Catalysis of Organic Reactions Using Immobilised Transition Metal Nanoparticles

Hussam Yahya Alharbi

A thesis submitted in partial fulfilment of the requirements for the degree of

Doctor of Philosophy in Chemistry

School of Natural and Environmental Sciences

Newcastle University

May 2022

Abstract

The synthesis and properties of polymer immobilised ionic liquids (PIILs) have been extensively studied. In particular, the Knight-Doherty group has explored and developed novel functionalised PIIL systems as supports for transition metal- and nanoparticles-based catalysts for a range of chemical reactions.

Chapter 2 describes the completion of a study of iridium-catalysed aromatic C-H borylation under homogeneous conditions, which does not involve PIIL but was used to gain experience in catalysis. *In situ* generated Ir-complexes, formed from [Ir(COD)(acac)] or [Ir(COD)(OMe)]$_2$ and tmphen catalysed the C-H borylation of diethyl phenylphosphonate (**A**, R = H) with B$_2$pin$_2$ or HBpin under mild conditions but were nonselective, producing a mixture of 3-, 3,5-di- and 4-boryl substituted aryl phosphonates (**B**). In contrast, aryl phosphonates carrying an existing 3-substituent undergo C-H borylation with very high regioselectivity to give the product in which the boronate ester is *meta* to both existing substituents. The resulting *meta*-substituted arylboronic esters were then utilised as the nucleophilic coupling partner for the Pd-catalysed Suzuki–Miyaura cross-coupling reaction with a variety of aryl halides to prepare a diverse range of *meta*-phosphonate substituted biphenyls (**C**).
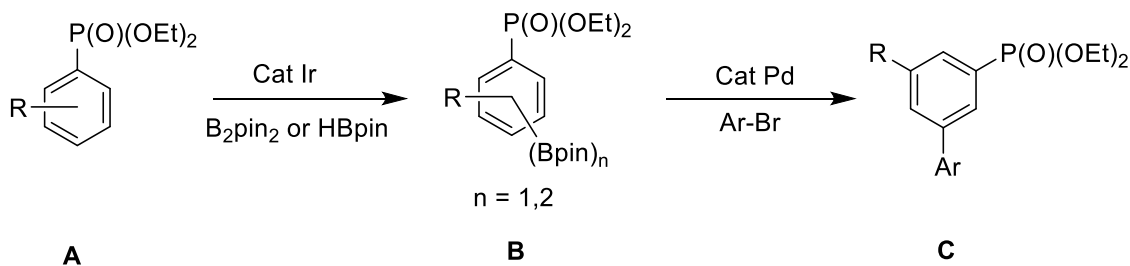
Chapter 3 builds upon the work carried out in a paper published by our research group in PIIL supported AuNPs for the reduction of nitroarenes. The impregnation of a phosphine-decorated PIIL with KAuCl$_4$ was anticipated to result in oxidation of the phosphine and reduction of the Au(III) to Au(I). A series of ^{31}P NMR experiments were performed with triphenylphosphine, as a model compound, which confirmed that treatment with KAuCl$_4$ results in formation of a transient Ph$_3$PCl$_2$ species, and ultimately the major products Ph$_3$PO and Ph$_3$PAuCl, together with a small amount of Ph$_3$PAuCl$_3$. The PIIL Au(I) phosphine complex **D** (AuCl, Z = PPh$_2$) and Au(III) phosphine oxide complex **D** (AuCl$_4^-$, Z = O=PPh$_2$) were prepared, together with the *in situ* generated Au(I)

containing phosphine oxide **D** (AuCl, Z = O=PPh$_2$) PIIL in order to investigate the effect of gold precursor and the heteroatom donor in the polymer support on the catalyst performance and selectivity for reduction of nitroarenes by the derived nanoparticle-containing PIILs **E**.
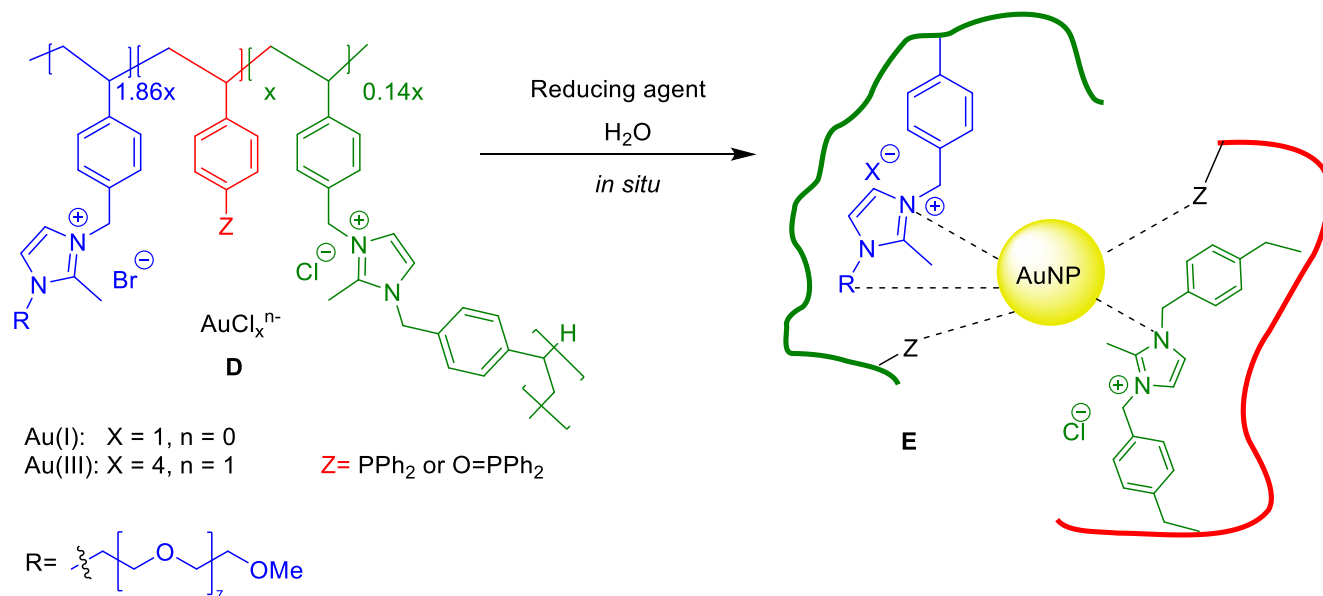
These catalytic systems reduce nitrobenzene under mild reaction conditions and with low catalyst loading into three distinct products; *N*-phenylhydroxylamine (**NOH**), azoxybenzene (**N2O**), and aniline (**NH2**). Using water as the reaction solvent the phosphine oxide based Au(III) and Au(I) precursors were both extremely active and selective for reduction of nitrobenzene (**NO2**) to form the thermodynamically unfavourable *N*-phenylhydroxylamine (**NOH**) with either NaBH$_4$ or (CH$_3$)$_2$NH·BH$_3$ as the stoichiometric hydrogen source. Changing the solvent system from water to ethanol under similar reaction conditions provided azoxybenzene (**N2O**) as the sole product with NaBH$_4$ but the reaction was unselective when using (CH$_3$)$_2$NH·BH$_3$ as hydrogen source. Finally, by increasing the number of equivalents of NaBH$_4$, using longer reaction time and higher temperature, aniline (**NH2**) was afforded in almost quantitative yields.
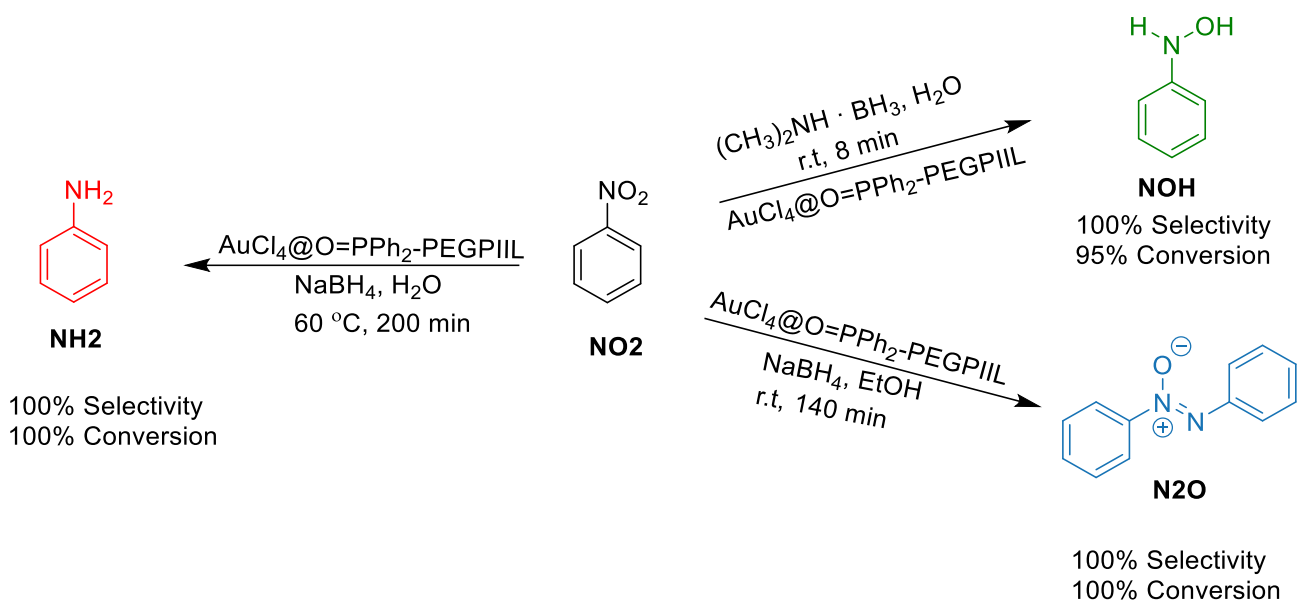
In chapter 4, a strongly hydrophobic decyl hydrocarbon chain was incorporated into the polymer to investigate the influence of replacing the strongly hydrophilic PEG. Both PdNP@PPh$_2$-PEGPIIL (**F**) and PdNP@PPh$_2$-*N*-decylPIIL (**G**) are efficient and selective systems for quinoline hydrogenation in the presence of NaBH$_4$ or (CH$_3$)$_2$NH·BH$_3$ under mild conditions and delivered 100% selectivity for 1,2,3,4-tetrahydroquinoline (THQ). The polyethylene glycol modified catalyst (PdNP@PPh$_2$-PEGPIIL, **F**) had a higher activity than the *N*-decyl analogue (PdNP@PPh$_2$-*N*-decylPIIL, **G**).
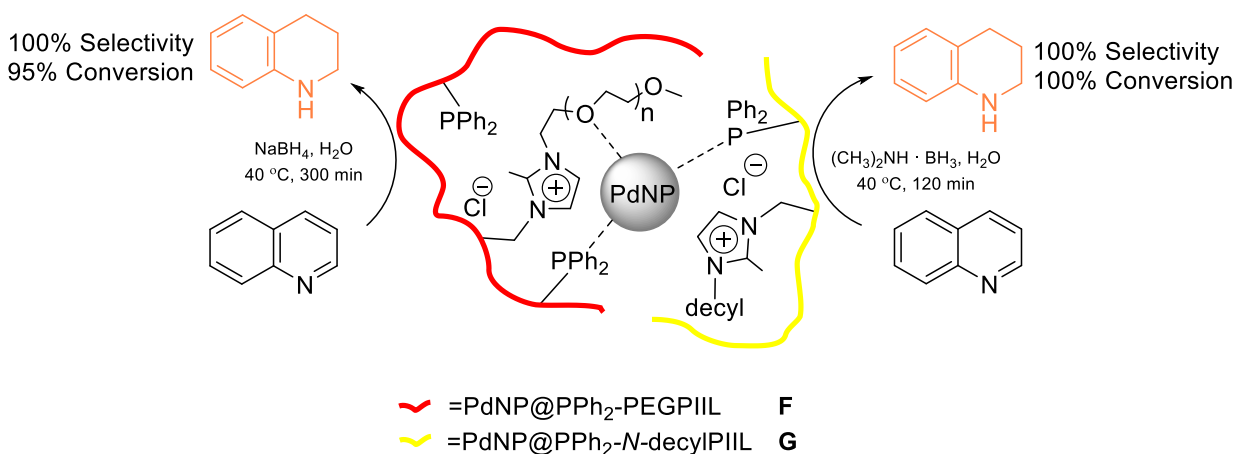
In chapter 5, PIIL supported PtNPs were found to catalyse the aqueous hydrolysis of NaBH$_4$ efficiently under mild conditions to produce hydrogen. The composition of the polymer effects the efficiency of the catalyst. PtNP@PPh$_2$-PEGPIIL (**H**) was found to be more active as compared to

PtNP@PPh$_2$-*N*-decylPIIL (**I**). A maximum initial TOF of 169 moleH$_2$.molcat^{-1}.min^{-1} with PtNP@PPh$_2$-PEGPIIL (**H**) loading of 0.08 mol% was achieved under mild conditions. This represents one of the highest TOF values reported for the aqueous hydrolysis of NaBH$_4$ in the presence of a PtNP-based system. Arrhenius plots indicated an activation energy (Ea) of 23.9 kJ mol^{-1} for the aqueous hydrolysis of NaBH$_4$ catalysed by PtNP@PPh$_2$-PEGPIIL (**H**) and 35.6 kJ mol^{-1} for PtNP@PPh$_2$-*N*-decylPIIL (**I**). The mechanism of the reaction was explored by primary kinetic isotope effect, using either H$_2$O or D$_2$O which produced a k$_H$/k$_D$ of 1.8 for hydrolysis catalysed by PtNP@PPh$_2$-PEGPIIL and 2.1 for PtNP@PPh$_2$-*N*-decylPIIL. These values are consistent with cleavage of the O-H bond being involved in the rate determining step. The PtNP@PPh$_2$-PEGPIIL was recycled up to five times. The drop in conversion to 70% after the fifth cycle was ascribed to poisoning by the accumulated byproduct, metaborate.

= PtNP@PPh$_2$-PEGPIIL   **H**
= PtNP@PPh$_2$-*N*-decylPIIL   **I**
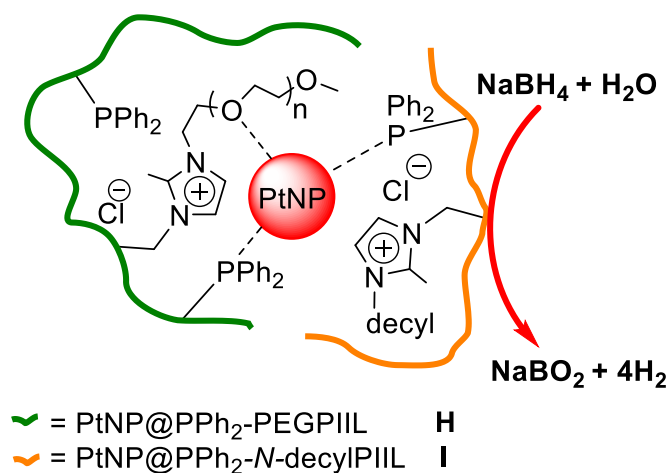
Dedication

This thesis is dedicated to my mother, Fatimah Alhazmi, and my father, Yahya Alharbi, for their endless prayer, support, and encouragement. And to my wife Enas Alahmadi and my children Lara and Mishary for their sacrifice and supporting me all the time.

Acknowledgements

enough to extend my appreciation to my brother, my sister in-law, my sisters, my father in-law, my mother in-law and my friends. Thank you very much

Above all, I am so grateful to Allah Almighty for providing me with all the blessings in my life.

List of Publications

1. Doherty, S.; Knight, J. G.; Tran, T. S. T.; **Alharbi, H. Y**.; Perry, D. O. The Synthesis of Biarylmonophosphonates *via* Palladium-Catalyzed Phosphonation, Iridium-Catalyzed C-H Borylation, Palladium-Catalyzed Suzuki–Miyaura Cross-Coupling. *Catal. Lett.* **2022**, *152* (2), 398–413. https://doi.org/10.1007/s10562-021-03643-3.

2. Doherty, S.; Knight, J. G.; **Alharbi, H. Y**.; Paterson, R.; Wills, C.; Dixon, C.; Šiller, L.; Chamberlain, T. W.; Griffiths, A.; Collins, S. M.; Wu, K.; Simmons, M. D.; Bourne, R. A.; Lovelock, K. R. J.; Seymour, J. Efficient Hydrolytic Hydrogen Evolution from Sodium Borohydride Catalyzed by Polymer Immobilized Ionic Liquid-Stabilized Platinum Nanoparticles. *ChemCatChem* **2022**, *14* (4), e202101752. https://doi.org/10.1002/cctc.202101752.

3. Doherty, S.; Knight, J. G.; Backhouse, T.; Tran, T. S. T.; Paterson, R.; Stals, F. M. E.; **Alharbi, H. Y**.; Chamberlain, T. W.; Bourne, R.; Stones, R.; Griffiths, A.; White, J.; Aslam, Z.; Hardacre, C.; Daly, H.; Hart, J.; Temperton, R.; O'Shea, J.; Rees, N. Highly Efficient and Selective Aqueous Phase Hydrogenation of Aryl Ketones, Aldehydes, Furfural and Levulinic Acid and Its Ethyl Ester Catalyzed by Phosphine Oxide-Decorated Polymer Immobilized Ionic Liquid-Stabilized Ruthenium Nanoparticles. *Catal. Sci. Technol.* **2022**,12 (11), 3549-3567. https://doi.org/10.1039/D2CY00205A.

List of Abbreviations

acac	Acetylacetonate
AIBN	Azobisisobutyronitrile
B_2pin_2	Bis(pinacolato)diboron
C_2C_1Im	1-Ethyl-3-methylimidazolium
$C_4C_1C_1Im$	1-Butyl-2,3-dimethylimidazolium
C_4mim	1-Butyl-3-methylimidazolium
CNTs	Carbon nanotubes
COD	1,5-Cyclooctadiene
Conv.	Conversion
DCM	Dichloromethane
DLS	Dynamic light scattering
DLVO	Derjaguin-Landau-Verwey-Overbeek
DMF	*N,N*-Dimethyl formamide
DNB	Dinitrobenzene
DSC	Differential scanning calorimetry
Dtbpy	4,4′-Di-*tert*-butyl-2,2′-dipyridyl
EDX	Energy dispersive X-Ray spectroscopy
eq.	Equivalent
FT-IR	Fourier transform infrared spectroscopy
g	Gram
h	Hour
HBpin	Pinacolborane
ICP-OES	Inductively coupled plasma optical emission spectrometry
IL	Ionic liquid
J	Coupling constant
mg	Milligram
Min	Minutes
mL	Millilitre
MOFs	Metal organic frameworks
N2O	Azoxybenzene

NO2	Nitrobenzene
NH2	Aniline
NHC	*N*-heterocyclic carbene
nm	Nanometres
NMR	Nuclear magnetic resonance
NOESY NMR	Nuclear Overhauser effect spectroscopy
NOH	*N*-Phenylhydroxylamine
NPs	Nanoparticles
PEG	Polyethylene glycol
PIIL	Polymer immobilised ionic liquid
PIL	Poly ionic liquid
POM	Polyoxometalates
ppm	parts per million
ROMP	Ring-opening metathesis polymerisation
RTIL	Room temperature ionic liquid
SCIL	Solid catalyst with ionic liquid layer
Selec.	Selectivity
SEM	Scanning electron microscopy
SILP	Supported ionic liquid phase
TEM	Transmission electron microscopy
TGA	Thermal gravimetric analysis
THF	Tetrahydrofuran
THQ	Tetrahydroquinoline
THT	Tetrahydrothiophene
tmphen	3,4,7,8-Tetramethyl-1,10-phenanthroline
TOF	Turnover frequency
TON	Turnover number
TSIL	Task specific ionic liquid
wt. %	Weight percentage of total mass
XPhos	2-Dicyclohexylphosphino-2′,4′,6′-triisopropylbiphenyl
XPS	X-ray photoelectron spectroscopy
δ	Chemical shift

Table of Contents

Chapter 1. Introduction

1.1 Catalysis

A catalyst is a substance that accelerates a chemical reaction by facilitating the breaking and making of bonds in reactions by changing the activation energy of the pathway without being consumed in the process. The catalytic pathway has lower activation energy than that for the uncatalysed reaction (Figure **1.1**). Therefore, only a very small amount of catalyst is generally required to convert a large quantity of reactants, and this process occurs under milder conditions than those required in the absence of the catalyst. If there is a possibility of forming more than one product, then the use of a catalyst may change the distribution of products compared to the uncatalysed process, hence, enabling control over the selectivity of the chemical reaction.[1–3]
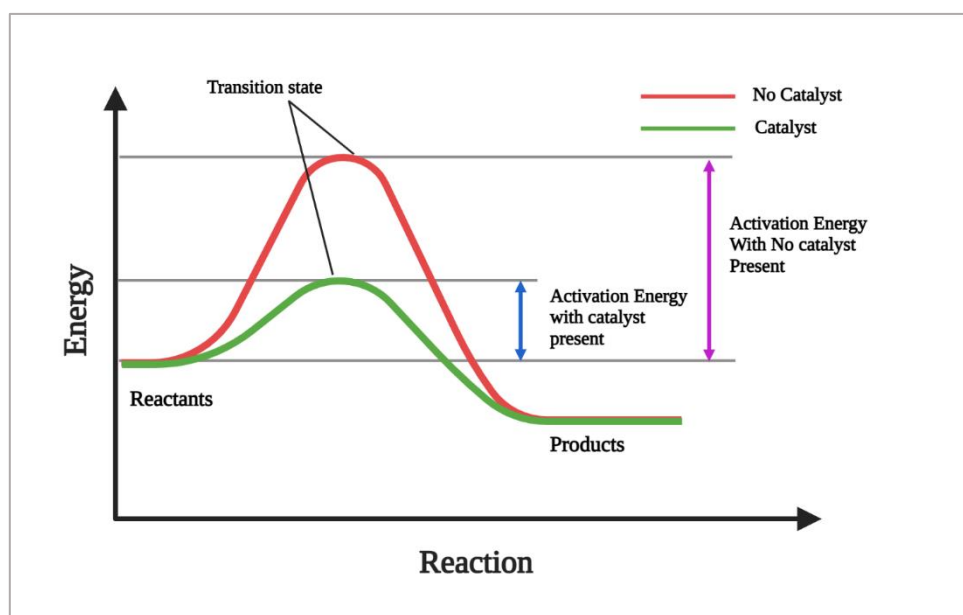
Figure 1.1: The effect of a catalyst on a reaction/energy coordinate.

Catalysts can be usefully classified into homogenous and heterogeneous. In homogeneous catalysis, the catalyst exists in the same phase as the reaction mixture (usually in the liquid phase). Under such conditions, the catalyst species are spatially separated from each other and the nature of the active sites is identical, leading to uniform catalysis throughout the reaction. Although homogeneous catalysts usually display high activities and selectivities under mild conditions of

reaction, the similar solubility properties of the catalyst and products make catalyst separation and recycling difficult.[4,5]

Heterogeneous catalysis occurs when the catalyst is in a dissimilar phase (usually solid/liquid, solid/gas or solid/liquid/gas). Heterogeneous catalysis has an important role in the development of procedures since it has the potential to satisfy the objectives of industrial catalysis, and at the same time meet the principles of green chemistry. Separation and recovery of the catalyst is often simple, and there are fewer challenges due to the distinct differences in solubility and miscibility of the catalyst and product. The key challenge in the design of newer heterogeneous catalysts is to reach high levels of activity and selectivity that can compete with those of homogeneous catalysts.[1,6]

1.2   Ionic Liquids

Low melting organic salts, which exist in the liquid state below 100 °C, are generally known as ionic liquids. Many of the ionic liquids (ILs) with lower melting points are also known as room temperature ionic liquids (RTILs). The reason behind the lower melting point of ionic liquids is their low lattice energy. In recent years, ILs have strongly attracted much research attention due to their widespread potential for applications in various fields. For instance, they are well known as neoteric solvents or designer solvents, possessing several desirable properties like high thermal stability, low volatility, and non-flammability, ease of handling, immiscibility with various organic solvents, and the IL can be used several times, i.e., they can be recyclable.[7] Additionally, ILs can be functionalised through careful choice of the anion and cation, which in turn provides the opportunity to fine-tune the intrinsic properties of the ILs such as polarity, stability, density, conductivity, viscosity and hydrophilicity/hydrophobicity, etc.[8] Much of the initial work in this area was founded on imidazolium based ILs, however, nowadays a variety of anions and cations have been developed to obtain desirable properties. (Figure **1.2**) displays some of the structures of the various typical cations and anions used for ILs.

Cations

Anions

Imidazolium
Pyridinium
Pyrrolidinium

halide
$Tf_2N^{\ominus}$

$PF_6^{\ominus}$
$BF_4^{\ominus}$

Ammonium
Phosphonium
Sulfonium

$AlCl_4^{\ominus}$
$NO_3^{\ominus}$

$CF_3SO_3^{\ominus}$
$Al_2Cl_7^{\ominus}$
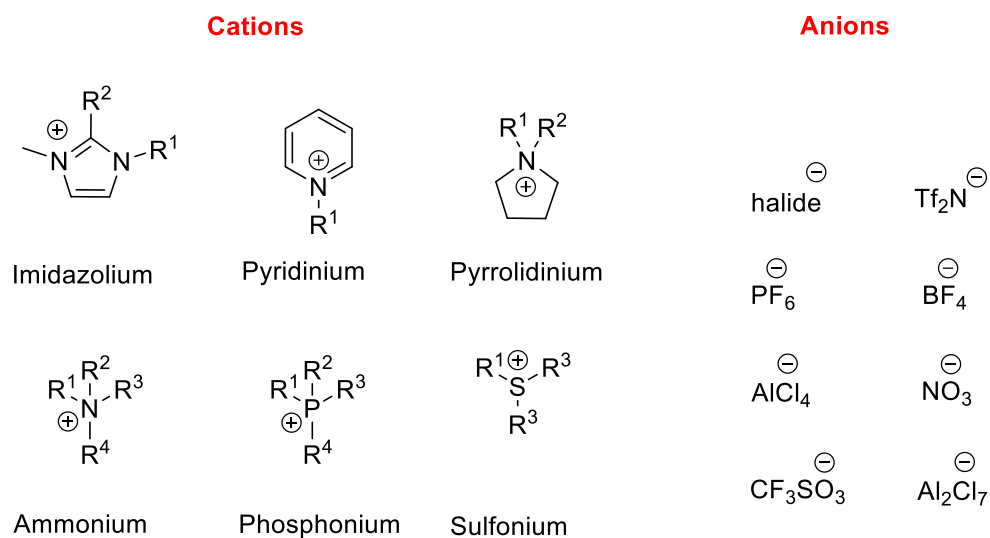
Figure 1.2: Examples of ionic liquid cations and anions.

The use of ionic liquids as solvents in the field of catalysis also suffers from some disadvantages such as their need to be stored under an inert atmosphere, leaching, and high viscosity. The biodegradability of ILs and the associated long-term toxicity is yet unknown and also the high cost associated with them has prevented their use for commercial purposes.[9–11] As ILs are composed only of ions (cations/anions), they can serve as an ideal medium to stabilise reactive charged intermediates, which in turn improves the selectivity and reaction rate of several catalytic reactions. Accordingly, they have been widely used in organic synthesis. For example, ILs have proved to be an effective medium for the dehydration reaction of carbonyl compounds for imine formation.[12]

Since ILs have exceptionally broad and diverse properties due to the possibility of functionalisation of different cation/anion counterparts, the most significant characteristic associated with an IL is its polarity. It is believed that ILs act as super polar solvents due to their ionic nature, nevertheless, an accurate measurement the polarity of an IL has yet not been established. Many ILs appear to possess moderate polarities similar to acetonitrile, and methanol.[13]

The polarities of ILs are thought to be controlled by inter- and intramolecular forces and the ion pair Coulombic interactions within the liquid. The most common type of IL is based on the dialkylimidazolium cation (**Figure 1.3**),[14] which display several intra and intermolecular interactions, including:

a) Hydrogen-bond formation between protons in the cation, which serve as donors, and the anion as acceptor.

b) Possible Van der Waals interactions among the different side chain alkyl groups and π-π-stacking due to the aromatic imidazolium ring.[14]
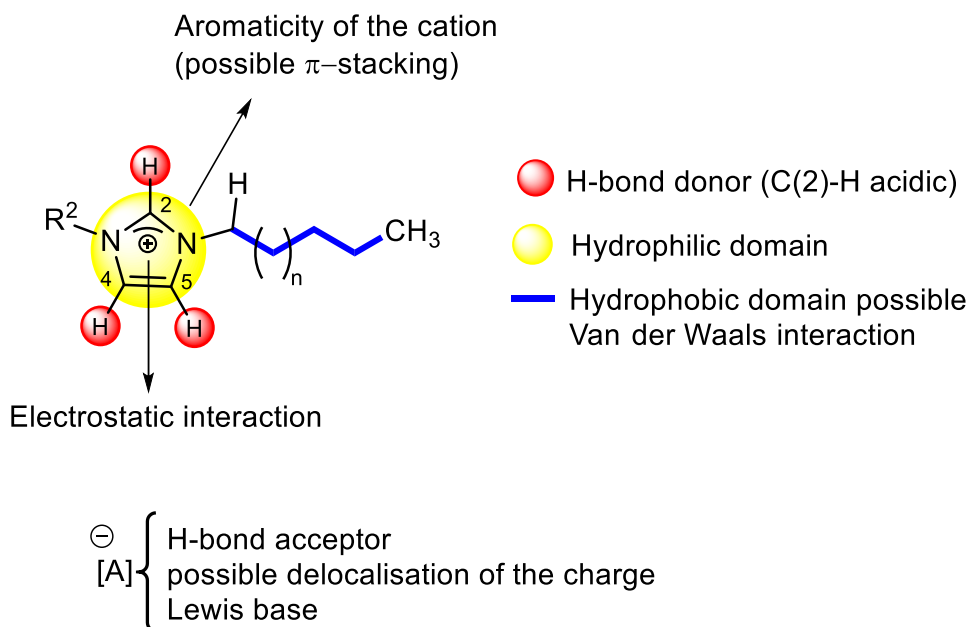
Figure 1.3: The different types of interactions present in imidazolium-based ILs.[14]

ILs present unique solubility characteristics which allow them to dissolve several polar and nonpolar substances.[13] In addition, the three-dimensional structure of the IL can play a vital role in defining its role in different reactions. The H-bonding interactions involved in dialkylimidazolium chloride-based ILs can form polymeric networks which can be identified by using a variety of different techniques, for instance, NMR, X-ray diffraction, and NOESY spectroscopy.[14–16] Choice of a specific anion for a specific cation has also been found useful in perturbing the melting points of the ILs. For example, a cation which can coordinate with the hydrophilic anions strongly, like halides increases the melting point of the IL whereas a cation which coordinates weakly with the hydrophobic anions, like triflates ([OTf]$^-$) and triflimides ([NTf$_2$]$^-$), lowers the melting point. Another way to alter the melting point of the IL is by the fine-tuning of the alkyl side chain length. For instance, alkyl side chains with longer lengths decrease the melting point of the IL.[17] ILs generally possess higher viscosities as compared to conventional organic solvents, which in turn has a disadvantageous effect on the dynamics and the kinetics of a particular reaction since mass

transfer might be limited. In the field of catalysis, this concept plays a vital role as the reactant must possess easy access to the active sites. The viscosity of the IL can often be decreased by adding small quantities of water, even as low as the parts-per-million range or by adjusting the ILs where the choice of anion has the greater effect.[18]

Ionic liquids can be prepared by many routes (Scheme **1.1**). Each route has its own inherent advantages and disadvantages. IL synthesis has mainly been done by a metathesis process using a halide salt of alkali metals having an organic cation or ammonium salt with a suitable anion (Scheme **1.1**, Route A).[19] However, this route often causes many adverse halide by-products which are difficult to remove from the desired product. An alternate approach can be neutralisation of a base with suitable Brønsted acids (Scheme **1.1**, Route B) or by alkylimidazole direct alkylation (Scheme **1.1**, Route C). Using route B, it is very difficult to get ILs with high purity because traces of alkylimidazole or Brønsted acids remain in the final product. (Scheme **1.1**, Route C) has been reported for synthesis of phosphate, sulfate or sulfonate based ILs.[14] Route D is a relatively new route which also does not have halides and other by-products by using dimethyl carbonate (DMC) instead of alkyl halides as a clean methylating agent.[20]

Route A) Anion Methathesis
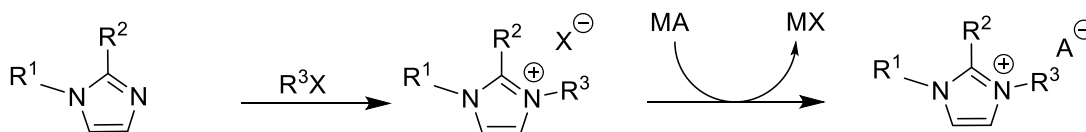
Route B) Neutralisation

X= Halide
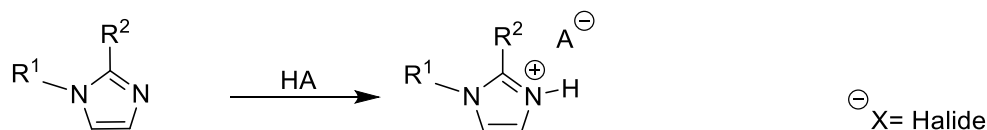
Route C) Direct Alkylation
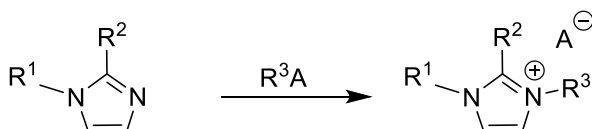
Route D) Carbonate Route
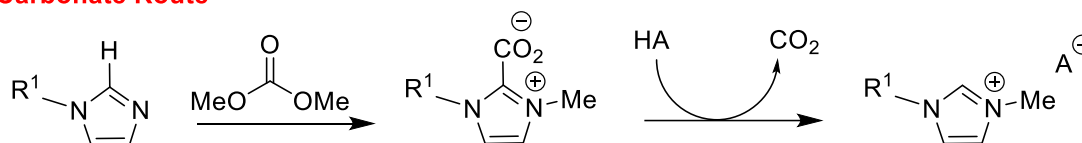
Scheme 1.1 Preparative routes used to synthesise imidazolium based ionic liquids

Since the discovery of ionic liquid science and technology, catalysis appeared as one of the most suitable areas of application because of their unique features. These features include their unusual and highly tunable solubility and miscibility and their extraordinary combinations of polarity and nucleophilicity. The main strategies that have emerged for the use of ILs in catalysis are liquid – ionic liquid biphasic catalysis and ionic liquid thin film catalysis.[21,22]

One of the most well developed applications of ionic liquids in liquid-ionic liquid biphasic catalysis is the use of acidic chloroaluminate melts in Friedel-Crafts reaction (also known as refinery alkylation). The ionic liquids used here actually constitute the catalytically active part of the reaction system.[23] Another extensively investigated area is the use of the IL as the bulk solvent for a transition metal catalyst, forming a catalytically active ionic catalyst solution. In these two cases, catalyst recycling and product isolation are made easier by the immiscibility of the organic phase, in which the product usually resides, and the ionic liquid phase, in which the catalyst resides. Mass

transfer limitations are, however, often serious due to the higher viscosity of the catalyst-containing ionic liquid phase in comparison to organic phase.[24] The relatively high liquid viscosity of ionic liquid catalysts slows the transfer of substrates in the reaction mixture.[25]

Catalysis involving a thin film of ionic liquid can be one of the best approaches to overcome these problems in which a catalytically active phase consists of a thin film that reduces the pathway of diffusion, and therefore the characteristic diffusion time. There are two conceptually different approaches for the use of thin films of IL (Figure **1.4**):

- "Supported Ionic Liquid Phase (SILP)" which contains a catalyst species that is dissolved in a thin IL film on the surface of a support material. This is therefore supported homogeneous catalysis.[26]
- "Solid Catalyst with Ionic Liquid Layer (SCILL)" in which a catalytically active solid, or a solid support containing the catalyst, is coated with a thin IL film. This case represents IL modified heterogeneous catalysis.[26]
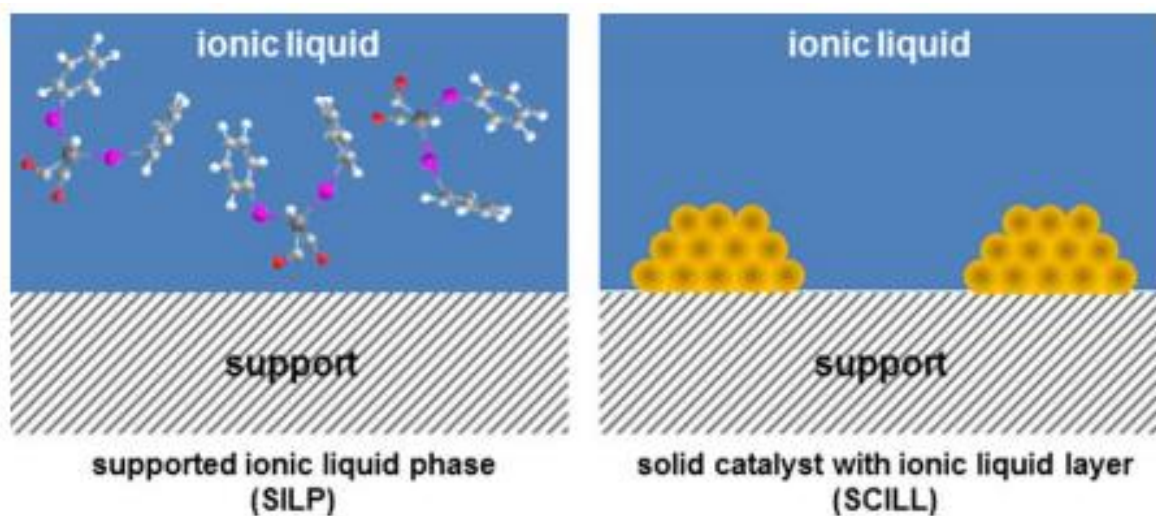
Figure 1.4: Two fundamentally different types of IL thin film catalysis. Supported Ionic Liquid Phase (SILP) and Solid Catalyst with Ionic Liquid Layer (SCILL).[26]

There are some situations when these cases overlap with each other. For example, when under the particular conditions of reaction, thermal degradation occurs to a SILP catalyst in a system that contains nanoparticles of IL-stabilised catalyst. Moreover, under the particular conditions of reaction, it is also possible that transformation of a SCILL catalyst can occur and it becomes a SILP-like system due to active species from the solid surface dissolving into the film of IL. Thus,

it must be kept in mind that the nature of an IL film under the conditions of catalysis may become very complex due to the presence of dissolved side-products, products and substrate with the inclusion of catalyst. The occurrence of the interface plays an essential role in the catalytic applications of ILs: as in liquid-ionic liquid biphasic catalysis the major concern is the interface between the organic phase and IL phase and in IL thin film catalysis both IL-solid support and the IL-fluid (liquid or gas) phase interfaces are important.

1.2.1   Liquid-Ionic Liquid Biphasic Catalysis

As discussed above, there are two cases that are covered by liquid-ionic liquid biphasic catalysis:

(i)   the presence of IL as an active liquid for catalysis, and

(ii)   the presence of IL as a solvent that dissolves the catalyst (e.g. a transition metal species).

There is a special case that belongs to case (ii) in which stable nanoparticles for catalysis form a constant suspension in an IL.

Acid catalysis is used in many key processes in the chemical, petrochemical and oil refining industries. Strong and cheap acids i.e., H_2SO_4 or $AlCl_3$, are traditionally used and product isolation typically involves the complete hydrolysis of the catalyst. At the end of the process, the wastewater which is corrosive is formed in huge quantities that must be eliminated with refined down-stream procedures because they contain the residues of organic product. Furthermore, hydrolysis of the catalyst renders it inactive. Acidic ILs offer specific advantages in these applications because they can be highly acidic liquids that can be adjusted in their acid strength, miscibility and solubility.[18,27,28] The chloroaluminate ILs are the best established and well investigated example, which are manufactured by mixing an organic salt of chloride with an excess quantity of $AlCl_3$. In all practical applications of the chloroaluminate in its melt state, it contains a degree of water contamination because they are found to be highly hygroscopic.[29] Consequently, chloroaluminate ILs as an acid must contain traces of molecular hydrochloric acid (HCl) and hydroxy/oxychloroaluminate species. Brønsted superacidity was discovered during the late 1980's, in which HCl in the gaseous state is added to melts of acidic chloroaluminate. $[C_2C_1Im]Cl/AlCl_3$ has been used for the quantitative examination of HCl acidity as function of IL composition (51 to 66.4 mol% of $AlCl_3$) and HCl pressure.[30] Interestingly the acidic nature of chloroaluminates can change during vacuum conditions, because of the sublimation/evaporation of $AlCl_3$ and HCl from

the IL, therefore the melt's acidity and composition can be changed. Carbonylation reactions,[31] Friedel–Crafts acylation[32] and Friedel–Crafts alkylation[33] are the best examples of fundamental applications of acidic chloroaluminate ILs with liquid-ionic liquid biphasic catalysis. Refinery alkylation reactions, [34] cracking[35] and oligomerisation[36] are the best examples of liquid-ionic liquid biphasic catalysis that are successfully operated as acidic catalysis reactions.

1.2.2   Liquid-Ionic Liquid Biphasic Transition Metal Catalysis

Aside from their use in acid catalysed reactions, in the past twenty years ILs have been intensively studied for the immobilisation of transition metals that are dissolved homogeneously. There is a need for successful methods for the immobilisation of homogenous catalysts for industrial usage in order to solve the problem of the separation of catalyst/product. Moreover, it is very expensive to recycle and recover dissolved complexes of transition metals. The following properties need to be satisfied by the polar ionic–liquid phase for use in multi-phase homogenous catalysis by transition metal species:

- Adequate solubility of the reactants and the starting materials which must have fast mass transfer into the catalyst-containing phase.
- The desired product(s) should not dissolve well in the IL.
- Extremely good catalyst solvation to ensure complete immobilisation of the catalyst and to avoid leaching.
- The solvent must not cause the deactivation of the catalyst that is immobilised.

Due to nucleophilicity properties, polarity and adjustable solvation, ionic liquids are well suited to these complex requirements.[37] Furthermore, liquid-ionic liquid biphasic catalyst reactions permit the efficient recycling of the applied transition metal catalyst, although ionic liquids are relatively expensive. Therefore, the application of ILs on a commercial level may offer significant advantages and has not yet been fully explored.

In liquid-ionic liquid biphasic catalysis using transition metal catalysts, the ligands must be highly ionic or polar to minimise the leaching of catalyst. In the study of biphasic reactions, much has been done to address this issue and to develop versions of ligands carrying an ion-tag that maintains the steric and electronic effect of the ligand[38,39] Some ion-tagged ionic ligands are shown in Figure **1.5** that have been effectively used for hydroformylation, oxidation and hydrogenation reactions.[18]
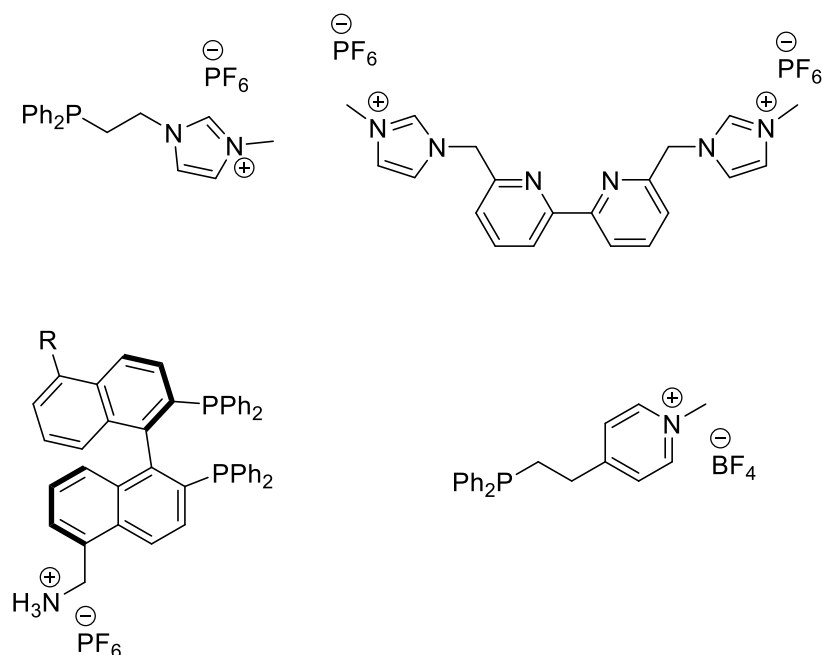
Figure 1.5: Examples of ion-tagged ionic ligands used to immobilise transition metal complexes in liquid-ionic liquid biphasic reactions.

IL media have been used for stabilising and preparing nanoparticles with catalytic properties.[40,41] One possible mechanism of nanoparticles stabilisation involves the formation of a protective layer composed of loosely bound *N*-heterocyclic carbenes (in the case of some 2-unsubstituted imidazolium-based ILs) or anions. However, these surface-bound protective species can be replaced by other substances. This protective layer improves the comparatively low stability of nanoparticles towards agglomeration/aggregation. The addition of polymeric stabilisers or ligands can be helpful to achieve stable nanoparticle-based catalysis in ILs and transition metal nanoparticles distributed in ILs have been used as active catalysts for many different reactions, such as the hydrogenation of ketones, arenes and alkenes.[42] In these liquid-ionic liquid biphasic systems the catalyst phase is formed by the IL with dispersed nanoparticles in it and the upper organic phase is formed by the product and starting material. A simple decantation process has been used for the recovery of the IL-nanoparticle phase. There are many reports concerning the application of imidazolium-based ILs within catalysis because of the resulting improvement in reaction rate and chemoselectivity.[10,43]

1.3 Nanoparticles (NPs) for Catalysis

Catalysis based on transition metal nanoparticles (NPs) is now among the most versatile and powerful technologies because of their nanoscale size dimensions (1-100 nm). In addition, the quantum confinement effects of NPs induce several unique physical properties due to which they have found applications in various fields including electrochemistry,[44] biotechnology,[45] drug delivery in medicine,[46] fuel cell technology,[47] etc. The high catalytic activities of metal nanoparticles arise due to their high surface area to volume ratio as compared to their bulk analogues.[48] However, highly active NPs with smaller diameters though kinetically stable, undergo rapid agglomeration if a stabilising agent or capping ligand has not been added. The overall process has been well understood by using the principle of Ostwald ripening (Figure **1.6**).[49] According to this principle, partially or non-coordinated unsaturated atoms present at the surface of the small particles are energetically less stable as compared to those which are completely coordinated and well-organised in the bulk material. Larger particles usually possess a lower surface to volume ratio and hence, a lower surface energy. The system therefore will reorganise to reduce its overall energy *via* removal of atoms or molecules from the surface of smaller particles and then undergo attachment to the surface of the larger particles. As a result, the number of smaller particles decreases.
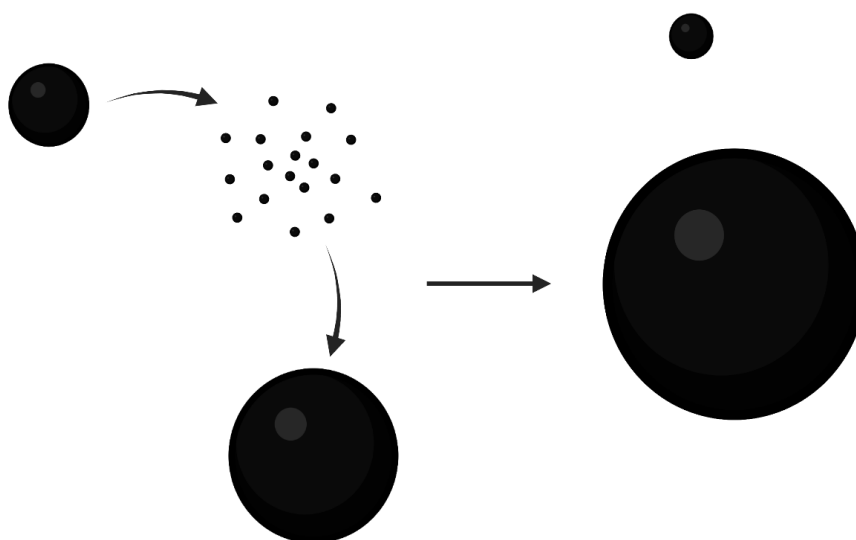
Figure 1.6: Schematic illustration of Ostwald ripening

Since, NPs have very small sizes and high catalytic activities, they can be easily used in both homogenous and heterogeneous catalysis. A variety of synthetic strategies have been designed to synthesise NPs with well-defined size and surface properties. One can immobilise and impregnate the NPs with a variety of materials making them advanced and green materials for different purposes including efficient recycling.

1.3.1   Synthesis of Metal Nanoparticles

Generally, two main approaches are followed for the synthesis of metal nanoparticles as shown in Figure **1.7**.
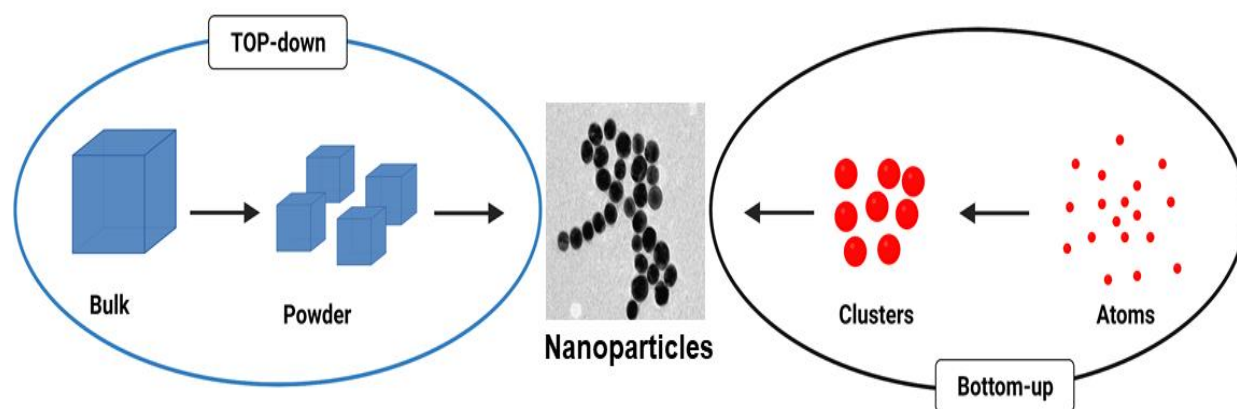
Figure 1.7: Different approaches to nanoparticles synthesis.

1. Top-Down approach

In the top-down approach, also known as the destructive method, the reduction of the bulk material into powder to nano-meter scale particles is carried out *via* attrition or mechanical milling and thermal decomposition. However, this method of nanoparticle synthesis is not preferred (Figure **1.7**).[50–52]

2. Bottom-Up approach

The more practical and common method for the synthesis of metal nanoparticles is the bottom-up method. It is conventionally achieved by reduction or decomposition of organometallic precursors in the presence of different stabilising agents followed by aggregation into nanoparticles (Figure

1.7). This method enables catalyst design due to the possibility of controlling the shape, size and dispersity of the nanoparticles. Besides this, the factors that can ultimately govern the catalytic activity and selectivity of the newly formed catalyst can also be controlled and tuned.[48,53] Additionally, this method is more applicable to scale-up for its use in commercial purposes.[54] Therefore, the stabilisation of metal nanoparticles is crucial for the synthesis of highly selective and active catalysts. A significant amount of research in this context has been accomplished by using different nanoparticle stabilisers; for instance, functionalised polymers with organic heteroatom donors,[55,56] carbon nanotubes (CNTs),[57] ionic liquids (IL),[58] inorganic polyoxometallates (POM)[59] and metal organic frameworks (MOFs).[60]

1.3.2   Nanoparticles Stabilisation

The stabilisation of metal nanoparticles typically occurs by three methods (Figure **1.8**).

Electrostatic   Steric   Electrosteric
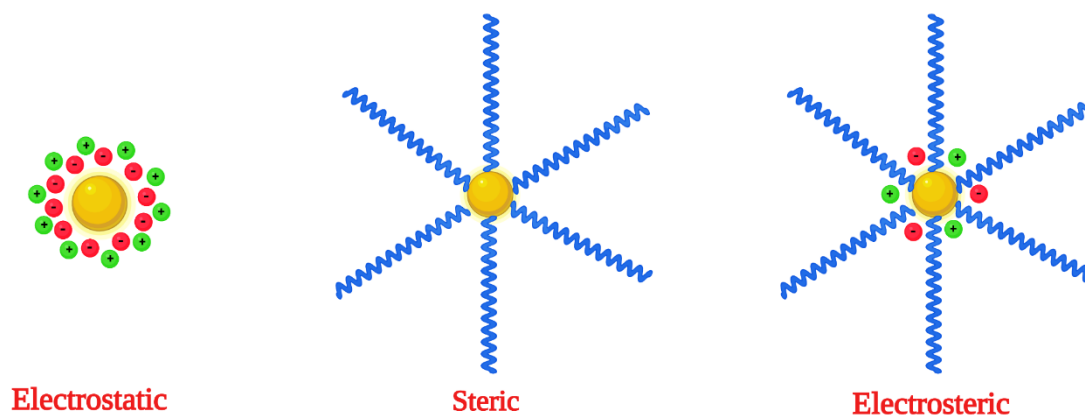
Figure 1.8: Schematic representation of different stabilisation methods of metal nanoparticles.

a) Electrostatic stabilisation

The nanoparticles experience a repulsive force when they are surrounded by a double layer of electric charges. The Derjaguin, Landau, Verwey and Overbeek (DLVO) theory proposes charged colloidal particles at first and then the electric charges are uniformly distributed over the surface of the nanoparticles. According to the DLVO theory, the electrostatic stabilisation of the metal nanoparticles is provided by the IL *via* a 'protective shell' formation around the nanoparticles. Therefore, the inner shell will be anionic and this initial shell is the main and primary source

responsible for providing stability to the metal nanocluster.[61] The use of ionic liquid (IL) in order to improve the stability of metal NPs and the electrostatic protection to prevent NPs from undergoing aggregation has been well documented.[62–64]

Stabilisation of AuNPs and PtNPs by using imidazolium-based IL has been well reported.[65,66] For instance, AuNPs of ~5 nm have been successfully prepared by reducing an aqueous solution of $HAuCl_4$ with an excess $NaBH_4$ by using the ionic liquid, 3,3′-[disulfanylbis(hexane-1,6-diyl)]-bis(1-methyl-*1H*-imidazol-3-ium) dichloride. The corresponding $[BF_4]^-$ or $[PF_6]^-$-based derivatives were simply prepared by an ionic exchange process. Similarly, AuNPs of approximately 3.6 nm have also been prepared and stabilised by using a zwitterionic imidazolium based ionic liquid carrying both a terminal thiol and a pendent sulfonate group. These nanoparticles have shown an unusually high stability in aqueous solutions of electrolytes and ionic liquid (IL).[67]

b) Steric stabilisation

The second stabilisation method is based on the concept that the steric repulsion between the molecules or ions adsorbed on adjacent particles influences the size and chemical nature of these molecules or ions, which in turn then determines the degree of stabilisation (Figure **1.8**).[68] For example, the geometric limitations around the surface of the nanoparticles usually permits large, and bulky molecules to provide an effective stabilisation, whereas an oblong or round geometry is beneficial to keep the approaching nanoparticles apart from each other (Figure **1.9a**).[68,69]
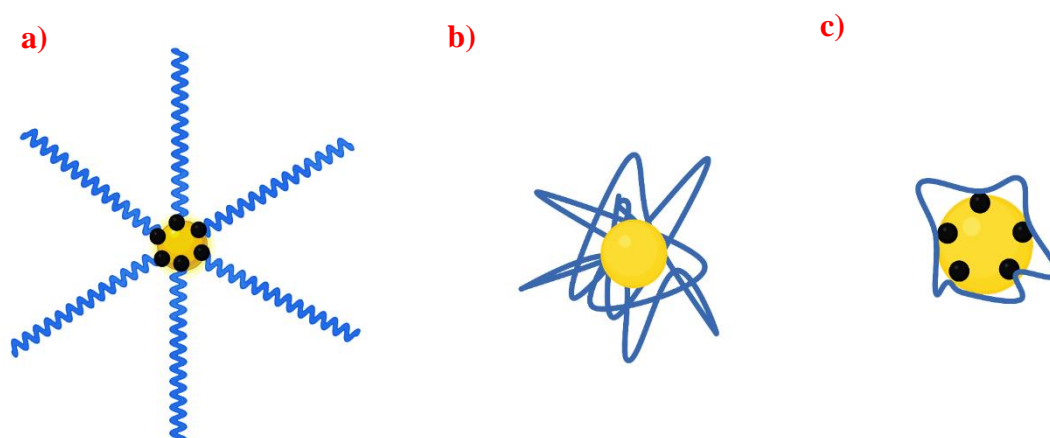
Figure 1.9: Representation of steric stabilisation: a) A round geometry resulting from molecules adsorbed through anchoring centres, b) Long stabiliser species encapsulate a nanoparticle, c) Chelate effect, involving a stabiliser with more than one adsorption centre.

Similarly, when the chain length of the stabiliser used is considerably longer than the characteristic size of the nanoparticles, then the probability of formation of a sphere encapsulating the nanoparticle is more likely (Figure **1.9b**).[70] It is for this reason, large molecular weight polymers are frequently used as nanoparticle stabilisers. Another key condition for the stabiliser is that it must strongly adsorb to the surface of the nanoparticles in order to provide longer lifetime at the surface and that it must not undergo spontaneous desorption. A stabiliser with more than one adsorption centre thus has many advantages, as the chelating effect of the stabiliser increases, the probability that the stabiliser remains adsorbed also increases (Figure **1.9c**). Chemisorption is the key driving force for the strong binding between the stabiliser and the nanoparticle surface of the metal.[71]

Metals with empty valence orbitals have an "electron deficient" surface, therefore, strongly electron "donating" atoms with free lone pair of electrons, such as sulphur (II), phosphorus (III) and nitrogen (III) moieties or molecules with π-electrons, such as aromatic systems usually adsorb strongly to the surface of the metal nanoparticles.[71–73] Thus, the concept of steric stabilisation is very important and plays a vital role during process of nanoparticles synthesis.

Wang and co-workers have prepared several bimetallic Au-Pd nanoparticles by using graphene oxide as the stabiliser. They have been employed as effective catalysts for the selective oxidation of a range of alcohols. A study by using varying amounts of the metal:graphene oxide ratio was carried out in order to fine tune the size of the nanoparticle by minimising the space for growth of nanoparticles inside the cavities of the graphene oxide sheets. Moreover, incorporating titania oxide (TiO_2) as a templating agent, the catalytic activity was further improved *via* formation of a two-dimensional graphene oxide layer to inhibit aggregation of the particles under catalysis conditions. The beneficial aspect of using this strategy is that no organic surfactants are required which might prevent the substrate from reaching the active sites of the catalyst.[74]

c) Electrosteric stabilisation

The use of bulky and highly charged adsorbents in order to achieve the stabilisation of nanoparticles rather than a neutral stabilising agent results in electrosteric stabilisation. Stabilisers which are ionic in nature, adsorb strongly to the surface and meet the concepts of steric and electrostatic stabilisation simultaneously are considered the best stabilisers. This can be conventionally accomplished by using amphiphilic block copolymers,[75] polyacrylate,[76] metal oxide

nanoparticles,[77] and synthesis of ionic liquids containing long alkyl chains to encapsulate the nanoparticles. In this way, the stabilisation is achieved by an electrostatic type of protective layer at the nanoparticle surface along with a sterically bulky hydrophobic outer layer.[78]

Heteroatom-modified polymer immobilised ionic liquid (PIIL) supports can be considered to provide the three types of stabilisation methods (Figure **1.8**), providing electosteric stabilisation to the nanoparticles against agglomeration. Therefore, the tunable nature of polymer chemistry is very advantageous and could enable rational design to control the particle size, particle distribution and morphology of the desired nanoparticles. This could be achieved *via* variations of the heteroatom, charge density, charge distribution, hydrophobicity, hydrophilicity, and the ratio of cross linkage of the polymer support. Additionally, through the introduction and variation of functional co-monomers it could be possible to enhance catalyst activity and/ or selectivity. By controlling the phase behaviour, or designing insoluble polymers, it could be possible to enable easy and efficient recovery and reuse of the catalyst.

In this context, the use of PIIL based supports to stabilise metal nanoparticles is proving to be an effective strategy in catalysis. For example, ionic co-polymers based on 1-vinyl-3-alkyl imidazolium chloride and *N*-vinylpyrrolidone functionalities have been used to stabilise RhNPs along with polyvinylpyrrolidone (PVP) stabiliser. The resulting catalysts were found to possess longer life time and the total turnover numbers were found to be 5 times greater than those previously observed for the hydrogenation of benzene by using IrNPs in $[C_4mim][PF_6]$.[18,79] The stabilisation achieved by using these copolymers emphasised a key synergistic effect between the ionic liquid and the polymer, since the reaction proceeds poorly and forms a black precipitate in the absence of either the co-polymer or $[C_4mim][PF_6]$. Lately, AgNPs, AuNPs and NiNPs stabilised by 1-vinyl-3-alkyl imidazolium polymers have been prepared in which the alkyl chain length is found to exert a strong effect on the size of the nanoparticle.[80,81] Additionally, imidazolium-decorated styrene-based copolymers have also been found to stabilise AuNPs, PdNPs and PtNPs *via* an electrosteric mechanism.[82–84]

Nanoparticles have been shown to be exceptionally active catalysts that combine the advantages of homogeneous and heterogeneous catalysis, providing a more environmentally friendly alternative to both. Optimisation of the performance of nanoparticle catalysts requires the understanding of the role of the catalyst in the manufacturing processes, structure of the active sites

on nano-scales and atomic scales, mechanism of reactions in the chemical process and also the efficiency, lifetime and selectivity of the catalyst. Hence, the shape, size, structure, support and promoters of the catalyst particles all influence the efficiency and the properties of a catalyst.

1.4 Supported Ionic Liquid Phase (SILP) Catalysis

The use of ILs in homogeneous catalysis has been well established, however, the major disadvantage associated with their use is mostly the product isolation from the reaction mixture including the requirement for excess quantities of IL, especially when the reaction is performed on large scale. The requirement of excess quantities of IL is not ideal primarily because of the high cost associated with the ILs, in addition to the potential toxicity, since there is a lack of proper understanding of their biology and also of their long-term stability. The desire to use small quantities of ILs, and the profound influence on the homogenous catalysis, prompted the concept of the supported IL phase (SILP). Therefore, a representative SILP system (Figure **1.10**) comprises of small quantities of thin film of IL homogenously dispersed on a large surface area of a support material, for instance silica, alumina or activated carbon. In this way, the SILP system displays dual properties of homogeneous as well as heterogeneous catalyst; the material thus can be easily isolated and reused and also has the beneficial aspect of being a homogeneous system.[85] Another beneficial aspect of the SILP system is that the homogenously dispersed catalyst within the IL phase is very near to the reaction interface, which drastically reduces the length of diffusion pathways and minimises the adverse effects which arise due to viscosity associated with the bulk or biphasic IL usage. More importantly, SILP systems can display enhanced reaction rates as compared to bulk ILs. Some of the very early examples of the use of the SILP system includes the saturation of a silica surface by Lewis acid based ILs such as aluminium chloride based derivatives which have the capability to catalyse several Friedel-Crafts reactions.[86]
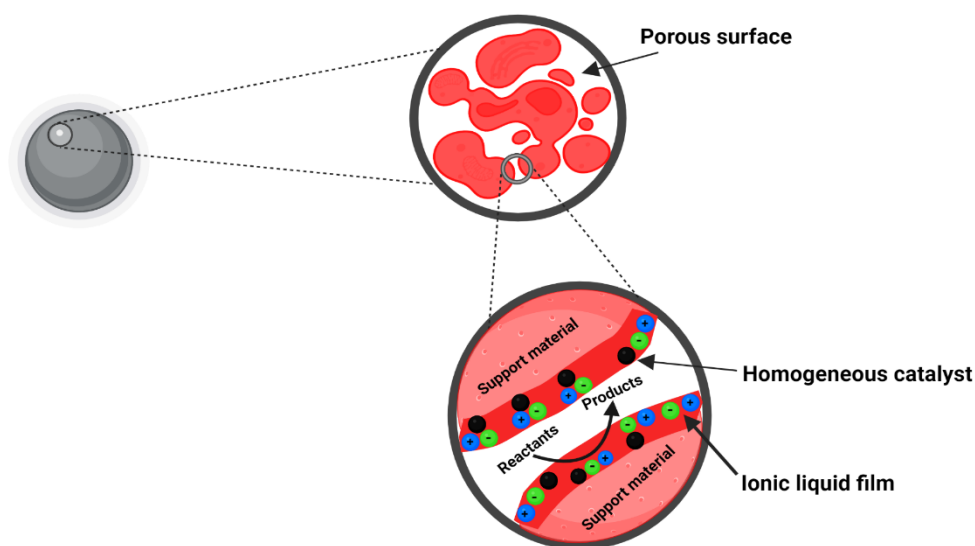
Figure 1.10: A supported ionic liquid phase catalyst (SILP).

In the context of SILP material preparation, generally four different methodologies have been used, as shown in Figure **1.11**. Among them, the immersion method (Figure **1.11A**) has been used more frequently to generate SILP based catalysts.
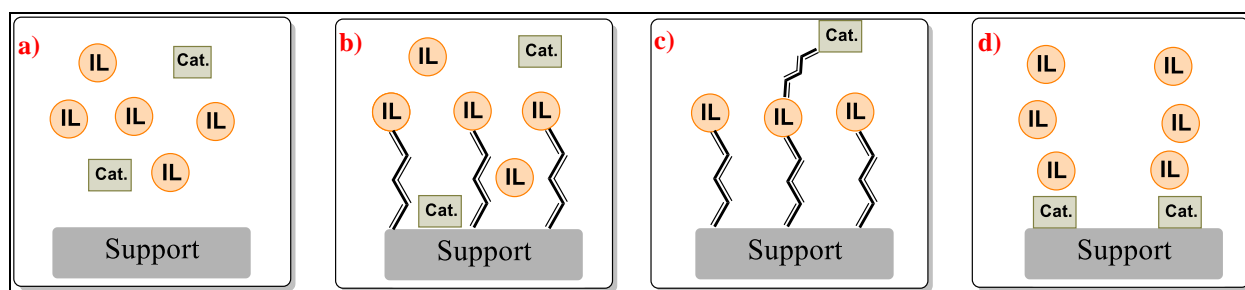
Figure 1.11: Four main methodologies in the preparation of SILP materials.

This method has been very commonly used especially for the immobilisation of a homogenous metal complex. In this method, the supporting material is saturated simply by dipping in a solution of the catalyst or pre-catalyst in IL in the presence of an organic solvent (wet impregnation). Then, the organic solvent is evaporated *in vacuo* leaving the desired dry SILP material, since the IL is non-volatile only the organic solvent evaporates in this method. Highly porous silica gels with large surface area have been used frequently as the supporting materials, although mesoporous silica and silica-alumina based systems like zeolites have also been employed for this purpose.[87,88] Other

inorganic support materials, such as alumina, have been occasionally employed, since they possess small pore volumes, however, they might be beneficial under specific circumstances as they tolerate various pHs. Among organic support materials chiral polymer chitosan,[89] membranes based on advanced materials,[90] carbon based nanotubes (CNTs) and sintered fiber metal[91] have been frequently used. SILP systems generated in this way have been used to catalyse a variety of reactions including hydroformylation reactions, olefin metathesis reactions, carbonylation reactions, hydroamination reactions, carbon-carbon coupling reactions.[85,87,92,93] An unexpected scenario has been observed in the SILP system upon confinement to the support material. For instance, the results of Rh-catalysed hydroformylations performed on silica-based SILP materials indicated that the organometallic complex formed in the impregnated thin IL layer, possessed drastically reduced mobility and this resulted in some unusual behavior in the supported complexes.[94] Similarly, the immobilisation of copper bis(oxazoline) complexes in $[C_4mim][PF_6]$ on silicate Laponite support imposed several rotational restrictions on the catalyst, resulting in the reversal in the enantioselectivity for a cyclopropanation reaction as compared to their homogenous analogues.[95]

One of the major issues associated with the immersion method based SILP system is the leaching from SILP materials. In order to overcome this issue, the covalent anchoring method (Figure **1.11B**) was introduced. Hence, modifications on the surface of the support are carried out either *via* a covalent attachment of a particular functionalised IL fragment or through a sol-gel synthetic protocol.[96] Finally, the catalyst can then be immobilised following the wet impregnation method either with or without the use of additional IL. For instance, the surface of the silica can be modified through covalent attachment followed by immobilisation using the catalyst in IL.[97] Such modified materials, using organocatalysts have been widely use in aldol catalysis. These materials have delivered a very high catalytic activity and enantioselectivity as compared to their homogeneous analogues. Another major beneficial aspect of these materials is that they can be easily isolated and can be recyclable with a slight drop in the catalytic efficiency. In the same way, a comparable outcome was seen when salen complexes of Mn(III) were immobilised on an imidazolium-functionalised silica support along with a better enantioselective performance.[98] An IL monolayer functionalisation method has also been used with other support materials, for instance carbon nanotubes (CNTs) (Figure **1.12**) have been used for this purpose, as they display better mechanical strength, better chemical stability and have large surface to volume ratio. In addition, CNTs surface

functionalisation with [C$_4$mim][PF$_6$] allows high loadings of IL, up to 55 wt% with no detectable leaching issue.[99] Immobilisation of Rh complexes provided a material which was shown to be highly active for the hydrogenation of 1-hexene. These SILP materials displayed outstanding hydrogenation performance as compared to their oxide-based counterparts and also retained the Rh/IL phase completely upon recycling.[85,99]
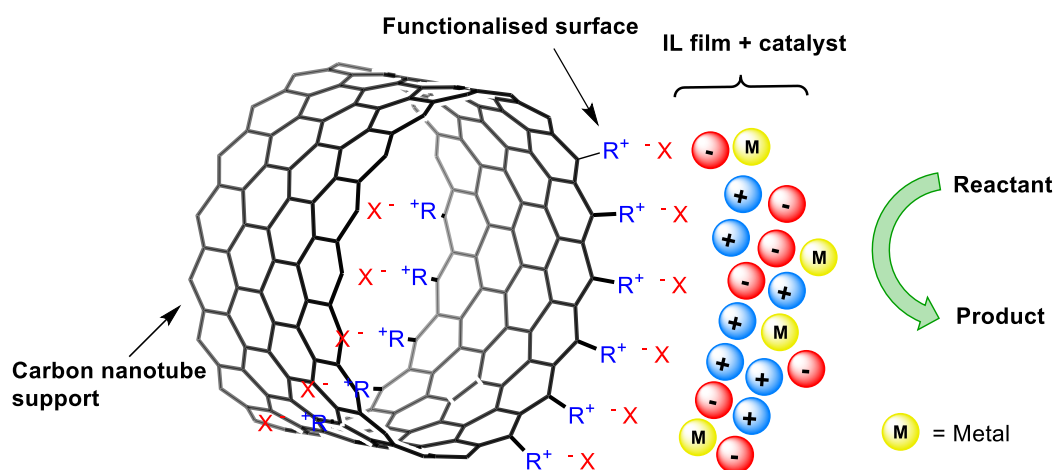
Figure 1.12: Surface functionalisation of CNTs with imidazolium based ionic groups.[99]

The covalent anchoring of SILP support materials is not restricted to the tethering of IL but also the ligand or the catalyst can be covalently anchored to the IL (Figure **1.11C**). For instance, a silica surface was functionalised with methylimidazolium IL fragments by Dieter et al., which form *N*-heterocyclic carbenes on adding Pd(OAc)$_2$. The materials obtained in this manner were highly active in catalysing the Heck reaction of a wide variety of haloarenes with olefins.[100]

Finally, SILP materials (Figure **1.11D**) can also be prepared by using a very thin layer of IL coating over a preformed heterogeneous catalyst in an analogous manner as the immersion method, this method is commonly termed as solid catalyst with ionic liquid layer (SCILL).[92,101] The materials prepared in this way avoid leaching of the active species from the material surface. For instance, a thin layer of hydrophobic IL added over a covalently immobilised Sc-catalyst on silica support provided a marked difference in the catalytic activity in the aqueous phase Mukaiyama-aldol reaction.[102] The utilisation of preformed heterogeneous catalysts is very attractive, since it prevents complex functionalisation during immobilisation. Jess and co-workers described the utilisation of an imidazolium-based IL on a commercially accessible Ni catalyst in this context.[103]

Supported ionic liquids have recently attracted attention for the use with oxidised metal complexes. It was demonstrated that using $CuCl_2$ as a modifier of supported ionic-liquid-phase Au(III) catalysts stabilised the Au(III) catalysts against reduction to metallic Au(0). The reduced Au(0) can also be re-oxidised to Au(III) species using $CuCl_2$. When the Au-Cu-IL/ on activated carbon (AC) catalysts were evaluated for production of vinyl chloride (VCM) during acetylene hydrochlorination, they displayed a high turnover frequency (TOF) of $168.5\ h^{-1}$ that is 1.8 times greater than that of the non-promoted catalyst and high selectivity i.e. 99.8%. Beside this, they also showed stable catalytic performance under industrial reaction conditions for acetylene hydrochlorination with negligible loss of acetylene (C_2H_2) after 500 hrs. It was proposed from XRD, BET, TEM, ICP-MS, XPS, and TGA analyses that the greater catalytic performance is because of electronic interaction and inhibition of cationic gold (Au) species by adding Cu^{2+} to reoxidise the reduced metallic Au(0).[104]

Ru-based supported ionic liquid phase (SILP) systems effectively catalyse the low-temperature water-gas shift reaction (WGSR). Previously, it was suggested that Ru-carbonyl species played a significant role in the mechanism although a detailed knowledge regarding active catalytic species is lacking. Ru-carbonyl complexes were identified using *in situ* diffuse reflectance infrared Fourier transform spectroscopy (DRIFTS) and density functional theory (DFT). It was shown by using catalyst $[Ru(CO)_3Cl_2]_2/[C_4C_1C_1Im]Cl/Al_2O_3$ that dimer splitting is induced by Cl^-. Consequently, equilibrium was established among many $[Ru(CO)_xCl_y]_n$ in which the ionic liquid served as an effectively infinite Cl^- reservoir. It was found that the major species in the system synthesised from $[Ru(CO)_3Cl_2]_2$ is indeed $[Ru(CO)_3Cl_3]^-$. Smaller quantities of chloride-rich species $[Ru(CO)Cl_4]_2^-$ or $[Ru(CO)_2Cl_4]_2^-$ and $[Ru(CO)_2Cl_3]^-$ were also found in the SILP. Carbonylation of $RuCl_3/[C_4C_1C_1Im]Cl/Al_2O_3$ using another robust WGSR catalyst led to similar Ru-carbonyl species. These results confirmed the presence of the proposed equilibrium.[105]

It was investigated during recovery of scandium from its ore bauxite residue (red mud) that scandium can be adsorbed in acidic solutions using a supported ionic liquid phase (SILP). For this purpose, SILP betainium sulfonyl (trifluoromethanesulfonylimide) poly(styrene-co-divinylbenzene) [Hbet–STFSI–PS–DVB] was synthesised by covalent linking from IL to the resin. It was confirmed from batch experiments during recovery of the Sc(III) which was adsorbed on SILP in 1 M sulfuric acid solution that the SILP was stable and can be reused without effecting its efficiency; repeating adsorption/desorption cycles seven times. In addition, the ionic liquid was

immiscible with the aqueous phase. Thus, SILPs could be designed for the recovery of Sc(III) as adsorbents from bauxite residue.[106]

Several difficulties arise from the support materials in the SILP methodology, which in turn have an effect on the reaction outcome. The complex nature of interactions due to the support material and the catalyst and IL hampers complete understanding of the mechanism and kinetics of a particular reaction. Confinement of catalyst particles in a narrow IL layer prevents limitations due to mass transport, nonetheless, this imposes undesired geometric restrictions on the organometallic complexes. Further limitations are associated with the chemical stability of the support material under severe conditions of a particular reaction. For instance, silica-based support materials display a prominent decline in the catalytic efficiency of Rh-catalysed hydroformylation reaction of propene due to an irreversible side reaction occurring between the catalyst, the ligand and the acidic silanol groups on the surface of the silica.[107]

These difficulties limit the application of SILP materials on large scale and prevent generalisation regarding SILP catalysis. Therefore, every catalytic process requires a detailed mechanistic insight including an in-depth investigation and understanding about the reaction kinetics. In this context, current work is focused on improving the systems, basic understanding of the support, and development of novel support materials.[108]

1.5   Polymer Immobilised Ionic Liquid (PIIL) Phase Catalysis

A new class of polymers which consists of a polymer backbone attached to an IL-like group is poly (ionic liquid)s (PILs). Materials based on PILs allow easy tuning of the properties of IL-like groups attached to the polymers.[109] One of the major beneficial aspect of PILs over SILP based analogues is that the PILs show flexibility and swelling characteristics in solution which contrasts to the conventional heterogeneous versions obtained from inorganic materials. The swelling property of the polymer support may enhance access of the reactants to the catalytically active sites, which in in case of rigid SILP-based systems was not possible.[110] Moreover, the component-based assembly of PILs permits a wide range of ILs to be tagged to monomers and the inclusion of various other neutral task specific monomers which in turn provides the opportunity to regulate the ionic micro-environment and optimisation of the physical properties of the polymer, for instance the flexibility, integrity and porosity *via* the degree of crosslinking, the thermal stability and the compatibility with a variety of solvents. Such advantages have permitted their use in a variety of scientific fields

such as biotecchology,[111] applications in fuel cell technology,[112] energy based materials,[113] and in the field of drug delivery.[114] Polymer Immobilised Ionic Liquid (PIIL) Phase materials can be used in place of Supported Ionic Liquid Phase (SILP) to aid catalyst recovery and reuse. The covalent attachment of the IL-like component of a PIIL prevents leaching into the surrounding conventional solvent and one major advantage is it is possible to design a cross-linked polymer network that encapsulates the active species. Figure **1.13** shows a visual representation of the concept of Polymer Immobilised Ionic Liquid (PIIL) Phase.
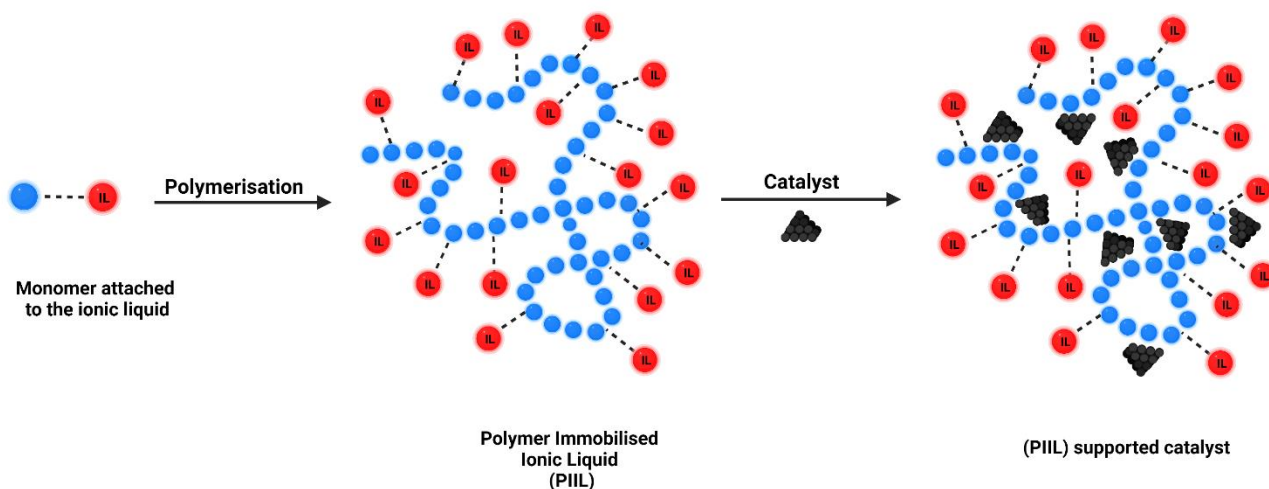
Figure 1.13: Polymer Immobilised Ionic Liquid (PIIL) Phase Concept

Materials based on PIIL are now well recognised in catalysis, and the incorporation of metal nanoparticles into polymer matrices is a simple process.[115,116] Several methods for preparing polymeric materials based on PIIL are present in the literature, however, the most general method is through NPs stabilisation *via* rational design of IL-like monomers. These monomers are then combined with a neutral comonomers *via* polymerisation.[109,116] It is also possible to assemble the PIIL through post polymerisation, for example by modifying imidazole functionalised polymers, but this process is unlikely to be quantitative and suffers issues related to the uniformity of the resulting polymer, and the purification and isolation of the product. The direct synthesis of styrenic imidazolium IL monomers delivers an easy method for preparing IL-based polystyrene. The PIIL produced in this way are then impregnated with an appropriate precursor of a specific metal before reduction with sodium borohydride or other reducing agents to obtain the respective metal NPs. The NPs obtained *via* this method can be electrosterically protected by the PIIL, which overcomes

the problem of aggregation *via* weak interactions among the IL and the NP surface including steric protection from the polymer backbone. The nature of various interactions present at the interface of the polymer and catalyst can be easily controllable through polymer composition tuning, which in turn has proved to be very useful in improving the rates and selectivity for different reactions.[117]

The Knight/Doherty research group has extensively investigated the development of PIIL phase catalysis to address the difficulties associated with ILs in homogenous/biphasic catalysis. As discussed above, the modular preparation of PIIL permits incorporation of IL-like monomers and task specific monomers into the polymer backbone easily and fine tuning of the material properties, catalytic activity and selectivity in a rational and systematic way.

For instance, the peroxometalate-based PIIL system [PO$_4${WO(O$_2$)$_2$}$_4$]@PIIL **1.1** (Scheme **1.2**) developed by the Knight and Doherty group was prepared through a Ring-Opening Metathesis Polymerisation (ROMP) strategy between *cis*-cyclooctene and a pyrrolidinium-functionalised norbornene, using the first-generation Grubbs catalyst. This catalyst efficiently and selectively catalyses the epoxidation of allylic alcohols and oxidation of sulphides mediated by hydrogen peroxide and could easily be recycled.[118]

1.1
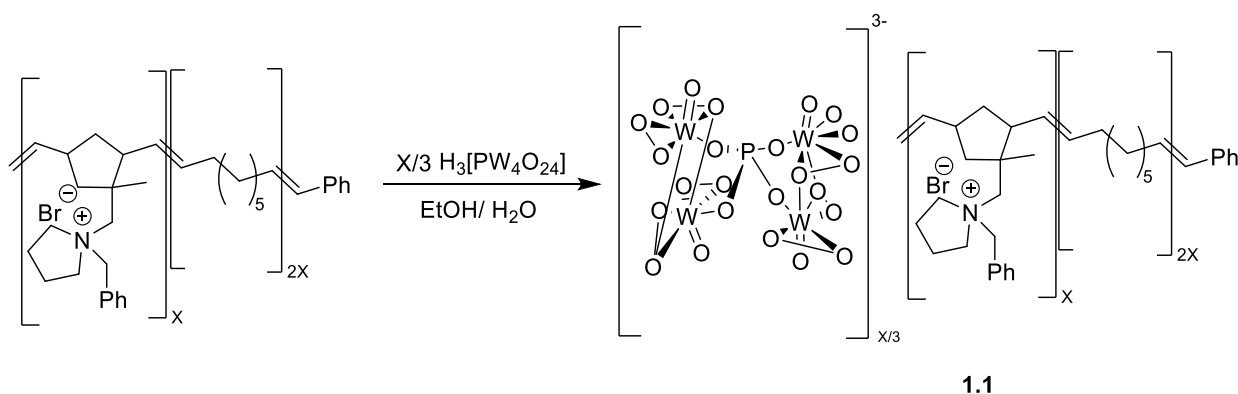
Scheme 1.2: Peroxometallate PIIL catalyst for epoxidation of allylic alcohols and oxidation of sulphides.

An efficient Suzuki-Miyaura cross-coupling between phenyl boronic acid and aryl bromides was developed in aqueous media under mild conditions using ionic liquids immobilised on polystyrene-based, heteroatom donor-modified polymers (PdNP@HAD-PIIL; HAD = PPh$_2$ **1.5**, NH$_2$ **1.6**, CH$_2$CN **1.7**, OMe **1.8**, *N*-pyrrolidone **1.9**) which can stabilise palladium nanoparticles (Figure **1.14**).
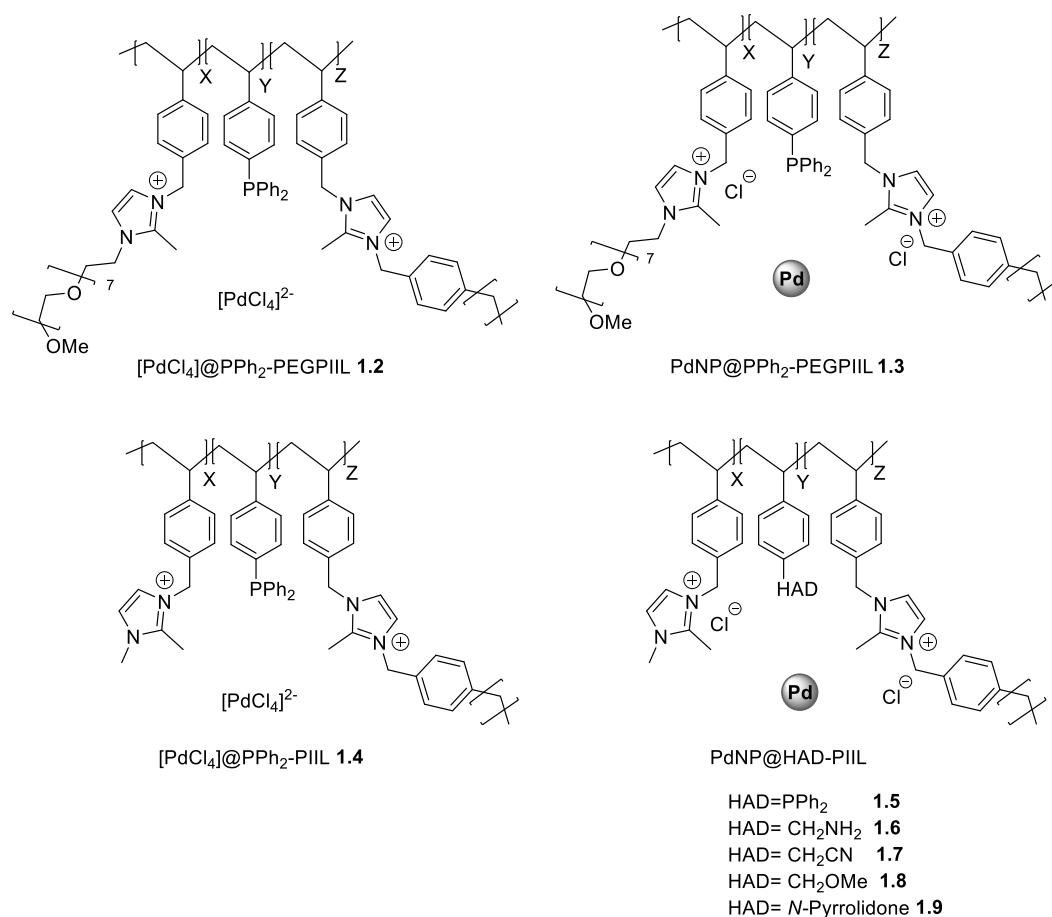
Figure 1.14: Composition of polymer immobilised ionic liquids PdNP@R-PIIL.

This catalyst system was more efficient for a variety of substrates than the other examined heteroatom donor-modified systems. The catalytic activity was further improved when polyethylene glycol (PEG) was incorporated into the phosphine modified immobilised ionic liquid support which was proposed to be due to improved access and dispersibility to the active site. Catalyst generated *in situ* from either [PdCl₄]@PPh₂-PIIL **1.4** or its PEGylated counterpart [PdCl₄]@PPh₂-PEGPIIL **1.2**, by reduction with phenylboronic acid, outperformed their pre-formed Pd(0) counterparts for several substrates. The turnover frequency i.e. 16,300 h^{-1} is one of the highest for Suzuki-Miyaura cross-couplings catalysed by palladium nanoparticles **(Scheme 1.3)**.[82]
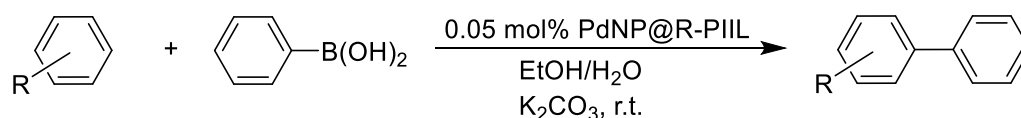
Scheme 1.3: PdNP@R-PIIL catalysed Suzuki-Miyaura cross-coupling between phenyl boronic acid and aryl bromides.

The research group has also prepared mildly cross-linked phosphine functionalised PIIL to stabilise palladium nanoparticles. A comparison between PEGylated (PEGPIIL) **1.3** and non-PEGylated analogues (PIIL) **1.5** indicated that the PEGylated counterparts (PEGPIIL) **1.3** are highly effective catalysts for aqueous phase hydrogenation. A wide range of nitro-aromatic and -heteroaromatic compounds were reduced with sodium borohydride using PIIL supported palladium under mild conditions with low catalyst loading. The extensive cross-linking of tris(4 vinylphenyl) phosphine on PEGylated (PSty$_3$-PEGPIIL) **1.10** and non-PEGylated analogues (PSty$_3$-PIIL) **1.11** were explored as a way to isolate the phosphine-based heteroatom and limit the number of phosphines bound to the surface of the Pd. In fact, no significant influence on catalyst performance was evident as a result of this modification. PdNPs immobilised on lightly cross-linked phosphine-decorated PEGylated polymer **1.3** was shown to be a highly active catalyst for aqueous phase reduction of nitroarenes using H$_2$ as reducing agent with a TON of 36,000 and even higher performance (TON of 274,000, TOF = 17,125 h^{-1}) for the transfer hydrogenation using NaBH$_4$ as reducing agent, the highest reported value for this process at room temperature. A continuous flow nitrobenzene reduction in a packed bed reactor operated over a 250 min time period with no sign of catalyst deactivation.[119] Figure **1.15** shows the composition of polymer imobilised ionic liquid supports palladium nanoparticles.
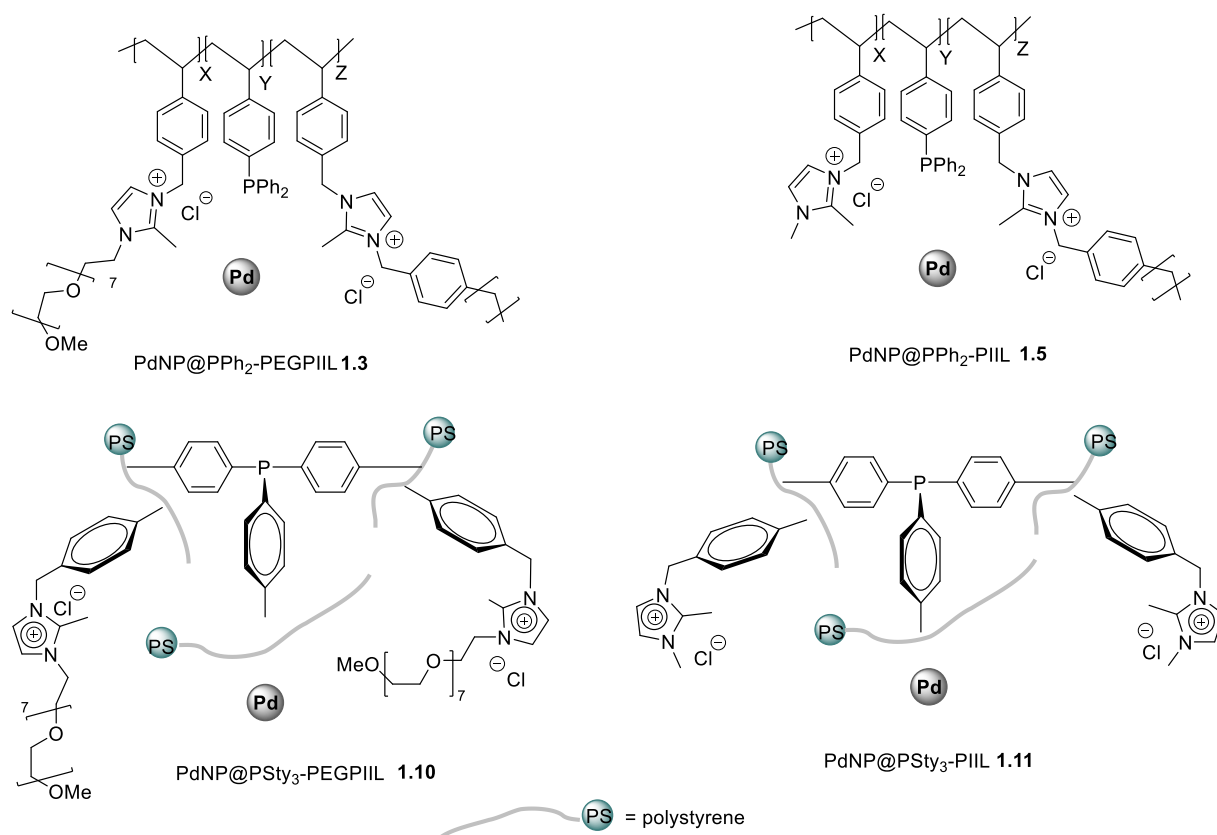
Figure 1.15: Composition of polymer immobilised ionic liquid supports palladium nanoparticles.

A tandem Suzuki-Miyaura cross coupling-nitroarene reduction sequence was also catalysed by the same system. That allows a high yield of biaryl amine **1.12** in an operationally straight forward single-pot procedure from an arylboronic acid and a nitro-substituted aryl or heteroaryl halide and offers a simple route for the synthesis of a diverse range of amines.[119]
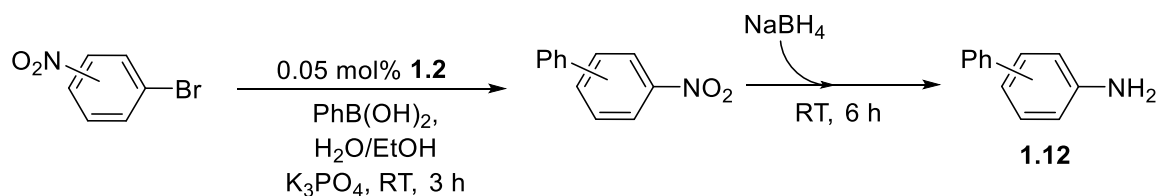
Scheme 1.4: Tandem Suzuki-Miyaura cross coupling hydrogenation for biarylamines synthesis.

Most recently, the research group have published PdNP@PPh$_2$-PEGPIIL **1.3** and PdNP@PPh$_2$-PIIL **1.5** stabilised by phosphine-decorated polymer immobilised ionic liquid and have shown these to be active and exceptionally selective catalysts for the aqueous phase hydrogenation of α,β -unsaturated aldehydes, ketones, esters and nitriles. Full conversion and 100% selectivity for the

reduction of the double bond (C=C) were achieved with PdNP@PPh$_2$-PEGPIIL **1.3** under mild conditions. This is the most selective PdNP-based system reported for the aqueous phase hydrogenation of this class of substrate.[120]

The group also recently published the use of phosphine-decorated polymer immobilised ionic liquids for the stabilisation of gold nanoparticles (AuNP@R-PIIL **1.13**). The resulting catalytic system is extremely effective and selective for the NaBH$_4$-mediated reduction of nitroarenes (Figure **1.16**). This catalytic system under milder reaction conditions and with a very low catalyst loading reduces nitrobenzene (**NO2**) into three distinct products; *N*-phenylhydroxylamine (**NOH**), azoxybenzene (**N2O**), and aniline (**NH2**). The partial and complete reduction of nitroarenes to obtain three distinct products by using a single nanoparticle-based catalytic system with an excellent selectivity is notable. Under optimised conditions using water as the solvent under inert atmosphere provides the thermodynamically less favoured *N*-phenylhydroxylamine (**NOH**) in almost quantitative yields, however, changing the solvent system from water to ethanol under similar reaction conditions in open air provides azoxybenzene (**N2O**) as the sole product. The high selectivity for *N*-phenylhydroxylamine (**NOH**) is associated with the use of a nitrogen atmosphere under which the reaction follows the direct reduction pathway, which is essentially irreversible, whereas the change in selectivity under air atmosphere is due to a competing condensation reaction pathway which allows reversible formation of *N*-phenylhydroxylamine (**NOH**) along with significant quantities of the azoxy-based product (**N2O**). Finally, under slightly different reaction conditions by careful adjustment of time and temperature aniline (**NH2**) is afforded selectively in almost quantitative yields. A dramatic enhancement in the catalytic efficiency of the catalyst was observed when PEG was introduced onto the polyionic liquid layer. For instance, *N*-phenylhydroxylamine (**NOH**) was obtained with a TOF of 73,000 h^{-1}, a TON of 100,000 and with a selectivity of >99%. Similarly, azoxybenzene (**N2O**) was obtained with a TOF of 37,000 h^{-1}, a TON of 55,000 and with a 100% selectivity, and finally the completely reduced product aniline (**NH2**) was obtained with a TOF of 62,500 h^{-1}, a TON of 500,000, and with a 100% selectivity. The key factors responsible for the better catalytic activity and selectivity are very difficult to identify precisely, however, the ionic liquid and phosphine combination is considered important to achieve a high activity and selectivity. Interfacial electronic effects, which directly affect the adsorption and thus selectivity and the channeling of the substrate by creating an electrostatic potential around the AuNPs are thought to be major factors for the higher catalytic activity.

Nevertheless, this is the only report of AuNP-based catalytic system for the selective reduction of nitroarenes, which also provides the foundation for the discovery and development of continuous flow processes for easy scale-up.[83]
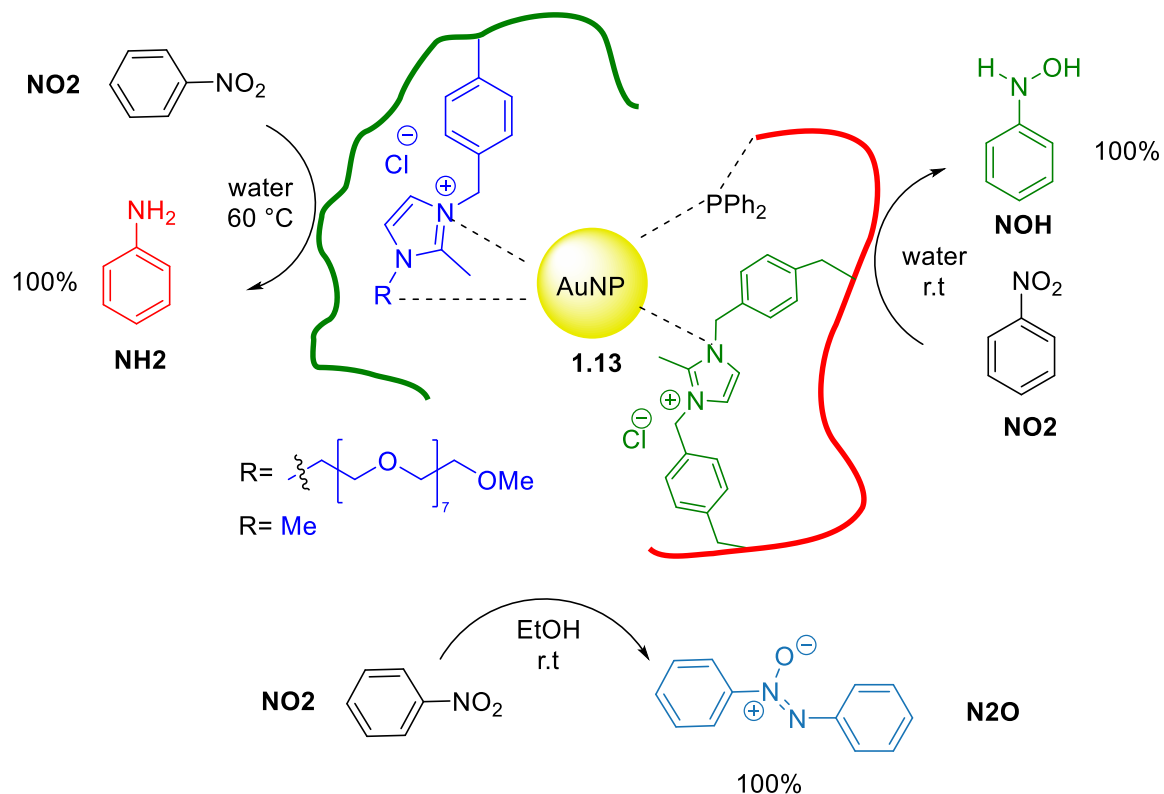
Figure 1.16: PIIL stabilised AuNPs

A variety of PIILs with differing structural architectures are possible, regardless of the same number of IL monomer units, for instance, linear shaped, hyper-branched shaped or star shaped polymers. Moreover, PIIL block copolymers are also accessible through covalent post modification between suitable block copolymers and the IL-like modification. PIIL have the capability of developing stabilising interactions with metal nanoparticles resulting in modification to the activity and selectivity of derived catalysts and this project aims to expand on our work in this area. The use of PIILs is not limited to academia but also has potential for applications in industries related to energy because of the tunable physicochemical properties of the PIIL.

1.6 Method of Polymerisation

The polymerisation method should allow a high degree of functionalisation so that the properties of the surface, the micro-structure, and the ionic micro-environment, the stability and the porosity can be altered in a controlled way, ideally using a straightforward synthetic protocol. As a result, the interactions at the catalyst surface, the easy accessibility to the substrate and efficiency can be optimised, which in turn enables an accurate property-function relationship and activity-selectivity relationship to be established.

1.6.1 Radical Polymerisation

Among the polymerisation techniques, the radical polymerisation method is the most versatile and commonly used method. The polymers obtained through radical polymerisation typically have high molecular weights, and are easily and cost effectively produced by using a wide range of different monomers. The mechanism of radical polymerisation is believed to proceed through successive addition of two or more unsaturated monomers to a terminal radical, generally known as the active center. The active center then in turn attacks the π-bond of a monomer which undergoes homolytic bond cleavage. The main condition of such processes is to create an air or oxygen free system before the activation in order to avoid inhibition of polymerisation by oxygen. In labs, such systems can usually be obtained by repeated freeze, pump and thaw processes.[121,122]

Initiation
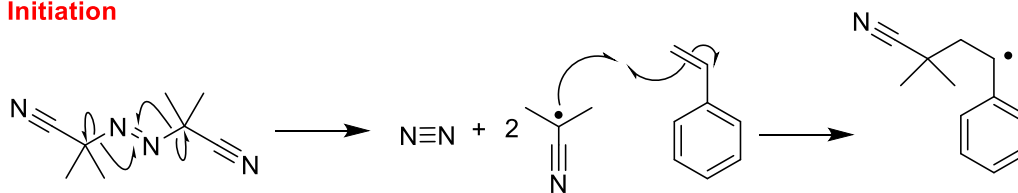
Azobisisobutyronitrile (AIBN)

Propagation
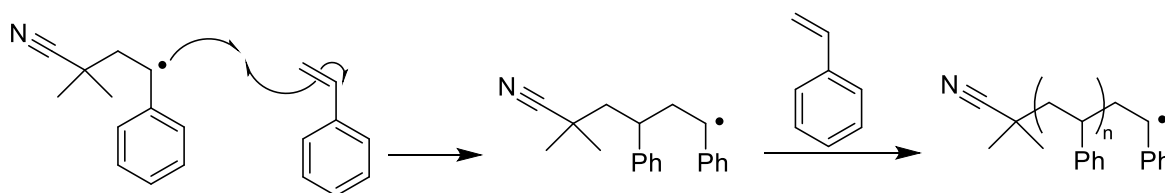
Scheme 1.5: Initiation and propagation steps of radical polymerisation of styrene initiated by AIBN.

Free radicals can form *via* a homolytic bond fission or *via* a single electron transfer pathway. In the homolytic pathway, the two bonding electrons of a bond are each transferred to the associated atoms forming two free radical species as a result, while the single-electron transfer pathway involves transfer of a single electron to or from an ion or molecule.[121,122] Scheme **1.5** shows an azobisisobutyronitrile (AIBN) initiated radical polymerisation pathway during which homolysis through a thermolytic bond cleavage at low temperature occurs to form N_2 which is the thermodynamic driving force of the initiation reaction. In addition, benzoyl peroxide, and *tert*-butyl hydroperoxide can also be used as thermal initiators. Photolytic bond cleavage using UV radiation can also be used for homolysis, for instance, benzophenone can be used as an appropriate photolytic initiator. The photolytic pathway of homolysis has the beneficial aspect of producing or ceasing the free radicals efficiently, since the UV source can be easily turned on and off.

Finally, the radical polymerisation can be terminated *via* an irreversible bimolecular reaction of two propagating chains to form one single polymer. The other termination pathway proceeds *via* a disproportionation during which a hydrogen atom is abstracted from the penultimate carbon of one chain by an active center, as a result two deactivated polymer molecules are formed. Among the two polymers formed one contains a saturated terminus while the other contains an unsaturated terminus (Scheme **1.6**).

a) **Homolytic termination pathway**
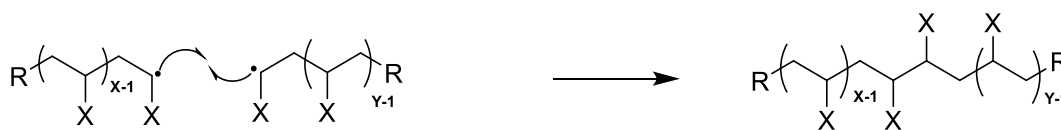
b) **Disproportionation termination pathway**
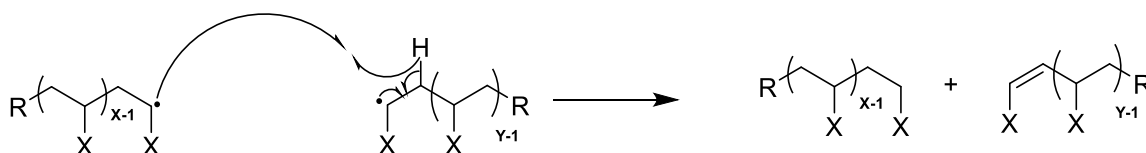
Scheme 1.6: Mechanisms of combination and disproportionation termination.

One of the major disadvantages of radical polymerisation is the uncontrolled nature of free radical formation which results in the formation of various poorly and unevenly distributed molecular weight polymer mixtures. In the same way, this issue also prevents controlled formation of block co-polymers.[121,122]

1.7 Polymer and NPs Characterisation

A variety of methods will be used to characterise the polymer and nanoparticles materials synthesised in this project:

- **X-ray Photoelectron Spectroscopy (XPS)** is a quantitative technique used for analysis of the material surface, in particular allowing measurement of the elemental composition and the electronic state of the atoms on the material surface. XPS uses a focused beam of X-rays that cause the excitation, and emission of photoelectrons from the top 1-10 nm of the sample surface being studied. The energy of the photoelectron emission is measured by an electron energy analyser. The identity of the elements present, their chemical states, and quantity can be determined from the measured binding energy and photoelectron peak intensity. Spectral analysis, peak fitting and deconvolution are carried out using CasaXPS software.

- **Inductively Coupled Plasma Optical Emission Spectrometry (ICP-OES)** is an analytic technique which is used for the quantitative detection of elements. The atoms and ions are

excited by means of an inductively coupled plasma. Elements are identified by the characteristic wavelengths of the electromagnetic radiation emitted from exited atoms and ions. The elemental concentration inside the sample is indicated by the emission intensity.

- **Transmission Electron Microscopy** (**TEM**) is a microscopy technique in which an electron beam is used to produce an image by transmission through a sample or specimen. The specimen can be a suspension or ultra-thin sample section with thickness less than 100 nm. When the beam of electrons is passed through the specimen the electrons interact with the sample ultimately producing an image. An imaging device, for example photographic film layer and fluorescent screen, or sensors, such as a charge coupled device, are used for magnifying and focusing the specimen image.

- **ThermoGravimetric Analysis** (**TGA**) is a thermal analysis in which the sample's mass is measured with change of temperature over time. This method can provide details about physical changes, including desorption, absorption and phase transitions; and chemical facts, including solid-gas reactions i.e., oxidation or reduction reactions, thermal decomposition, and chemisorptions.

- **Scanning Electron Microscopy (SEM)** produces an image of a sample by detecting secondary electrons which are emitted from the surface of material as it is scanned with a focused beam of electrons. The technique is most often used to provide information about the morphology of the sample.

- **Energy Dispersive X-Ray Spectroscopy (EDX)** is an analytical method used to identify, characterise, and quantify the elemental compositions of a sample. EDX is based on the emission of specific X-rays from the sample. A focused beam of high-energy charged particles such as electrons or protons is directed into the sample being studied. This beam interacts with the atom, ejecting an electron from its shell and creating a void in its place. Another electron from higher binding energy falls into the void and an X-ray with the energy of the difference of the electron level binding energies is released. EDX analysis provides a spectrum that shows the peaks associated with the elemental composition of the studied sample.

- **Dynamic Light Scattering (DLS)** is an analysis method used to measure the hydrodynamic diameter of nanoparticles which have been dispersed in a liquid. A laser beam is focused on a cuvette containing the sample. The differences in scattered light are detected over time at a specific scattering angle and this signal used to determine the mean particle size.

1.8   Project Aims

The main objective of this project was to extend the Polymer Immobilised Ionic Liquid (PIIL) concept previously developed by the Knight/Doherty research group and primarily focus on the styrene-based heteroatom donor modified PIIL based systems for the stabilisation of metal nanoparticles. The significance of this project lies in the systematic modification of the PIIL support by introducing additional functionalities to design the catalyst rationally. These modifications affect the catalyst-support interactions and are crucial to probing the factors responsible for improving the catalyst lifetime, selectivity profile, and recyclability. Additionally, to control the morphological growth, the activity of the nanoparticles and the ionic micro-environment can be tuned by modulating the charge density. Therefore, an in-depth investigation to identify the optimum property performance profiles of the polymer immobilised ionic liquid (PIIL) supported nanoparticle catalysts is of much significance. In order to investigate these things, we chose to study the selective reduction of nitroarenes, quinoline hydrogenation and hydrolytic hydrogen evolution from sodium borohydride.

Chapter 2. Iridium-Catalysed C-H borylation of diethyl phenylphosphonate

This chapter describes the completion of a study of iridium-catalysed aromatic C-H borylation under homogeneous conditions, the initial work for which was undertaken by previous member of the group, but which does not involve PIIL. This work was used to gain experience in catalysis and in order to complete the study for publication.

2.1   Introduction

Arylphosphonates are a versatile class of organic compounds whose structure is found in some natural products and agrochemicals.[123–126] They serve as precursors for several classes of organic compounds such as phosphonic acids and phosphines which in turn play a significant role in the field of organometallic synthesis and catalysis.[127–133] For these reasons, a substantial amount of research has been dedicated to this field. Numerous approaches for the synthesis of C-P bonds are found in the literature. Among them, the transition metals-based synthesis of C-P bonds has been extensively studied. For instance, arylphosphonates have been prepared by using Ni, Cu and Pd-catalysed reaction of aromatic halides or pseudo-halides with a dialkyl phosphonate.[134–145] Similarly, in the presence of Ni, Cu, and Pd-catalysts oxidative cross-coupling reaction of aromatic boronic acids or silanes with dialkyl phosphonates,[146–151] decarbonylative C-P bond formation in the presence of a Ni-catalyst,[152–154] coupling of diaryliodonium salts and a dialkyl phosphonate in the presence of Cu,[155] and phosphorylation of aromatic C-H bonds by using Pd-catalysts[156–162] have been explored for the synthesis of arylphosphonates. Moreover, a late-stage modification by utilising transition-metal-catalysed C-H arylation methodology in which the phosphonate serves as a directing group,[163–171] and Suzuki-Miyaura cross-coupling of halogenated aryl phosphonates are also among some of the effective approaches for the synthetic elaboration of arylphosphonates,[172–180] allowing the synthesis of biaryl phosphonates which are potential precursors to chiral biarylphosphines. In addition, some reports of P–H dehydrative cross-coupling,[181] transition metal-free photo-induced cross-coupling of heteroaryl and aryl halides with H-phosphonates,[182,183] and direct P-arylation of arynes which was accomplished through a Michaelis-Arbuzov-type reaction,[184] are also available in the literature. One of the major drawbacks of all the methodologies

described above is that these methods require a pre-functionalised substrate, hence limiting the scope and access to a variety of substrate combinations.

For the synthesis of substituted biaryl and heterobiaryl phosphonates, the Knight and Doherty group developed a new strategy by coupling *ortho*-phosphonate functionalised aryl- and naphthylboronate esters as the nucleophilic partners (Figure **2.1a**).[185] Previous literature protocols had introduced the *o*-phosphonate group as an electrophile in multiple steps. A general and efficient protocol for the synthesis of *o*-boryl arylphosphonates has been recently reported by Clark and Watson *via* a regioselective C-H borylation strategy and by utilising the phosphonate group as the directing group (Figure **2.1b**).[186] Advantages of this method include tolerance towards various functional groups, readily accessible, commercially available starting materials and catalysts, and good levels of regioselectivity. Furthermore, the boronic esters so obtained can be converted into a variety of further functionalised organic compounds. Previously, phosphines have been widely explored as directing groups for the *o*-selective C-H borylation, however, the limitations of substrate scope restrict the use of phosphines. The use of arylphosphonate-directed *o*-selective C-H borylations, extends the substrate scope.[170,187–190]

We were interested in studying the C-H borylation of aryl phosphonates as a route to new cross-coupling partners to synthesise biaryl-based structural motifs. By using this method, phosphonate-substituted arylboronic esters will be prepared without the need of pre-functionalisation of the aryl phosphonate (Figure **2.1c**). Aryl borylation has been achieved *via* an Ir-catalysed C-H borylation strategy in which the regioselectivity is primarily controlled by steric factors.[191–193] The regio-selective *meta*-selective C-H borylation of 1,3-disubstituted arenes is a well-established protocol for the preparation of 3,5-disubstituted arylboronic esters. A plethora of *meta*-substituted products such as phenols,[194] ethers, arylamines and arylamine boronate esters,[195,196] arylboronic acids, trifluoroborates and pentafluorosulfanyl-substituted aryltrifluoro-borates,[197,198] aryl nitriles and nitrated arenes,[199,200] alkylarenes and disubstituted bromoarenes,[201,202] difluoro- and trifluoromethylated arenes [203–205] and borylated aryl alkynes,[206] *etc.* have already been reported in the literature. Alternative strategies to achieve *meta*-selective C-H borylation have also been reported. For example, by a directed non-covalent secondary interaction between a modified bipyridine and the substrate by using Ir-catalyst has been recently reported.[207,208] Other strategies towards regioselective *meta*-borylation of aromatic substrates include: noncovalent ion-pair interaction between a cationic substrate and anionic liqand;[209] Lewis acid−Lewis base (LA−LB)

direct C–H borylation by using bifunctional catalysts,[210] or a mixture of electrostatic interactions between a ligand-substrate complex and B-N-based secondary interactions;[211] nevertheless, each strategy needs the preparation of a dedicated ligand backbone. Among them, the simple use of steric factors is very reliable for controlling the regioselectivity of C-H borylation, therefore, we have chosen the Ir-catalysed C-H borylation of 3-substituted aryl phosphonates as a route to phosphonate-substituted arylboronic esters (Figure **2.1c**).
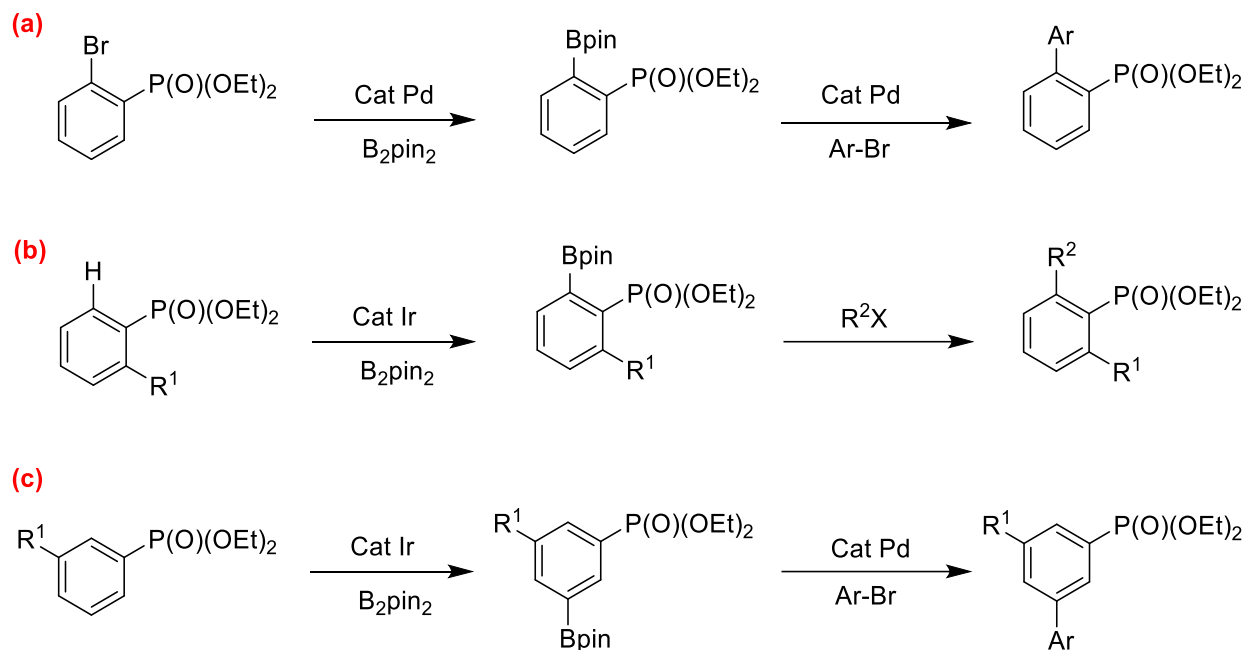
Figure 2.1: Preparation of phosphonate substituted arylboronic ester. (a) 2-bromo substituted aryl phosphonate borylation, (b) Ir-catalysed arylphosphonate-directed *ortho*-selective C-H borylations and (c) Ir-catalysed *meta*-aryl phosphonate C-H borylation.

A recent report of the aryl and acyl cross-coupling of amides by using an Ir-catalyst in a highly selective and divergent manner *via* a C-H borylation/N-C(O) activation strategy for the preparation of ketones and biaryl ketones[212] and Clark's strategy of aryl phosphonate-directed *ortho*-C-H borylation[186] motivated us to explore the borylation of aryl phosphonates.

2.2 Results and Discussion

Iridium-catalysed C-H borylation is a well-established protocol in organic synthesis,[213,214], therefore, the initial experiments were performed by following a literature procedure.[215] We investigated diethyl phenylphosphonate **2.1** as the benchmark substrate in order to determine the selectivity by optimising the procedure for simple analysis. The initial reaction was performed in hexane using 2.5 mol% of Ir-catalyst loadings at room temperature and monitoring the conversion and products through ^{31}P NMR spectroscopy since the substrate and the products display distinct and perfectly separated resonances as shown in Figure **2.2**.
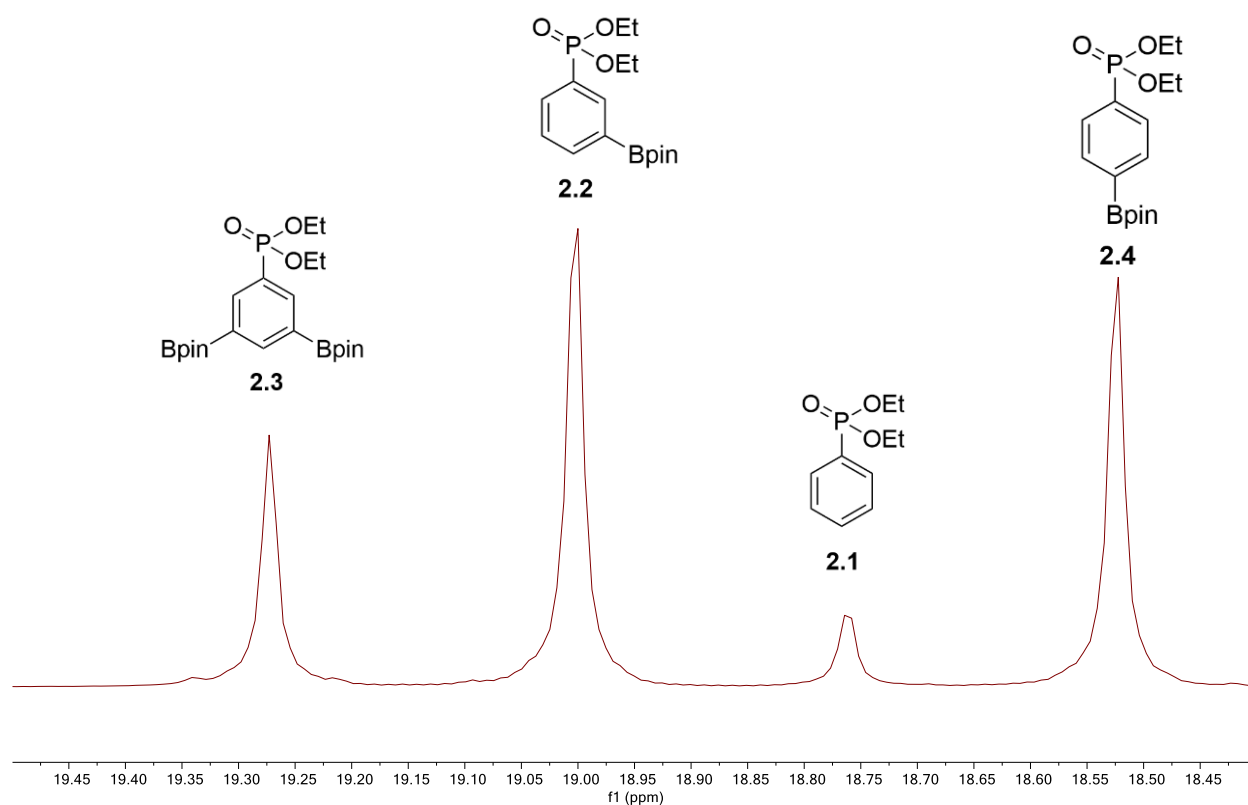
Figure 2.2: ^{31}P NMR (121 MHz, CDCl$_3$) spectrum of a reaction mixture after 1 hour at 50 °C in hexane indicating phenylphosphonate **2.1**, *m*-substituted **2.2**, 3,5-diboryl substituted product **2.3** and *p*-substituted **2.4**.

The active catalyst was generated *in situ* from the dimeric precursor (1,5-cyclooctadiene)(methoxy)iridium(I) in the presence of 3,4,7,8-tetramethyl-1,10-phenanthroline (tmphen) ligand (Table **2.1,** entry 1). This catalyst was used because it has been extensively explored for the non-directed Ir-catalysed C-H borylations of several alky, aryl, and heteroaryl C-

H bonds. It has been reported that this electron rich catalyst and the corresponding complexes obtained activate C-H bonds more effectively than corresponding electron poor counterparts.[216–219] The reaction after 24 hours at room temperature with 2.5 mol% of catalyst loading in hexane showed a conversion of 97%. The *m*-substituted and *p*-substituted arylphosphonates **2.2** and **2.4** were formed in approximately the same amount (40±5% and 35±5% by ^{31}P NMR), while 3,5-diboryl substituted product **2.3** (22%) was found to be the minor product (Table **2.1**, entry 1).

Interestingly under identical reaction conditions, except that the reaction temperature was increased to 50 °C, almost quantitative conversions were achieved only after 1 hour. However, the regioisomer product distribution was similar to the products achieved at room temperature (Table **2.1**, entry 2). Then, the effect of different solvents on the reaction was evaluated under the conditions of 2.5 mol% catalyst loadings at 50 °C for 1 hour. Excellent conversions were observed when the reaction was performed in hexane (94%) and methylcyclohexane (91%), while dioxane (88%) and tetrahydrofuran (70%) provided moderate conversions, and a very low conversion was observed when the reaction was performed in DMF (3%) (Table **2.1**, entries 2-6). Considering the best results were observed in hexane, this solvent was selected as the best choice for further experimental studies.

Catalyst loading experiments were then performed first by reducing the catalyst loading to 1.25 mol%, a corresponding lower conversion of only 71% was observed. However, the product distribution was not affected. On the contrary, when the catalyst loading was increased to 5 mol%, a conversion of 96% after 30 min was observed (Table **2.1**, entries 7 and 8).

Next, we evaluated the effected of the Ir-source, although [Ir(COD)(OMe)]$_2$ is well-known for C-H borylations, other efficient Ir-sources for C-H borylations are also reported in the literature, therefore, [Ir(COD)(acac)], [Ir(COD)Cl]$_2$ or [Ir(COD)$_2$]BF$_4$ in the presence of tmphen ligand were investigated. C-H borylation by using B$_2$pin$_2$ with diethyl phenylphosphonate **2.1** under the optimised reaction conditions of 1 hour at 50 °C in hexane provided 93% conversion when [Ir(COD)(acac)] was used as the catalyst precursor, a 77% conversion for [Ir(COD)$_2$] BF$_4$ and only 7% conversion was observed when [Ir(COD)Cl]$_2$ was used as the catalyst precursor. However, a conversion of 51% for [Ir(COD)Cl]$_2$ after 1 hour was observed when the reaction temperature was increased from 50 °C to 70 °C (Table **2.1**, entries 9-11). The product distribution for each catalytic system was nonetheless comparable to that observed for [Ir(COD)(OMe)]$_2$. Since the highest

conversions were obtained by employing [Ir(COD)(OMe)]$_2$ as the precursor, we used it to evaluate the effect of different ligands on the reaction. The use of 4,4'-di-*tert*-butyl-2,2'-bipyridine (dtbpy), 4,4'-dimethyl-2,2'-bipyridine (4,4'-Me$_2$bpy) or 4,4'-dimethoxy-2,2'-bipyridine [4,4'-(OMe)$_2$bpy] instead of tmphen under optimum conditions of 1 hour at 50 °C in hexane showed no significant difference on the conversion and yield of the desired products (Table **2.1,** entries 12-17).

The effect of the boron source was then investigated as the Ir-catalysed C-H borylation of phosphines had shown some dramatic enhancements on the overall outcome of the reaction when a different type of borylation agent was employed.[190] Therefore, HBpin was used instead of B$_2$Pin$_2$ under the optimum conditions. Reactions conducted in hexane and dioxane delivered 95% and 86%, respectively, with 2 eq. of HBpin. The product distribution for *m*-substituted **2.2,** 3,5-diboryl substituted product **2.3** and *p*-substituted **2.4** was similar to that observed when using B$_2$pin$_2$ (Table **2.1,** entries 18 and 19). When a 1:1 ratio of HBpin:substrate was used, the conversion dropped significantly (Table **2.1,** entry 20). However, complete conversion was observed when the ratio was increased to 3 or 5. Additionally, 3,5-diboryl substituted **2.3** was obtained as the main product when 5 eq. of HBpin was used (Table **2.1,** entries 21 and 22 cf. 20).

Furthermore, the sequence of addition also demonstrated significant effects on the reaction. When [Ir(COD)(OMe)]$_2$ and tmphen were added first and then HBpin, a slightly lower conversion was observed. However, when HBpin and catalyst were added first, and then the ligand, a significantly higher conversion was observed (Table **2.1,** entries 2 and 23). This observation is consistent with the literature.[215]

Table 2.1: Ir-catalysed C-H borylation of diethyl phenylphosphonate **2.1**.

Entry	Ir source	Ligand	Solvent	Boron source	%Conv[a]	%**2.2**[a]	%**2.3**[a]	%**2.4**[a]
1[b]	[Ir(COD)(OMe)]$_2$	tmphen	hexane	B$_2$pin$_2$	97	40	22	35
2	[Ir(COD)(OMe)]$_2$	tmphen	hexane	B$_2$pin$_2$	94	42	18	34
3	[Ir(COD)(OMe)]$_2$	tmphen	dioxane	B$_2$pin$_2$	88	40	18	30
4	[Ir(COD)(OMe)]$_2$	tmphen	Me-Cy	B$_2$pin$_2$	91	43	16	32
5	[Ir(COD)(OMe)]$_2$	tmphen	THF	B$_2$pin$_2$	70	29	20	21
6	[Ir(COD)(OMe)]$_2$	tmphen	DMF	B$_2$pin$_2$	3	3	0	0
7[c]	[Ir(COD)(OMe)]$_2$	tmphen	hexane	B$_2$pin$_2$	71	42	8	29
8[d]	[Ir(COD)(OMe)]$_2$	tmphen	hexane	B$_2$pin$_2$	96	36	26	34
9	[Ir(COD)(acac)]	tmphen	hexane	B$_2$pin$_2$	93	38	21	34
10	[Ir(COD)$_2$]BF$_4$	tmphen	hexane	B$_2$pin$_2$	77	39	14	24
11	[Ir(COD)Cl]$_2$	tmphen	hexane	B$_2$pin$_2$	7	4	1	2
12	[Ir(COD)(OMe)]$_2$	dtbpy	hexane	B$_2$pin$_2$	91	44	21	26
13	[Ir(COD)(OMe)]$_2$	4,4'-(OMe)$_2$-bpy	hexane	B$_2$pin$_2$	83	44	10	29
14	[Ir(COD)(OMe)]$_2$	4,4'-Me$_2$-bpy	hexane	B$_2$pin$_2$	93	39	25	29
15	[Ir(COD)(acac)]	dtbpy	hexane	B$_2$pin$_2$	91	43	21	27
16	[Ir(COD)(acac)]	4,4'-(OMe)$_2$-bpy	hexane	B$_2$pin$_2$	87	43	16	28
17	[Ir(COD)(acac)]	4,4'-Me$_2$-bpy	hexane	B$_2$pin$_2$	79	41	11	27
18	[Ir(COD)(OMe)]$_2$	tmphen	hexane	HBpin	95	40	23	32
19	[Ir(COD)(OMe)]$_2$	tmphen	dioxane	HBpin	86	36	21	29
20[e]	[Ir(COD)(OMe)]$_2$	tmphen	hexane	HBpin	54	33	2	19
21[f]	[Ir(COD)(OMe)]$_2$	tmphen	hexane	HBpin	100	33	30	37
22[g]	[Ir(COD)(OMe)]$_2$	tmphen	hexane	HBpin	100	38	27	35
23[h]	[Ir(COD)(OMe)]$_2$	tmphen	hexane	HBpin	67	34	10	23

Reaction conditions: 0.37 mmol of diethyl phenylphosphonate **2.1**, 0.28 mmol B$_2$pin$_2$ or 0.74 mmol HBpin, 1.25 or 2.5 or 5 mol% Ir-catalyst, 5 mol% ligand, 4 mL solvent, 1 or 24 hour, 50 or 70 °C.

a   Yields determined by ^{31}P NMR spectroscopy. Average of at least three runs. Error ±5%.

c   Reaction conducted with 1.25 mol% [Ir(COD)(OMe)]$_2$ and 2.5 mol% ligand under identical conditions.

d   Reaction conducted with 5 mol% [Ir(COD)(OMe)]$_2$ and 10 mol% ligand for 30 min under otherwise identical conditions.

e   Reaction run with 0.37 mmol HBpin.

f   Reaction run with 1.1 mmol HBpin

g   Reaction run with 1.85 mmol HBpin

h   0.74 mmol of HBpin added after the tmphen.

We also investigated the effect of reaction time at 50 °C in hexane by using B$_2$pin$_2$ and HBpin as borylation agents and the results obtained are shown in Figure **2.3a** and **2.3b** for B$_2$pin$_2$ and HBpin, respectively. The composition time profile experiments revealed that by using 2.5 mol% of [Ir(COD)(OMe)]$_2$ and 5 mol% tmphen, B$_2$pin$_2$ undergoes an induction period initially and then reacts with diethyl phenylphosphonate **2.1** with simultaneous formation of *m*-substituted **2.2** and *p*-substituted **2.4**, while 3,5-diboryl substituted **2.3** was observed to be formed after significantly longer reaction times (Figure **2.3a**). The composition time profile is in agreement with the previously reported non-regioselective C-H borylation because the ratio of (*m*-substituted **2.2** + 3,5-diboryl substituted **2.3**):(*p*-substituted **2.4**) is almost 2 throughout, reflecting the fact that there are two *meta*-hydrogen atoms and just one *para* in the substrate.[191] In contrast, the composition-time profile experiments with HBpin (Figure **2.3b**) revealed that diethyl phenylphosphonate **2.1** consumption was very fast and provided *m*-substituted **2.2** and *p*-substituted **2.4** as major products while 3,5-diboryl substituted **2.3** was provided in only small quantities. Nevertheless, the reaction with HBpin for longer reaction times (> 1 hour) showed a similar composition time profile as observed for B$_2$pin$_2$ (Figure **2.3a**). Moreover, no induction period was observed for HBpin (Figure **2.3b**). The induction time with B$_2$pin$_2$ is attributed to the necessity for reduction of 1,5-cyclooctadiene to form the corresponding active bipyridine-ligated iridium trisboryl complex catalyst.[220] It has been reported that elimination of this induction period observed for B$_2$pin$_2$ in the presence of [Ir(COD)Cl]$_2$/dtbpy, can be achieved by addition of a small amount of HBpin to the reaction mixture.[220] It has also been reported for Ir-catalysed C-H borylation that HBpin performs similarly to B$_2$Pin$_2$ when added prior to the ligand and the addition order for the Ir-catalysed C-H borylations has a significant influence on the performance of the catalyst.[215]
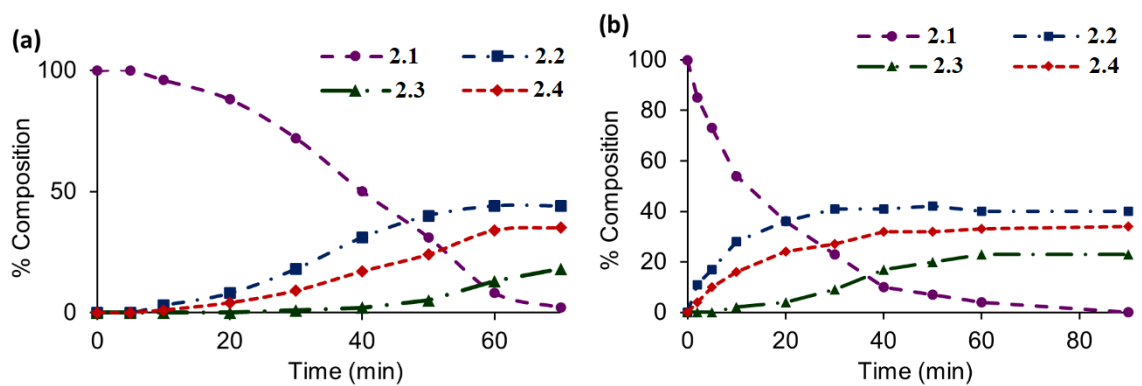
Figure 2.3: Composition time profile of Ir-catalysed borylation of diethyl phenylphosphonate **2.1** in hexane at 50 °C using 2.5 mol% [Ir(COD)OMe)]$_2$, 5 mol% tmphen, (a) 2 mole eq. of B$_2$(pin)$_2$ and (b) 2 mole eq. of HBpin.

2.3   Conclusion

The C-H borylation of diethyl phenylphosphonate **2.1** with B$_2$pin$_2$ and HBpin by using catalytic of Ir-catalyst generated *in situ* from the catalyst precursors [Ir(COD)(acac)]/tmphen or [Ir(COD)(OMe)]$_2$/tmphen proceeds under mild reaction conditions to deliver a mixture of *m*- and *p*-borylated products, however, apart from the lack of any *ortho*-borylation (presumably due to steric control) the reaction was found to be non-regioselective.

After this work, other students in the group completed this study by following the C-H borylation strategy thus employed to synthesise *m*-substituted phosphonate-functionalised arylboronic esters with complete regioselectivity by incorporating 3-substituted aryl phosphonates as the substrates. The presence of an additional substituent *meta* to the phosphonate in the substrate leaves only one position which is not sterically encumbered. The resulting *m,m'*-disubstituted arylboronic esters were then utilised for the Pd-catalysed Suzuki–Miyaura cross-coupling reaction as the nucleophilic coupling partners with a variety of aryl halides to prepare a diverse range of *m*-phosphonate substituted biphenyls, as shown in Figure **2.4**.[221]
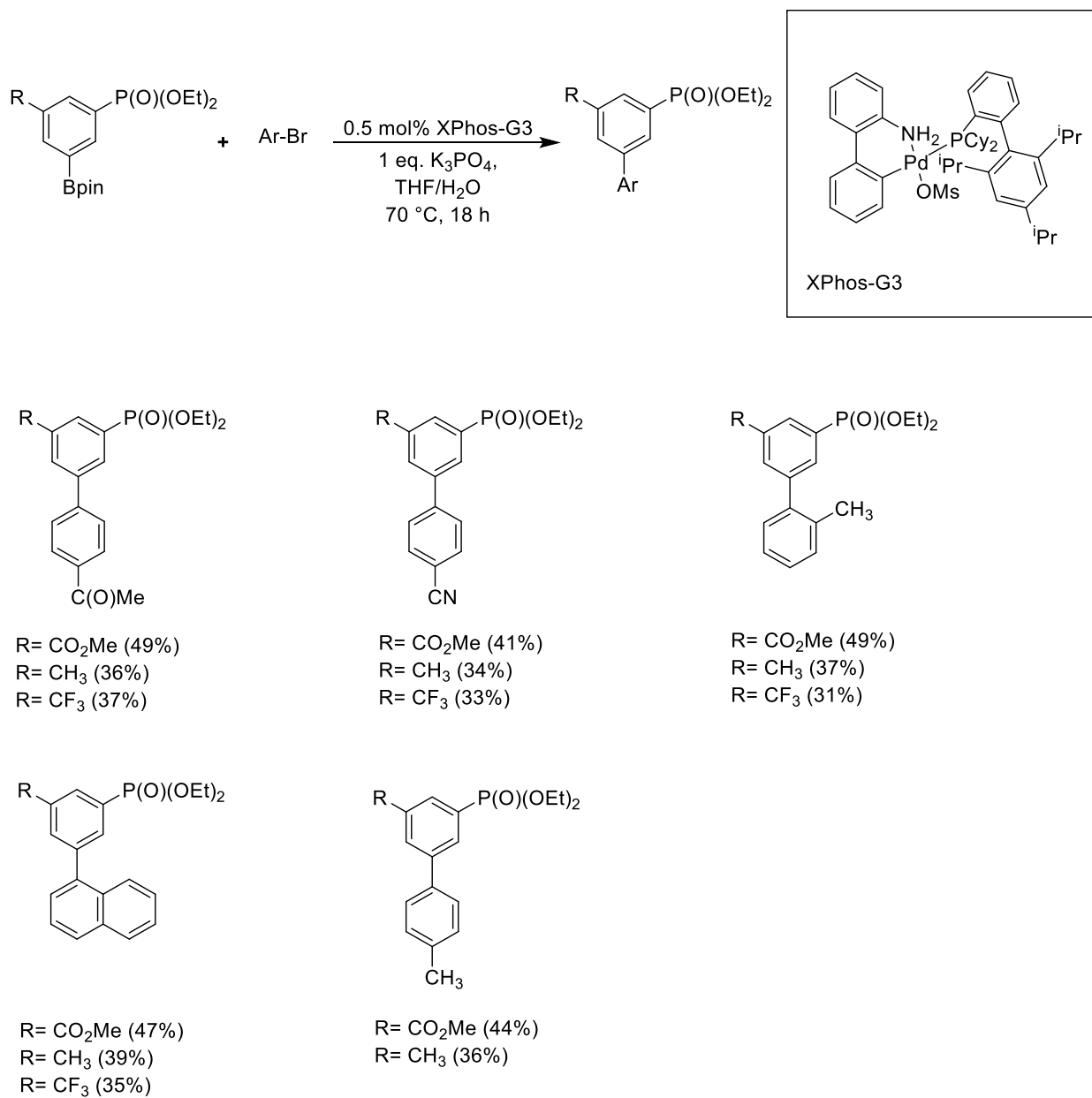
Figure 2.4: Suzuki–Miyaura cross-coupling reaction of aryl bromide and *m*-phosphonate substituted esters.

Chapter 3. Selective Transfer Hydrogenation of Nitroarenes Using PIIL-Stabilised Gold Nanoparticles

3.1   Introduction

Aromatic amines represent an important class of organic compounds due to their applications in pharmaceuticals, agrochemicals, dyes and pigments.[222] Many synthetic approaches for the synthesis of aromatic amines have been well documented in the literature, including metal-catalysed *N*-arylation of simple amines. Nevertheless, these protocols suffer from limitations of using stoichiometric quantities of metals, including requirement of toxic additives, and sometimes require high catalyst loadings.[223] In addition, the use of volatile, flammable, and potentially toxic organic solvents is often required due to the solubility profile of most of the organic substrates. Finally, poor selectivity for the desired product remains to be addressed with priority for their frequent use, especially during the large scale production of these useful synthetic precursors.[224] Furthermore, the accumulation of residual organic solvent, leaching of precious metals and the continuous deposition of toxic by-products based on azo-derivatives all lead to contamination of the product streams and makes the industrial application less sustainable. The undesired azo-based by-products are formed due to the condensation of intermediates during the reaction.[225] The most widely accepted reaction mechanism for nitrobenzene (**NO2**) reduction was first proposed by Haber (Scheme **3.1**). This mechanism generally involves two competing pathways, the direct pathway (**a**) and the condensation pathway (**b**).[226]
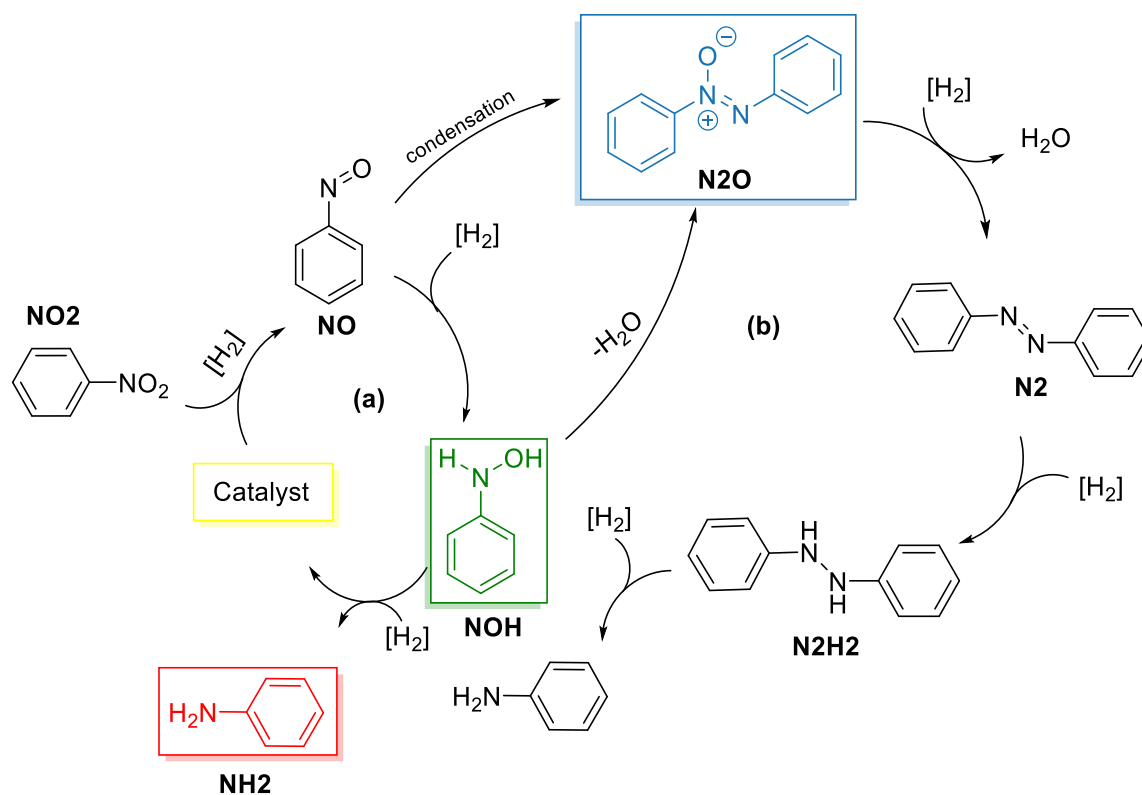
Scheme 3.1: General mechanisms (Haber) for the reduction of nitroarenes (a) direct pathway (b) condensation pathway.

The first step of nitrobenzene (**NO2**) reduction is generally identical in either pathway and involves the addition of one equivalent of H_2 molecule to nitrobenzene (**NO2**) on the surface of the catalyst followed by removal of a water molecule, resulting in nitrosobenzene (**NO**) formation, which then reacts with another equivalent of H_2 to form the thermally labile *N*-phenylhydroxylamine (**NOH**). The *N*-phenylhydroxylamine (**NOH**) in the direct pathway further undergoes hydrogenation to give the completely hydrogenated aryl amine. Most of the Pd-based catalysts are known to follow this common pathway during nitroarene reduction.[113] The *N*-phenylhydroxylamine (**NOH**), in some cases, does not undergo complete reduction, rather accumulates on the surface of the catalyst under certain reaction conditions to form azoxybenzene (**N2O**) *via* the condensation pathway. A low concentration of reducing agent and/or substrate might be responsible for this condensation pathway, as reported by Kralik *et.al.*[227] Consequently, the reaction may then proceed from the azoxybenzene (**N2O**) *via* a cascade of two successive hydrogenations, i.e., *via* azobenzene (**N2**) and diphenyl hydrazine (**N2H2**) formation before producing the desired final product aryl amine. As a result, six different products are expected under slightly different reaction conditions,

emphasising design and discovery of more selective catalysts for the efficient production of a single product in high yields.

Both homogeneous and heterogeneous metal catalysts for the reduction of nitroarenes have been studied extensively. For instance, Ru and Rh-based catalytic systems have been used for nitroarene reduction under homogenous conditions. However, the homogeneous catalytic process is not considered a preferred route since the recovery and reuse of the expensive metals are often challenging, and the majority of these reactions only proceed with the use of expensive metals, often also with the requirement for complex and specific ligands.[228,229] In this aspect, heterogeneous catalysts, including Pd,[119,230] Au,[83,231] and Ru[232,233] display several beneficial aspects compared to their homogeneous counterparts. For example, the use of heterogeneous catalytic systems offers simple removal or recovery of the catalyst from the complex reaction mixture and provides the opportunity to reuse the catalytic system multiple times with no significant loss of catalytic activity. Several metal nanoparticles (MNP's) stabilised by either carbon-containing or inorganic-based materials have displayed outstanding efficiencies for the reduction of nitroarenes into corresponding amines. These catalytic systems demonstrate excellent catalytic activity and selectivity, along with the advantage of recycling.

Catalytic systems based on heterogeneous supports with encouraging reaction capability for either hydrogenation or transfer hydrogenation of nitroarenes include palladium nanoparticles (PdNPs) of controlled size immobilised on carbon nanospheres,[234] gold nanoparticles (AuNPs) supported on imidazolium based organic polymers[235] and ruthenium nanoparticles (RuNPs) stabilised and supported on polystyrene.[236] Recent heterogeneous catalytic systems with excellent catalytic activities include nitrogen-doped carbon-based ruthenium nanoparticles (RuNPs),[237] mesoporous titanium dioxide,[238] or functionalised phosphine based ionic liquid polymers.[239] Only a few of these examples possess all of the essential features required for a sustainable and environmentally green catalytic system. For instance, only a few catalytic systems have shown the capability to operate under mild conditions in short reaction times with high selectivity and low catalyst loadings, making the synthetic pathway operationally straightforward and efficient with the beneficial aspect of recyclability the catalytic system. Thus, there is still a need, opportunity and potential to design and develop new catalyst technologies with improved catalytic efficiency to synthesise useful organic compounds.

A heterogeneous catalytic system developed in our lab recently has demonstrated the potential to fulfil the majority of the requirements described above, displaying eco-friendly and selective aqueous phase reduction of nitroarenes at room temperature. This catalytic system is comprised of Au or Pd nanoparticles based on immobilised phosphine decorated PEGylated polymer.[83,119]
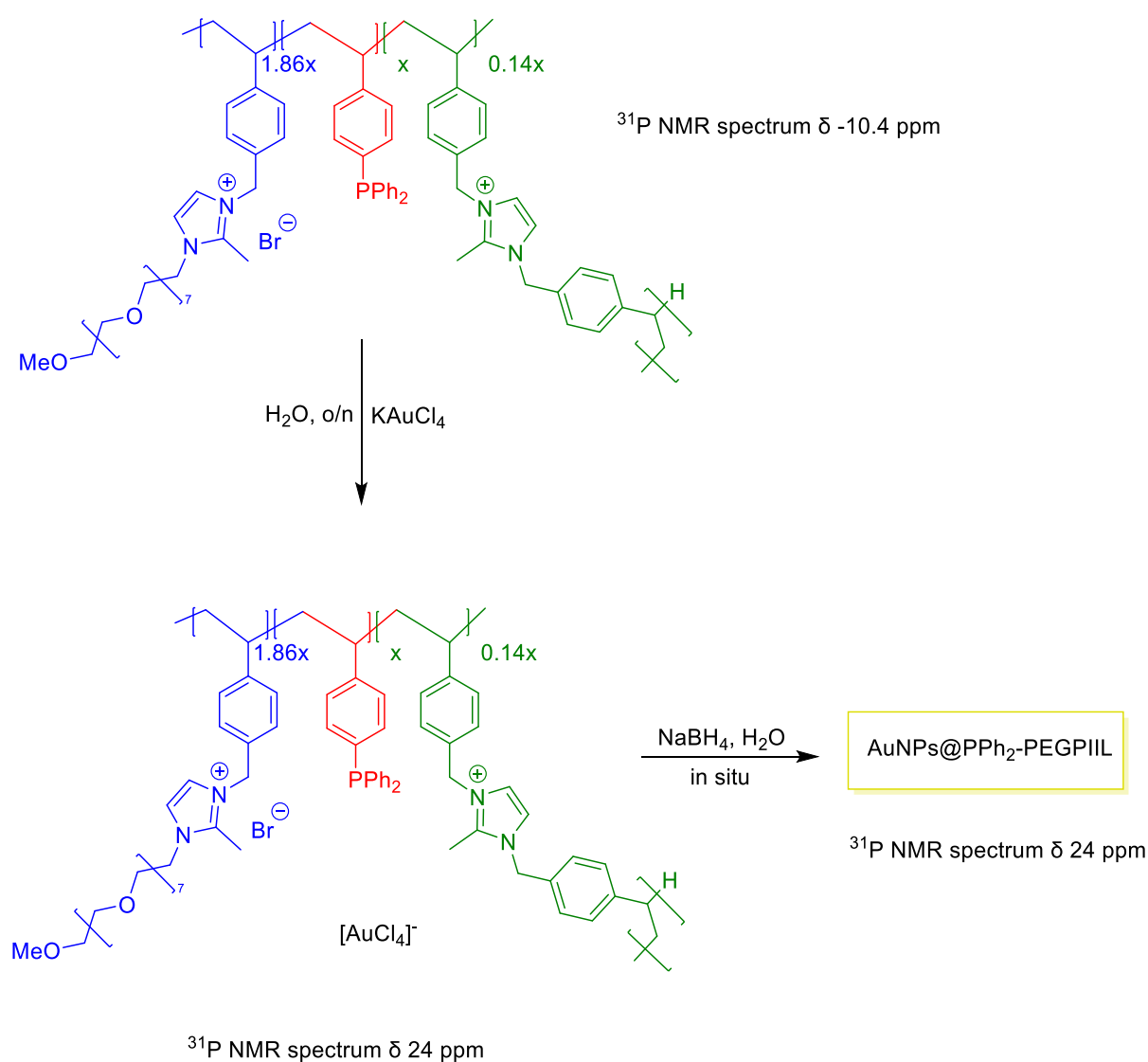
Scheme 3.2: Reported ^{31}P NMR shift and proposed structures of the AuNP@PPh$_2$-PEGPIIL catalyst from reference.[83]

As indicated in Scheme **3.2**, the previous report[83] from the Knight and Doherty groups indicated that the gold nanoparticles used as catalysts for the reduction of nitrobenzene (**NO2**) were supported on a phosphine-functionalised polymer. However, it can be seen that the ^{31}P NMR

chemical shift (δ 24 ppm) observed for the postulated gold(III) loaded material $[AuCl_4]@PPh_2$-PEGPIIL remains unchanged on subsequent *in situ* reduction by $NaBH_4$ to obtain the active AuNP-based catalyst. Although the chemical shift of phosphine-bound Au(0) might be expected to appear below δ 24 ppm, the literature value for Ph_3P-capped gold nanoparticles is actually δ 56 ppm.[240] Nonetheless, the value of δ 24 ppm which we observed is surprising insofar as the chemical shift obtained for the postulated Au(III)-phosphine material remains unchanged on reduction with $NaBH_4$. In fact, the reaction of PPh_2-PEGPIIL with $KAuCl_4$ to give a ^{31}P NMR peak at δ 24 ppm suggests that the reaction product is actually due to phosphine oxide and not gold(III)-coordinated phosphine since $NaBH_4$ does not reduce $O=PPh_2$. Therefore, it is possible that the higher activity of the nanoparticles reported in the previous work may be attributed to P=O - Au in the precursor used for the generation of the nanoparticles.

In the reported work, nitrobenzene (**NO2**) was used as the model substrate to optimise the initial catalytic reaction conditions for the 'AuNP@PPh_2-PIIL'-based system using an identical procedure previously reported for the corresponding PdNPs-based system.[119] When the reaction was performed by using 0.05 mol% of 'AuNP@PPh_2-PIIL' loading, the reaction of nitrobenzene (**NO2**) in water under a nitrogen atmosphere at room temperature (25°C) for 2 hours showed a complete conversion of the substrate and provided *N*-phenylhydroxylamine (**NOH**) with a 97% selectivity (Scheme **3.3**). Under similar reaction conditions, the corresponding PEGylated polymer-based catalyst, 'AuNP@PPh_2-PEGPIIL', also showed complete conversion. However, the selectivity for *N*-phenylhydroxylamine (**NOH**) was increased to 99% after 40 mins. Next, the effect of different solvents on the catalytic reaction was studied which revealed a complete inversion in selectivity for the reduction of nitrobenzene (**NO2**) to azoxybenzene (**N2O**) instead of *N*-phenylhydroxylamine (**NOH**) when the solvent was changed from water and water/ethanol mixture to dry ethanol. A complete conversion of nitrobenzene (**NO2**) in 2.5 hours at room temperature by using 0.05 mol% loading of the 'AuNP@PPh_2-PEGPIIL'-based system in dry ethanol provided azoxybenzene (**N2O**) as the only reduced product (Scheme **3.3**).[83]
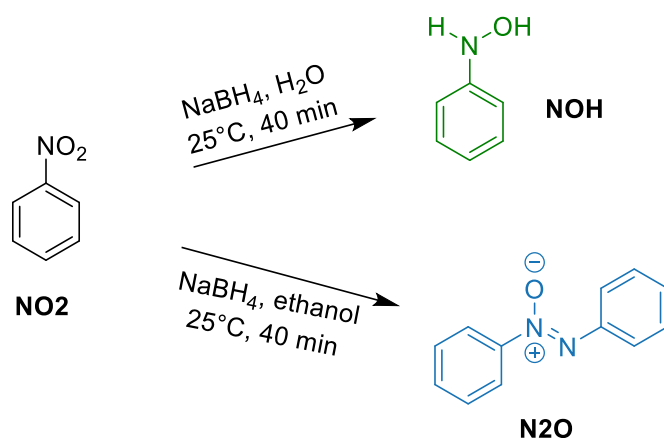
Scheme 3.3: Solvent dependent selective reduction of nitrobenzene (**NO2**) catalysed by 0.05 mol% AuNP@PPh$_2$-PEGPIIL.[83]

In following these initial results, and particularly to investigate the role of phosphine oxides, we aimed to synthesise: phosphine polymers that will be coordinated to gold(I); phosphine oxide polymers that will be coordinated to gold(III); and phosphine polymers coordinated to gold(III). Additionally, the catalytic activity of the nanoparticle generated from each of the precursors will be determined towards the reduction of nitrobenzene (**NO2**). Synthesis of the phosphine modified polymer immobilised ionic liquid phase requires the three functionalised styrene monomers shown in Figure **3.1** which were chosen to be incorporated into the PIIL materials to achieve required functionality such as swelling, dispersion, structural integrity and catalyst efficiency.[120]
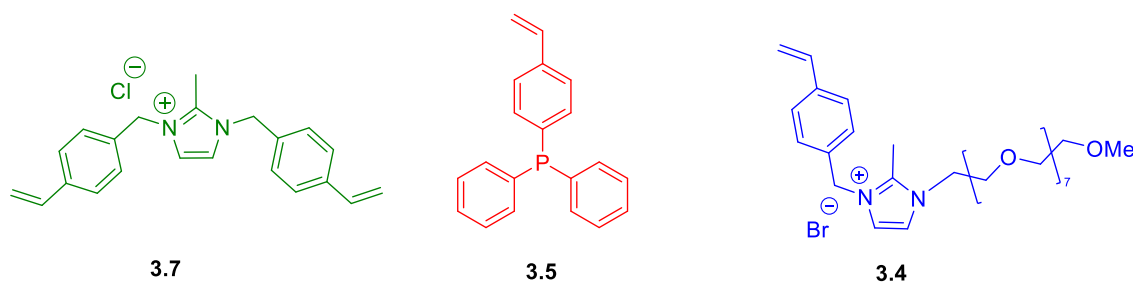
Figure 3.1: Target monomers; cross-linker **3.7**, neutral functionalised monomer **3.5** and PEGylated monomer **3.4**

A Polymer-Immobilised Ionic Liquid (PIIL) can be defined as a polymer/copolymer formed from one or more types of prefabricated ionic liquid-like monomer. Our chosen PIIL system incorporates the imidazolium cationic monomer **3.4** based on the extensive uses of imidazolium-based ionic liquids for catalytic applications.[241] The imidazolium-centred bis (styrene) **3.7** would act as a cross-linker, the amount of which can be varied to control structural integrity and physical characteristics

(such as porosity) of the resulting polymer and the neutral phosphine **3.5** is included due to its ability to coordinate to metals, potentially controlling the growth of metal nanoparticles and modulating their ultimate catalytic activity (Figure **3.2**).
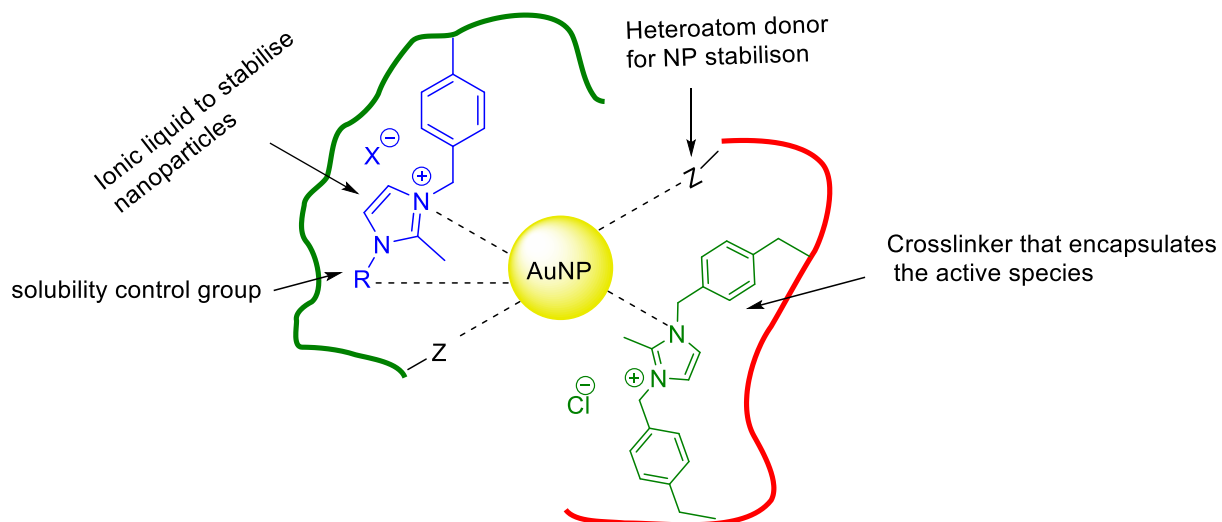
Figure 3.2: Polymer Immobilised Ionic Liquid Phase (PIIL) concept.

3.2   Results and Discussion

3.2.1   Synthesis of Monomers

3.2.1.1 Synthesis of 2-methyl-1-PEG-3-(4-vinylbenzyl) imidazolium bromide (3.4)

A PEG functionalised imidazolium-based ionic liquid, 2-methyl-1-PEG-3-(4-vinylbenzyl) imidazolium bromide (**3.4**), was employed as the monomeric unit for the preparation of the PPh$_2$-PEGPIIL support. A four-step convergent strategy was used to prepare this compound **3.4** (Scheme **3.4**).
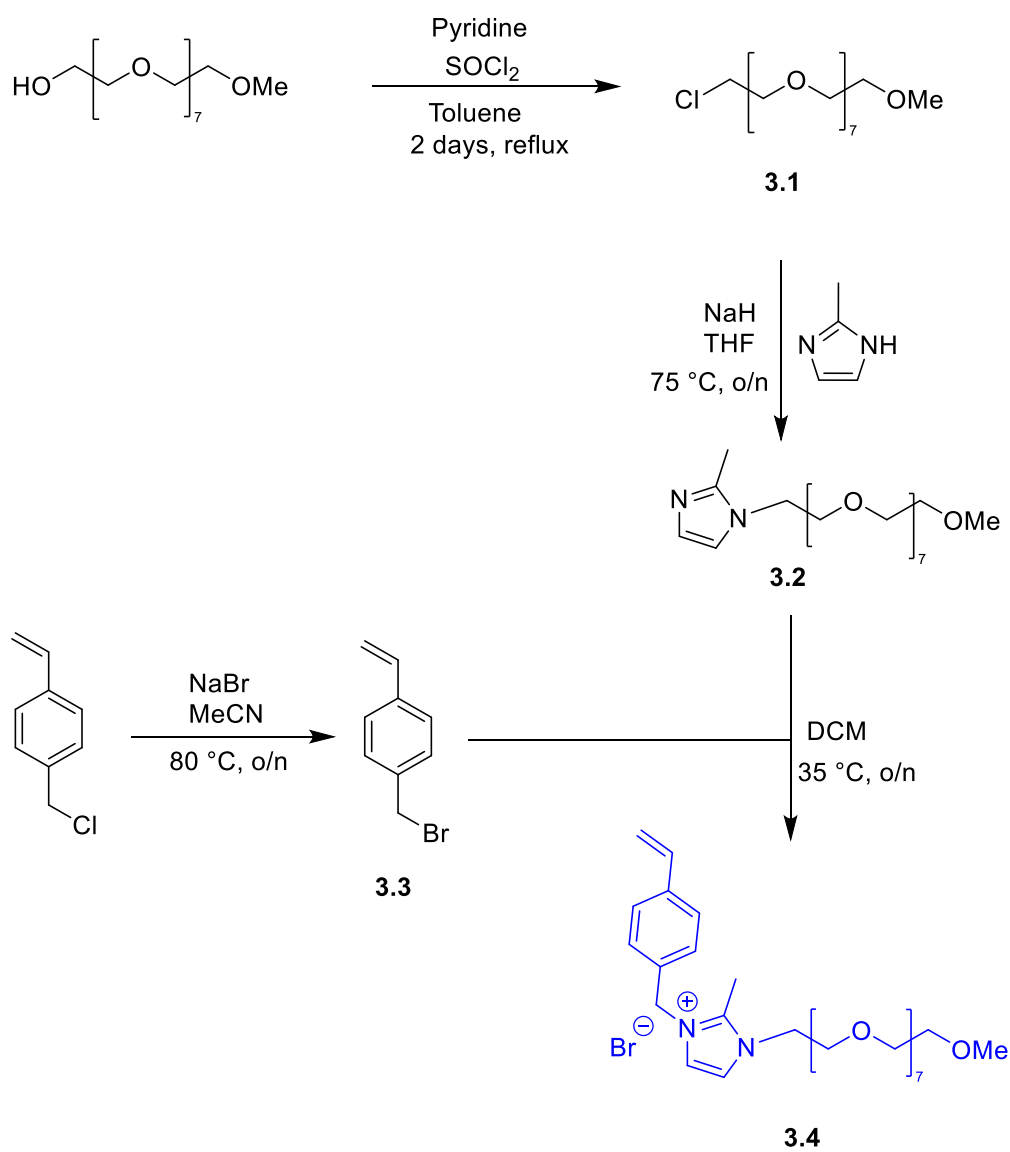
Scheme 3.4: Synthesis of PEGylated monomer **3.4**

Firstly, PEG-chloride **3.1** was prepared as shown in Scheme **3.4**. For this, a toluene solution of polyethylene glycol monomethyl ether and pyridine was gently stirred and heated until 80 °C, followed by the addition of thionyl chloride, and heating under reflux for two days. The reaction mixture was quenched by adding water, the mixture was extracted with toluene and the solvent was removed under reduced pressure to give PEG-chloride **3.1** as a red oil in 89% yield. Overall, this reaction (Darzens halogenation) displays a nucleophilic substitution of an –OH group from the polyethylene glycol monomethyl ether by a halide (Cl⁻). The ¹H and ¹³C NMR spectra were consistent with the data previously reported for compound **3.1**.[120]

Deprotonation of 2-methylimidazole by reaction with NaH in THF was followed by dropwise addition of the PEG-chloride **3.1** and the reaction mixture was stirred overnight at 75 °C. The reaction was then quenched by adding water, the solvent was removed by external trap, and the residue was washed with diethyl ether to produce the pure PEG-imidazole **3.2** as a red oil in 90% yield. The structure of compound **3.2** was confirmed by analysis of the ¹H spectrum (Figure **3.3**), which showed a key singlet peak at δ 2.27 ppm corresponding to the methyl group on the imidazole ring and a slight downfield shift of the triplet corresponding to the CH$_2$ protons at δ 3.90 ppm compared to δ 3.69 ppm in PEG-chloride **3.1** due to the greater electron-withdrawing effect of the imidazole nitrogen compared to the chloride.[120]
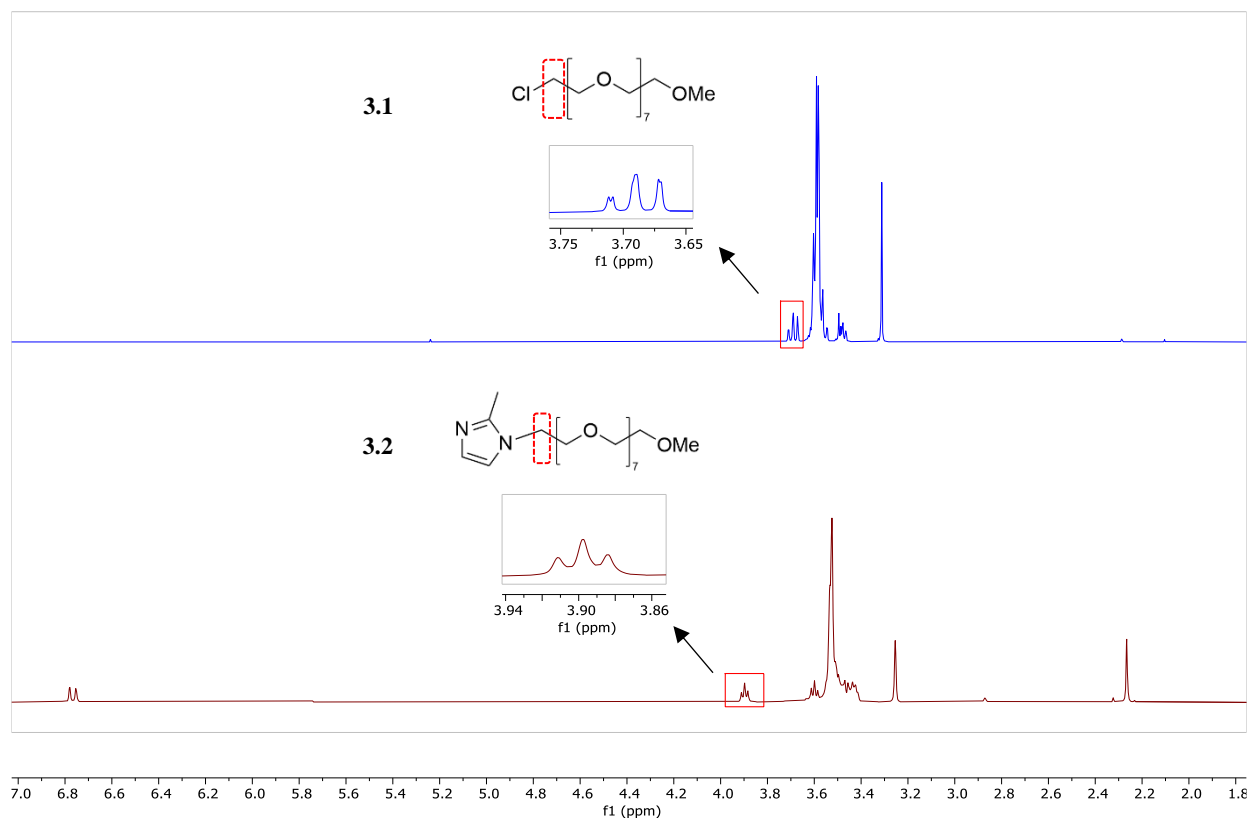
Figure 3.3: ^{1}H NMR spectrum (300 MHz, CDCl$_3$) of PEG-Cl **3.1** and 2-methyl-1-PEG-imidazole **3.2**

4-Vinylbenzyl bromide **3.3** was prepared by a Finkelstein-type reaction from 4-vinylbenzyl chloride as shown in (Scheme **3.4**). Thus, a mixture of 4-vinylbenzyl chloride and 4 equivalents of NaBr in acetonitrile was allowed to react overnight at 85 °C. 4-Vinylbenzyl bromide **3.3** was isolated as a yellow oil in 86% yield. In the ^{1}H NMR spectrum the singlet due to the benzylic protons in the benzyl bromide **3.3** was shifted upfield to δ 4.41 ppm in comparison to the corresponding resonance for 4-vinylbenzyl chloride (δ 4.7 ppm). In addition,^{13}C NMR spectroscopy was used to confirm the differences in chemical shift between 4-vinylbenzyl chloride and 4-vinylbenzyl bromide **3.3** (δ 46.55 ppm for C-Cl and δ 33.50 ppm for C-Br).[242]

Finally, quaternisation of the 2-methyl-1-PEG-imidazole **3.2** was accomplished by treatment with 4-vinylbenzyl bromide **3.3** in dichloromethane and allowing the reaction mixture to stir overnight at 35 °C to produce 2-methyl-1-PEG-3-(4-vinylbenzyl) imidazolium bromide **3.4** (Scheme **3.4**). The solvent was removed under reduced pressure and the residue was triturated with diethyl ether and dried under high vacuum to provide the imidazolium bromide **3.4** as a yellow oil in 89% yield.

As the ionic liquid component, the resulting imidazole-based ammonium cation is expected to play a vital role in stabilising the gold nanoparticles and for the catalytic activity. The ^{1}H spectrum of the imidazolium salt **3.4** (Figure **3.4**), showed a downfield shift of the singlet peak corresponding to the CH$_2$ protons at δ 5.45 ppm compared to δ 4.50 ppm in **3.3** due to the greater electron-withdrawing effect of the imidazolium nitrogen compared to the bromide confirming successful synthesis of the monomer unit containing PEG functionalised, imidazolium-based ionic liquid.[120]
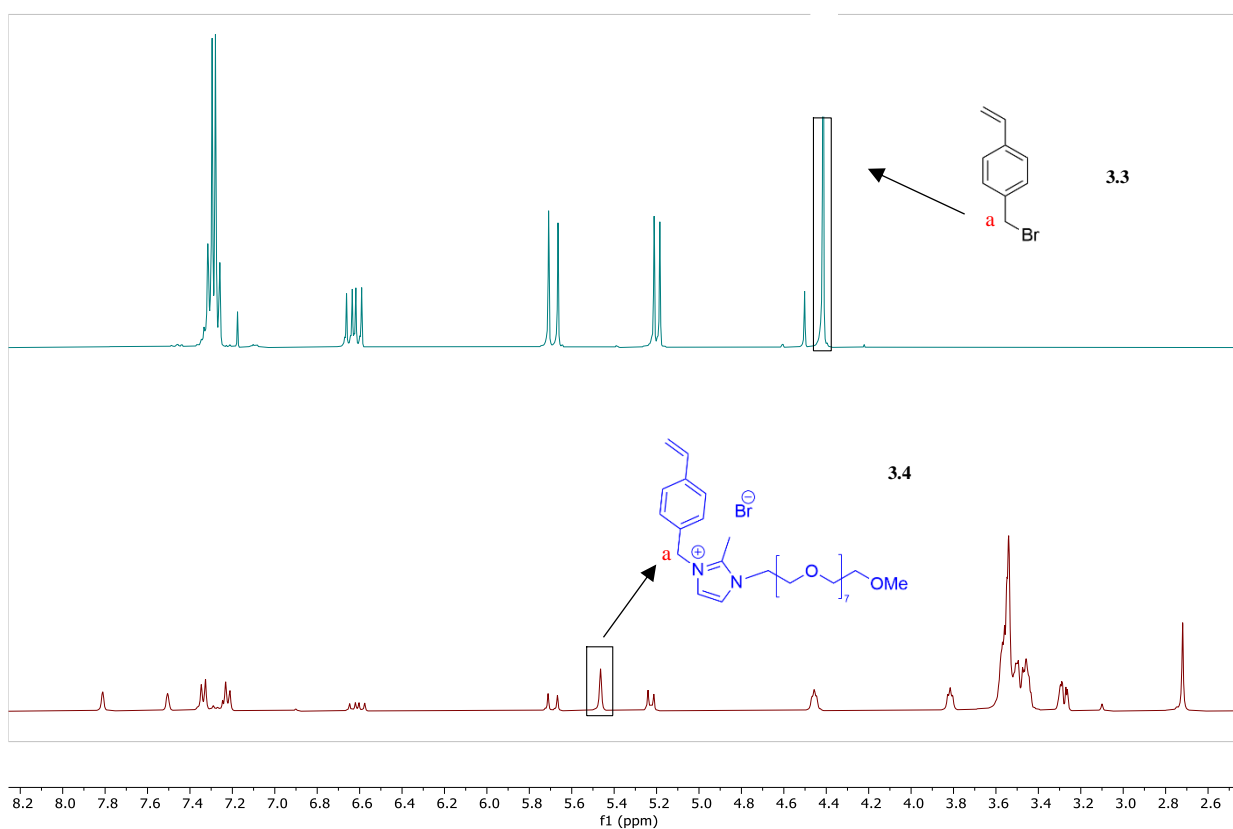
Figure 3.4: ^{1}H NMR spectrum (300 MHz, CDCl$_3$) of 4-vinylbenzyl bromide **3.3** and 2-methyl-1-PEG-3-(4-vinylbenzyl) imidazolium bromide **3.4.**

3.2.1.2 Synthesis of diphenyl(4-vinylphenyl) phosphine (3.5)
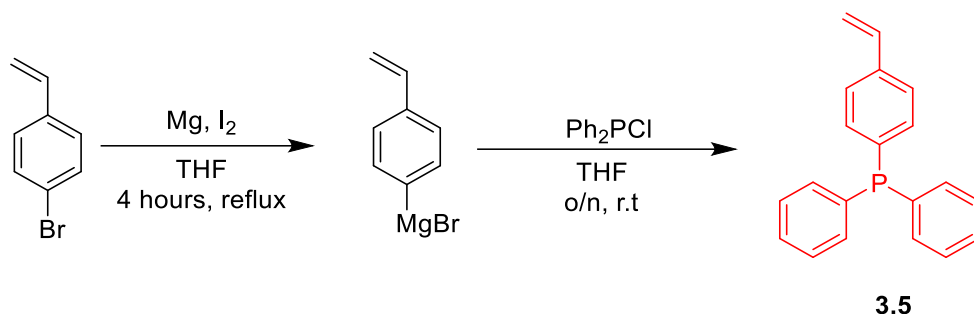
Scheme 3.5: Synthesis of phosphine neutral functionalised monomer

Tertiary phosphines (PR$_3$) are excellent ligands for various metal ions and transition metals. By varying the R groups, phosphines can be electronically and sterically tuned systematically and predictably. Like amines, phosphines can behave like π acids. The characteristics of phosphines allow them to stabilise transition metal ions in low oxidation states and they are significant components of homogeneous and heterogeneous catalysts. Steric influences also affect the behaviour of phosphines as a ligand.[243]

The synthesis of the known diphenyl(4-vinylphenyl) phosphine **3.5** monomer for the preparation of PIIL support is shown in Scheme **3.5**. For this, a Grignard reagent was prepared by treating 4-bromostyrene with Mg turnings in dry THF in the presence of a crystal of iodine under reflux for 4 hours. This particular phosphine was found to be rather easily oxidised, so all the steps must be performed exclusively under N$_2$. All the solvents must be degassed to prevent the formation of the phosphine oxide. The resulting Grignard reagent formed *in situ* was then added dropwise to a solution containing chlorodiphenylphosphine in dry THF *via* a cannula and left for overnight stirring. After work-up and solvent evaporation in vacuo, the desired diphenyl(4-vinylphenyl) phosphine **3.5** was obtained as a white powder in 64% yield. Observation of a single peak in the ^{31}P spectrum at δ -5.74 ppm, indicated a successful reaction with no peaks appearing between δ 25-30 ppm (Figure **3.5**) which would indicate the presence of phosphine oxide. 4-Diphenylphosphinostyrene **3.5** was stored under N$_2$ to prevent oxidation.[244]
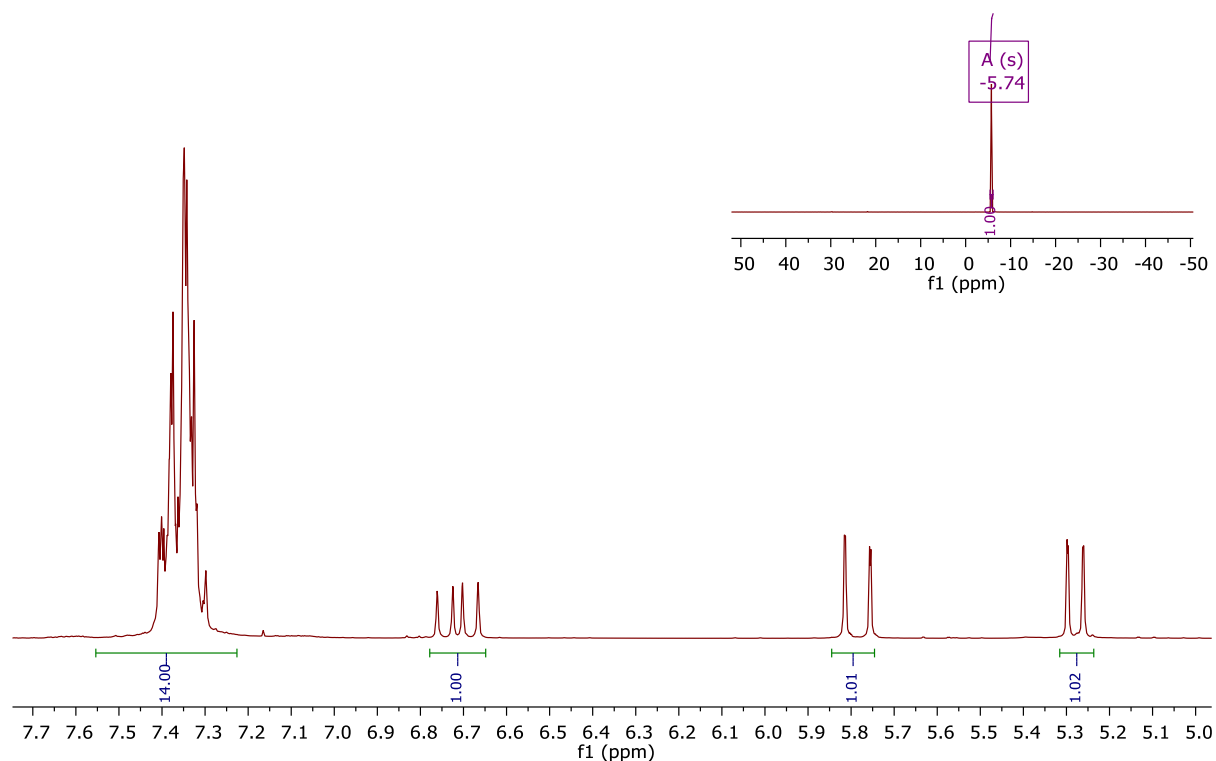
Figure 3.5: [1]H (400 MHz, CDCl[3]) and [31]P (121 MHz, CDCl[3], inset) NMR spectra of phosphine monomer **3.5.**

3.2.1.3 Synthesis of 2-methyl-1,3-bis(4-vinylbenzyl)-*1H*-imidazol-3-ium chloride (3.7)

The preparation of the cross-linking monomer was accomplished by utilising a two-step synthetic protocol according to the previously reported method (Scheme **3.6**).[245]
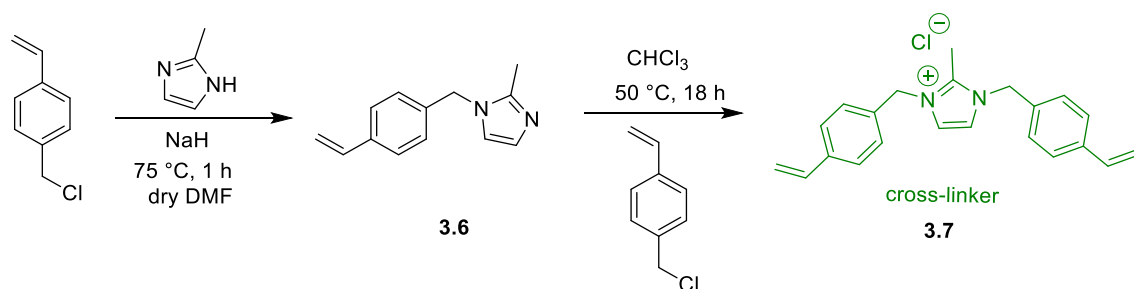
Scheme 3.6: Synthesis of 2-methyl-1,3-bis(4-vinylbenzyl)-*1H*-imidazol-3-ium chloride **3.7**.

Firstly, 2-methyl imidazole was deprotonated by reacting it with sodium hydride in dry DMF followed by dropwise addition of 4-vinylbenzyl chloride at 75 °C for 1 hour. The use of the polar, aprotic solvent DMF facilitates the S[N]2 reaction. This reaction produced the imidazole **3.6** as a yellow oil in 95% yield.

The resulting pale yellow coloured oil intermediate imidazole **3.6** was subsequently reacted by dropwise addition of 4-vinylbenzyl chloride in chloroform and stirring at 50 °C overnight. After removing the solvent under reduced pressure, the residue was dissolved in DCM and added dropwise to a large volume of diethyl ether with stirring. The resulting precipitate was filtered, washed with diethyl ether, and dried under high vacuum to afford the desired imidazolium salt **3.7** as a white powder in 98% yield.

3.2.2   Synthesis and Characterisation of PPh₂-PEGPIIL (3.8)

PPh₂-PEGPIIL was prepared by the free radical copolymerisation of the PEGylated styryl imidazolium salt **3.4** with styryl diphenyl phosphine **3.5** and the cross-linker **3.7** in a ratio of 1.86:1:0.14, respectively, as shown in (Scheme **3.7**). The monomers and 5 mol% AIBN were dissolved in dry ethanol:THF (1:1). In the (extensive) previous work in the group a molar ratio of 2:1 has been used for the cationic, ionic-liquid like monomers to the neutral phosphine monomer (i.e. a 2:1 charge:P ratio). This ensures that, in the case of metal precursors such as $PdCl_4^{2-}$ and $PtCl_4^{2-}$ exhaustive metal loading by ion exchange results in a metal:phosphine ratio of 1:1. Although, in the present case using the monoanionic $AuCl_4^-$ exhaustive ion exchange between the metal source and polymer-associated halides during the catalyst loading would lead to a Au to phosphine ratio = 2:1 , the nature of the polymer was not changed in order to enable comparison to previous work and also because the other physical properties of the polymer (tractability, solubility etc.) would not be in doubt. Eventually, achievement of the desired 1:1 Au:P ratio in the metal-loaded polymer would require control of the stoichiometry during the metal loading step (see later) rather than relying on exhaustive ion exchange.[83,120] The polymerisation reaction mixture was then degassed six times using the freeze-pump-thaw technique to remove the oxygen from the system, which might interfere with the reaction and produce ultimately undesired compounds. The reaction was stirred at 80 °C for four days, after which a further 5 mol% of AIBN was added to the mixture, and the degassing process was repeated six times. Subsequently, the reaction was heated for one more day to ensure complete polymerisation.
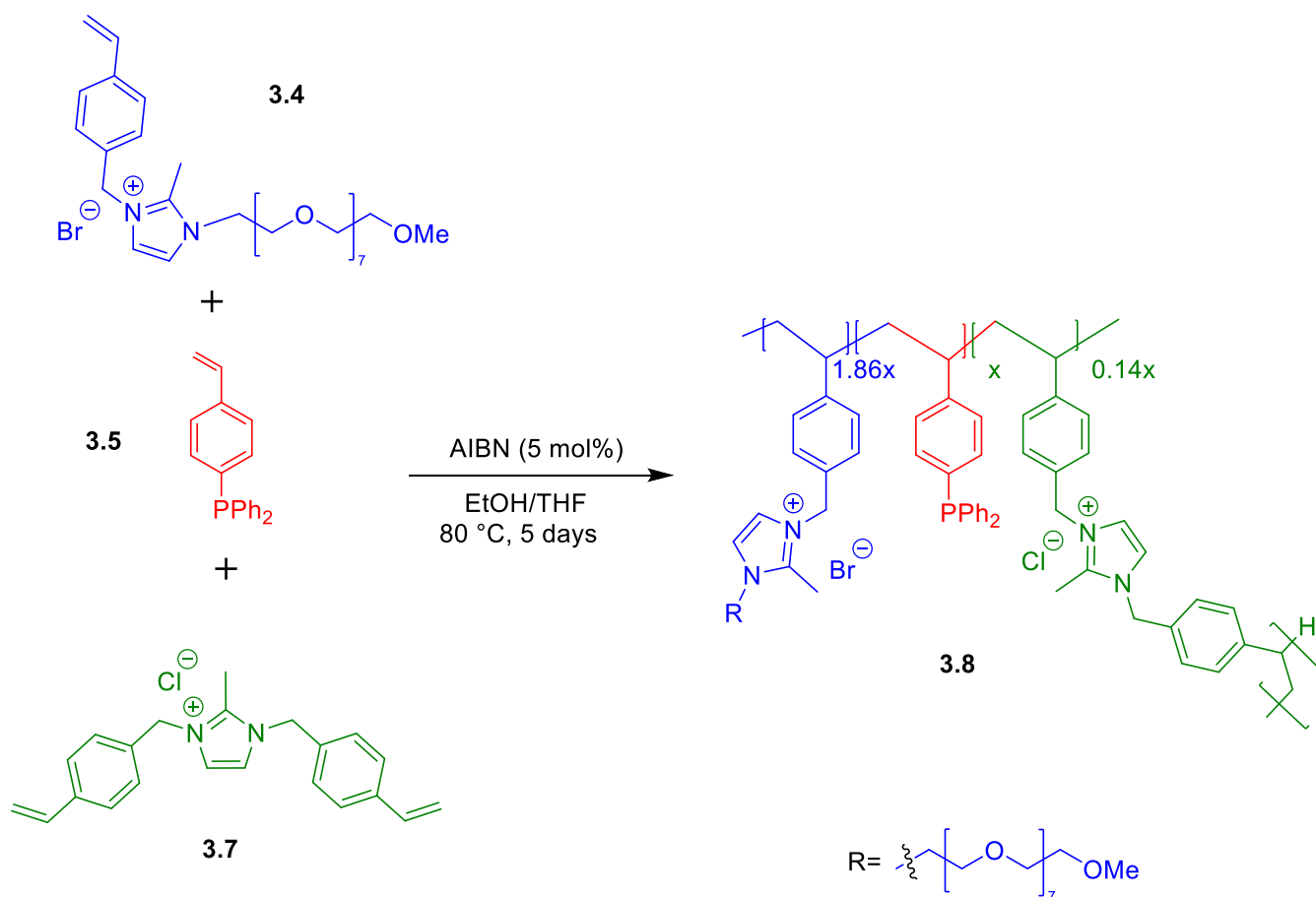
Scheme 3.7: Synthesis of PPh$_2$-PEGPIIL functionalised PIIL **3.8**

After completion of the reaction, the solvent was removed under reduced pressure and the residue was re-dissolved in DCM followed by re-precipitation in diethyl ether to remove unreacted monomers to afford the polymer **3.8** as a fine off-white powder in 90% yield. The absence of vinylic signal peaks (which would appear at δ 5.2, 5.7, 6.7 ppm) in the ^{1}H NMR spectrum (Figure **3.5**) indicates the completion of the polymerisation. Furthermore, because of the random nature of the polymer and the tumbling effects of polymer molecules in solution, the spectrum showed significant peak broadening, confirming that the reaction was completed successfully. The ^{31}P NMR spectrum revealed a single peak at δ -6.95 ppm, indicating a tertiary phosphine group. The PPh$_2$-PEGPIIL **3.8** obtained was extremely hygroscopic because it consists of a hydrophilic PEG chain, absorbing atmospheric moisture. Due to this reason, and the potential for air oxidation of the phosphine to the undesired phosphine oxide, the product **3.8** was stored under a nitrogen atmosphere.

The ^{1}H NMR spectrum of PPh$_2$-PEGPIIL **3.8** (Figure **3.6**), was used to measure the actual ratio of monomer units incorporated in the polymer. The peaks at δ 2.78 ppm were assigned to the methyl groups on the two imidazolium rings, δ 3.30-3.40 ppm were assigned to the methoxy protons in the PEG functionalised monomer and the signal at ca. δ 5.50 ppm was assigned as the CH$_2$ adjacent to the imidazolium ring. The aromatic and imidazolium protons were assigned at δ 6.70-7.80 ppm. Integration of each of these peaks enables the calculation of the relative proportions of each monomer. The values obtained agreed with the expected 2:1 ratio of imidazolium groups:phosphine.
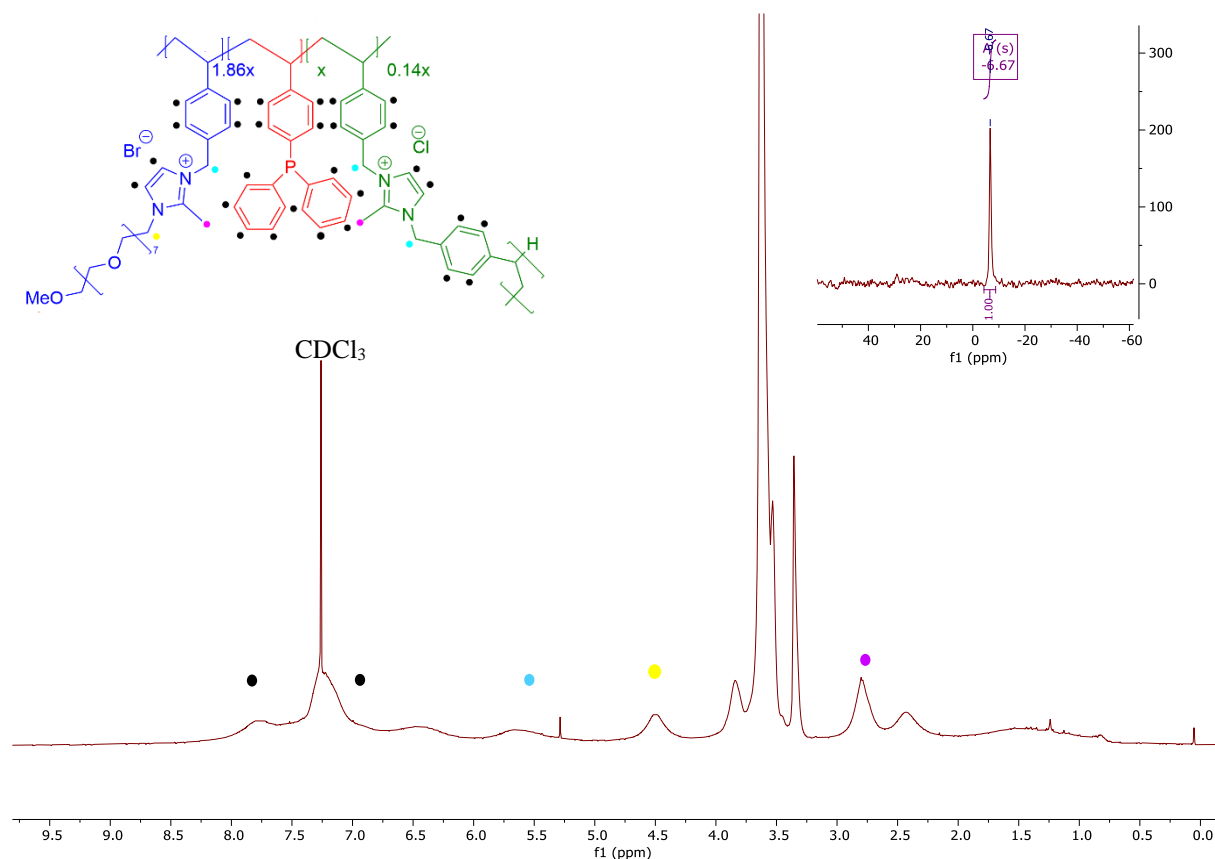
Figure: 3.6 ^{1}H (400 MHz, CDCl$_3$) and ^{31}P (121 MHz, CDCl$_3$, inset) NMR spectra for PPh$_2$-PEGPIIL **3.8.**

3.2.2.1 FT-IR analysis of the PPh$_2$-PEGPIIL (3.8)

The PPh$_2$-PEGPIIL **3.8** was characterised by FT-IR and the spectrum is shown in Figure **3.7,** which contains a characteristic broad band at 3404 cm^{-1} assigned to H$_2$O because the compound was hygroscopic, bands at 3126 and 3050 cm^{-1} assigned to imidazolium and aryl (C-H) stretching, a band at 2870 cm^{-1} to aliphatic C-H stretching, bands at 1600, 1525, 1513 cm^{-1} to the various

aromatic (C=N) and (C=C). In addition, a band stretching at 1118 cm^{-1} to imidazolium skeletal symmetric stretch, and a band at 1094 cm^{-1} assigned to ether (C-O-C).
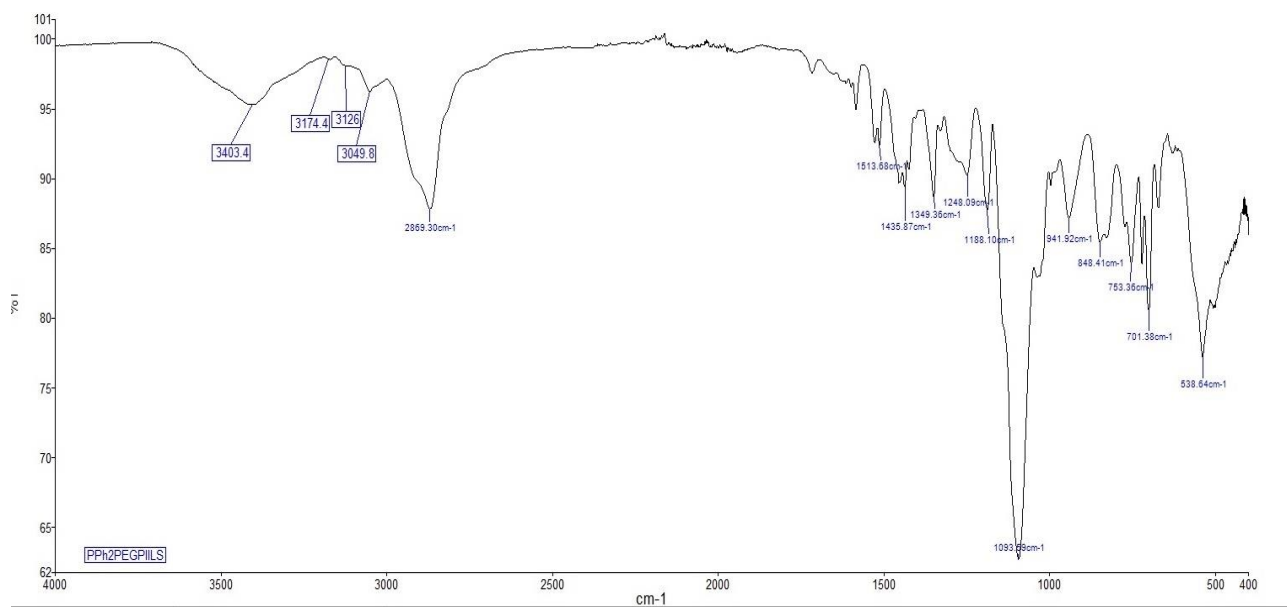
Figure 3.7: FT-IR spectrum of PPh$_2$-PEGPIIL

3.2.2.2 Scanning Electron Microscopy (SEM)

The surface morphology of PPh$_2$-PEGPIIL (**3.8**) was studied by Scanning Electron Microscopy (SEM), as shown in Figure **3.8**.
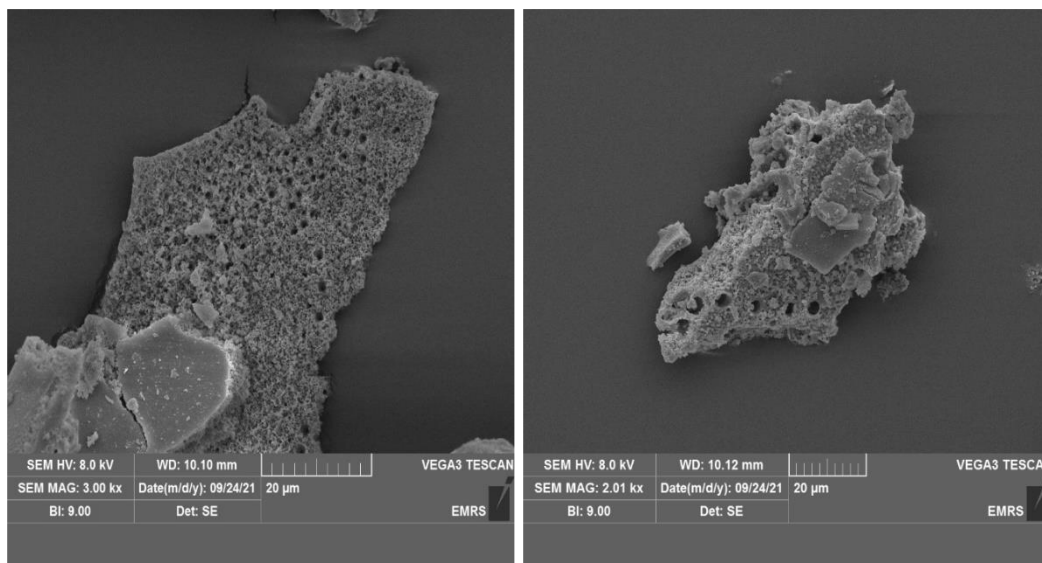
Figure 3.8: High-resolution scanning electron microscopy (SEM) images of PPh$_2$-PEGPIIL (**3.8**)

The high-resolution SEM images were taken on a Tescan Vega 3LMU scanning electron microscopy with digital image collection. The SEM images in Figure **3.8** show that the surface morphology of PPh$_2$-PEGPIIL **3.8** appeared as porous, which may be due to the hydrophilic PEG group.

Unfortunately, due to the intrinsic porosity and hydrophilicity of PEGPIIL material, a significant amount of solvent was trapped, making elemental analysis inaccurate for determining the polymer composition and causing difficulty in filling the rotor to record the solid-state NMR.

3.2.3 Synthesis and Characterisation of Gold-loaded Catalyst Precursors

3.2.3.1 Synthesis of '[AuCl$_4$]@PPh$_2$-PEGPIIL' adduct (3.9)
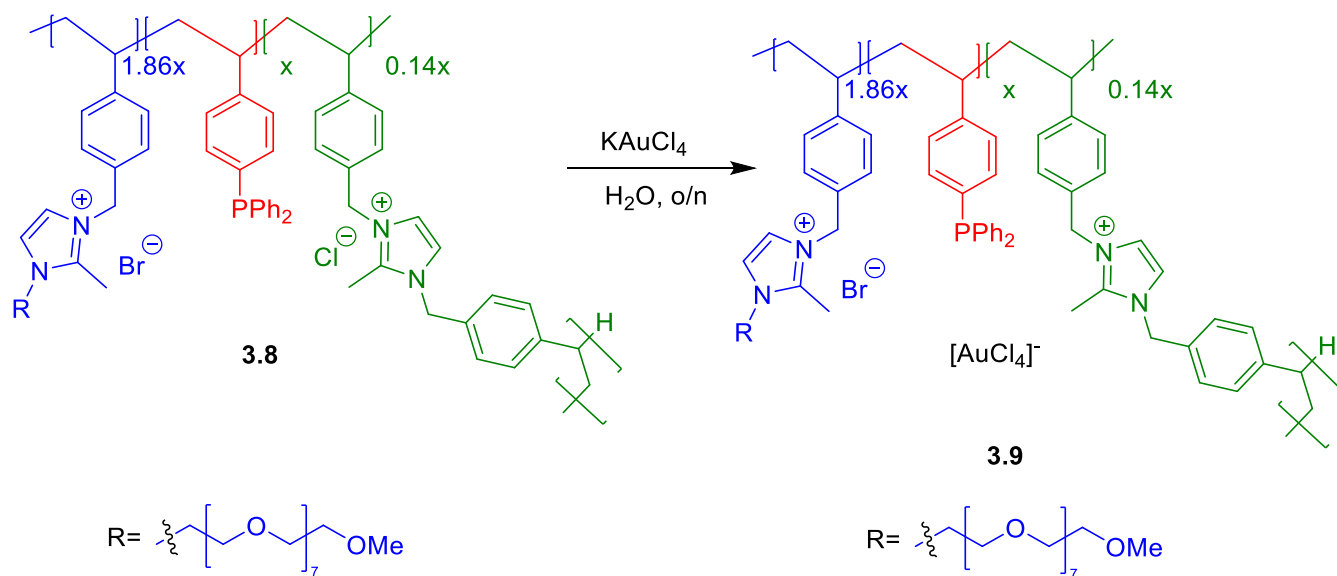
Scheme 3.8: Synthesis of '[AuCl$_4$]@PPh$_2$-PEGPIIL' adduct **3.9.**

In order to synthesise the '[AuCl$_4$]@PPh$_2$-PEGPIIL', we followed the published method[83] for anionic exchange of [AuCl$_4$]$^-$ with the halide anions in the polymer as shown in Scheme **3.8**. The AuCl$_4$ loaded catalyst precursor was synthesised by impregnation of PPh$_2$-PEGPIIL **3.8** with KAuCl$_4$. This procedure required stirring PPh$_2$-PEGPIIL **3.8** in water, and an aqueous solution of one equivalent of K[AuCl$_4$] per phosphine was added. After stirring overnight at room temperature, the water was removed by an external trap and the residue was re-dissolved in DCM, then reprecipitated in diethyl ether, filtering, washing, and drying under high vacuum to afford '[AuCl$_4$]@PPh$_2$-PEGPIIL' adduct **3.9** as an orange powder in 80% yield and which was stored in a Schlenk flask under N$_2$. PPh$_2$-PEGPIIL **3.8** support was chosen to determine the effect of various modifications on the activity and selectivity of the catalyst. The ^{31}P NMR spectrum of '[AuCl$_4$]@PPh$_2$-PEGPIIL' adduct **3.9** showed a single peak at δ 29.7 ppm, as shown in Figure **3.9**.
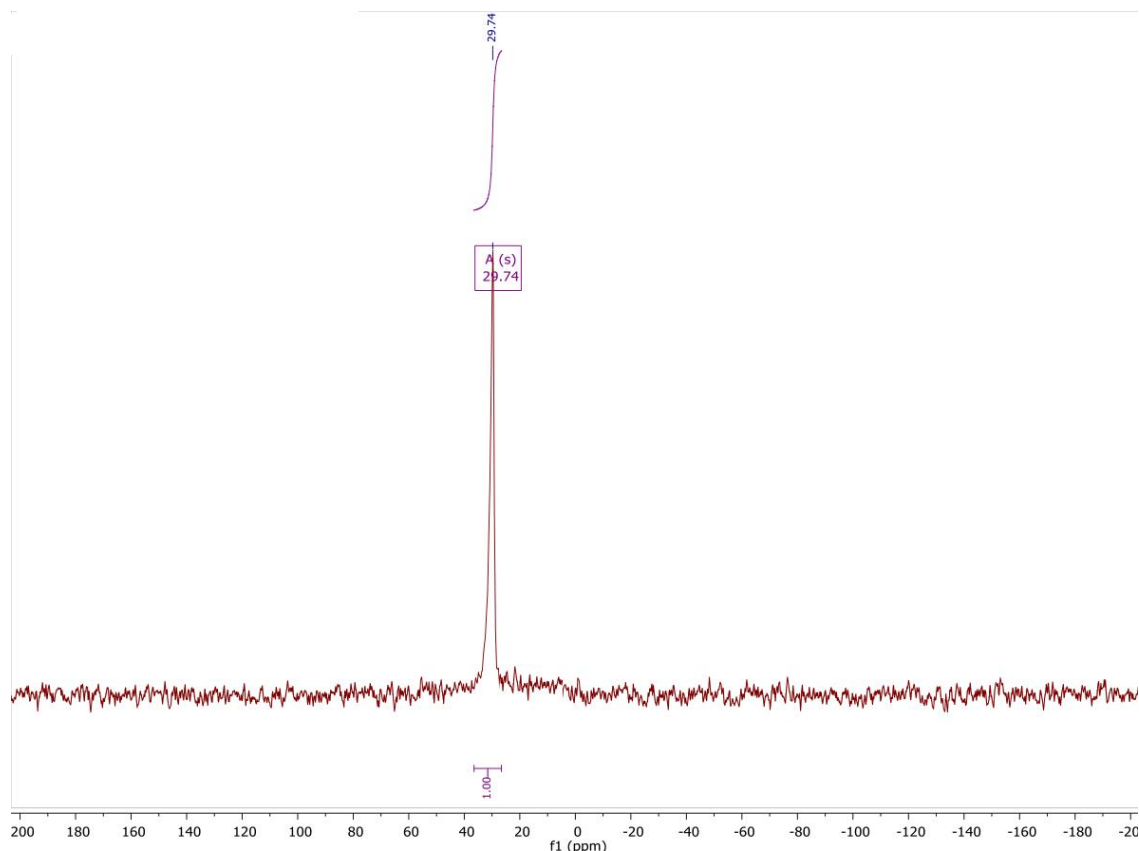
Figure 3.9: ^{31}P (121MHz, CDCl$_3$) NMR spectrum for [AuCl$_4$]@PPh$_2$-PEGPIIL adduct **3.9**.

Although, in the published work,[83] the resulting gold-loaded PIIL was proposed to be a gold(III)-phosphine as shown in Scheme **3.9**, it was suspected that oxidation of the phosphine occurs, concomitant with reduction of Au(III) to give a phosphine oxide-gold adduct. It should be noted that O=PPh$_3$ in ^{31}P NMR shows a single peak at δ 29 ppm.[246–248]

In fact, preparation of a *true* Au(III):phosphine complex Au^I(PPh$_3$)Cl$_3$ has been reported in the literature.[249,250] This literature method reports that the Au(III) species must be prepared first from Au^I(PPh$_3$)Cl and then by subsequent oxidation to form the Au^{III}(PPh$_3$)Cl$_3$ by bubbling of Cl$_2$ gas into the solution of Au^I(PPh$_3$)Cl. There is no previous report for the synthesis of Au^{III}(PPh$_3$)Cl$_3$ directly from KAuCl$_4$ and PPh$_3$, and the resulting Au(I) species and O=PPh$_3$ were proposed to be formed from a redox type reaction. Thus, *in situ* reduction of Au(III) would result in the formation of a Au(I) species, and concomitant oxidation of PPh$_3$ might occur to generate O=PPh$_3$. Considering this possibility, if KAuCl$_4$ reacts with PPh$_2$-PEGPIIL, the postulated structure of the *actual* product **3.9** would be the corresponding diphenylphosphine oxide from oxidation of PPh$_2$-PEGPIIL, associated with the Au(I)Cl species (Scheme **3.9**).
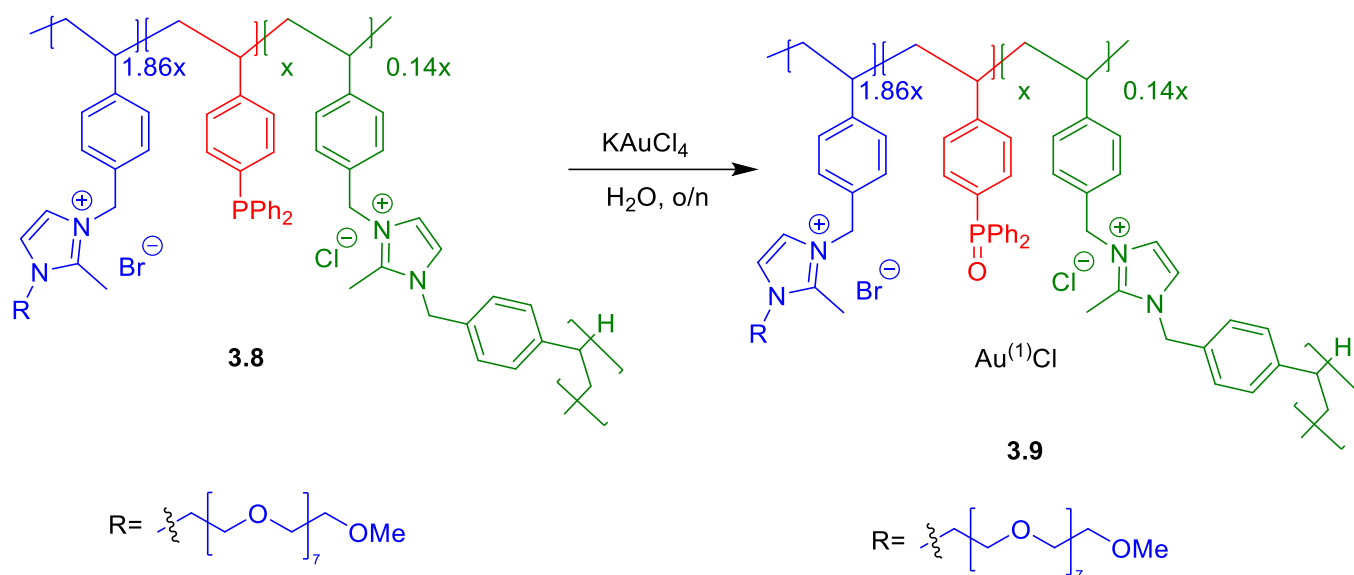
Scheme 3.9: The suspected potential reaction occurring during the synthesis of catalyst precursor **3.9**.

In order to support this hypothesis, we planned to attempt to prepare the authentic [AuCl$_4$]@PPh$_2$-PEGPIIL by Cl$_2$-induced oxidation of a Au(I) precursor. Before attempting this chemistry on the polymer-supported system, we first chose to undertake all of the necessary reactions on the simple Ph$_3$P series: this would entail preparation of O=PPh$_3$ **3.10**, Au^I(PPh$_3$)Cl **3.12**, and then Au^{III}(PPh$_3$)Cl$_3$ **3.15** by subsequent oxidation using Cl$_2$ gas. These model compounds would also be useful for exploring the NMR characteristics of each species.

3.2.3.2 Synthesis of O=PPh$_3$ (3.10)
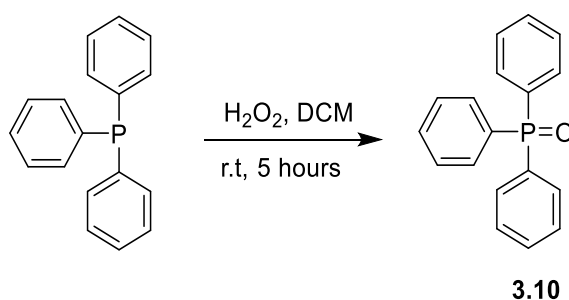
Scheme 3.10: Synthesis of O=PPh$_3$ **3.10**.

The oxidation of triphenylphosphine to triphenylphosphine oxide was performed using H$_2$O$_2$ in order to confirm the method to be used later for the polymer supported phosphine. The preparation

of O=PPh$_3$ **3.10** was carried out according to a method used previously b**y** Dubován et *al*. [247] PPh$_3$ was oxidised by H$_2$O$_2$ in 5 hours using dichloromethane as solvent. After that time, the two layers were separated, and the solvent was removed to afford O=PPh$_3$ **3.10** as a fine white powder in 94%. The ^{31}P NMR spectrum of O=PPh$_3$ **3.10** indicated a change in chemical shift from δ -5.46 ppm for PPh$_3$ to δ 29.4 ppm for O=PPh$_3$, which agrees with the literature.[247]

3.2.3.3 Synthesis of Au^I(PPh$_3$)Cl (3.12)

3.11

3.12
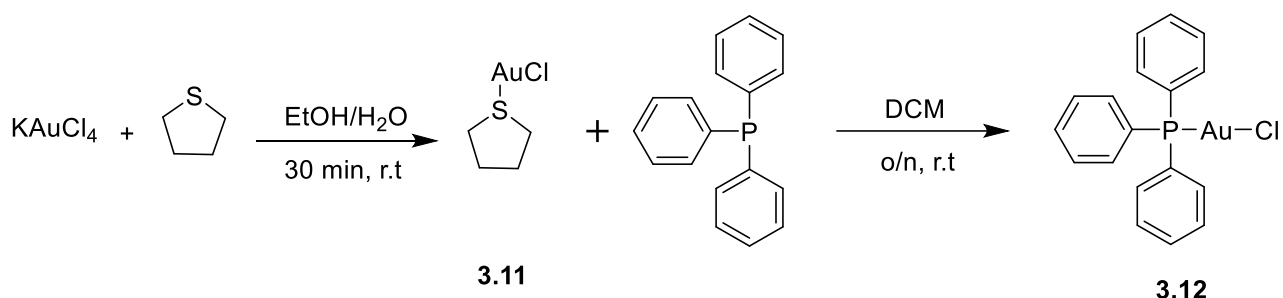
Scheme 3.11: Synthesis of Au^I(PPh$_3$)Cl **3.12**.

Au^I(PPh$_3$)Cl **3.12** was synthesised in two steps following literature procedures, shown in Scheme **3.11**. Firstly, we started by synthesising Au^I(THT)Cl **3.11** by the reaction of KAuCl$_4$ with excess THT in ethanol/water mixture, which resulted in the formation of a white precipitate.[392] The obtained white precipitate was isolated by filtration and washed with ethanol. In this reaction, the Au(III) is reduced to Au(I), and one equivalent of the THT is oxidised to tetrahydrothiophene-1-oxide. In the next step, Au^I(THT)Cl **3.11** and triphenylphosphine were dissolved in dichloromethane and stirred overnight at room temperature. The resulting white precipitate was filtered and washed with ethanol, diethyl ether, dried under high vacuum and then recrystallised from chloroform/hexane to give **3.12** in 71%. The ^{31}P NMR spectrum of **3.12** showed a single peak at δ 33.19 ppm, as shown in Figure **3.10**, and this agrees with work reported by Price et *al*.[251]
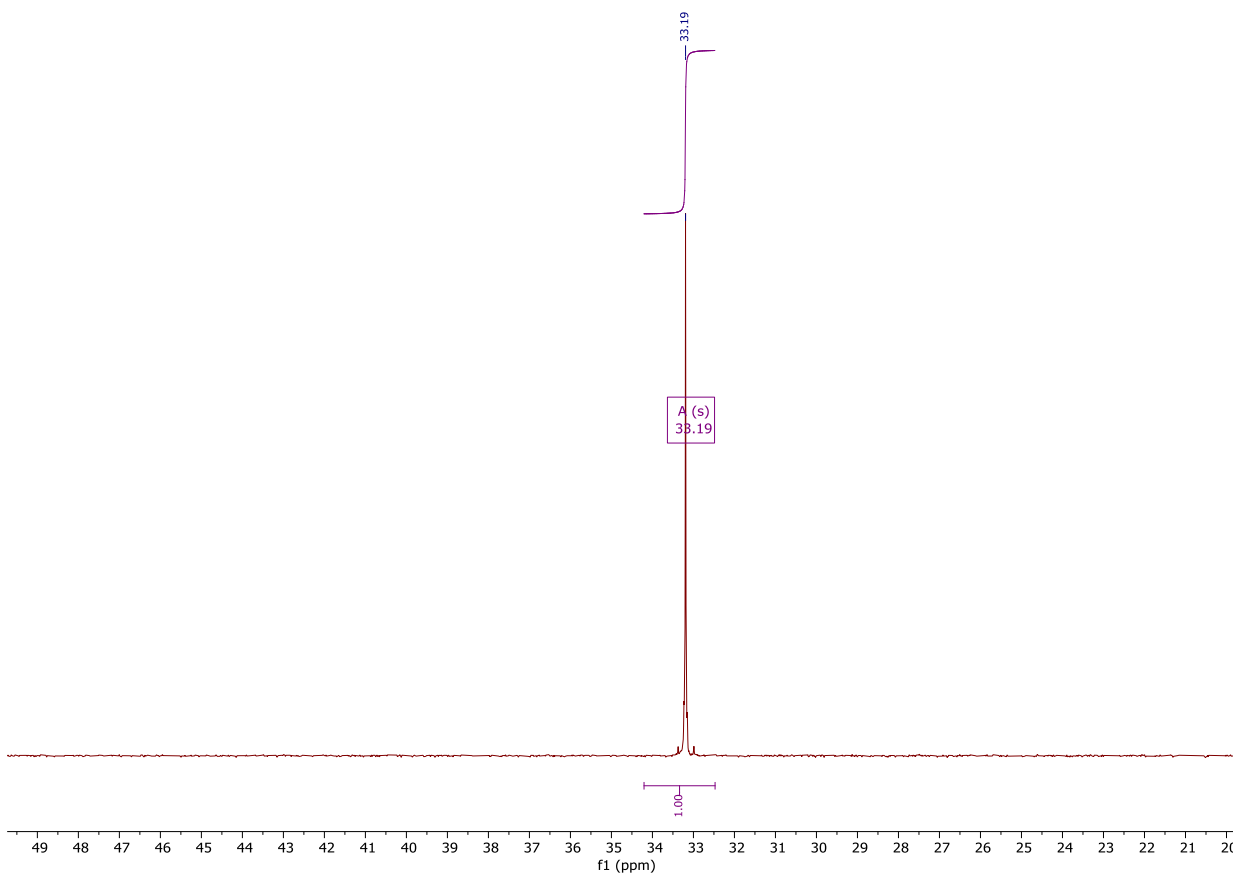
Figure 3.10: ^{31}P (121 MHz, CDCl$_3$) NMR spectrum of Au^I(PPh$_3$)Cl **3.12**.

Figure **3.11** shows the stacked ^{31}P NMR spectra of pure samples of PPh$_3$, O=PPh$_3$ **3.10**, and Au^I(PPh$_3$)Cl **3.12** and illustrates the chemical shift differences between the three species.
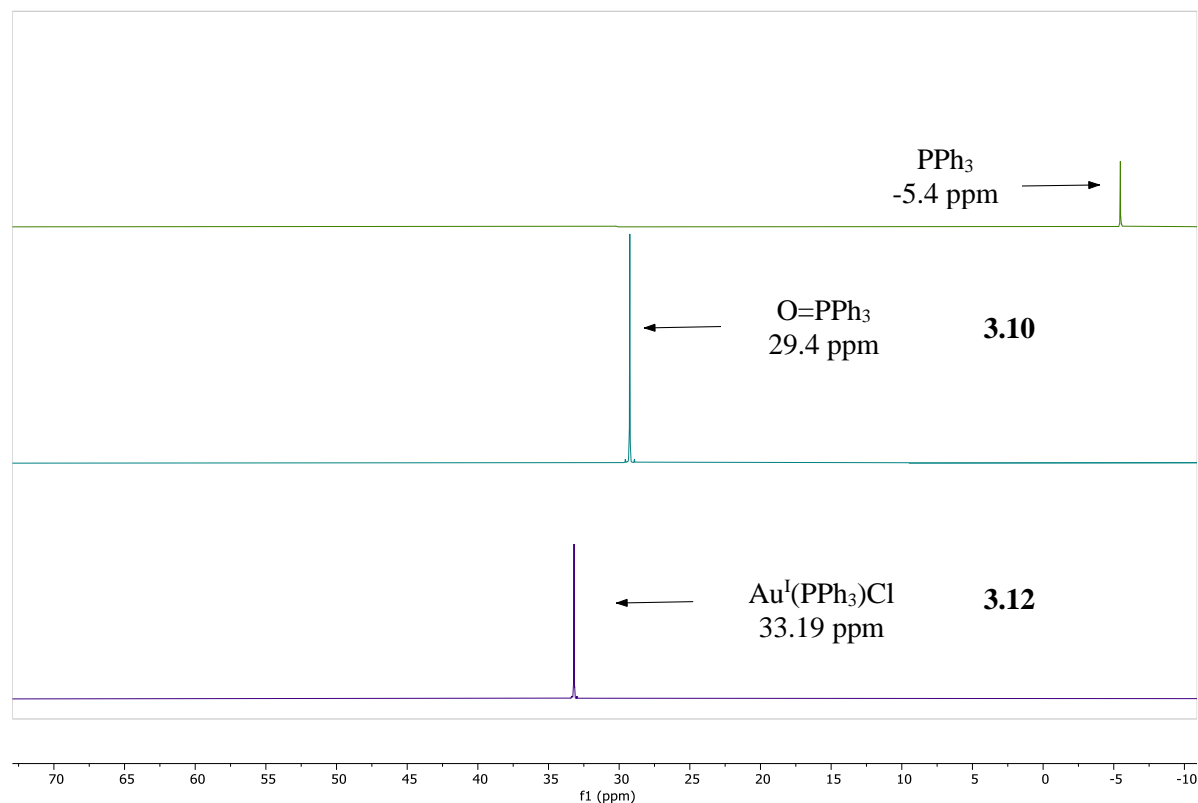
Figure 3.11: ^{31}P (121 MHz, CDCl$_3$) NMR spectra of PPh$_3$, O=PPh$_3$ **3.10** and Au^{I}(PPh$_3$)Cl **3.12.**

In order to explore the proposed Au(III)-induced phosphine oxidation, a solution of KAuCl$_4$ in dry ethanol and a solution of PPh$_3$ in dry dichloromethane were mixed in a Schlenk flask under N$_2$ and stirred vigorously overnight. The ^{31}P NMR spectrum of the resulting mixture revealed that PPh$_3$ was completely consumed. In addition to a singlet at δ 33 ppm, assigned to Au^{I}(PPh$_3$)Cl, a singlet at δ 29 ppm was confirmed to be due to O=PPh$_3$ by subsequent spiking of the mixture with pure O=PPh$_3$ **3.10**. In addition, a new peak appeared at δ 62 ppm, which was assigned as a PPh$_3$Cl$_2$-based transient intermediate. This assignment was confirmed by spiking the sample with a small amount of the commercially-available PPh$_3$Cl$_2$.[246] In a separate experiment, after 15 hours of stirring, a white precipitate was obtained through filtration and ^{31}P NMR analysis indicated that it was Au^{I}(PPh$_3$)Cl (Figure **3.12**).
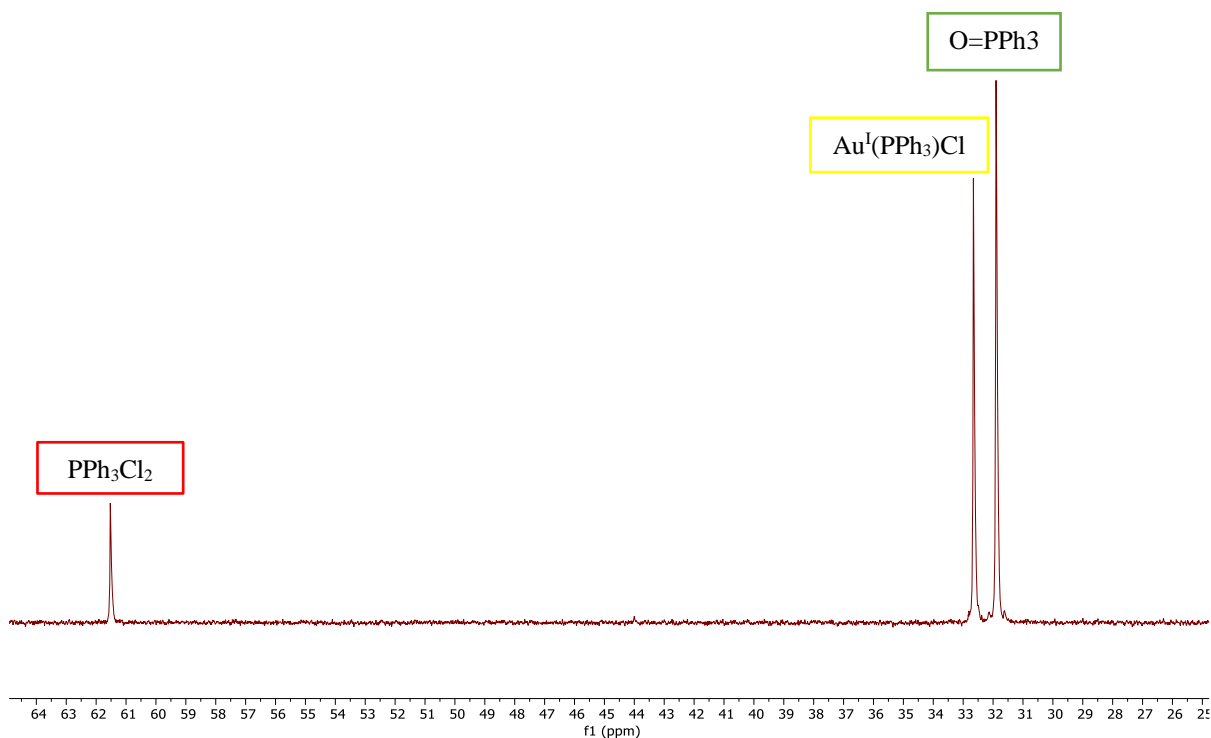
Figure 3.12: ^{31}P (202 MHz, EtOH/CH$_2$Cl$_2$) NMR spectrum of the reaction mixture (KAuCl$_4$ + PPh$_3$) after 15 hours.

A similar experiment was scaled down to fit inside an NMR tube, allowing us to monitor the reaction at different times using ^{31}P NMR. Over 18 hours, this experiment showed that the intensity of the O=PPh$_3$ **3.10** peak at δ 29 ppm rises with time, the Au^I(PPh$_3$)Cl **3.12** signal at δ 33 ppm also rises with time, but much less strongly, while the signal at δ 62 ppm diminishes over time (Figure **3.13**).
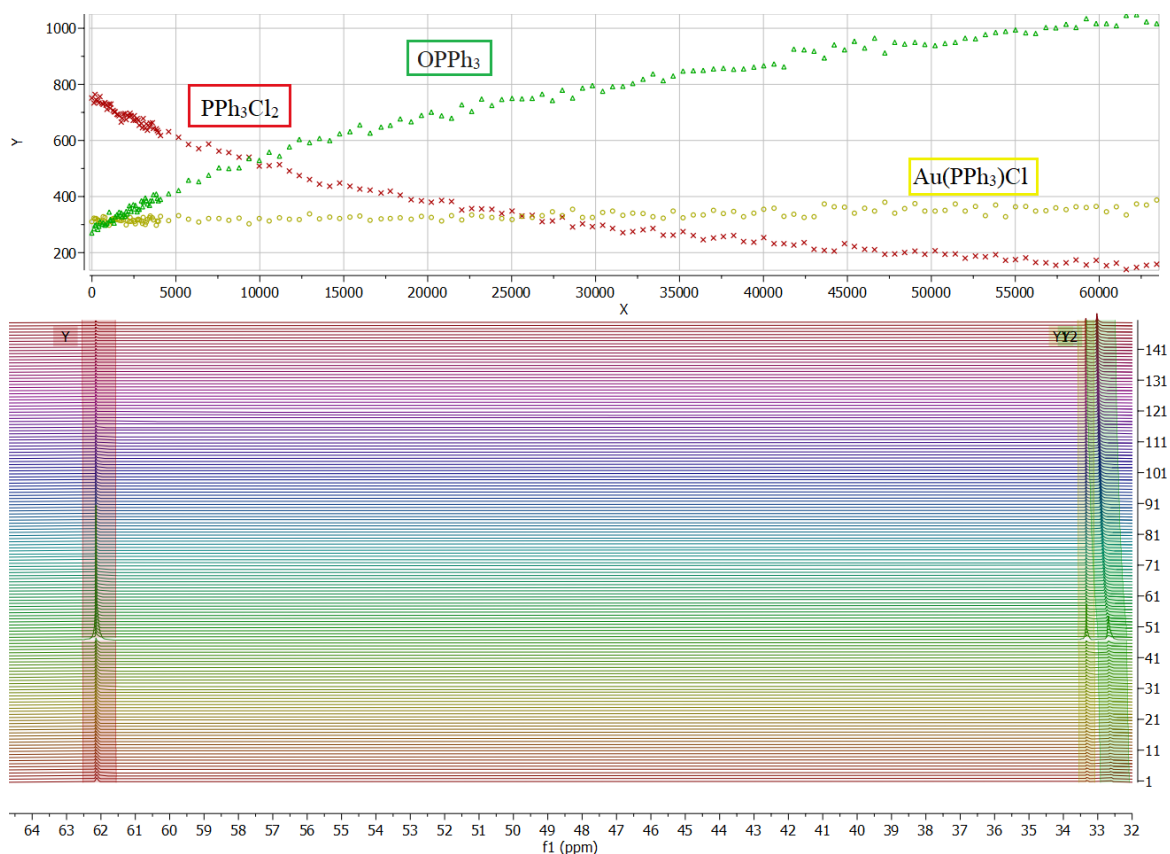
Figure 3.13: A stacked plot of ^{31}P (202 MHz, EtOH/CH$_2$Cl$_2$) NMR spectra over 18 hours.

Interestingly, a new peak appeared at δ 44 ppm after 24 hours, as shown in Figure **3.14**. The chemical shift of this peak would be consistent with $Au^{III}(PPh_3)Cl_3$ as reported by Attar et al.[249], who oxidised $Au^I(PPh_3)Cl$ to $Au^{III}(PPh_3)Cl_3$ by treatment with Cl_2 gas. Consequently, we decided to synthesise $Au^{III}(PPh_3)Cl_3$ by oxidising $Au^I(PPh_3)Cl$ **3.12** in order to enable an NMR spiking experiment to confirm the identity of the new species in the reaction mixture.
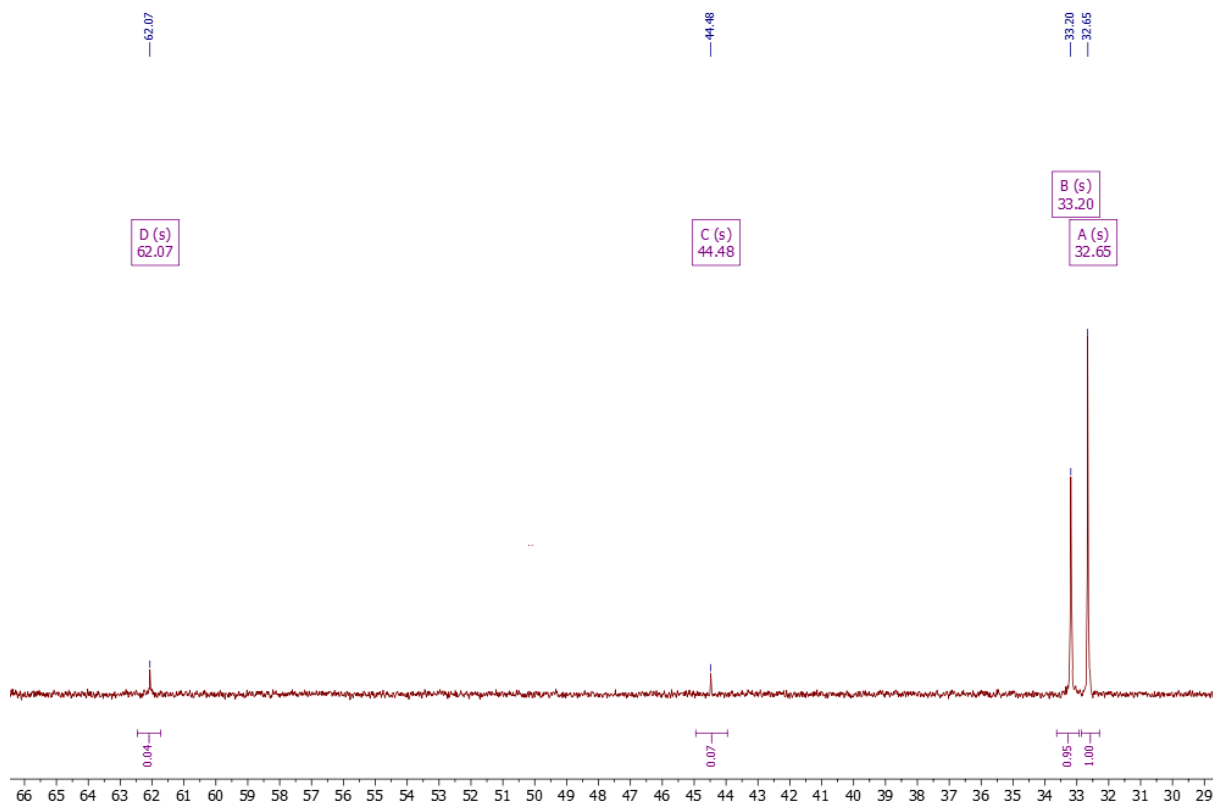
Figure 3.14: ^{31}P (202 MHz, EtOH/CH$_2$Cl$_2$) NMR spectrum of the reaction mixture (KAuCl$_4$ + PPh$_3$) after 24 hours indicating the possible formation of a gold(III) phosphine complex (δ 44.5 ppm).

3.2.3.4 Synthesis of Au^{III}(PPh$_3$)Cl$_3$ (3.13)
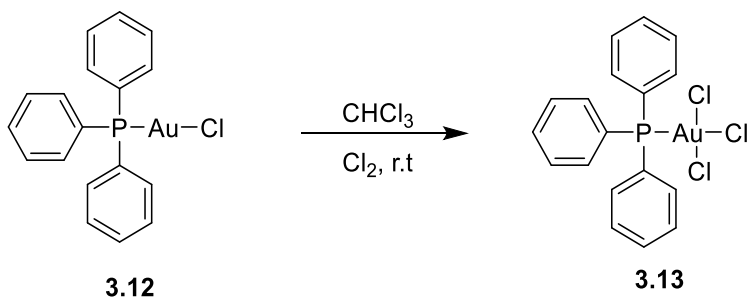
Scheme 3.12: Synthesis of Au^{III}(PPh$_3$)Cl$_3$ **3.12**

Following Attar's procedure, chlorine gas was bubbled through a chloroform solution containing Au^{I}(PPh$_3$)Cl **3.12** while the solution was stirring. The solution turned from colourless to bright yellow within seconds. The solvent was removed, and the solid result was washed with hexane and

diethyl ether. The ^{31}P spectrum of Au^{III}(PPh$_3$)Cl$_3$ **3.13** revealed (Figure **3.15**) a single peak at δ 44 ppm, consistent with that previously reported by Attar et *al.*[249]
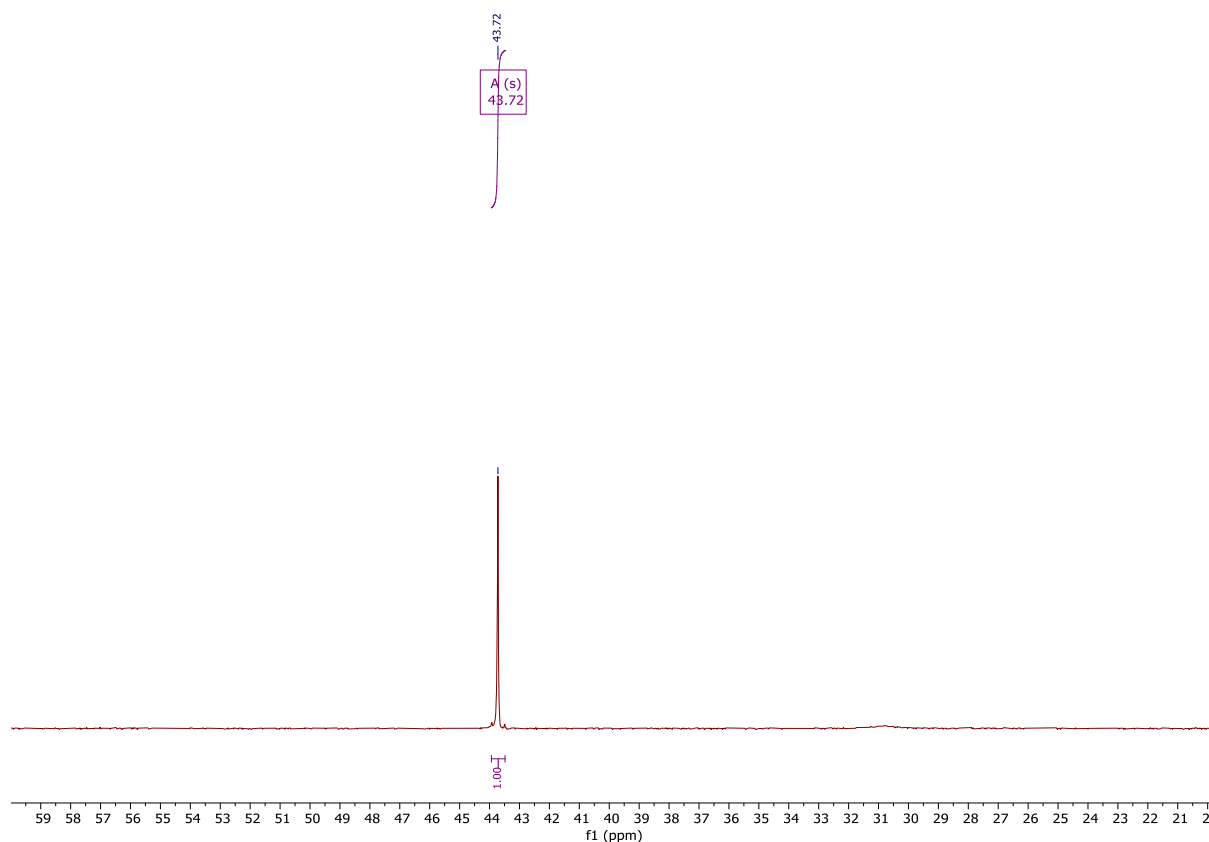
Figure 3.15: ^{31}P (162 MHz, CDCl$_3$) NMR spectrum of Au^{III}(PPh$_3$)Cl$_3$ **3.13**.

Therefore, with the desired Au^{III}(PPh$_3$)Cl$_3$ **3.13**, we proceed to do a spiking experiment by addition to the NMR sample we had in Figure **3.14**. Notably, an increase in the peak that appeared at δ 44 ppm confirmed that this peak indeed corresponds to Au^{III}(PPh$_3$)Cl$_3$. (Figure **3.16**).
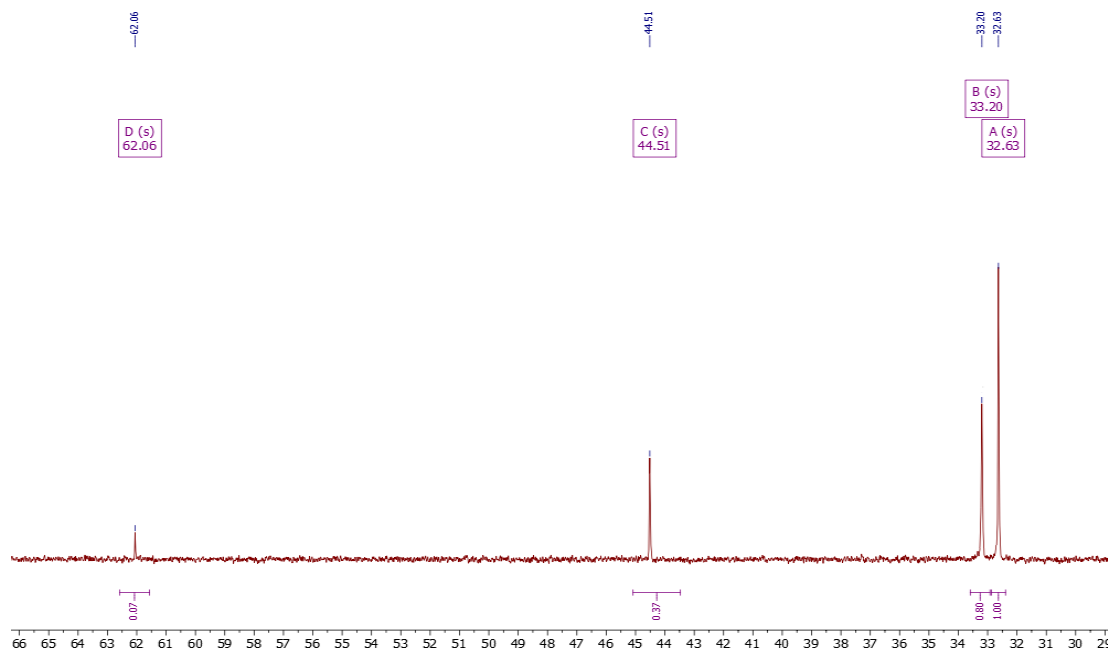
Figure 3.16: The spiking ^{31}P (202 MHz, EtOH/CH$_2$Cl$_2$) NMR spectrum after adding Au^{III}(PPh$_3$)Cl$_3$ **3.13** (compare to Figure **3.14**).

The previous experiments demonstrated that when triphenylphosphine is mixed with KAuCl$_4$, a redox reaction occurs, with most of the phosphine being oxidised to triphenylphosphine oxide and most of the gold(III) being reduced to gold(I). In addition, a small amount of the gold(III)-phosphine complex is also formed. A question remains over the source of the oxygen atom which becomes incorporated into the phosphine oxide. It is possible that this arises simply from a very small amount of adventitious water, which is difficult to exclude from ethanol. Alternatively it may come from ethanol itself, which would require the concomitant formation of either chloroethane or diethyl ether. A proposed mechanism for the formation of O=PPh$_3$, Au(I), and Au(III) species is shown in the scheme below (Scheme **3.13**); the use of both ethanol and water as potential nucleophilic sources of the oxygen are included for illustration.
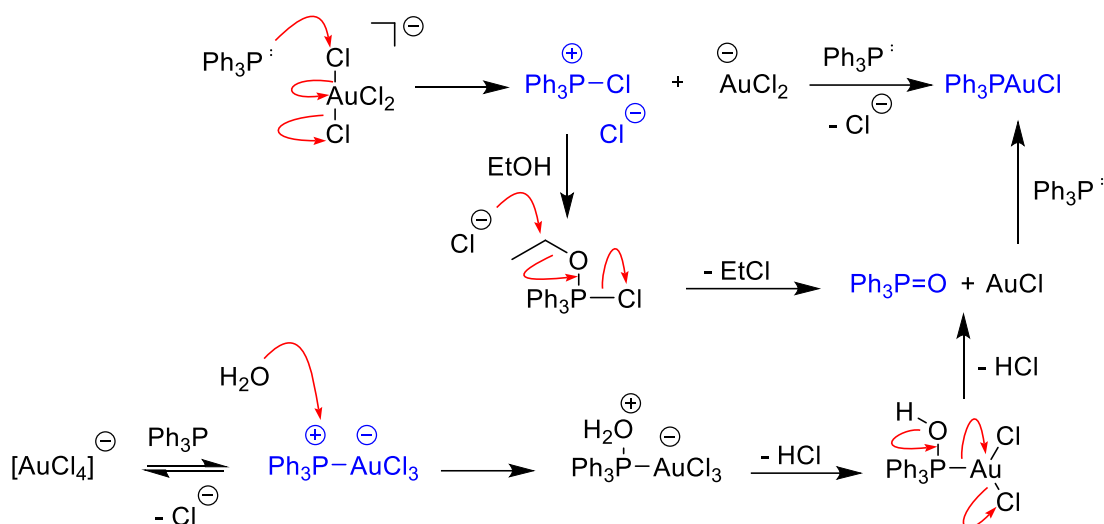
Scheme 3.13: Proposed redox mechanism for reaction between Au(III) and phosphine.

We have established that, in practice, attempted formation of [AuCl$_4$]@PPh$_2$-PEGPIIL adduct **3.9** proceeds by unexpected oxidation of the phosphine and reduction of the gold(III) to gold(I) during the impregnation of the PPh$_2$-PEGPIIL support **3.8** with KAuCl$_4$ to give a mixture of phosphine oxide, Au(I) and a small amount of Au(III) after 24 hours.

Thus, the next plan was to synthesise an authentic sample of [AuCl$_4$]@PPh$_2$-PEGPIIL by oxidation of the corresponding gold(I) to gold(III) by treatment with Cl$_2$ gas in the same way as was used above to prepare Au^{III}(PPh$_3$)Cl$_3$ **3.13**.

3.2.3.5 Synthesis [AuCl]@PPh2-PEGPIIL (3.14)
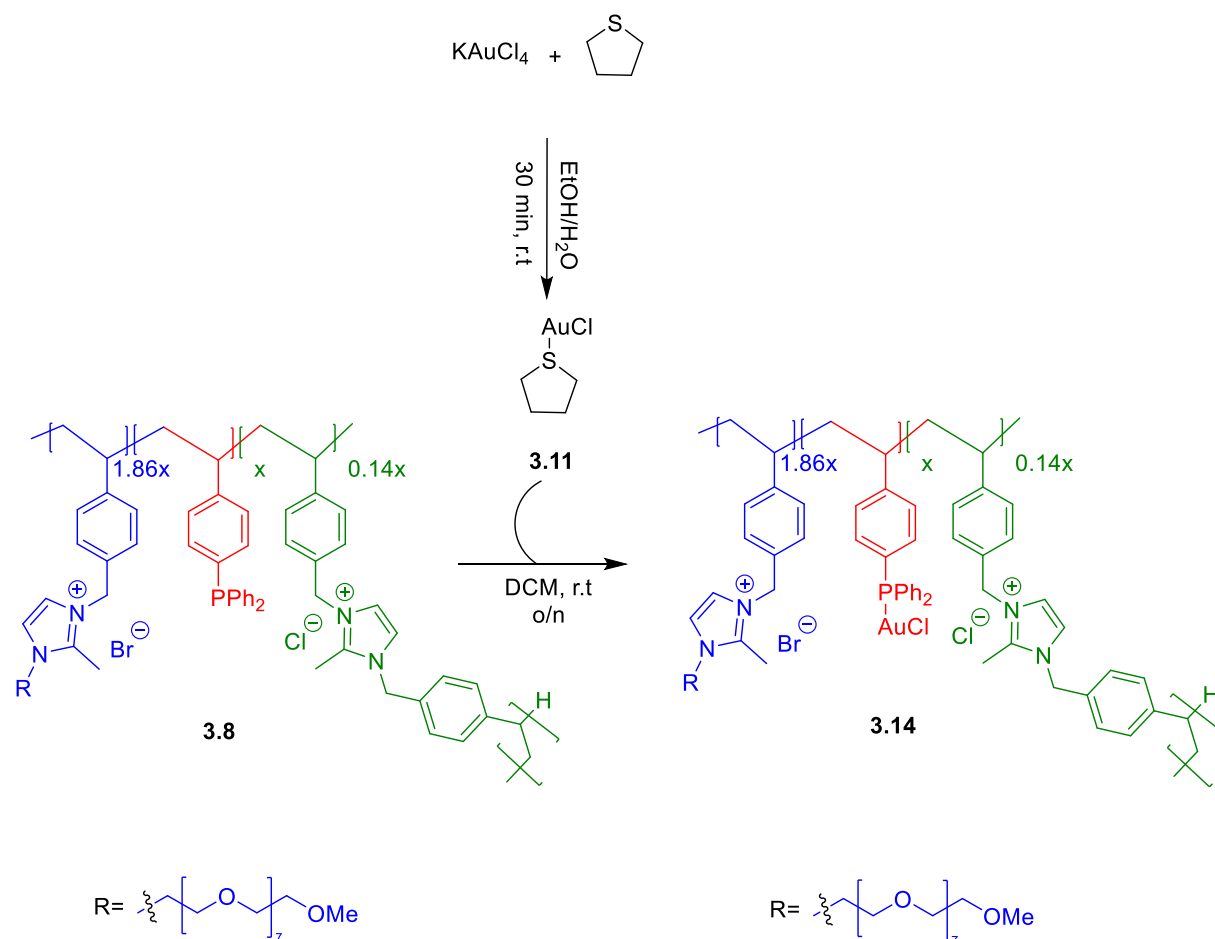
Scheme 3.14: Synthesis of [AuCl]@PPh$_2$-PEGPIIL **3.14**.

[AuCl]@PPh$_2$-PEGPIIL **3.14** was synthesised in two steps, as shown in Scheme **3.14**. Firstly, Au(THT)Cl **3.11** was prepared as reported previously in the synthesis of Au^I(PPh$_3$)Cl **3.12**. Secondly, Au(THT)Cl **3.11** was reacted with PPh$_2$-PEGPIIL **3.8** in DCM overnight. After that, the solvent was removed under reduced pressure. The residue was dissolved in dichloromethane and purified by re-precipitation in diethyl ether, filtering, washing, and drying under high vacuum to afford [AuCl]@PPh$_2$-PEGPIIL **3.14** as an off-white solid in 95% yield. The ^{31}P NMR spectrum of **3.14** indicated complete disappearance of the singlet around δ -5 to -8 ppm for PPh$_2$-PEGPIIL and appearance of a single peak at δ 33.65 ppm, indicating the formation of phosphine coordinated to AuCl.

3.2.3.6 Attempted synthesis of [AuCl₄]@PPh₂-PEGPIIL (3.15)
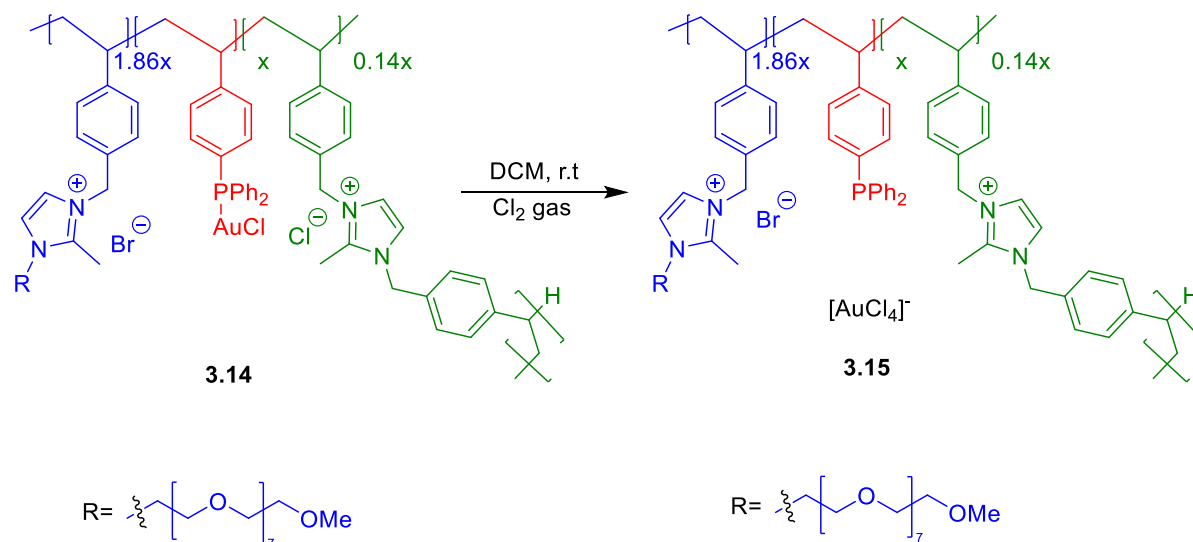
Scheme 3.15: Attempted synthesis of [AuCl₄]@PPh₂-PEGPIIL **3.15**.

Following Attar's procedure,[249] chlorine gas was bubbled through a dry dichloromethane solution containing [AuCl]@PPh₂-PEGPIIL **3.14** while the solution was stirring. As observed in the corresponding reaction using triphenylphosphine, the solution turned from colourless to bright yellow within seconds. The solvent was removed by an external trap, and the resulting oily product was washed with hexane, diethyl ether and dried under high vacuum to afford what was hoped to be [AuCl₄]@PPh₂-PEGPIIL **3.15** as a yellow oil. Unfortunately, the ^{31}P NMR spectrum indicated two peaks; the first peak appeared at δ 44 ppm, which was assigned to the desired gold(III) phosphine complex, and the second was an intense peak at δ 29 ppm which was assigned to the formation of the phosphine oxide. Also, no peak was observed at δ 33 ppm, which indicates the Cl₂ oxidised all the gold(I) to the gold(III) (Figure **3.17**).
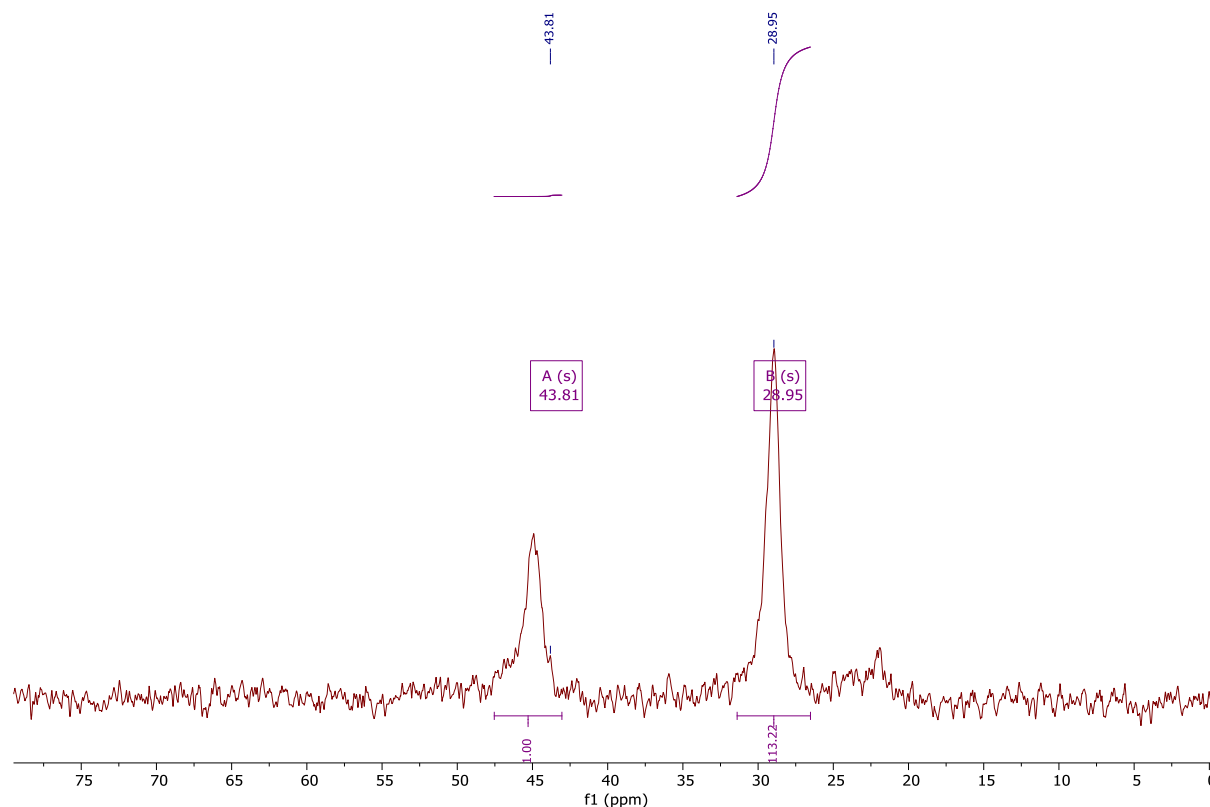
Figure 3.17: ^{31}P (121 MHz, CDCl$_3$) NMR spectrum for [AuCl$_4$]@PPh$_2$-PEGPIIL **3.15**.

The reaction was repeated increasing both the reaction time and Cl$_2$ gas amount bubbling through the solution to ensure complete oxidation of the gold(I) to gold(III) and minimise formation of O=PPh$_3$, but still we got the same results. In addition, the colour of the (impure) gold(III) complex was observed to change from a yellow oil to black overnight. The [AuCl$_4$]@PPh$_2$-PEGPIIL appears to be thermally unstable and decomposed even in the absence of light, when stored in an inert atmosphere in the freezer. Due to the difficulty and high cost of preparation, the formation of a mixture with phosphine oxide, and the instability of the gold(III)-phosphine containing polymer we chose not to undertake further work on this species.

Consequently, we choose to oxidise the polymer in order to synthesise a phosphine oxide-derived gold precursor, to enable testing and comparison of the selectivity and activity to *in situ* formed gold(I) phosphine oxide adduct **3.9**.

3.2.3.7 Synthesis of O=PPh₂-PEGPIIL (3.16)
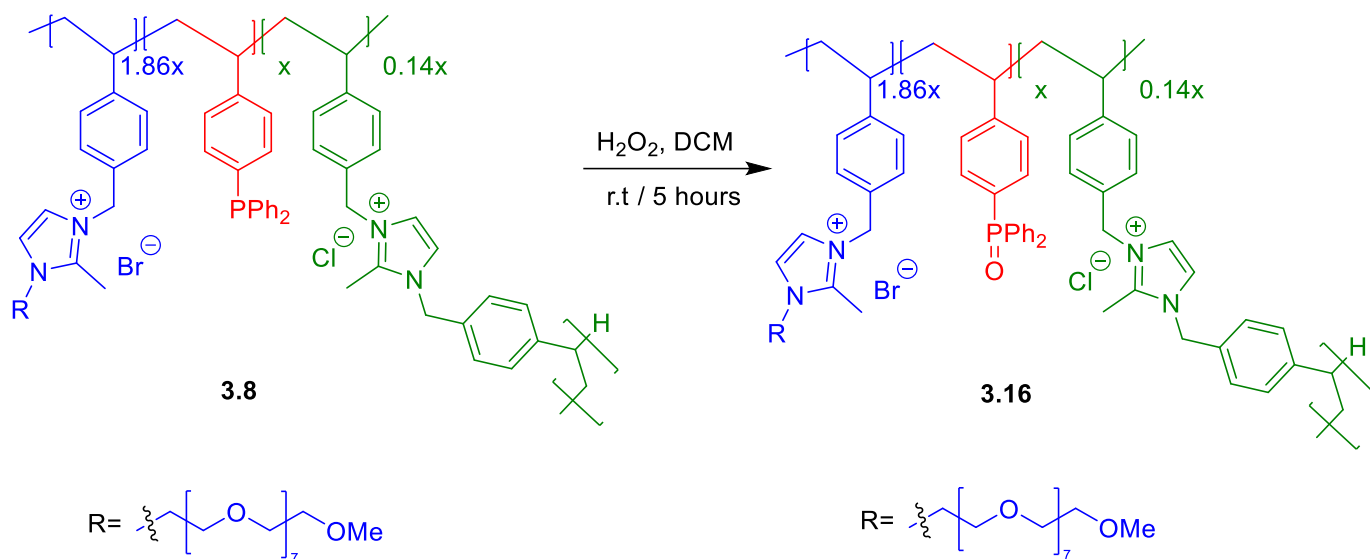
Scheme 3.16: Synthesis of O=PPh₂-PEGPIIL **3.16**.

O=PPh$_2$-PEGPIIL **3.16** was synthesised in the same manner as O=PPh$_3$ **3.10**. Hydrogen peroxide was used to oxidise PPh$_2$-PEGPIIL **3.8** and delivered a clean product **3.16** as a white solid in a 90% yield. A single peak at δ 29.63 ppm was observed in ^{31}P NMR spectrum of **3.16**, indicating phosphine oxide formation. Also, no peak was observed between δ -5 to δ -8 ppm, indicating complete phosphine consumption.

3.2.3.8 Synthesis of [AuCl₄]@O=PPh₂-PEGPIIL (3.17)
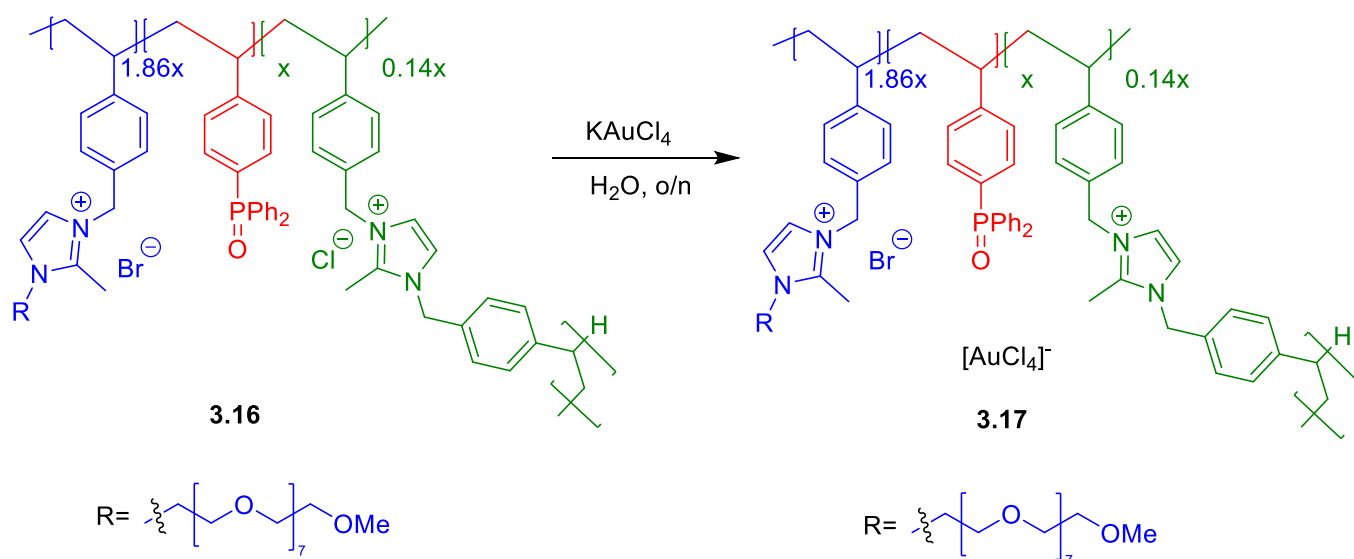
Scheme 3.17: synthesis of [AuCl₄]@O=PPh₂-PEGPIIL 3.17.

To synthesise the [AuCl₄]@O=PPh₂-PEGPIIL, we followed the published method[83] as shown in Scheme 3.17. The phosphine oxide-containing polymer 3.16 and KAuCl₄ were dissolved in water, and the mixture was stirred overnight at room temperature. After that, the water was removed by an external trap. The residue was re-dissolved in DCM followed by re-precipitation in diethyl ether filtering, washing, and drying under high vacuum to afford [AuCl₄]@O=PPh₂-PEGPIIL 3.17 as an orange powder in 92% yield and stored in a Schlenk flask under N_2.

3.2.3.9 ICP Optical Emission Spectrometry (ICP-OES)

The gold content in the precursors *[AuCl]@O=PPh₂-PEGPIIL* 3.9, [AuCl]@PPh₂-PEGPIIL 3.14 and [AuCl₄]@O=PPh₂-PEGPIIL 3.17 was determined by inductively coupled plasma optical emission spectroscopy (ICP-OES) (Table 3.1).

Table 3.1: Gold content of PIIL precursors as determined by ICP-OES.

Entry	precursor	mmol Au/ g	Au wt%
1	*[AuCl]@O=PPh₂-PEGPIIL* adduct **3.9**	0.43	8.61
2	[AuCl]@PPh$_2$-PEGPIIL **3.14**	0.45	8.94
3	[AuCl$_4$]@O=PPh$_2$-PEGPIIL **3.17**	0.41	8.15

The low Au contents are likely because of the PEG functionality, which may be associated with absorbed solvent and moisture from the air.

3.2.3.10 Scanning Electron Microscopy (SEM)

SEM analysis of the freshly prepared gold precursors exposed a clear difference in the surface morphology against the polymer **3.8** (Figure **3.8**). In this instance, the gold precursors materials have a more granular texture, potentially due to the additional processing step during the impregnation with the polymer materials.
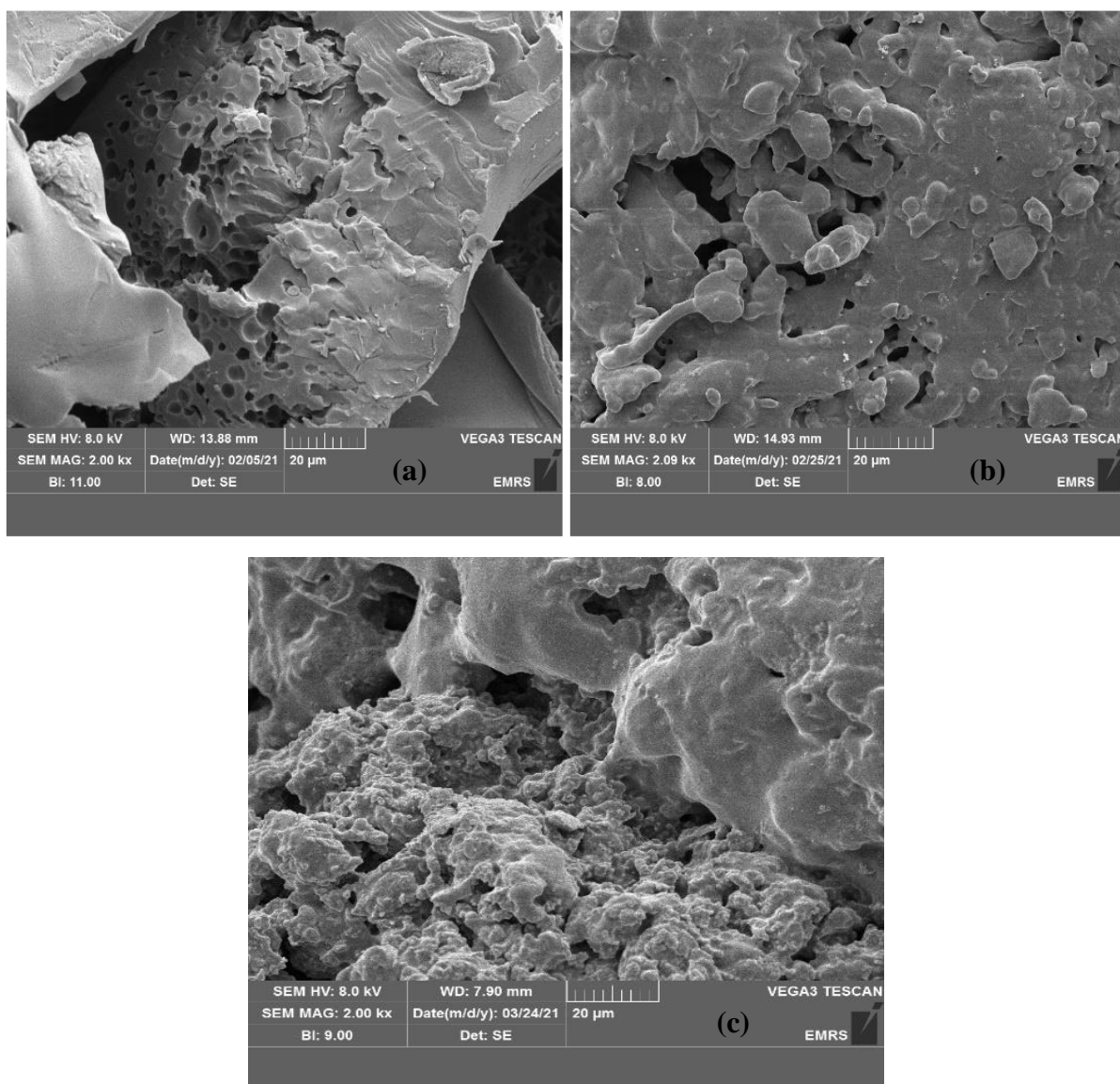
Figure 3.18: SEM images of (a) *[AuCl]@O=PPh₂-PEGPIIL* adduct **3.9**, (b) [AuCl]@PPh₂-PEGPIIL **3.14** and (C) [AuCl₄]@O=PPh₂-PEGPIIL **3.17**.

3.2.3.11 Transmission Electron Microscopy (TEM) of Gold Nanoparticle-Containing PIIL

In order to generate gold nanoparticle-containing PIIL, each of the three precursors *[AuCl]@O=PPh₂-PEGPIIL* adduct **3.9**, [AuCl]@PPh₂-PEGPIIL **3.14** and [AuCl₄]@O=PPh₂-PEGPIIL **3.17** was reduced *in situ* by treatment with water and 2.5 equivalents of NaBH₄ under the conditions used for nitrobenzene (**NO2**) reduction.

TEM analysis was performed to characterise the isolated AuNPs and to determine their mean diameters. TEM micrographs revealed that the AuNPs are small, near monodisperse with average diameters of 2.9 ± 0.9, 1.7 ± 0.5 and 2.1 ± 0.7, respectively. The representative micrographs and histograms of particle distribution based on >100 particles are shown in Figure **3.19**.
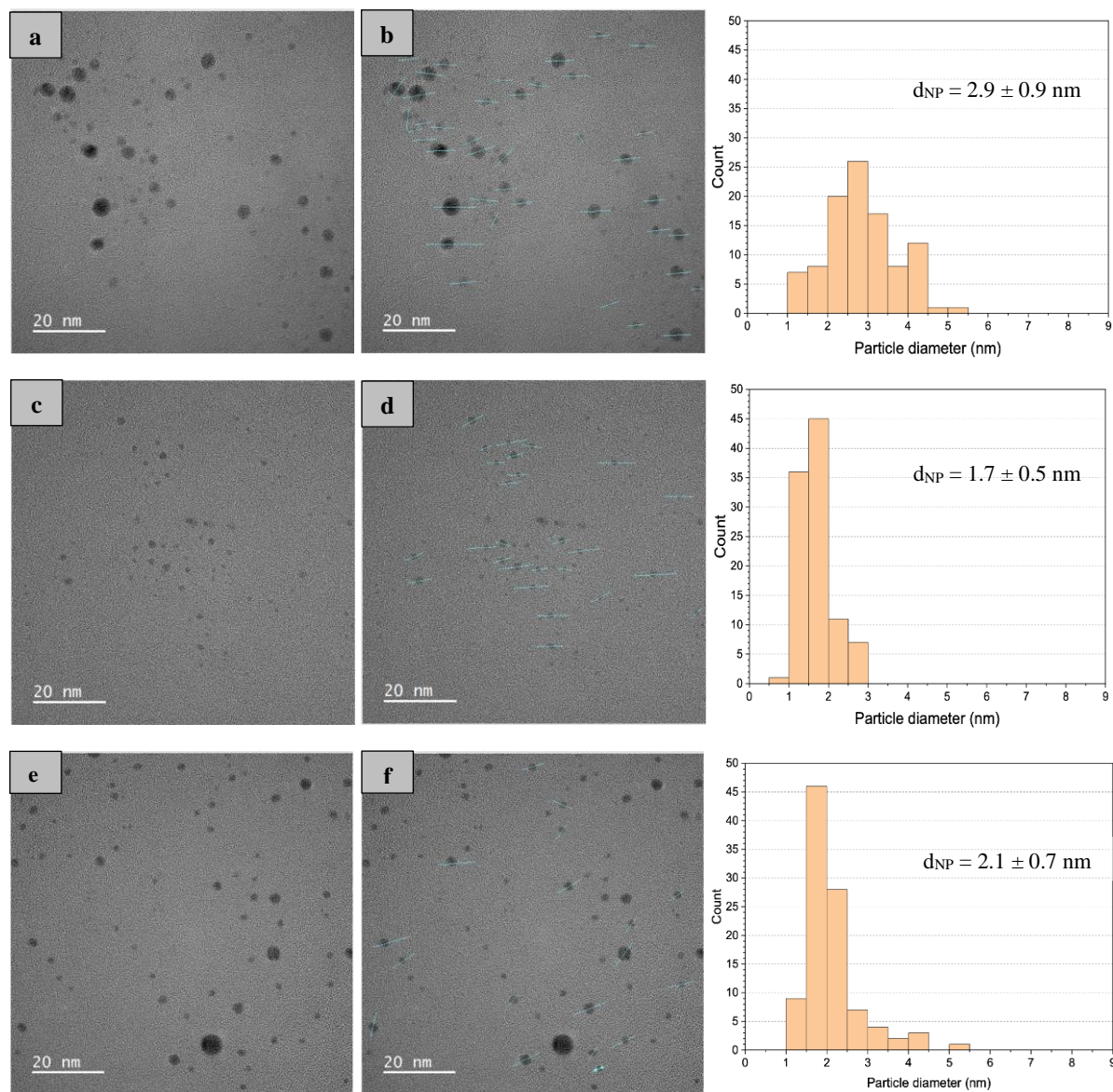
Figure 3.19: HRTEM micrographs of nanoparticles formed from: (a-b) *[AuCl]@O=PPh$_2$-PEGPIIL* adduct **3.9**, (c-d) [AuCl]@PPh$_2$-PEGPIIL **3.14** and [AuCl$_4$]@O=PPh$_2$-PEGPIIL 3.**17** (e-f) and corresponding size distributions determined by counting >100 particles.

It can be seen from the histograms that nanoparticles generated from [AuCl$_4$]@O=PPh$_2$-PEGPIIL **3.17** have a mean diameter of 2.1 ± 0.7 nm, which is similar to those formed from the *in situ-*

generated *[AuCl]@O=PPh₂-PEGPIIL* adduct **3.9.** The size distribution of the nanoparticles generated from **3.9** is similar to that reported in the previously published paper.[83]

In contrast, the TEM images of nanoparticles derived from [AuCl]@PPh$_2$-PEGPIIL **3.14** show that gold nanoparticles are smaller than the other two catalysts. While this result is unexpected, this may help to explain differences in catalyst performance caused purely by the Au-support interaction.

3.2.4   Catalytic Reduction of Nitrobenzene (NO2)

3.2.4.1 Sodium borohydride as reducing agent

The catalytic reduction of nitrobenzene (**NO2**) was thus explored in order to assess and compare the catalytic efficiency of AuNP@PPh$_2$-PEGPIIL derived from the *[AuCl]@O=PPh$_2$-PEGPIIL* adduct **3.9** with that of [AuCl]@PPh$_2$-PEGPIIL **3.14** and [AuCl$_4$]@O=PPh$_2$-PEGPIIL **3.17**. For this, we have followed and adopted the exact approach established previously[83] with the intention of comparing our findings with that of the previous results and to investigate the influence of the nature of both the support and nanoparticles on the catalytic efficiency. The transfer-hydrogenation reaction of nitrobenzene (**NO2**) mediated by NaBH$_4$ was therefore selected as the benchmark for the catalyst testing experiments. NaBH$_4$ plays a dual role in these reactions, it not only serves as the hydrogen source for nitro group reduction but also reduces the Au-based catalyst precursors *[AuCl]@O=PPh$_2$-PEGPIIL* adduct **3.9**, [AuCl]@PPh$_2$-PEGPIIL **3.14** and [AuCl$_4$]@O=PPh$_2$-PEGPIIL **3.17** *in situ* to form the corresponding AuNPs (Scheme **3.18**).
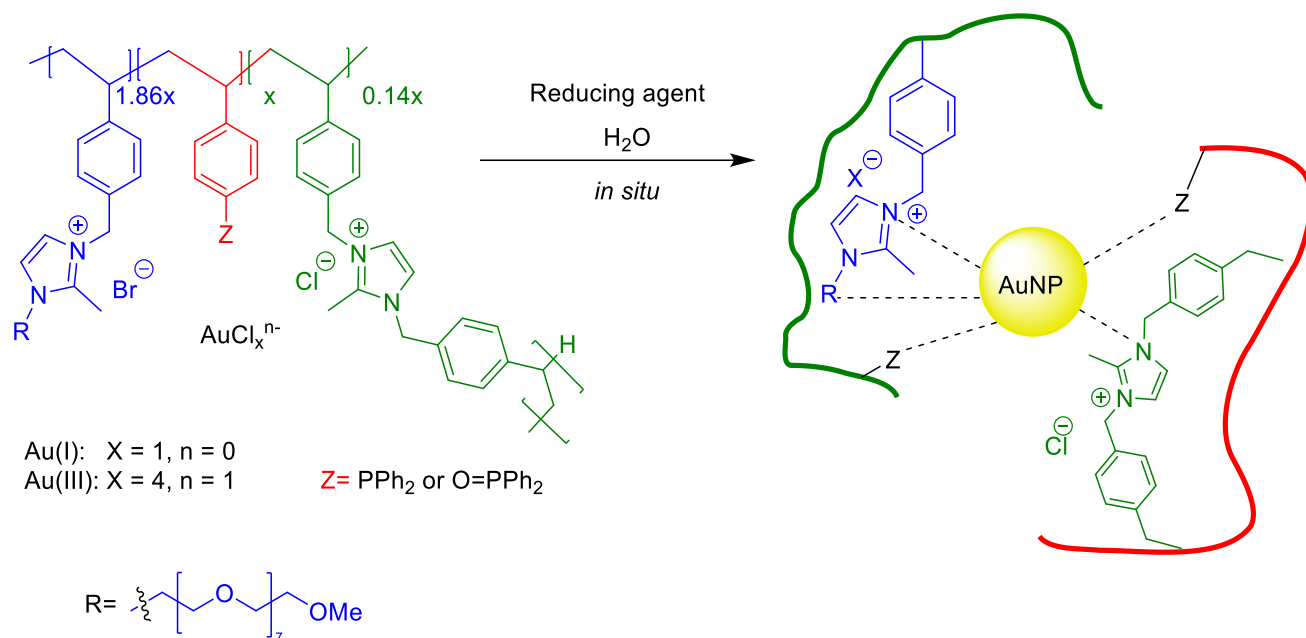
Scheme 3.18: Preparation of AuNP@PPh$_2$-PEGPIIL catalysts from gold precursors.

The conversion and selectivity of the reduction of nitrobenzene (**NO2**) by using the AuNPs were calculated by utilising ^{1}H NMR spectroscopy. For this, the reaction mixture was directly analysed by ^{1}H NMR. All the key intermediates of reduction of nitrobenzene (**NO2**) were identified by careful determination of their characteristic signals (Figure **3.20**).
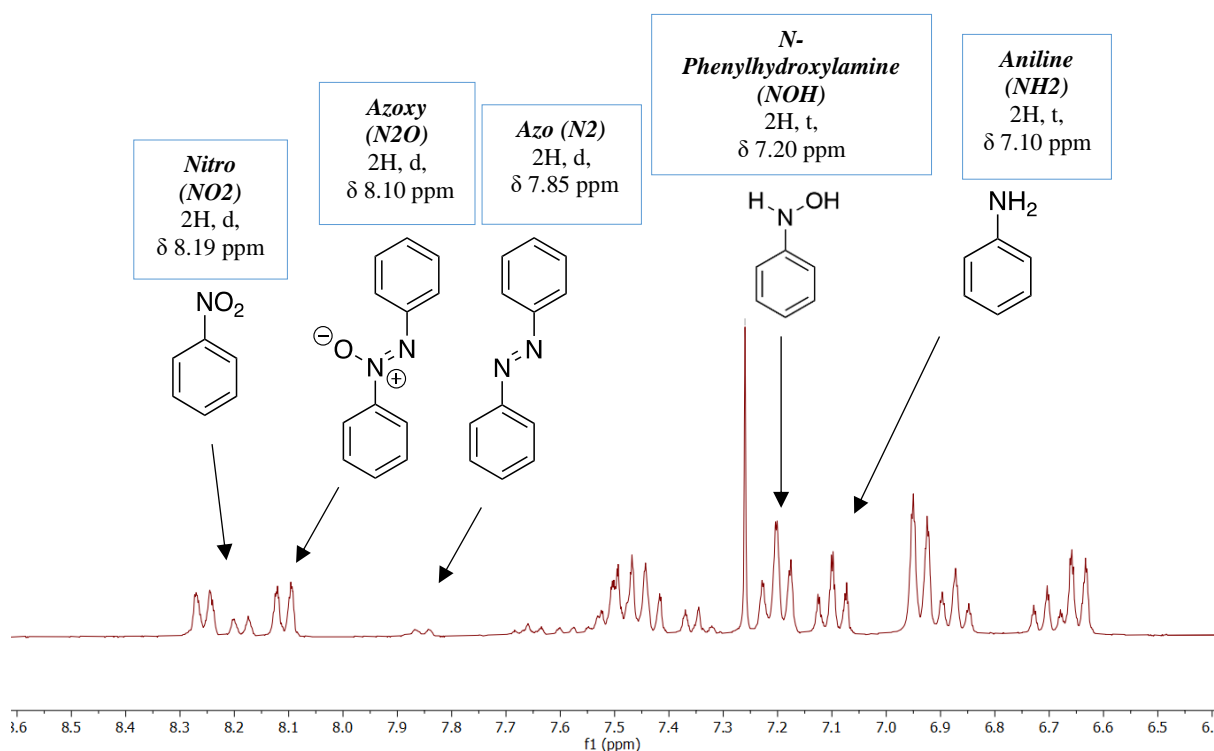
Figure 3.20: ^{1}H NMR spectrum (300 MHz, CDCl$_3$) of a mixture of the commercially available materials; Characteristic signals are indicated with their splitting and chemical shifts.

All reactions were carried out in triplicate, and the results are the average of the three runs, with a maximum error of 10% to ensure the reliability of the results. Then, the integration of each characteristic signal was used to calculate the corresponding conversions and selectivity following Equations **3.1**.

Equation 3.1:

$$Selectivity = \frac{Integral\ of\ desired\ product}{Total\ integral\ of\ all\ products} \times 100$$

$$Conversion = \frac{Total\ integral\ of\ all\ products}{Total\ integral\ of\ products\ \&\ reactant} \times 100$$

3.2.4.1.1 Initial optimisation:

In the beginning, we focused on the selective partial reduction of nitrobenzene (**NO2**) into *N*-phenylhydroxylamine (**NOH**). A complete and selective reduction of nitrobenzene (**NO2**) into the corresponding (**NOH**) using *[AuCl]@O=PPh₂-PEGPIIL* adduct **3.9** has been achieved previously with an excellent selectivity of 99%. This reaction in water with a catalyst loading of 0.05 mol% (based on ICP) at room temperature and 60 minutes delivers the desired *N*-phenylhydroxylamine (**NOH**) in excellent yield. Therefore, a test reaction under a similar reaction was undertaken first using *[AuCl]@O=PPh₂-PEGPIIL* adduct **3.9** to confirm the reproducibility of the reaction followed by test reactions using [AuCl₄]@O=PPh₂-PEGPIIL **3.17** and [AuCl]@PPh₂-PEGPIIL **3.14** under identical conditions to evaluate the comparative potential between the three catalysts precursors. Gratifyingly, complete reduction of nitrobenzene (**NO2**) into *N*-phenylhydroxylamine (**NOH**) with a 100% selectivity was observed for *[AuCl]@O=PPh₂-PEGPIIL* adduct **3.9** and [AuCl₄]@O=PPh₂-PEGPIIL **3.17**. However, only a 24% conversion of nitrobenzene (**NO2**) with a 100% selectivity for *N*-phenylhydroxylamine (**NOH**) was observed for [AuCl]@PPh₂-PEGPIIL **3.14** (Figure **3.21**). The poor conversion of the Au(I)-phosphine derived catalyst might be due to the difference in nature of nanoparticles formed from the Au(I) catalyst precursor **3.14** and may be influenced by the difference in the interaction between the nanoparticles and the phosphine heteroatom donor compared to the corresponding phosphine oxide.
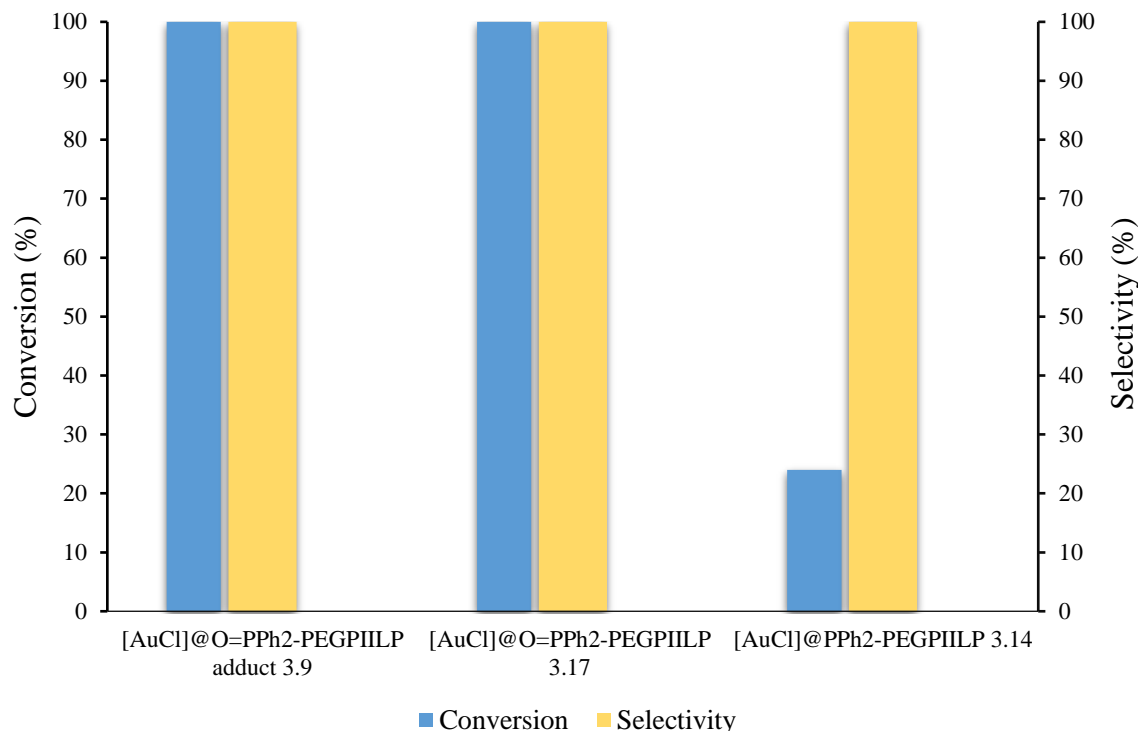
Figure 3.22: Conversion and selectivity of nitrobenzene (**NO2**) reduction toward *N*-phenylhydroxylamine (**NOH**) using 0.05 mol% **3.9, 3.14** and **3.17** precursors, 1mmol nitrobenzene (**NO2**), 2 mL H_2O and 2.5 mmol $NaBH_4$. Reactions were carried out in water at room temperature for 60 min.

3.2.4.1.2 Reaction time profile

In order to investigate the differences in activity of the gold precursors, *[AuCl]@O=PPh$_2$-PEGPIIL* adduct **3.9**, [AuCl]@PPh$_2$-PEGPIIL **3.14** and [AuCl$_4$]@O=PPh$_2$-PEGPIIL **3.17** a study was undertaken to determine the variation in composition of the reaction mixture with time. Therefore, several experiments were performed using 0.05 mol% of each of the gold precursors **3.9**, **3.14** and **3.17** based on ICP-OES catalyst loadings and 2.5 equivalents of $NaBH_4$ for the selective reduction of nitrobenzene (**NO2**) between 0 min and 300 min under a N$_2$ atmosphere. Then conversion and selectivity for each experiment were determined by ^{1}H NMR spectroscopy using 1,4-dioxane as internal standard. The results obtained are summarised in Figure **3.23**.
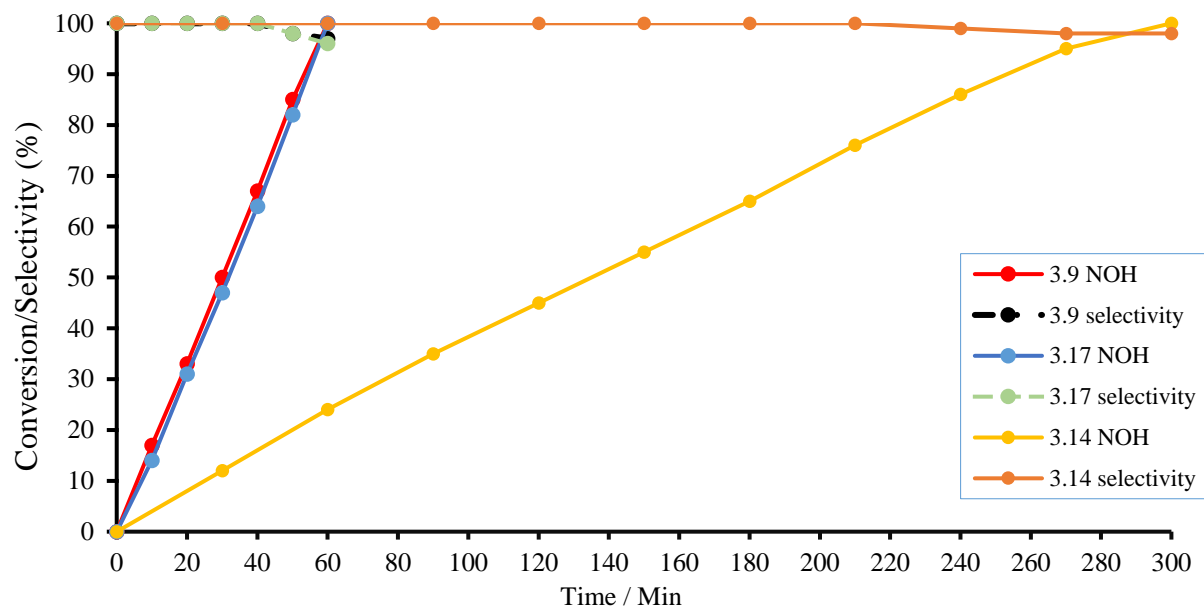
Figure 3.23: Time profile for reducing nitrobenzene (**NO2**) to *N*-phenylhydroxylamine (**NOH**) catalysed by *[AuCl]@O=PPh₂-PEGPIIL* adduct **3.9**, [AuCl₄]@O=PPh₂-PEGPIIL **3.17** and [AuCl]@PPh₂-PEGPIIL **3.14**. Reaction conditions: 1 mmol nitrobenzene (**NO2**), 2.5 mmol NaBH₄, 0.05 mol% catalyst (based on ICP), 2 mL water, room temperature. Conversion and selectivity were determined using ¹H NMR spectroscopy with dioxane as the internal standard. Selectivity for *N*-phenylhydroxylamine (**NOH**) = [% *N*-phenylhydroxylamine (**NOH**) / (% *N*-phenylhydroxylamine (**NOH**) + % aniline (**NH2**) + % azoxybenzene (**N2O**))] x 100.

The time-conversion profile studies for reducing nitrobenzene (**NO2**) catalysed by *[AuCl]@O=PPh₂-PEGPIIL* adduct **3.9**, [AuCl]@PPh₂-PEGPIIL **3.14** and [AuCl₄]@O=PPh₂-PEGPIIL **3.17** indicate that a significant catalytic efficiency of AuNPs was observed when the phosphine oxide in *[AuCl]@O=PPh₂-PEGPIIL* adduct **3.9** and [AuCl₄]@O=PPh₂-PEGPIIL **3.17** was incorporated into the support. *N*-Phenylhydroxylamine (**NOH**) was obtained with 97% and 96% selectively respectively and 100% conversion for both catalysts within 60 minutes. In contrast, the AuNP catalyst derived from [AuCl]@PPh₂-PEGPIIL **3.14** without phosphine oxide showed a substantial drop in the catalytic efficiency and provided only 24% conversion of nitrobenzene (**NO2**) with a selectivity of 100% after 60 minutes and complete conversion nitrobenzene (**NO2**) with a selectivity of 98% for *N*-phenylhydroxylamine (**NOH**) after 300 minutes (Figure **3.23**). These results demonstrate that the activity of nanoparticle catalysts generated from phosphine oxide-functionalised gold precursors **3.9** and **3.17** is higher that of catalyst generated from the phosphine-functionalised gold precursor **3.14.** This marked difference in the catalytic efficiency of

the phosphine oxide incorporated catalyst might be due to the greater polarity of the phosphine oxide allowing improved access to the active site in the aqueous phase besides the small size of the AuNPs. One might also speculate that differences in activity could be due to the supplementary electronic interactions provided by the phosphine oxide in the polymer and the AuNPs surface. As a consequence, this might cause variations in the relative reaction barriers. Furthermore, the non-homogeneous dispersion of the AuNPs, providing uneven access to the corresponding active sites of the catalysts *[AuCl]@O=PPh2-PEGPIIL* adduct **3.9** and [AuCl4]@O=PPh2-PEGPIIL **3.17** might lead to slight differences in activity between these species. Despite the differences in activity, the *selectivity* of the catalysts appears to be very similar and all were highly selective for the formation of *N*-phenylhydroxylamine (**NOH**).

Several nanoparticle-based catalytic systems for the reduction of nitrobenzene (**NO2**) are present in the literature, however, there are only a very few reports available in the literature that demonstrate selective reduction of nitrobenzene (**NO2**) into *N*-phenylhydroxylamine (**NOH**), which includes amberlite supported PtNPs, titania-supported AuNPs or AgNPs, and polystyrene supported RuNPs.[252–255] In all cases, the selective formation of *N*-phenylhydroxylamine (**NOH**) is believed to be due to the interfacial electronic effects of the supports or additives, which stabilises the corresponding nanoparticles and allows slow and selective adsorption of *N*-phenylhydroxylamine (**NOH**) intermediate compared to the reactant. The catalytic efficiency and selectivity of catalysts *[AuCl]@O=PPh2-PEGPIIL* adduct **3.9** and [AuCl4]@O=PPh2-PEGPIIL **3.17** are superior to the reported catalytic systems since these systems require high catalyst loadings or require toxic additives and reducing agents, and in many cases, organic solvents. In contrast, the reaction of nitrobenzene (**NO2**) using *[AuCl]@O=PPh2-PEGPIIL* adduct **3.9** and [AuCl4]@O=PPh2-PEGPIIL **3.17** has been accomplished in water.

Thus, the superior selectivity obtained for reducing nitrobenzene (**NO2**) into *N*-phenylhydroxylamine (**NOH**) selectively by using precursors **3.9**, **3.14** and **3.17** under milder reaction conditions without any additives is unique and a pivotal discovery considering the challenging aspect of selective reduction.

3.2.4.1.3 The selective formation of azoxybenzene (N2O)

In the previously published work, unique solvent-dependent behaviour was observed for the selective reduction of nitrobenzene (**NO2**) into azoxybenzene (**N2O**).[83] This study led us to evaluate the effect of solvent on the outcome of reduction using each of our catalyst precursors.

A time-conversion profile experiment (Figure **3.24**) demonstrates that azoxybenzene (**N2O**) was obtained as the sole product of the reduction of nitrobenzene (**NO2**) using *[AuCl]@O=PPh$_2$-PEGPIIL* adduct **3.9** in neat ethanol and can be obtained with 100% conversion and 100% selectivity after 180 minutes. A comparative experiment under identical reaction conditions using [AuCl$_4$]@O=PPh$_2$-PEGPIIL **3.17** delivered 100% azoxybenzene (**N2O**), with a 100% selectivity after 120 minutes, faster than *[AuCl]@O=PPh$_2$-PEGPIIL* adduct **3.9**. The high activity obtained for *[AuCl]@O=PPh$_2$-PEGPIIL* adduct **3.9** and [AuCl$_4$]@O=PPh$_2$-PEGPIIL **3.17** might be attributed to the phosphine oxide modification since the reduction reaction using[AuCl]@PPh$_2$-PEGPIIL **3.14** under identical reaction conditions showed a complete conversion with 100% selectivity after 480 minutes. Apparently, the phosphine oxide modification again seems to be playing a critical role in improving the activity of the catalyst.
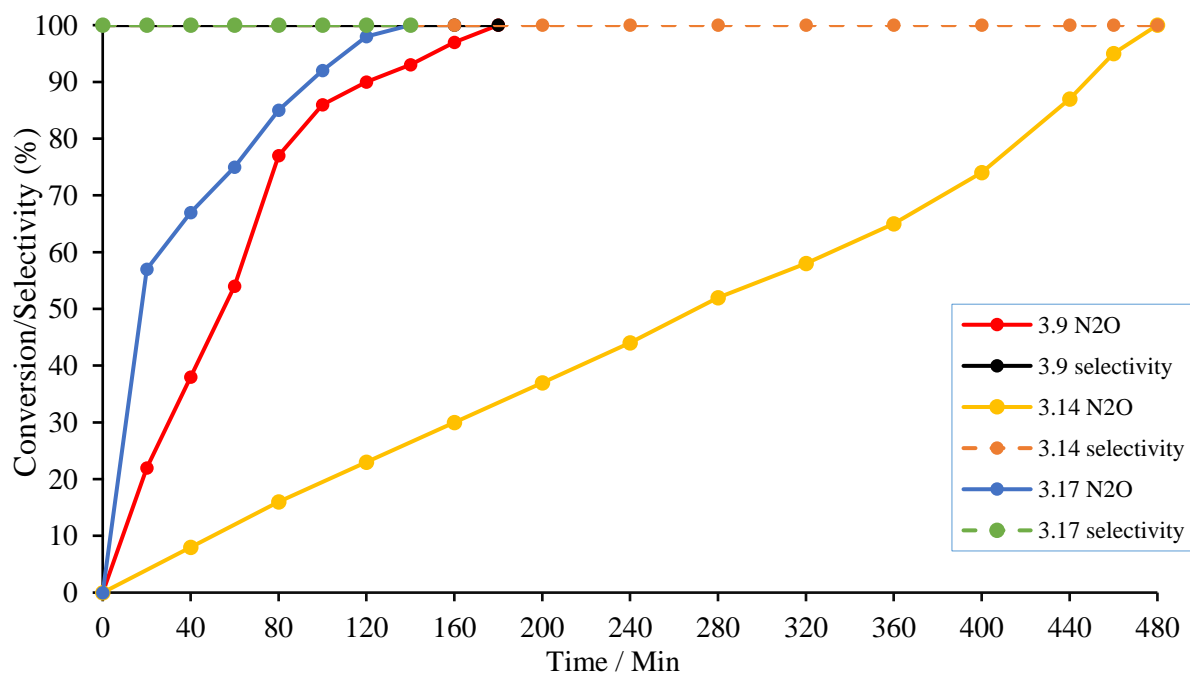
Figure 3.24: Time profile for reducing nitrobenzene (**NO2**) to azoxybenzene (**N2O**) catalysed by *[AuCl]@O=PPh₂-PEGPIIL* adduct **3.9**, [AuCl]@PPh₂-PEGPIIL **3.14** and [AuCl₄]@O=PPh₂-PEGPIIL **3.17**. Reaction conditions: 1 mmol nitrobenzene (**NO2**), 2.5 mmol NaBH₄, 0.05 mol% catalyst (based on ICP), 2 mL ethanol, room temperature. Conversion and selectivity were determined using ^{1}H NMR spectroscopy with dioxane as the internal standard. Average of three runs. Selectivity for azoxybenzene (**N2O**) = [100 x % azoxybenzene (**N2O**) / (% azoxybenzene (**N2O**) + % aniline (**NH2**) + % *N*-phenylhydroxylamine (**NOH**))].

A literature survey showed that catalytic systems for selective reduction of nitrobenzene (**NO2**) to azoxybenzene (**N2O**) are very rare. A comparative analysis of these catalytic systems with *[AuCl]@O=PPh₂-PEGPIIL* adduct **3.9** and [AuCl₄]@O=PPh₂-PEGPIIL **3.17** revealed that both precursors are superior catalysts in terms of catalytic efficiency and environmental compatibility since the reaction is performed in ethanol. For instance, magnetically separable urchin-like Ni/graphene nanocomposites have been shown to be effective catalysts for reducing nitrobenzene (**NO2**) to azoxybenzene (**N2O**) with the advantage of performing recycling experiments. However, this catalytic system requires hydrazine as a reducing agent, which is highly toxic. Likewise, AuNPs supported on mesostructured ceria (Au/meso-CeO₂) also retain switchable selectivity based on solvent composition since the addition of water to 2-propanol resulted in a drastic shift in the selectivity from azoxybenzene (**N2O**) to azobenzene (**N2**).[256] But this was obtained with 1 mol% catalyst loading, which is distinctly higher loading than that obtained with *[AuCl]@O=PPh₂-PEGPIIL* adduct **3.9** and [AuCl₄]@O=PPh₂-PEGPIIL **3.17**.

3.2.4.1.4 The selective formation of aniline (NH2)

Catalytic systems based on gold nanoparticles (AuNPs) have been extensively studied for the reduction of nitroarenes (**NO2**) into the corresponding anilines (**NH2**). Therefore, we aimed to explore and compare the catalytic efficiency of the catalysts *[AuCl]@O=PPh₂-PEGPIIL* adduct **3.9**, [AuCl]@PPh₂-PEGPIIL **3.14** and [AuCl₄]@O=PPh₂-PEGPIIL **3.17** with the existing literature systems to accomplish selective and complete reduction of nitroarenes into anilines (**NH2**). By employing the established protocol[83] using 0.05 mol% precursors, 1 mmol nitrobenzene (**NO2**) and 5 mmol NaBH₄ were stirred in water at 60 °C. The reduction of nitrobenzene (**NO2**) was then monitored as a function of time, while the composition was quantified using ^{1}H NMR. The composition-time profile (Figure **3.25a**) obtained displays a rapid conversion of nitrobenzene (**NO2**) into corresponding *N*-phenylhydroxylamine (**NOH**) within 10 min (82%), along with the aniline (**NH2**) (14%) as the minor product with *[AuCl]@O=PPh₂-PEGPIIL* adduct **3.9** and

complete conversion of *N*-phenylhydroxylamine (**NOH**) into aniline (**NH2**) was achieved after 220 minutes. As expected, the composition−time profile obtained for [AuCl$_4$]@O=PPh$_2$-PEGPIIL **3.17** (Figure **3.25b**) which shows complete conversion of *N*-phenylhydroxylamine (**NOH**) into aniline (**NH2**) after 200 minutes was closely similar to that obtained using *[AuCl]@O=PPh$_2$-PEGPIIL* adduct **3.9**.

(a) *[AuCl]@O=PPh$_2$-PEGPIIL* adduct **3.9**
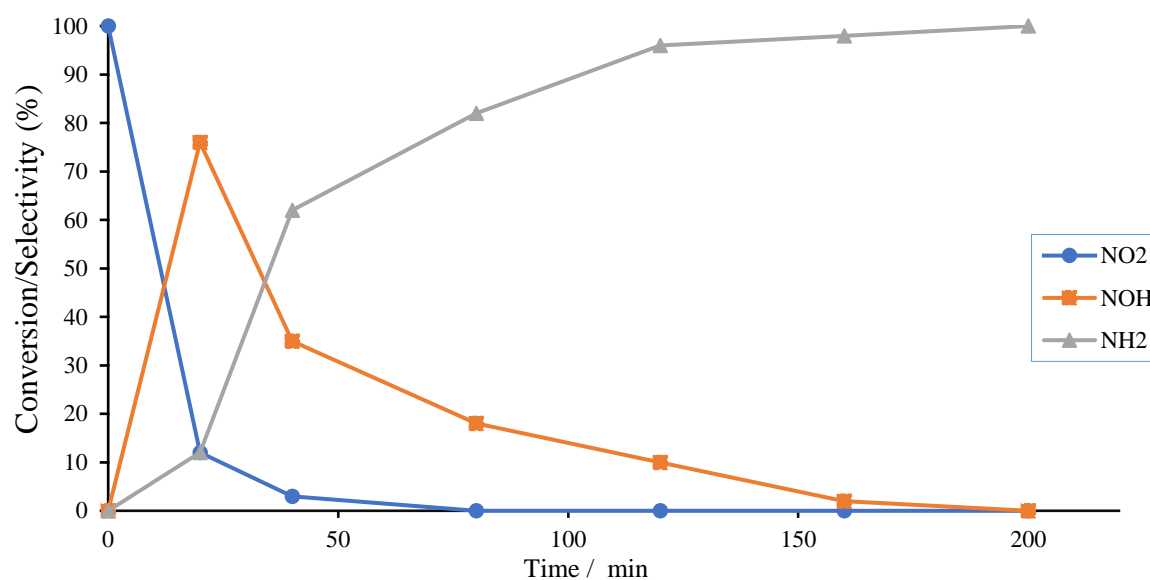
(b) [AuCl$_4$]@O=PPh$_2$-PEGPIIL **3.17**
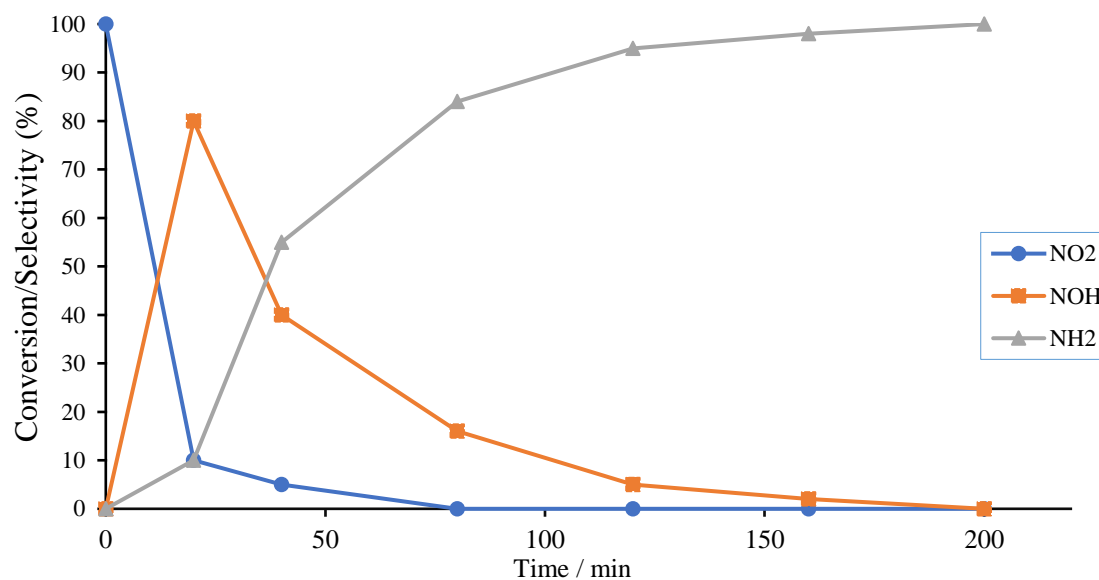
(c) [AuCl]@PPh$_2$-PEGPIIL **3.14**
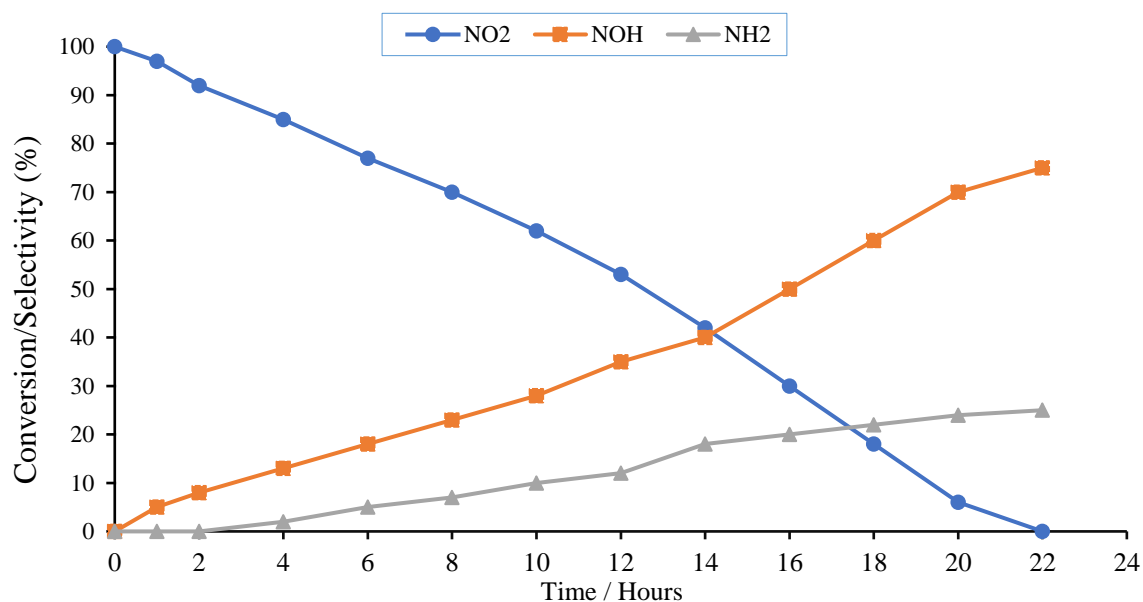
Figure 3.25: Time profile for reduction of nitrobenzene (**NO2**) to aniline (**NH2**) catalysed by (a) *[AuCl]@O=PPh$_2$-PEGPIIL* adduct **3.9**, (b) [AuCl$_4$]@O=PPh$_2$-PEGPIIL **3.17** and (c) [AuCl]@PPh$_2$-PEGPIIL **3.14**. Reaction conditions: 1 mmol nitrobenzene (**NO2**), 5.0 mmol NaBH$_4$, 0.05 mol% catalyst (based on ICP), 2 mL water, 60 °C. Conversion and selectivity were determined using ^{1}H NMR spectroscopy with dioxane as the internal standard. Average of three

runs. Selectivity for aniline (**NH2**) = [100 x % aniline (**NH2**) / (% aniline (**NH2**) + % *N*-phenylhydroxylamine (**NOH**))].

For comparison, the composition time profile obtained for the [AuCl]@PPh$_2$-PEGPIIL **3.14** (Figure **3.25c**) showed that complete conversion of nitrobenzene (**NO2**) into 75% *N*-phenylhydroxylamine (**NOH**) and 25% aniline (**NH2**) was achieved after 22 hours, a considerably slower reaction. For all three catalysts, the time profiles suggest a direct pathway for the formation of aniline (**NH2**) from *N*-phenylhydroxylamine (**NOH**) since no indication of the formation of azoxybenzene (**N2O**) was observed during the reaction.

3.2.4.2 Hydrogen source screening

The utility of gold precursors *[AuCl]@O=PPh$_2$-PEGPIIL* adduct **3.9**, [AuCl]@PPh$_2$-PEGPIIL **3.14** and [AuCl$_4$]@O=PPh$_2$-PEGPIIL **3.17** for nitrobenzene (**NO2**) reduction using H-sources other than sodium borohydride was explored. A range of potential hydrogen donors (the azeotropic mixture of formic acid/triethylamine (5:2)[257], hydrazine hydrate[258] and dimethylamine borane complex[259]) were selected, all of which have previously been reported in transfer hydrogen reactions.

Table **3.2** shows the results of nitrobenzene (**NO2**) reduction catalysed by *[AuCl]@O=PPh$_2$-PEGPIIL* adduct **3.9** using different hydrogen transfer agents. The azeotropic mixture of formic acid/triethylamine (5:2) and hydrazine hydrate were ineffective, giving no conversion (Table **3.2**, entries 1, 2). In contrast, the dimethylamine borane complex (Table **3.2**, entry 3) gave a high conversion and good selectivity toward *N*-phenylhydroxylamine (**NOH**).

Table 3.2: Screening of hydrogen source for the transfer hydrogenation of nitrobenzene (**NO2**).

Entry[a]	H-source	Conversion[a,b] (%)	Selectivity % NOH[b]	Selectivity % NH2[b]	Selectivity % N2O[b]
1	(5:2) HCOOH/Et$_3$N	0	0	0	0
2	NH$_2$-NH$_2$ hydrate	0	0	0	0
3	(CH$_3$)$_2$NH·BH$_3$	100	85	15	0

Reaction conditions: 1 mmol nitrobenzene (**NO2**), 2.5 mmol reducing agent, 0.05 mol% catalyst (based on ICP), 2 mL water, room temperature. [b]Conversion and selectivity were determined using ^{1}H NMR spectroscopy with dioxane as the internal standard. Average of at least 3 runs.

Dimethylamine borane complex ((CH$_3$)$_2$NH·BH$_3$) was chosen from the table **3.2** results as the best hydrogen source for further investigation due to the high conversion and selectivity toward *N*-phenylhydroxylamine (**NOH**).

3.2.4.2.1 Reaction time profile

Figure **3.25** shows the conversion and selectivity profile vs time for the nitrobenzene (**NO2**) reduction with dimethylamine borane complex using all three catalyst precursors.

(a) *[AuCl]@O=PPh₂-PEGPIIL* adduct **3.9** and [AuCl₄]@O=PPh₂-PEGPIIL **3.17**
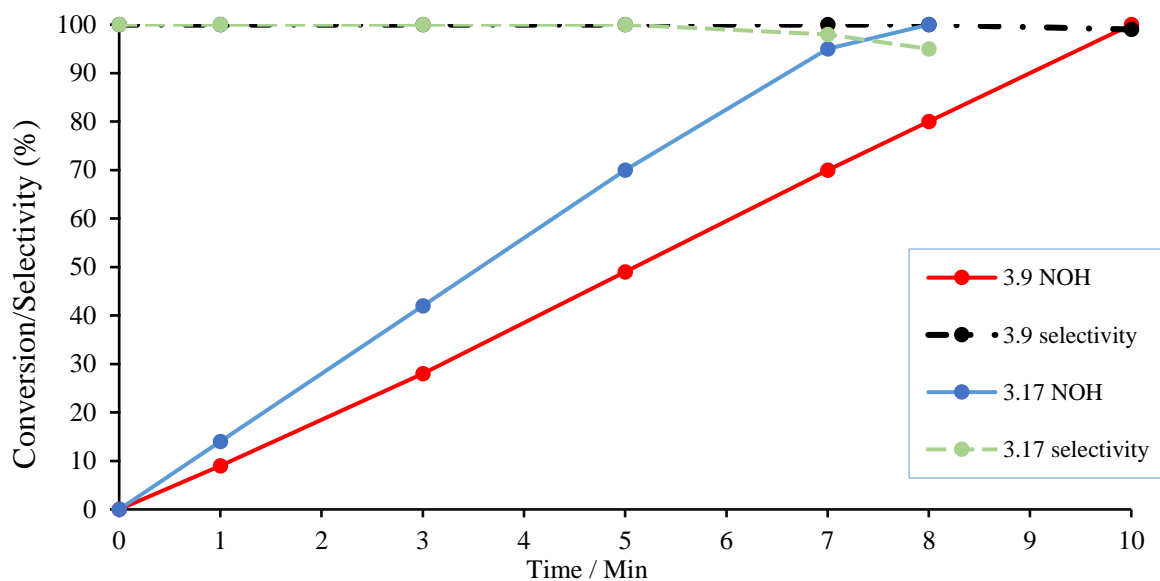
(b) [AuCl]@PPh₂-PEGPIIL **3.14**
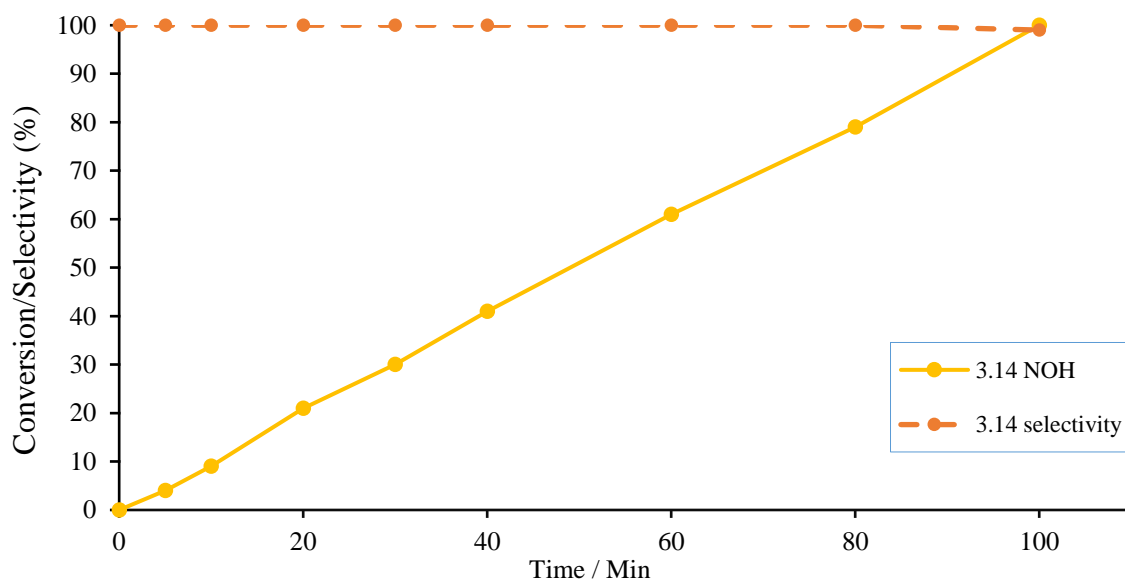
Figure 3.26: Time profile for reducing nitrobenzene (**NO2**) to *N*-phenylhydroxylamine (**NOH**) catalysed by (a) *[AuCl]@O=PPh$_2$-PEGPIIL* adduct **3.9**, [AuCl$_4$]@O=PPh$_2$-PEGPIIL **3.17** and (b) [AuCl]@PPh$_2$-PEGPIIL **3.14**. Reaction conditions: 1 mmol nitrobenzene (**NO2**), 2.5 mmol (CH$_3$)$_2$NH·BH$_3$, 0.05 mol% catalyst (based on ICP), 2 mL water, room temperature. Conversion and selectivity were determined using ^{1}H NMR spectroscopy with dioxane as the internal standard. Selectivity for *N*-phenylhydroxylamine (**NOH**) = [100 x % *N*-phenylhydroxylamine (**NOH**) / (% *N*-phenylhydroxylamine (**NOH**) + % aniline (**NH2**) + % azoxybenzene (**N2O**)].

After 10 minutes, *[AuCl]@O=PPh$_2$-PEGPIIL* adduct **3.9** had reached complete conversion (100%) and 99% selectivity for *N*-phenylhydroxylamine (**NOH**). Similarly, [AuCl$_4$]@O=PPh$_2$-PEGPIIL **3.17** had complete conversion and 95% selectivity within 8 minutes. However, as the reaction time increases above 8 minutes, the selectivity tends to decrease. In contrast, to achieve 100% conversion and 99% selectivity of [AuCl]@PPh$_2$-PEGPIIL **3.14**, the reaction time was increased to 100 minutes.

The conversion-selectivity profile in (Figure **3.26**) shows that the reaction rate is significantly higher upon using (CH$_3$)$_2$NH·BH$_3$ as a hydrogen source compared NaBH$_4$ with all three catalyst precursors (Figure **3.23**).

3.2.4.2.2 The selective formation of azoxybenzene (N2O)

In the case of NaBH$_4$ as a reducing agent, significant solvent-dependent behaviour was observed (see above) and the selectivity for nitrobenzene (**NO2**) reduction switched from *N*-phenylhydoxylamine to azoxybenzene (**N2O**) when changing from water to ethanol as solvent. We therefore explored the use of dimethylamine borane complex as a reducing agent in ethanol at room temperature (Figure **3.27**).

(a) *[AuCl]@O=PPh₂-PEGPIIL* adduct **3.9**
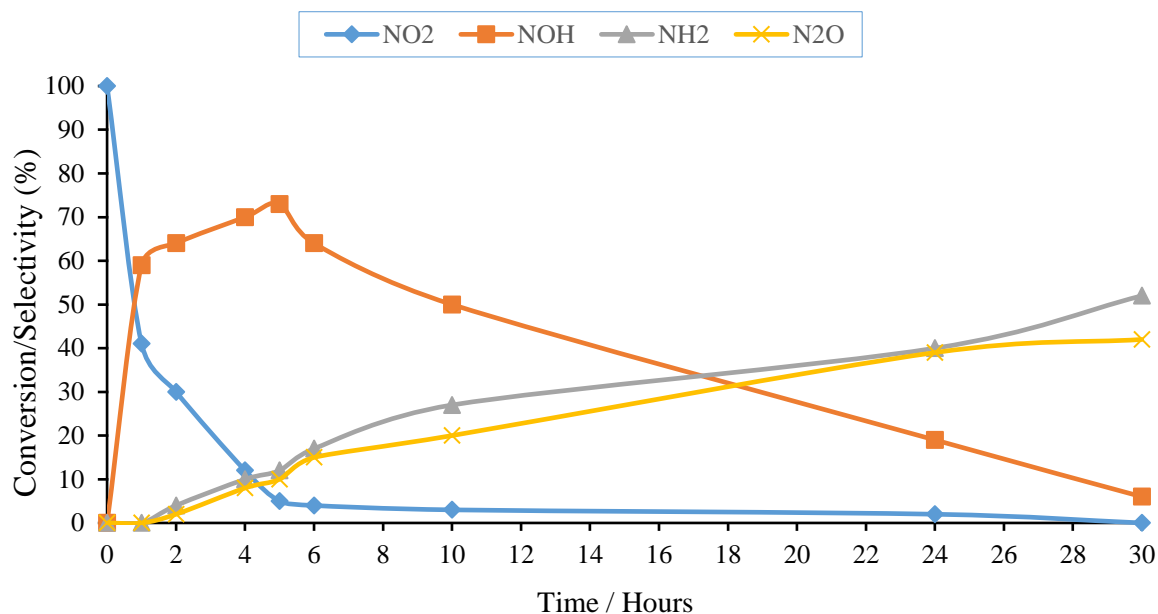
(b) [AuCl₄]@O=PPh₂-PEGPIIL **3.17**
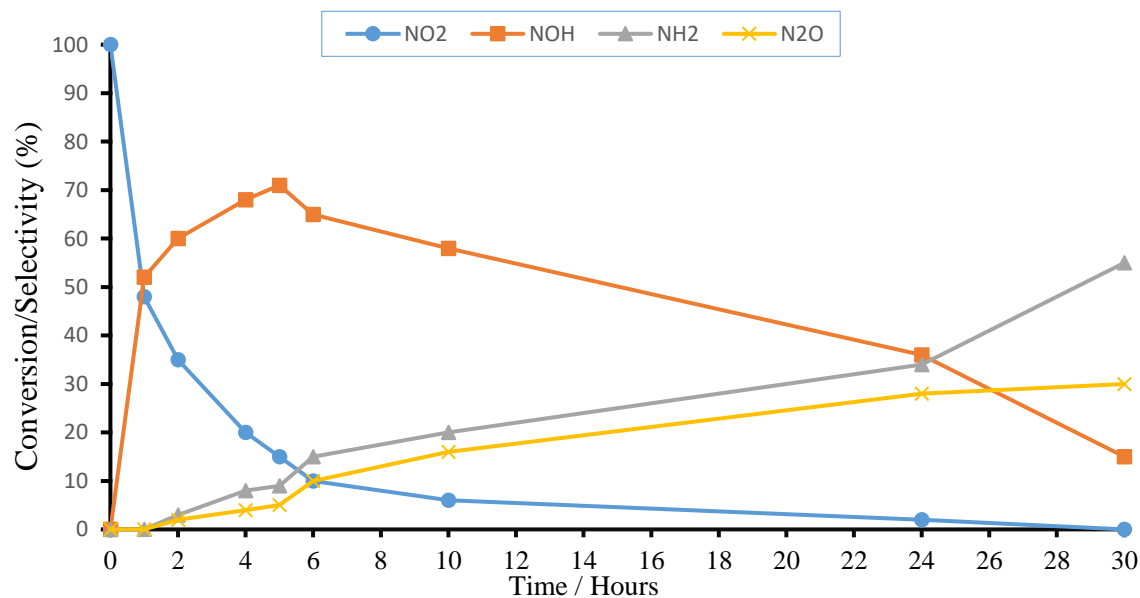
Figure 3.27: Time profile for reducing nitrobenzene (**NO2**) to azoxybenzene (**N2O**) catalysed by (a) *[AuCl]@O=PPh₂-PEGPIIL* adduct **3.9** and (b) [AuCl₄]@O=PPh₂-PEGPIIL **3.17.** Reaction conditions: 1 mmol nitrobenzene (**NO2**), 2.5 mmol $(CH_3)_2NH\cdot BH_3$, 0.05 mol% catalyst (based on ICP), 2 mL ethanol, room temperature. Conversion and selectivity were determined using ^{1}H NMR spectroscopy with dioxane as the internal standard.

Average of three runs. Selectivity for Selectivity for azoxybenzene (**N2O**) = [100 x % azoxybenzene (**N2O**) / (% azoxybenzene (**N2O**) + % aniline (**NH2**) + % *N*-phenylhydroxylamine (**NOH**))].

After 30 hours, the conversion of nitrobenzene (**NO2**) was complete and gave a mixture of 6% *N*-phenylhydroxylamine (**NOH**), 52% aniline (**NH2**) and 42% azoxybenzene (**N2O**) with *[AuCl]@O=PPh₂-PEGPIIL* adduct **3.9.** Moreover, [AuCl₄]@O=PPh₂-PEGPIIL **3.17** produced a mixture of 15% *N*-phenylhydroxylamine (**NOH**), 55% aniline (**NH2**) and 30% azoxybenzene (**N2O**).

Consequently, we decided to increase the catalyst loading from 0.05 to 0.25 mol% to increase the rate of reaction. Unfortunately, this attempt gave essentially the same product distribution as with 0.05 mol% loading but in a shorter time, as shown in Figure **3.28**.

(a) *[AuCl]@O=PPh₂-PEGPIIL* adduct **3.9**
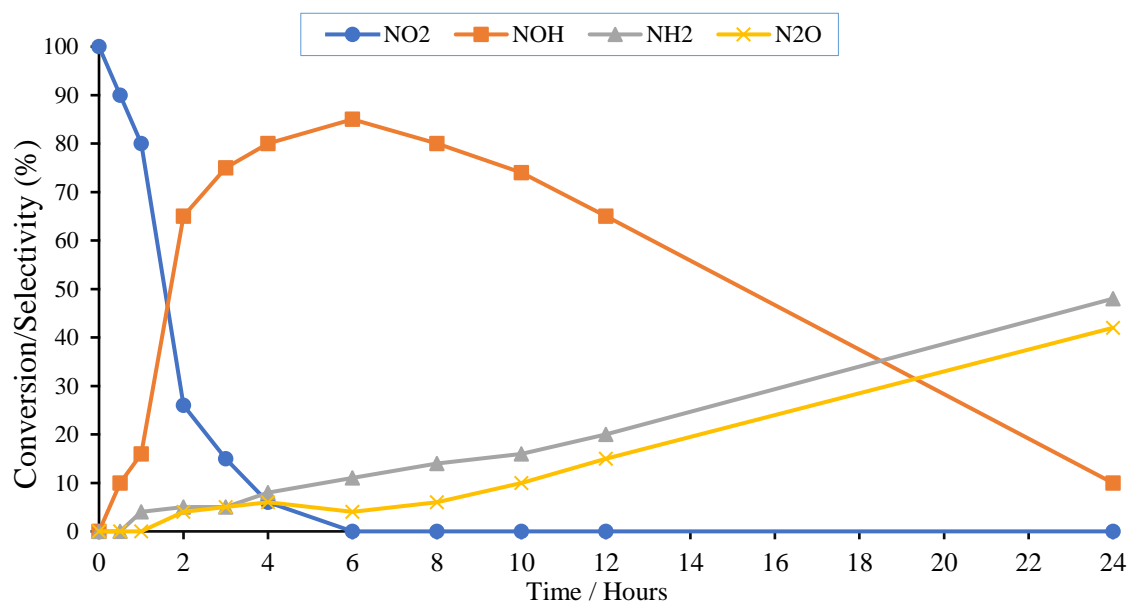
(b) [AuCl$_4$]@O=PPh$_2$-PEGPIIL **3.17**
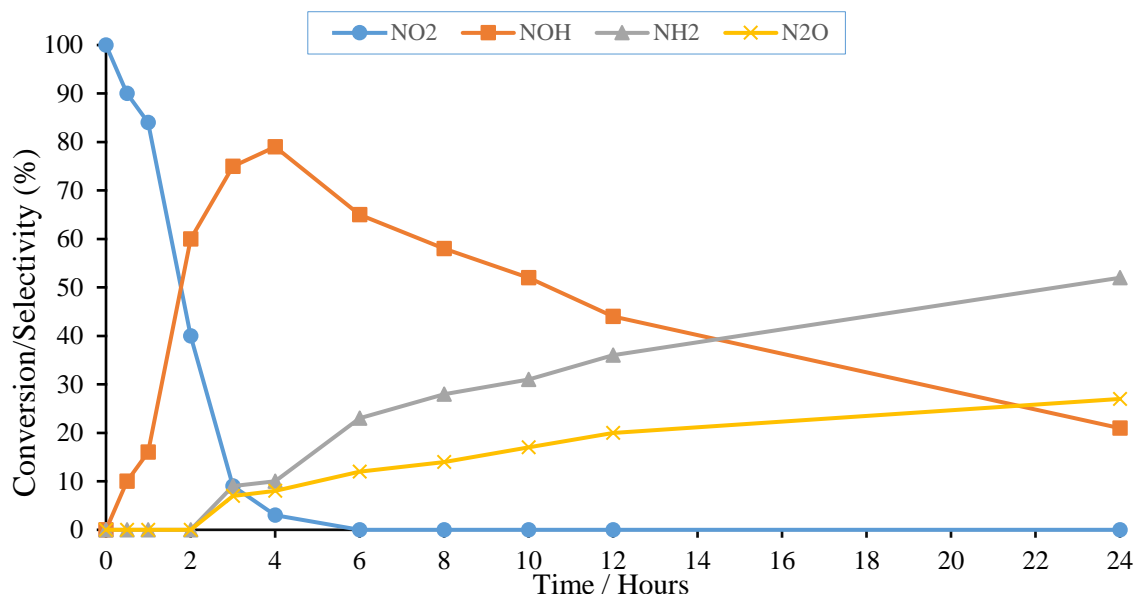
Figure 3.28: Time profile for reducing nitrobenzene (**NO2**) to azoxybenzene (**N2O**) catalysed by (a) *[AuCl]@O=PPh$_2$-PEGPIIL* adduct **3.9** and (b) [AuCl$_4$]@O=PPh$_2$-PEGPIIL **3.17** Reaction conditions: 1 mmol nitrobenzene (**NO2**), 2.5 mmol (CH$_3$)$_2$NH·BH$_3$, 0.05 mol% catalyst (based on ICP), 2 mL ethanol, room temperature. Conversion and selectivity were determined using ^{1}H NMR spectroscopy with dioxane as the internal standard. Average of three runs. Selectivity for Selectivity for azoxybenzene (**N2O**) = [100 x % azoxybenzene (**N2O**) / (% azoxybenzene (**N2O**) + % aniline (**NH2**) + % *N*-phenylhydroxylamine (**NOH**))].

The results of nitrobenzene (**NO2**) reduction using (CH$_3$)$_2$NH·BH$_3$ as a hydrogen source in ethanol toward azoxybenzene (**N2O**) catalysed by *[AuCl]@O=PPh$_2$-PEGPIIL* adduct **3.9**, [AuCl$_4$]@O=PPh$_2$-PEGPIIL **3.17** in (Figure **3.28**) revealed that the reactions are notably slower and less selective than the reactions using NaBH$_4$ (Figure **3.24**).

3.3 Conclusion

In conclusion, the research revealed that attempted preparation of AuCl$_4$@PPh$_2$-PEGPIIL by impregnation of PPh$_2$-PEGPIIL support **3.8** with K[AuCl$_4$] results in the unanticipated oxidation of the phosphine and reduction of the gold(III) to gold(I). Careful analysis of the ^{31}P NMR spectra provides solid evidence related to this precursor, and clearly indicates the presence of phosphine oxide. Attempted unambiguous synthesis of [AuCl$_4$]@PPh$_2$-PEGPIIL by oxidation of the corresponding gold(I) **3.14** to gold(III) **3.15** by treatment with Cl$_2$ gas was ultimately unsuccessful.

Unfortunately, the gold(III) species was unstable and decomposed even in the absence of light when stored in an inert atmosphere in the freezer. Consequently, we chose to oxidise the polymer in order to synthesise a phosphine oxide-derived gold precursor to enable testing and comparison of the selectivity and activity to *in situ* formed gold(I) phosphine oxide adduct **3.9.** TEM micrographs showed that in all cases the AuNPs are small, near monodisperse, with those derived from the gold(I) precursor having slightly smaller mean diameters.

The nitrobenzene (**NO2**) reduction in water-mediated by $NaBH_4$ in the presence of 0.05 mol% *[AuCl]@O=PPh$_2$-PEGPIIL* **3.9** and [AuCl$_4$]@O=PPh$_2$-PEGPIIL **3.17** displayed a 100% conversion of nitrobenzene (**NO2**) to *N*-phenylhydroxylamine (**NOH**) within 60 minutes, while [AuCl]@PPh$_2$-PEGPIIL **3.14** without phosphine oxide showed a substantial drop in the catalytic efficiency and complete conversion nitrobenzene (**NO2**) with a selectivity of 98% for *N*-phenylhydroxylamine (**NOH**) after 300 minutes. Furthermore, a solvent change to from water ethanol resulted in a shift in selectivity and yielded azoxybenzene (**N2O**) quantitatively.

The gold precursors were very efficient when $(CH_3)_2NH \cdot BH_3$ was used as a hydrogen source instead of $NaBH_4$ in water. *[AuCl]@O=PPh$_2$-PEGPIIL* adduct **3.9** and [AuCl$_4$]@O=PPh$_2$-PEGPIIL **3.17** had reached complete conversion 100% and (>95%) selectivity for *N*-phenylhydroxylamine (**NOH**) within 10 minutes. While [AuCl]@PPh$_2$-PEGPIIL **3.14** needed a longer time to achieve 100% conversion and 99% selectivity. On the contrary, the gold precursors were non-selective in ethanol.

The results reveal that nanoparticle catalyst formed from phosphine oxide-functionalised gold precursors **3.9** and **3.17** have a higher activity than catalysts derived from phosphine-functionalised gold precursor **3.14**. So, surface investigations, such as *in situ* DRIFTS, XAS and XPS analysis, would be required to demonstrate the nature of the P=O-Au interaction and understand how PIIL supports affect the catalyst's efficacy.

Chapter 4. Synthesis of PIIL Stabilised Palladium Nanoparticles and Application in the Selective Hydrogenation of Quinoline

4.1   Introduction

Functionalised 1,2,3,4-tetrahydroquinolines (1,2,3,4-THQs) are well known for being biologically active building blocks, key intermediates for several pharmaceuticals, agrochemicals, and other fine chemicals. Therefore, a substantial amount of research has been dedicated to methods for their synthesis during the last four decades.[260] Conventionally, three protocols have been extensively explored for the synthesis of 1,2,3,4-THQs, which includes chemoselective catalytic hydrogenation of *N*-heterocyclic compounds, catalytic cyclizations,[261,262] and Beckmann rearrangement of *N*-heterocycles (Scheme **4.1**).[263]
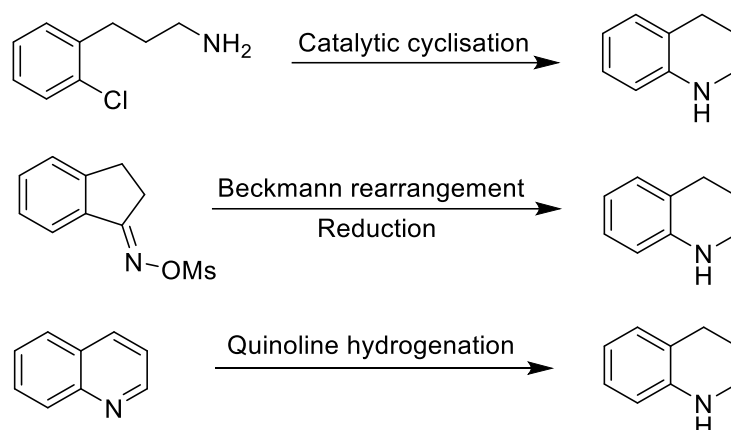
Scheme 4.1: Common synthetic routes to 1,2,3,4-THQ.

Among them, the catalytic hydrogenation of quinolines provides the most straightforward approach to access functionalised 1,2,3,4-THQs both in matter of simplicity and high atom efficiency. However, certain drawbacks associated with the catalytic hydrogenation of quinolines, such as the presence of high energy barriers, make the reaction inherently sluggish and, most of the time necessitates utilisation of drastic conditions limiting the scope of the reaction. Additionally, during hydrogenation, multiple intermediates and by-products may be formed (Scheme **4.2**), especially in the presence of other reducible functional groups such as unsaturated functional groups like alkenes

and alkynes, carbonyl compounds like aldehydes and ketones, nitriles, amines, and halogens, among other functional groups, ultimately creating selectivity issues. Lastly, the leaching of the active catalyst from the catalytic surface and the catalytic poisoning of the active sites of the catalyst due to coordination of the nitrogen atom of the *N*-heterocycles often results in poor efficiency and limits the reusability of the catalyst.
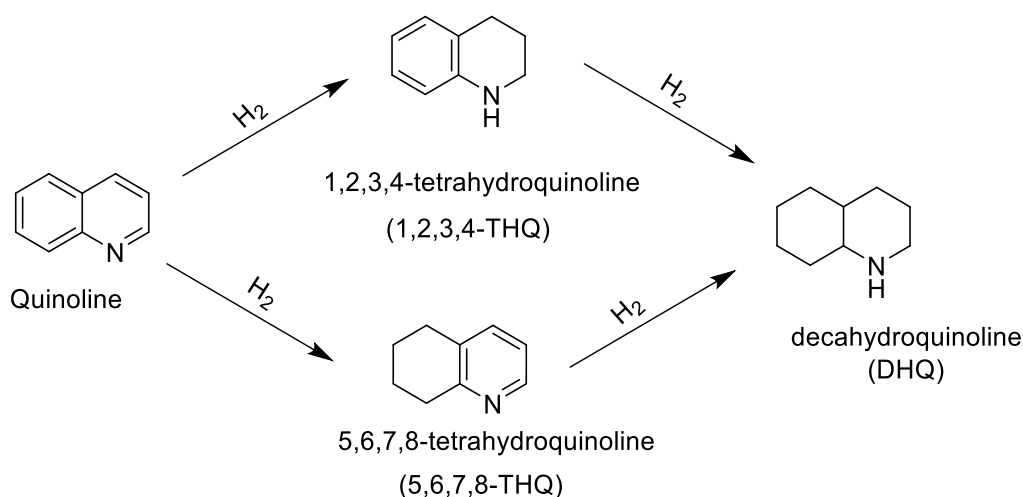
Scheme 4.2: Possible pathways for the hydrogenation of quinoline.

Despite all the drawbacks mentioned above, catalytic hydrogenations are still the most widely explored methodology for the selective and efficient hydrogenation of quinolines. Fish and co-workers achieved the first catalytic and selective hydrogenation of quinolines in 1982 using a Ru-based homogeneous catalyst.[264] Since then, various homogeneous catalysts based on several transition metals such as Ru,[265,266] Ir,[267,268] Rh,[269] Au,[270] and Co[271] have been synthesised and reported. Although the use of homogenous transition metals-based catalysts displays a better catalytic efficiency and selectivity, the difficulties associated during the separation of products and the recovery of the active catalyst from the reaction mixture limits the scope of the reaction, especially during large scale production. In addition, the need for certain additives such as iodine (I_2) for the catalytic hydrogenation of *N*-heterocycles by using Ir-based homogeneous catalysts sometimes limits the scope of the reaction, particularly when the reaction is applied on an industrial level.[272] Therefore, many research laboratories are currently focusing on designing and

synthesising novel and efficient heterogeneous catalysts for the selective and atom efficient synthesis of functionalised quinolines.

The beneficial aspect of using heterogeneous catalysts over homogeneous ones is that they are cost-effective, easily separated from the reaction mixtures, and recycled. Over 90% of all the chemicals produced worldwide are estimated to have been achieved by using transition metals based catalysts. Among them, the use of heterogeneous catalysts themselves alone accounts for 80% of chemical production.[273,274] Therefore, several Pd,[275,276] Pt,[277,278] Ru,[279,280] and Rh-based[281] catalysts have been transformed into chemoselective catalysts by choosing tuneable supports *via* fine-tuning of the support properties. For example, the surface of mesoporous silica hollow nanospheres (HMSNs) have been modified by using amino groups by Li and co-workers and found to be selective and with improved catalytic activity for the hydrogenation of *N*-heterocycles.[282] Similarly, homogeneously dispersed gold nanoparticles (NPs) on the relatively high surface area of TiO_2 have been synthesised successfully by Cao and co-workers for the selective hydrogenation of quinolines in the presence of other functional groups.[283] One of the drawbacks of using heterogeneous catalysts is that in most cases, high temperature and pressure are required to convert quinoline into 1,2,3,4-THQ, as a result the selectivity of the reaction is tuned by using various organic solvents.

Since water is a green solvent and plays a promoting role in several catalytic reactions by improving catalytic efficiency, water could be the most interesting solvent for these catalytic hydrogenations based on its green potential and cost-effective nature.[284] However, only a few heterogeneous catalysts are known for the aqueous phase catalytic hydrogenation of quinolines. For instance, silica spheres supported ruthenium nanoparticles (RuNPs) with an outer shell of microporous silica,[279] black wattle tannin stabilised palladium nanoparticles (PdNPs)[285,286] and polymer-supported PdNPs have been used to achieve aqueous phase hydrogenations of quinoline.[287] Unfortunately, even with these catalysts, the complete conversion of quinoline to 1,2,3,4-THQ still requires harsh reaction conditions, such as high temperature, high hydrogen pressure, long reaction times, need of large quantities of hydrogen sources and high catalyst loadings relative to quinoline.

Therefore, the design and synthesis of a chemoselective heterogeneous catalyst with industrially desirable and 'green credentials' and with the ability of operating under milder conditions is still anticipated. An ideal catalytic system in this aspect would be one operating at mild conditions with

low catalyst loadings in water and possessing high selectivity and short reaction times. The protocol must also display simple strategies for catalyst recovery, and finally, the catalyst must be sustainable in order to avoid the use of organic solvents.

The enhanced catalytic efficiency of PEG-modified PIIL-based catalysts for the aqueous phase reduction of nitroarenes in Chapter 3 and previous publications[82,83,120] might be due to mutual solvent-support interactions which promote polymer morphology/tertiary structure with enhanced properties for catalysis in the PIIL-based catalysis. Consequently, we aimed to evaluate the catalytic efficiency of the same systems for the chemoselective reduction of quinoline in an aqueous medium. The presence of heteroatom donor groups (e.g. phosphine) and modification in the PEG chain of the immobilised IL support are known to affect the catalytic activity of the catalyst in the hydrogenation of nitroarenes. Hence, we planned to investigate the influence of similar modifications for catalysis of other reductive reactions.

We aimed to develop an alternate and versatile, scalable, recyclable and environmentally friendly catalyst for such type of reactions. In terms of variation of the imidazolium side-chain, we proposed to investigate the influence of replacing the strongly hydrophilic PEG chain with a strongly hydrophobic decyl hydrocarbon chain **4.1**. This functional group substitution might influence the compatibility of catalysts with the aqueous phase but is also likely to influence the stability of the nanoparticles in theory because the PEG chain is likely to stabilise the metal nanoparticles *via* electrostatic interactions which are not available in the corresponding decyl chain.

4.2 Results and Discussion

4.2.1 Synthesis of 1-decyl-2-methyl-3-(4-vinylbenzyl)-1*H*-imidazol-3-ium bromide (4.1)
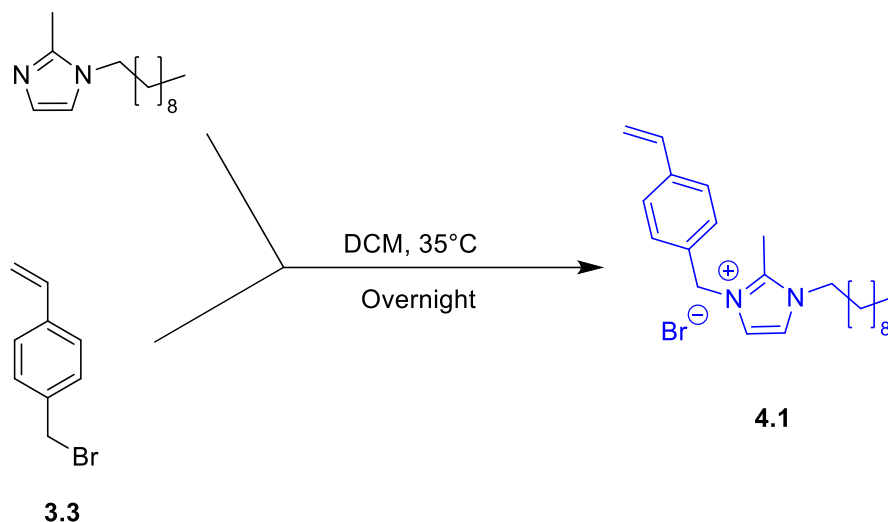
Scheme 4.3: Synthesis of 1-decyl-2-methyl-3-(4-vinylbenzyl)-1*H*-imidazol-3-ium bromide **4.1**.

In order to prepare the new hydrocarbon functionalised monomer **4.1**, 1-decyl-2-methyl imidazole was reacted with 4-vinylbenzyl bromide **3.3** in dichloromethane overnight at 35 °C. The solvent was removed, and the resultant residue was triturated with diethyl ether and dried under a high vacuum to afford 1-decyl-2-methyl-3-(4-vinylbenzyl)-1*H*-imidazol-3-ium bromide **4.1** as fine white powder in 94% yield. The ^{1}H NMR spectrum displayed all the characteristic signals consistent with that of **4.1**.

4.2.2 Synthesis and Characterisation of PPh₂-*N*-decylPIIL (4.2).

PPh₂-decylPIIL **4.2** was prepared by the free radical copolymerisation of 1-decyl-2-methyl-3-(4-vinylbenzyl)-1*H*-imidazol-3-ium bromide **4.1** with diphenyl(4-vinylphenyl) phosphine **3.5** and the cross-linker **3.7** in a ratio of 1.86:1:0.14, respectively, as shown in Scheme **4.4**. The monomers and 5 mol% AIBN were dissolved in dry ethanol/THF ratio 1:1. The reaction mixture was then degassed six times using the freeze-pump-thaw technique to eliminate the presence of oxygen, which might interfere with the radical reaction and also lead to unwanted phosphine oxidation. The reaction was carried out at 80 °C for four days, after which a further 5 mol% of AIBN was added to the mixture, and the degassing process was repeated six times. Subsequently, the reaction was heated for one more day to ensure complete polymerisation.
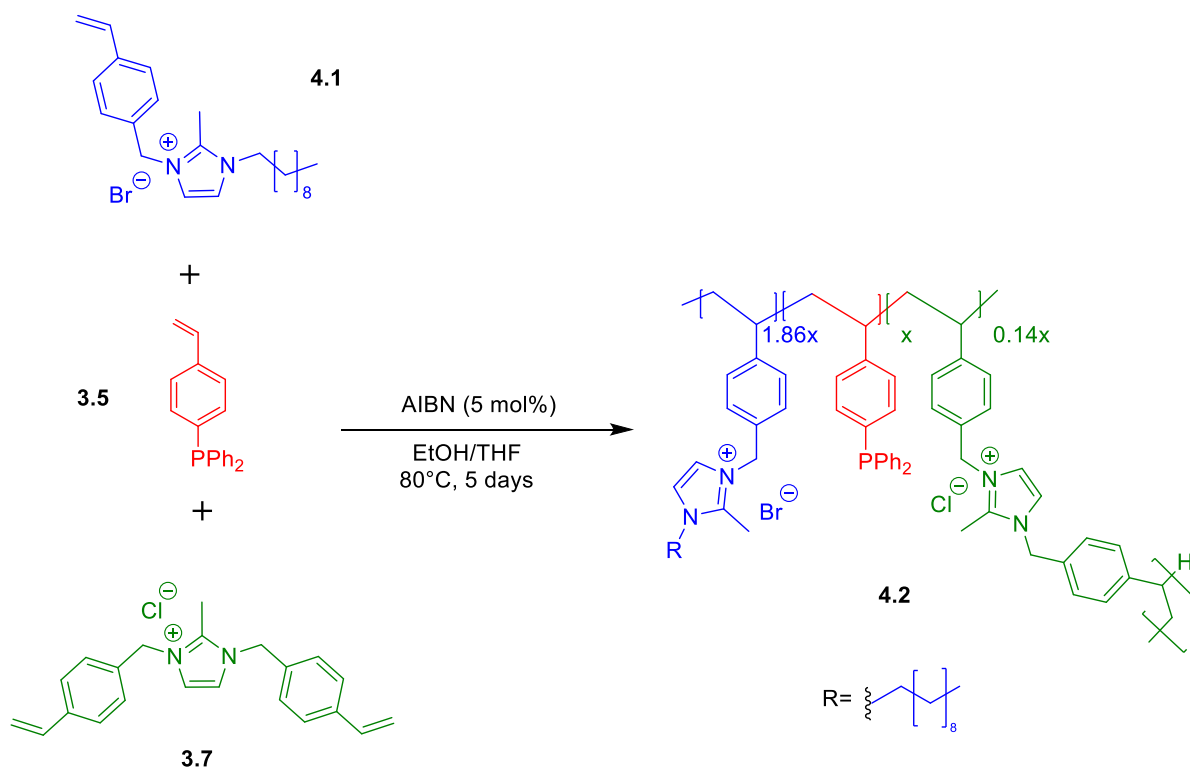
Scheme 4.4: Synthesis of PPh$_2$-*N*-decylPIIL **4.2**.

After completion of the reaction, the solvent was removed under reduced pressure. The residue was re-dissolved in DCM followed by re-precipitation in diethyl ether to remove unreacted monomer to afford the polymer **4.2** as a fine off-white powder in 91% yield. The absence of vinylic signal peaks in the ^{1}H NMR spectrum (Figure **4.1**) indicates the completion of the polymerisation and revealed well-defined signals with the characteristic broad peaks expected for the desired polymer **4.2**. The peaks at δ 0.87 ppm corresponding to CH$_3$ on the end of the decyl chain, the peaks at δ 1.24 ppm corresponding to methylene protons on the decyl chain and the saturated polymer backbone and the signal at ca. δ 5.65 ppm was assigned as the protons of the benzylic CH$_2$ groups adjacent to the imidazolium rings. The aromatic and imidazolium protons were assigned at δ 6.50-7.40 ppm. The ratio of imidazolium groups:phosphine 2:1 was calculated by comparison of the relative integrals. Also, the ^{31}P NMR spectrum showed a single peak at δ -6.64 ppm, indicating the phosphine group and absence of any unwanted phosphine oxide.
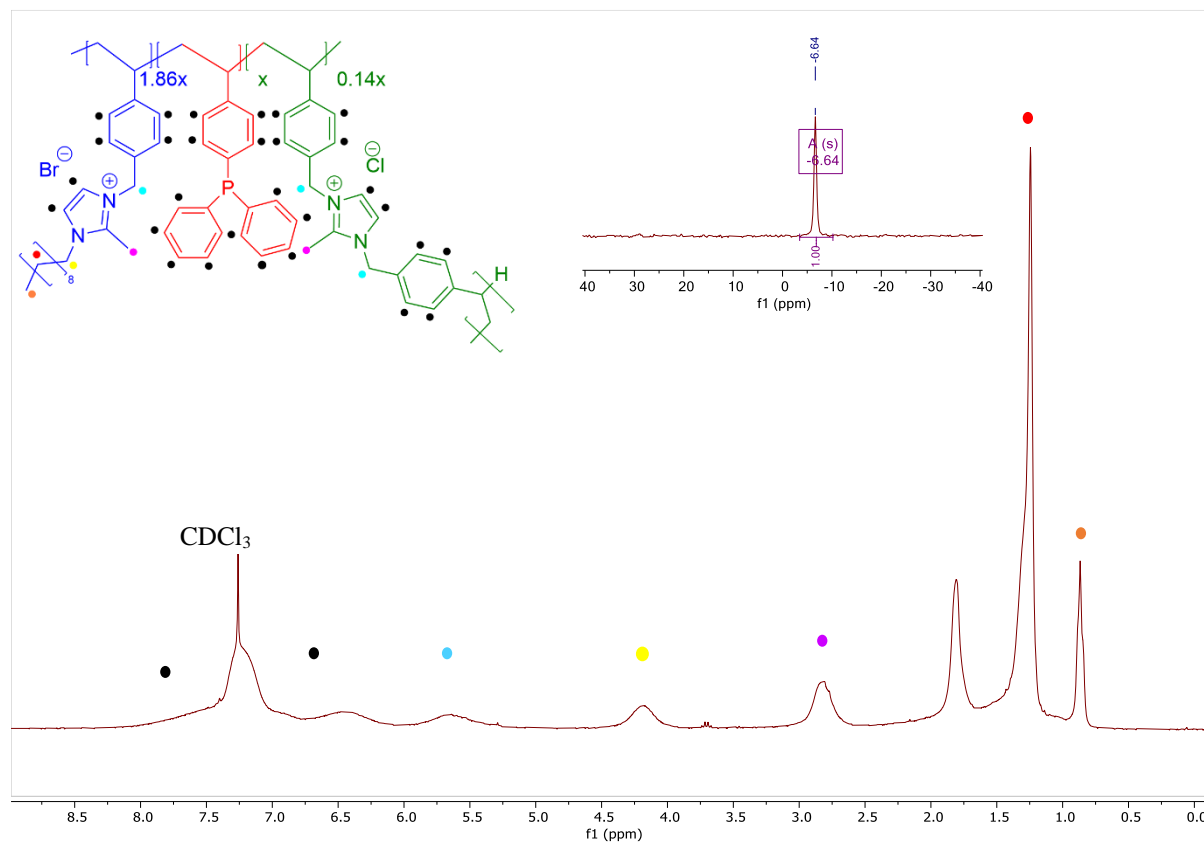
Figure 4.1: ^{1}H (400 MHz, CDCl$_3$) and ^{31}P (121 MHz, CDCl$_3$, inset) NMR spectra for PPh$_2$-*N*-decylPIIL **4.2**.

The solid-state ^{31}P NMR spectrum for PPh$_2$-*N*-decylPIIL **4.2**, as shown in Figure **4.2**, demonstrates one phosphorous containing species at δ -6.12 ppm with spinning side-bands. The value agrees with the value reported by Iwai *et al*. for the synthesis of Threefold Cross-Linked Polystyrene – Triphenylphosphane Hybrids.[288]
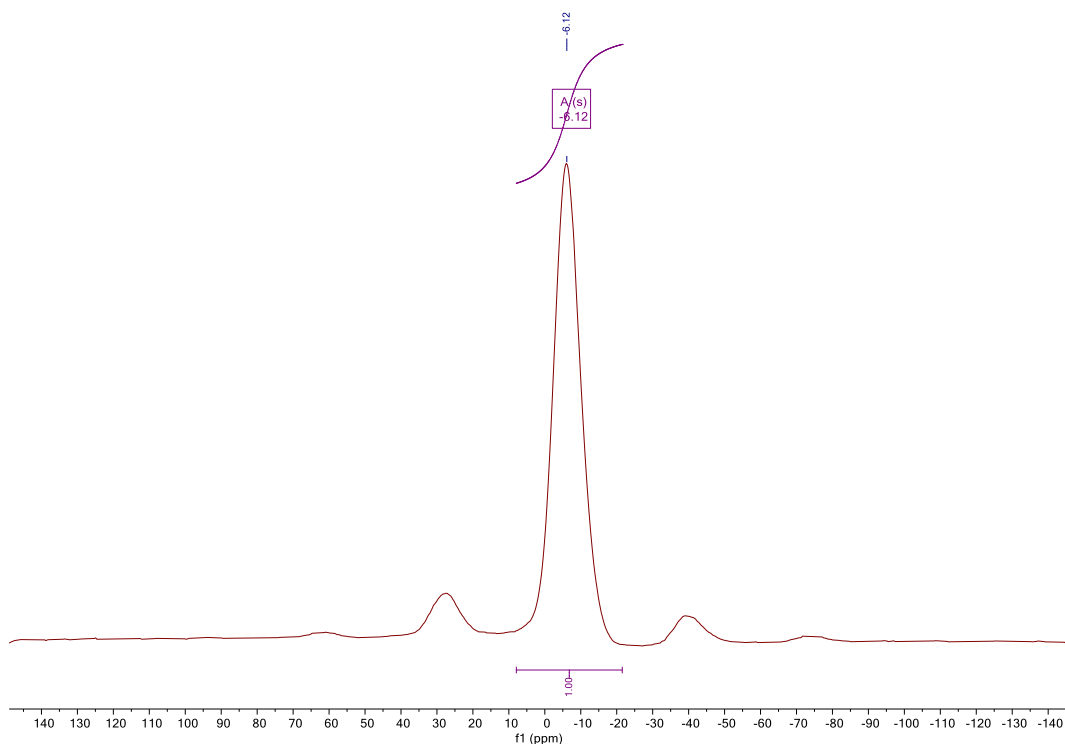
Figure 4.2: Solid-state ^{31}P NMR spectrum of PPh$_2$-*N*-decylPIIL **4.2**.

4.2.2.1 Scanning Electron Microscopy (SEM)

SEM analysis was used to determine the surface morphology of PPh$_2$-*N*-decylPIIL **4.2**. The SEM images in Figure **4.3** show that PPh$_2$-*N*-decylPIIL appears to have a smooth surface with only small areas of granular structure, which exhibit some porous features.
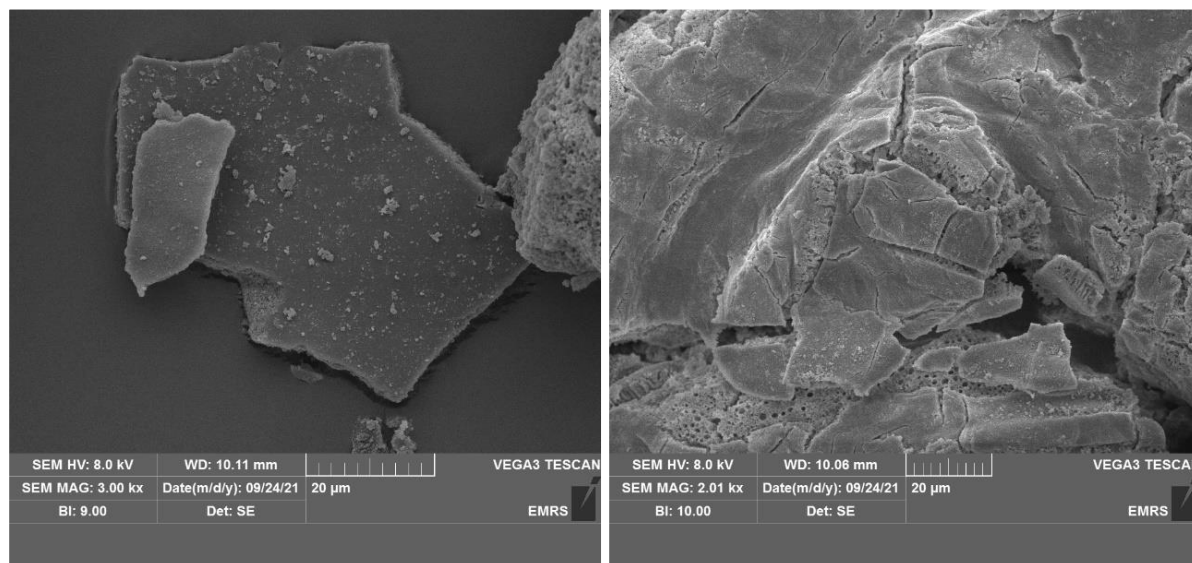
Figure 4.3: High-resolution scanning electron microscopy (SEM) images of PPh$_2$-*N*-decylPIIL **4.2**.

4.2.2.2 ThermoGravimetric Analysis (TGA)

The thermal stability of PPh$_2$-*N*-decylPIIL **4.2** was evaluated by thermogravimetric analysis (TGA) and differential scanning calorimetry (DSC). Figure **4.4** shows a slight initial weight loss (~5%) at approximately 100 °C, assigned to water or residual reaction solvent evaporation. The more significant weight loss observed at ~270 °C is likely to be due to degradation of the imidazolium pendants, which has been proven to happen in related polymers through dealkylation and carbene production.[289] This is followed by degradation likely to involve the PPh$_2$ moiety at 370 – 400 °C, and finally significant decomposition at around 550 °C,[290] which is associated with the polystyrene backbone. The analysis indicates that PIIL degradation occurred above 250 °C, indicating that the polymer is thermally stable above the temperature required for liquid-phase catalysis.
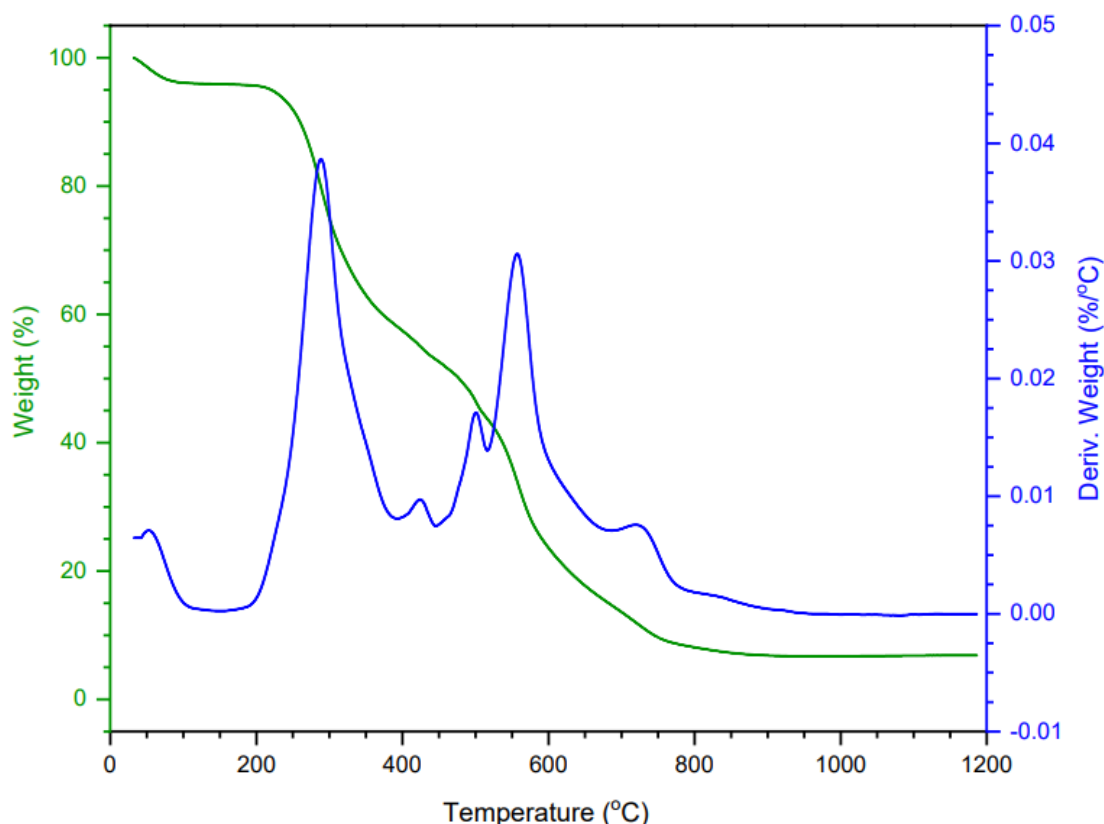
Figure 4.4: TGA curve for PPh$_2$-*N*-decylPIIL **4.2**; wt% v temperature (green) and (b) derivative wt% v temperature (blue). Heating rate of 10 °C min^{-1} in air.

4.2.3   Synthesis and Characterisation of PIIL Supported Palladium Nanoparticles (PdNP@PIIL)

Palladium loading experiments to the PIIL supports were performed by using an ion-exchange reaction protocol previously described in the literature (Scheme **4.5**).[82,119,291] The optimised ratio for the ionic liquid-like cations to the neutral phosphine of 2:1 in the PIIL supports was designed to facilitate achievement of a Pd to phosphine ratio in the final catalyst of 1:1 simply by complete ion exchange as long as the metal precursor has a charge of -2. This ratio is key for the activity of the catalyst because it ensures effective stabilisation of the surface of the Pd nanoparticles and prevents the PdNPs from agglomerate formation and ultimately decreased catalytic activity. Thus, the ion exchange reaction was accomplished by treating the desired PIIL with sodium tetrachloropalladate Na$_2$[PdCl$_4$] in water. As a result, the tetrachloropalladate anion substitutes both halides from PIIL. The imidazolium cations and the negatively charged Pd salt is expected to have a strong electrostatic attraction that will allow effective immobilisation of the Pd within the polymer. After stirring overnight at room temperature, the PdCl$_4$@PPh$_2$-PEGPIIL **4.3** and

PdCl$_4$@PPh$_2$-*N*-decylPIIL **4.4** were isolated by filtration as orange powders in >90% yield in each case.

The preparation of PdNP@PIIL catalysts was achieved by reducing the Pd^{II} species in the presence of excess NaBH$_4$ in ethanol. In each case, the solution immediately turned from orange to black colour, indicating that Pd^{II} had been reduced to Pd^0. The mixture was stirred overnight to ensure that the reaction was complete. The solvent volume was reduced, the residue was filtered, washed with water, ethanol, diethyl ether, and dried under high vacuum to afford PdNP@PPh$_2$-PEGPIIL **4.5** and PdNP@PPh$_2$-*N*-decylPIIL **4.6** as black powders in >70% yield.
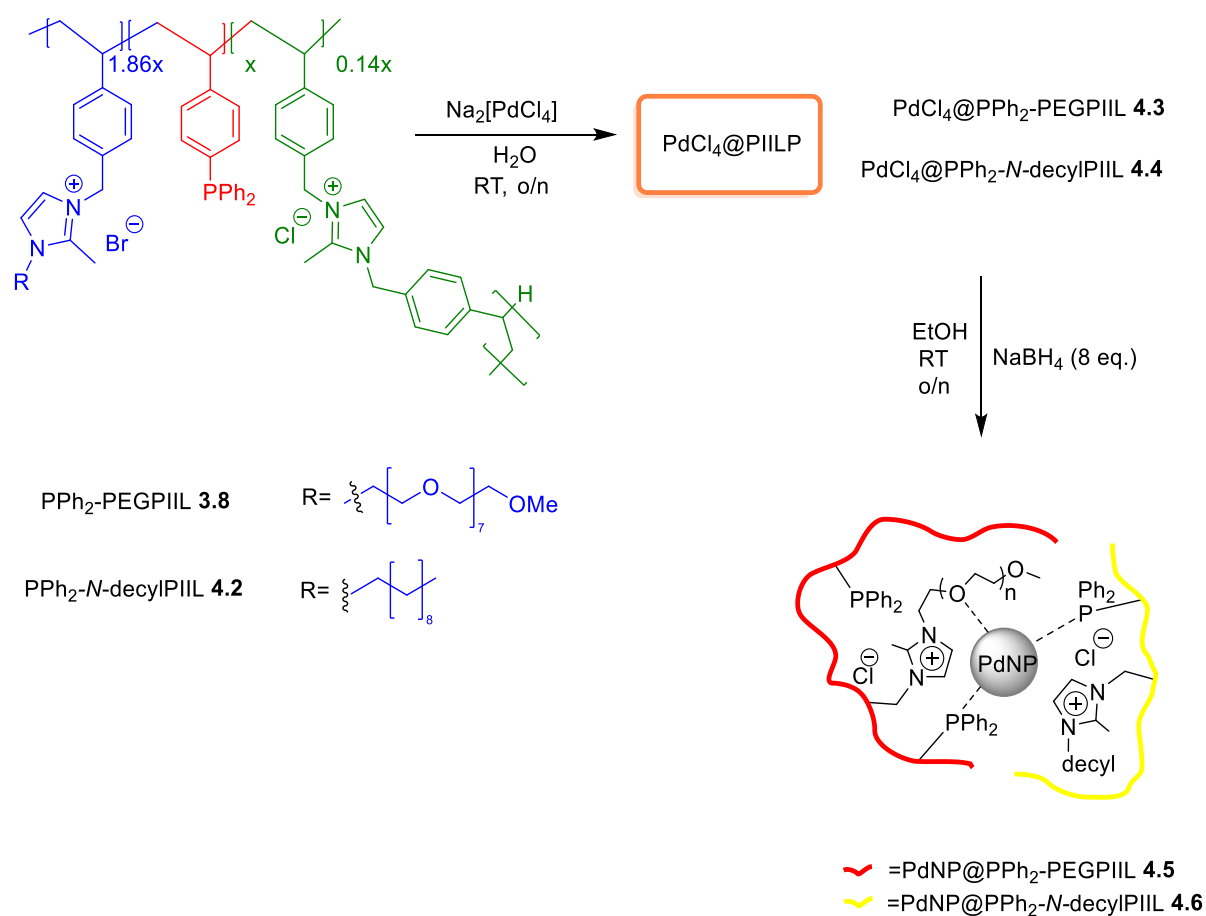
Scheme 4.5: Synthetic route used to impregnate the PIIL materials with Na$_2$[PdCl4] followed by NaBH$_4$ reduction to give the corresponding PIIL-stabilised PdNPs.

4.2.3.1 Solid-State Nuclear Magnetic Resonance (SSNMR)

The existence of Pd-P interactions in PdCl$_4$@PPh$_2$-PEGPIIL **4.3** and PdCl$_4$@PPh$_2$-*N*-decylPIIL **4.4** was examined by using solid-state ^{31}P NMR experiments (Figure **4.5**). Pd-P interactions were suggested by a significant shift of the signals resonating at δ -6 to 28 ppm for PdCl$_4$-PEGPIIL **4.3** (Figure **4.5a**) and δ -6 to 27 ppm for PdCl$_4$@PPh$_2$-*N*-decylPIIL **4.4** (Figure **4.5b**). A single peak (plus spinning side-bands) in the solid-state ^{31}P NMR spectrum of both **4.3** and **4.4** further confirmed the complete consumption of the starting material. The solid-state ^{31}P NMR spectrum of PdNP@PPh$_2$-PEGPIIL **4.5** (Figure **4.5c**) indicated two distinct signals, a signal resonating at δ 29 ppm was assigned for Pd(0) species while the minor signal resonating at δ 24 ppm was assigned for the Pd(II) species. In contrast, the solid-state ^{31}P NMR spectrum of PdNP@PPh$_2$-*N*-decylPIIL **4.6** (Figure **4.5d**) presented three signals resonating at δ 28, 10 and δ 0 ppm. The signal resonating at δ 28 ppm was assigned to PdNP@PPh$_2$-*N*-decylPIIL **4.6**, the small downfield shift to δ 10 ppm from the free phosphine may be due in part, to the coordination of the phosphine to more electron rich Pd^0 clusters and the δ 0 ppm signal might be due to different binding modes of phosphine functionalised supports with the non-homogenous PdNPs surface.[119,288,292] A survey of the relevant literature reveals that these values are consistent with the data previously reported. For instance, PdCl$_4$@PPh$_2$-PEGPIIL (δ 26.8 ppm), PdCl$_4$@PPh$_2$-PEGPIIL (δ 27.9 ppm), PdNP@PPh$_2$-PIIL (δ 29.5 ppm) and PdNP@PPh$_2$-PEGPIIL (δ 28.8 ppm), these values were reported previously by the Knight/Doherty group.[82,119,120] Also, from other research groups: PdNP stabilised by Phosphine-Functionalised imidazolium Ionic Liquids PdNP@PFILS (δ 29.5 ppm),[293] Pd nanoparticles stabilised with phosphine functionalised Porous Organic Polymer PdNP@POP-Ph$_3$P (δ 28.5 ppm),[55] phosphine-stabilised monodisperse palladium nanoparticles ((dba)Pd(0)TPP$_2$) (δ 29.4 ppm)[294] and phosphine modified binaphthyl palladium nanoparticles BINAP/Bin-PdNP (δ 28.6 ppm).[295]
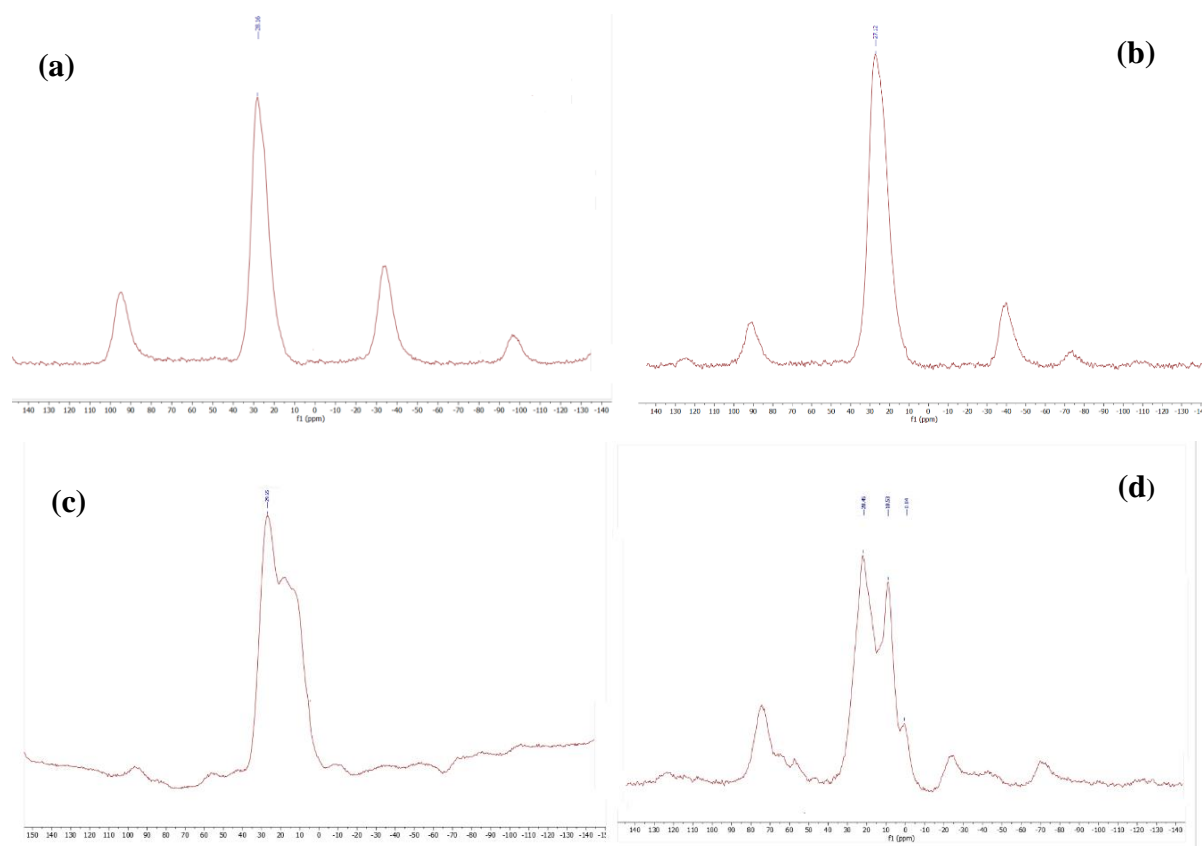
Figure 4.5: Solid state ^{31}P NMR spectrum of (a) PdCl$_4$@PPh$_2$-PEGPIIL **4.3**, (b) PdCl$_4$@PPh$_2$-*N*-decylPIIL **4.4**, (c) PdNP@ PPh$_2$-PEGPIIL **4.5** and (d) PdNP@PPh$_2$-*N*-decylPIIL **4.6**.

4.2.3.2 ICP Optical Emission Spectrometry (ICP-OES)

The palladium content of catalysts PdCl$_4$@PPh$_2$-PEGPIIL **4.3**, PdCl$_4$@PPh$_2$-*N*-decylPIIL **4.4**, PdNP@PPh$_2$-PEGPIIL **4.5** and PdNP@PPh$_2$-*N*-decylPIIL **4.6** was determined using ICP-OES analysis, and the values are listed in Table **4.1.** Interestingly, the palladium content in the PPh$_2$-*N*-decylPIIL tetrachloropalladate and the corresponding PdNP was higher than PPh$_2$-PEGPIIL, which may be due to a greater amount of absorbed solvent associated with the PEG functionality.

Table 4.1: Palladium content of PIIL catalyst as determined by ICP-OES.

Entry	Catalyst	mmol Pd/ g	Pd wt%
1	PdCl$_4$@PPh$_2$-PEGPIIL **4.3**	0.63	6.80
2	PdCl$_4$@PPh$_2$-*N*-decylPIIL **4.4**	0.72	7.68
3	PdNP@PPh$_2$-PEGPIIL **4.5**	0.51	5.45
4	PdNP@PPh$_2$-*N*-decylPIIL **4.6**	1.06	11.3

4.2.3.3 Scanning Electron Microscopy (SEM)

SEM microscopy was used further to investigate the morphology of PdCl$_4$@PPh$_2$-PEGPIIL **4.3**, PdCl$_4$@PPh$_2$-*N*-decylPIIL **4.4**, PdNP@PPh$_2$-PEGPIIL **4.5** and PdNP@PPh$_2$-*N*-decylPIIL **4.6** (Figure **4.6**) compared to the parent polymers. With the exception of PdCl$_4$@PPh$_2$-*N*-decylPIIL **4.4**, the samples have a much more granular texture, possibly due to the additional processing steps needed for the impregnation and reduction of PdCl$_4$ with the polymer materials.
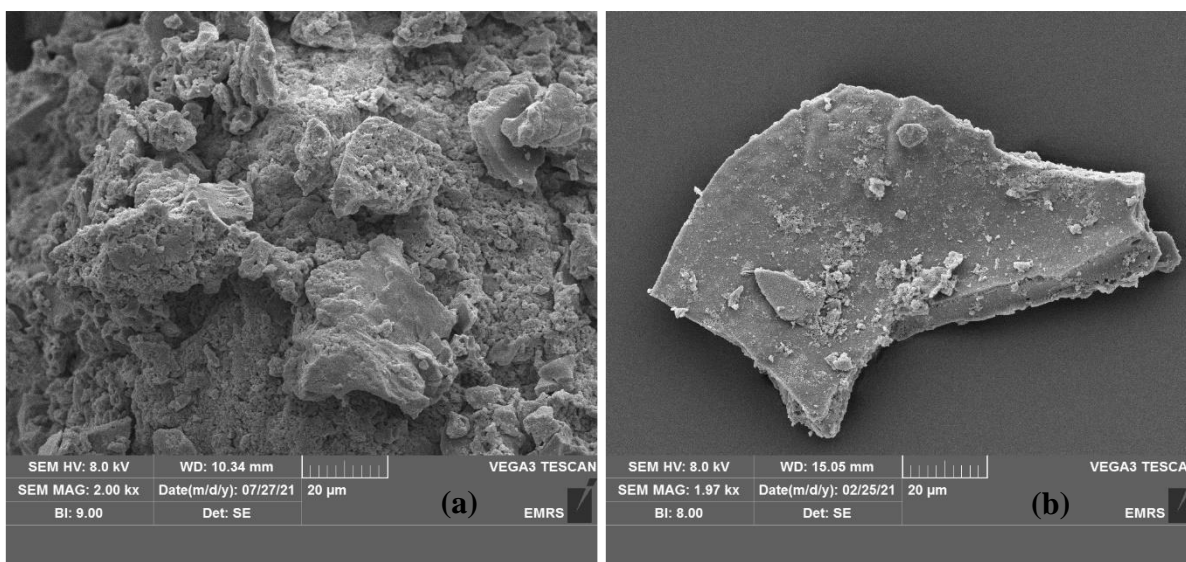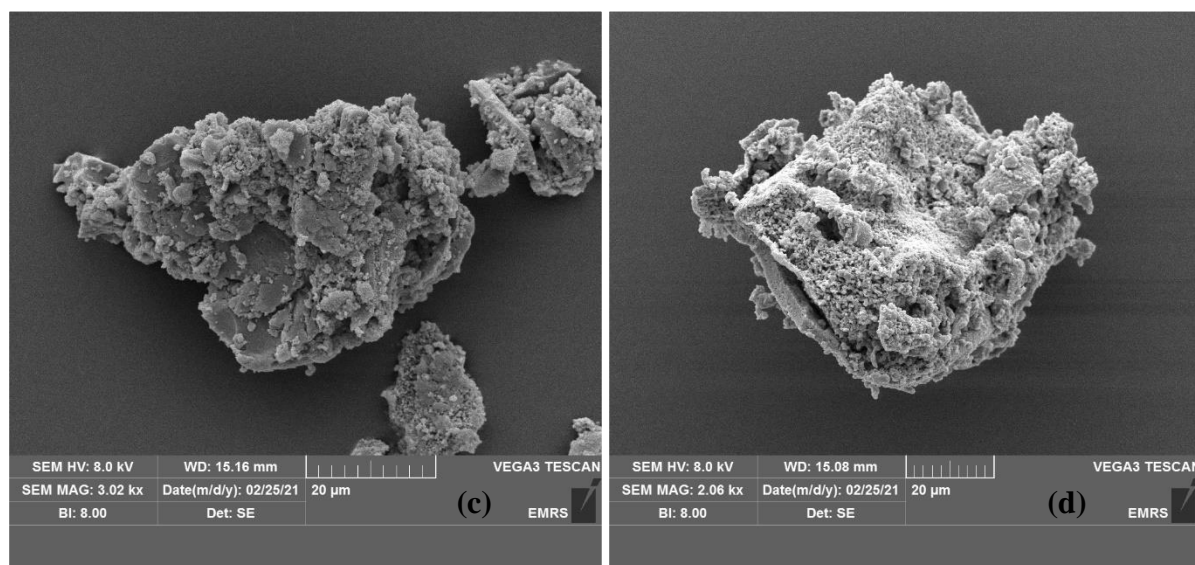
Figure 4.6: SEM images of (a) PdCl$_4$@PPh$_2$-PEGPIIL **4.3**, (b) PdCl$_4$@PPh$_2$-*N*-decylPIIL **4.4**, (c) PdNP@PPh$_2$-PEGPIIL **4.5** and (d) PdNP@PPh$_2$-*N*-decylPIIL **4.6**.

4.2.3.4 Transmission Electron Microscopy (TEM)

TEM analysis was used to determine the size distribution of Pd nanoparticles for PdNP@PPh$_2$-PEGPIIL **4.5** and PdNP@PPh$_2$-*N*-decylPIIL **4.6**. All the samples analysed consisted of small near monodisperse nanoparticles with an average diameter of 1.4 ± 0.3 nm and 1.3 ± 0. 3 nm respectively. The representative micrographs and histograms of particle distribution based on >100 particles are shown in Figure **4.7**.
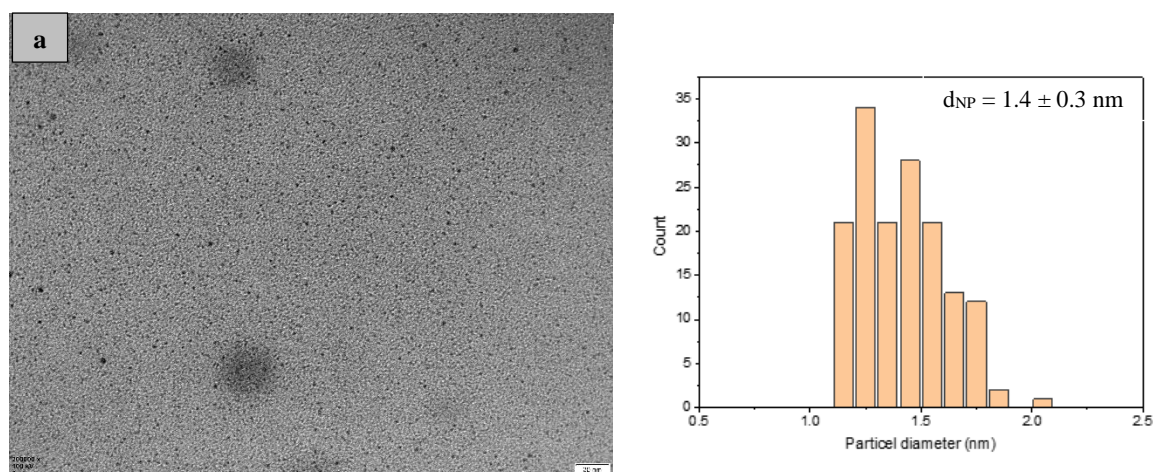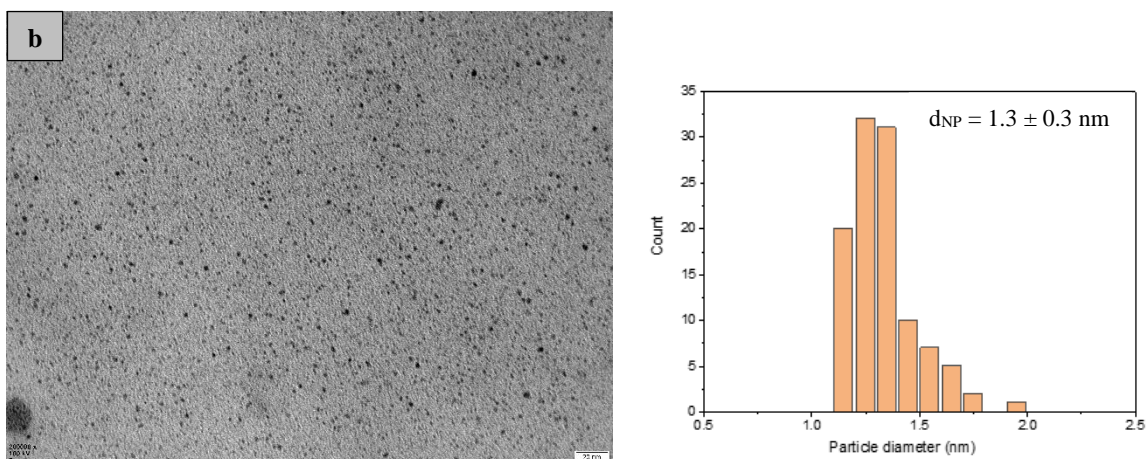
Figure 4.7: HRTEM micrographs of (a) PdNP@PPh₂-PEGPIIL **4.5** and (b) PdNP@PPh₂-*N*-decylPIIL **4.6** and corresponding size distributions determined by counting >100 particles. The white scale bar is 20 nm.

In comparison, the Lei *et al.* group has successfully generated highly active palladium NPs ex-situ stabilised with phosphine functionalised porous ionic polymer with an average diameter of 2.7 nm, which effectively catalysed the hydrogenation of nitroarenes in water.[55] The Luska *et al.* group has also succeeded in generating palladium nanoparticles stabilised by 6 different phosphine functionalised ionic liquids synthesised in imidazolium-based ionic liquids using H₂ to generate the PdNPs with an average diameter of 3 nm.[293]

4.2.4   Optimisation of Quinoline Hydrogenation

Hydrogenation of one, or both, rings in Quinoline may give three possible products (1,2,3,4-tetrahydroquinoline, 5,6,7,8-tetrahydroquinoline and decahydroquinoline), as shown in Figure **4.8**.
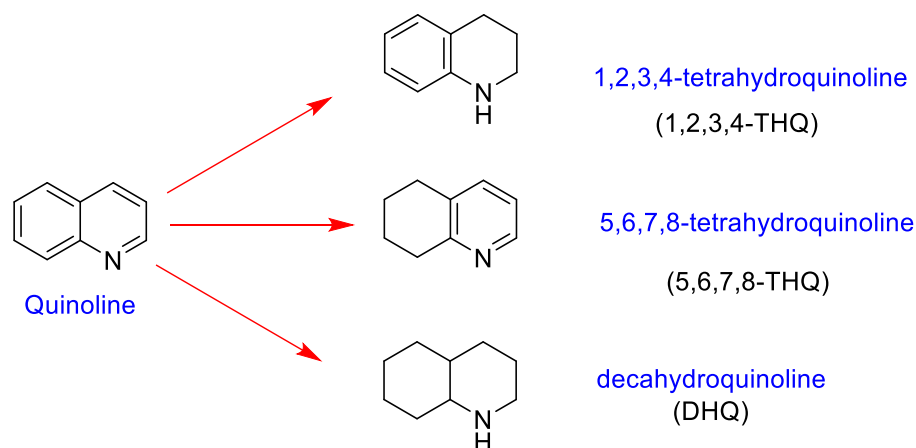
Figure 4.8: The main hydrogenation products of quinoline afford (5,6,7,8-THQ), (1,2,3,4-THQ), and (DHQ).

Quinoline is composed of a pyridine ring fused with a benzene ring and forms a conjugated π system of 10 atoms and 10 π electrons which is therefore overall aromatic since it obeys Hückel's rule of aromaticity. Because nitrogen is more electronegative than carbon, an inductive effect is induced within the pyridine ring and creates a stronger dipole than in the benzene-like ring, as shown in the electron density of quinoline (Figure **4.9**).
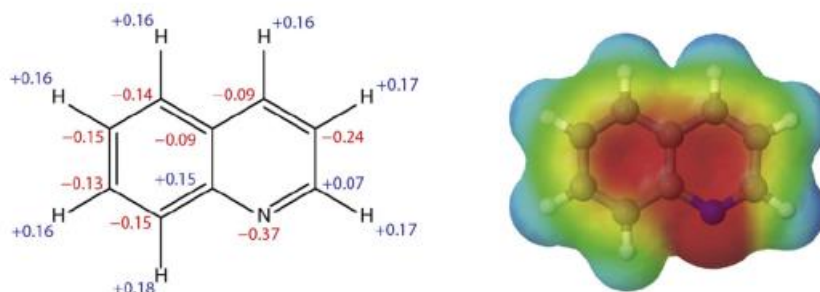
Figure 4.9: Net atomic charges of the nuclear sites in quinoline (left), along with the surface of the electrostatic potential, plotted from -0.1 V in red to +0.1 V in blue. (The image is adapted from reference 300).

The impact of the inductive effect in the pyridine ring towards its thermodynamic susceptibility for hydrogenation in comparison to benzene can be gauged by the delocalisation energy. The delocalization energy for benzene is 150 kJ mol^{-1}, while for pyridine is 117 kJ mol^{-1}.[296] This difference in energy suggests that hydrogenation of the pyridine ring in quinoline is likely to be easier than that of the benzene ring. Therefore, PdNP@PPh$_2$-PEGPIIL **4.5** and PdNP@PPh$_2$-*N*-decylPIIL **4.6** were expected to exhibit better chemoselectivity for the hydrogenation of quinoline toward 1,2,3,4-tetrahydroquinoline. In this research, quinoline is used as the benchmark substrate to examine the efficacy and selectivity of the catalyst for the quinoline hydrogenation using mild conditions and a green solvent with a hydrogen source.
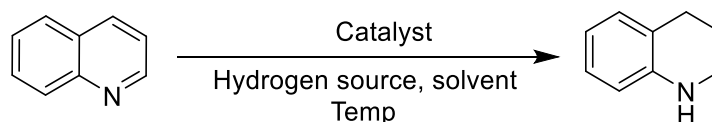
Scheme 4.6: General procedure for the hydrogenation reaction toward 1,2,3,4-tetrahydroquinoline.

The conversion and selectivity of quinoline hydrogenation by using the PIIL supported PdNPs and PdCl$_4$ were measured by adding 1 mmol of 1,3-dinitrobenzene to the reaction mixture after the

work-up, which serves as an internal standard for ^{1}H NMR analysis. Assignment of the components present in the product mixture of the hydrogenation was confirmed by comparison with a mixture of commercially available materials (Figure **4.10**).
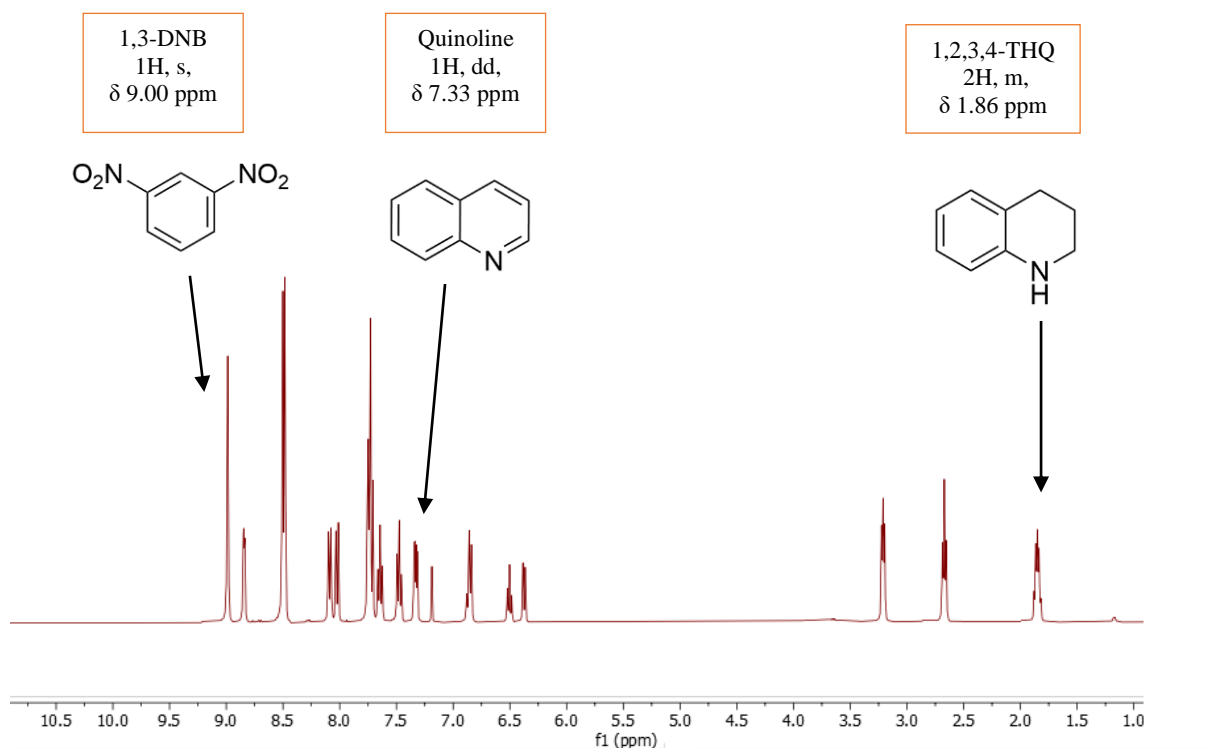
Figure 4.10: ^{1}H NMR spectrum (300 MHz, CDCl$_3$) of a mixture of quinoline, 1,2,3,4-THQ and the internal standard 1,3-dinitrobenzene; characteristic signals are listed with their splitting and chemical shifts.

4.2.4.1 Hydrogen source screening.

The catalytic transfer hydrogenation using hydrogen donors such as sodium borohydride,[297] formic acid,[298] dimethylamine borane complex,[259] hydrazine hydrate[258] and the azeotropic mixture of formic acid/triethylamine (5:2)[257] is a straightforward and versatile method that has been proposed as an alternative for conventional hydrogenation using H$_2$. PdNP@PPh$_2$-PEGPIIL **4.5** was chosen as the catalyst to be optimised since the Knight/Doherty group had previously discovered good results in PPh$_2$-PEGPIIL supported nanoparticles.[82,83,119,120]

Table 4.2: Screening of hydrogen source for the transfer hydrogenation of quinoline
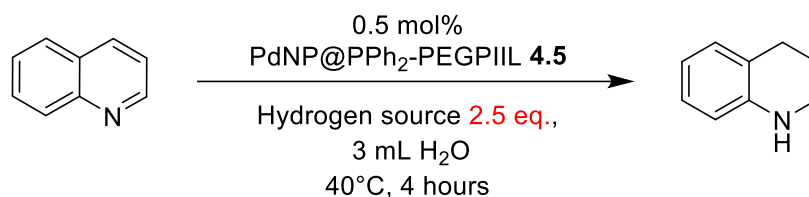
Entry[a]	**Hydrogen source**	**Conversion[a,b] (%)**	**Selectivity % 1,2,3,4-THQ**
1	(5:2) HCOOH/Et$_3$N	15	100
2	HCOOH	9	100
3	NH$_2$-NH$_2$ hydrate	4	100
4	NaBH$_4$	85	100
5	(CH$_3$)$_2$NH·BH$_3$	90	100

[a]Reaction conditions: 0.5 mol% catalyst (based on ICP), 3 mL H$_2$O and 2.5 mmol of a hydrogen source were stirred for 5 minutes before adding 1 mmol quinoline, then heated at 40 °C for 4 hours. [b]Conversion of quinoline and selectivity for 1,2,3,4-THQ were determined using ^{1}H NMR spectroscopy with 1,3-dinitrobenzene as the internal standard. Average of at least 3 runs.

The azeotropic mixture of formic acid/triethylamine (5:2) gave only 15% conversion with 100% selectivity toward 1,2,3,4-THQ (Table **4.2**, entry 1). Formic acid and hydrazine hydrate gave very low conversion 9% and 4%, respectively (Table **4.2**, entries 2 and 3). Interestingly, sodium borohydride and dimethylamine borane complex appeared to be the best hydrogen sources for quinoline hydrogenation and gave 85% and 90% conversion respectively and 100% selectivity toward 1,2,3,4-THQ (Table **4.2**, entries 4 and 5). Initially, sodium borohydride was used as a hydrogen source for further reaction optimisations before examining the use of dimethylamine borane complex.

4.2.4.2 Solvent optimisation

The solvent significantly influences the reaction rate and selectivity in catalytic hydrogenation reactions.[299] Furthermore, the solvent is pivotal in heterogeneous catalysis because it mediates and dictates the interaction between the catalyst surface and the reactants. A range of different reaction solvents were screened to achieve optimal performance of PdNP@PPh$_2$-PEGPIIL **4.5** ideally to find conditions which exhibit green credentials.

Table 4.3: Optimisation of reaction solvent for the transfer hydrogenation of quinoline
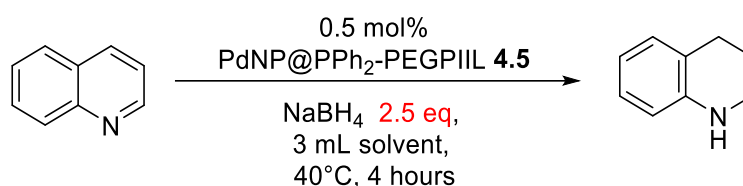
Entry[a]	Solvent	Conversion[a,b] (%)	Selectivity % 1.2,3,4 -THQ
1	H$_2$O	85	100
2	EtOH	71	100
3	EtOH/H$_2$O (1:1)	34	100
4	MeOH	0	0
5	THF	0	0

[a]Reaction conditions: 0.5 mol% catalyst (based on ICP), 3 mL solvent and 2.5 mmol NaBH$_4$ were stirred for 5 minutes before adding 1 mmol quinoline, then heated at 40 °C for 4 hours. [b]Conversion of quinoline and selectivity for 1,2,3,4-THQ were determined using ^{1}H NMR spectroscopy with 1,3-dinitrobenzene as the internal standard. Average of at least 3 runs.

As shown in Table **4.3**, the best result was obtained with H_2O as 85% conversion with 100% selectivity for 1,2,3,4 THQ (Table **4.3,** entry 1). In addition, EtOH gave a good result with 71% conversion and 100% selectivity for 1,2,3,4 THQ (Table **4.3,** entry 2). In contrast, the catalyst performed poorly in a 1:1 mixture of ethanol: water with 34% conversion. Although the conversion varied widely depending on the solvent used, the selectivity remained 100% for 1,2,3,4-THQ (Table **4.3,** entries 1-3). Besides the variation in the nature of the solvents, the low solubility of $NaBH_4$ in aprotic polar solvents (such as THF) and the decomposition of $NaBH_4$ in methanol may explain the lack of reaction in these cases (Table **4.3,** entries 4 and 5).[300] For the remaining studies, water was chosen as a solvent as it gave the highest conversion, is potentially a green solvent which is eco-friendly, accessible, and frequently reported to be a promoter in increasing the hydrogenation rate.[287,301,302]

4.2.4.3 Catalyst loading

To determine the optimum catalyst loading, several reactions were carried out in the presence of PdNP@PPh$_2$-PEGPIIL **4.5** and PdNP@PPh$_2$-*N*-decylPIIL **4.6** with a range of catalyst loading (0.05, 0.10 and 0.5 mol%). In addition, $NaBH_4$ 2.5 mmol was used as a hydrogen source and 3 mL H_2O at 40 °C for 1 hour (Table **4.4**).

Table 4.4: Catalyst loading optimisation for the transfer hydrogenation of quinoline

Entry[a]	Catalyst	Catalyst loading %	Conversion[a,b] (%)	Selectivity % 1.2,3,4 THQ
1	PdNP@PPh$_2$-PEGPIIL **4.5**	0.05	15	100
2	PdNP@PPh$_2$-*N*-decylPIIL **4.6**	0.05	11	100
3	PdNP@PPh$_2$-PEGPIIL **4.5**	0.1	15	100
4	PdNP@PPh$_2$-*N*-decylPIIL **4.6**	0.1	10	100
5	PdNP@PPh$_2$-PEGPIIL **4.5**	0.5	34	100
6	PdNP@PPh$_2$-*N*-decylPIIL **4.6**	0.5	22	100

[a]Reaction conditions: mol% catalyst (based on ICP), 3 mL H$_2$O and 2.5 mmol NaBH$_4$ were stirred for 5 minutes before adding 1 mmol quinoline, then heated at 40 °C for 1 hour. [b]Conversion of quinoline and selectivity for 1,2,3,4-THQ were determined using ^{1}H NMR spectroscopy with 1,3-dinitrobenzene as the internal standard. Average of at least 3 runs.

The selectivity for 1,2,3,4-THQ was excellent at all levels of catalyst loading, and the best conversions (34% and 22%) were achieved with 0.5 mol% of PdNP@PPh$_2$-PEGPIIL **4.5** and PdNP@PPh$_2$-*N*-decylPIIL **4.6** (Table **4.4,** entries 5 and 6) while there was no significant difference in conversion between 0.05% and 0.1 mol% loading (Table **4.4,** entries 1,2,3 and 4). As a result of Table **4.4,** 0.5 mol% loading was selected for further optimisation due to the higher conversion within one hour compared to other catalyst loadings.

4.2.4.4 *In-Situ* Nanoparticles Formation

The Knight-Doherty research group previously demonstrated that it is possible to generate PdNP@PPh$_2$-PEGPIIL **4.5** *in situ* from its precursor PdCl$_4$@PPh$_2$-PEGPIIL **4.3** immediately prior to the addition of the substrate for reaction, resulting in monodisperse nanoparticles with high activity.[119] Under the conditions determined previously, we aimed to study the selectivity and activity of the catalysts and their precursors (Table **4.5**).

Table 4.5: Comparison between pre-formed and *in situ* generated PdNP catalysts for quinoline reduction.

Entry	Catalyst	Conversion[b] (%)	Selectivity % 1.2,3,4 THQ
1[a]	No catalyst	8	100
2[c]	PdCl$_4$@PPh$_2$-PEGPIIL **4.3**	36	100
3[c]	PdCl$_4$@PPh$_2$-*N*-decylPIIL **4.4**	34	100
4[d]	PdCl$_4$@PPh$_2$-PEGPIIL **4.3**	66	100
5[d]	PdCl$_4$@PPh$_2$-*N*-decylPIIL **4.4**	51	100
6[c]	PdNP@PPh$_2$-PEGPIIL **4.5**	85	100
7[c]	PdNP@PPh$_2$-*N*-decylPIIL **4.6**	74	100

[a]Reaction conditions: 3 mL H$_2$O and 2.5 mmol NaBH$_4$ were stirred for 5 minutes before adding 1 mmol quinoline then heated at 40 °C for 4 hours.

[b]Conversion of quinoline and selectivity for 1,2,3,4-THQ were determined using ^{1}H NMR spectroscopy with 1,3-dinitrobenzene as the internal standard. Average of at least 3 runs.

[c]Reaction conditions: 0.5 mol% precursor or catalyst (based on ICP), 3 mL H_2O and 2.5 mmol $NaBH_4$ were stirred for 5 minutes before adding 1 mmol quinoline, then heated at 40 °C for 4 hours.

[d]Reaction conditions: 0.5 mol% precursor (based on ICP) and 3 mL H_2O were stirred overnight, then 2.5 mmol $NaBH_4$ was added stirred for 5 minutes before adding 1 mmol quinoline then heated at 40 °C for 4 hours.

Initially, a background test was done in the absence of the catalyst. As we expected, the conversion was very low 8% (Table **4.5**, entry 1) and advocates the need for an active catalyst for this hydrogenation reaction to achieve a substantial conversion of quinoline. *In situ* palladium reduction by direct use of the Pd(II) precursors PdCl$_4$@PPh$_2$-PEGPIIL **4.3** and PdCl$_4$@PPh$_2$-*N*-decylPIIL **4.4**, which were stirred in the presence of the $NaBH_4$ for five minutes prior to substrate addition, showed similar conversions but unfortunately gave low activity after 4 hours reaction at 40 °C (Table **4.5,** entries 2 and 3). In order to ensure maximal solvent-polymer saturation, we decided to stir the precursors overnight in water prior to adding $NaBH_4$, then stirring for 5 minutes before adding the quinoline. The longer stirring of the precursors with water shows a dramatic increase in the catalytic activity and achieved 66% and 51% conversion, respectively whilst retaining the 100% selectivity for 1,2,3,4-THQ after 4 hours (Table **4.5,** entries 4 and 5). Finally, the PdNP@PPh$_2$-PEGPIIL **4.5** and PdNP@PPh$_2$-*N*-decylPIIL **4.6** results clearly showed that performance is highly efficient with ex-situ formed (pre-prepared) nanoparticles and achieved conversions of 85% and 74%, respectively, and 100% selectivity for 1,2,3,4-THQ in 4 hours (Table **4.5,** entries 6 and 7). Therefore, the further study of the conversion time profile and a comparative catalyst test was undertaken using the ex-situ generated PdNP@PPh$_2$-PEGPIIL **4.5** and PdNP@PPh$_2$-*N*-PIIL **4.6** to gain further insight into the quinoline hydrogenation.

4.2.4.5 Conversion-time profile and comparative catalyst test for Quinoline hydrogenation

Having identified the optimum conditions, comparative catalyst testing was performed to determine the effect of the PEG chain, which has been shown to be critical for activity and selectivity of the catalyst in previously published papers[82,83,119] and Chapter 3 compared to the decyl alkyl chain we synthesised in this chapter. Hence, a series of reactions were performed between zero hour and 5 hours under the optimum conditions. The conversion and selectivity for

each experiment were determined by ^{1}H NMR spectroscopy using 1,3-dinitrobenzene as internal standard. The results obtained are summarised in Figure **4.11**.
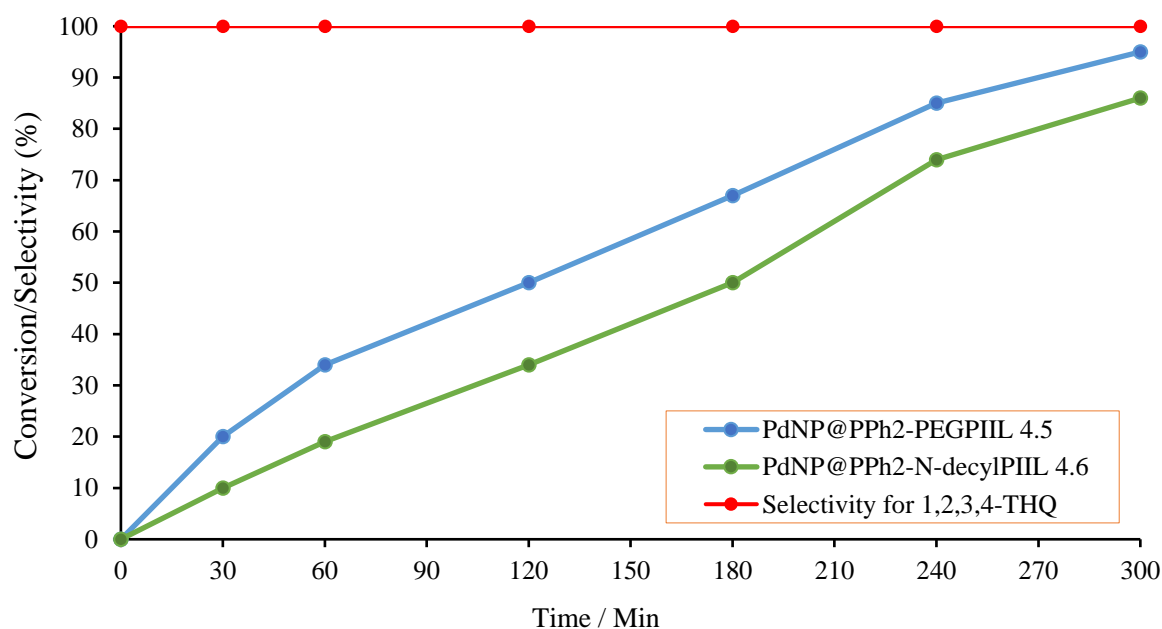
Figure 4.11: Time profile for quinoline hydrogenation to 1,2,3,4-THQ catalysed by PdNP@PPh$_2$-PEGPIIL **4.5** and PdNP@PPh$_2$-*N*-decylPIIL **4.6**. Reaction conditions: 0.5 mol% catalyst (based on ICP), 3 mL H$_2$O and 2.5 mmol NaBH$_4$ were stirred for 5 minutes before adding 1 mmol quinoline, then heated at 40 °C at different intervals of time. Conversion of quinoline and selectivity for 1,2,3,4-THQ were determined using ^{1}H NMR spectroscopy with 1,3-dinitrobenzene as the internal standard. Average of at least 3 runs.

The time conversion profile for quinoline hydrogenation catalysed by PdNP@PPh$_2$-PEGPIIL **4.5** and PdNP@PPh$_2$-*N*-decylPIIL **4.6** revealed 1,2,3,4-THQ was obtained in 95% and 86% conversion respectively and 100% selectivity for both catalysts after 5 hours (Figure **4.11**). Notably, high conversions were obtained with both catalysts, the PEGylated system slightly outperforming the alkyl chain system. The higher activity of PdNP@PPh$_2$-PEGPIIL **4.5** might be due to the presence of a hydrophilic influence. However, the excellent catalytic efficiency in water is mainly attributed to incorporating the highly hydrophilic polyethylene glycol into the PEG monomer within the catalyst's backbone. In this case, quinoline might efficiently coordinate to the catalysts active site in water, providing better molecular interactions *via* hydrogen bonding and organic interactions between the catalyst and the quinoline. In addition, a more homogenous dispersion of the catalyst in water might be achieved by PEGylation, which in turn will provide a quasi-homogeneous character with enhanced catalytic activity.

A literature survey showed that catalysts PdNP@PPh$_2$-PEGPIIL **4.5** and PdNP@PPh$_2$-*N*-decyPIIL **4.6** outperformed many reported catalytic systems for quinoline hydrogenation in water and NaBH$_4$ as a hydrogen source. For instance, 5 mol% of a polymer supported Pd catalyst (Pd-pol) gave 30% in conversion and >99% selectivity for 1,2,3,4-THQ after 9 hours at 60 °C in 5 mL water and 10 mmol of NaBH$_4$.[303] Also, nanoRu0@hectorite gave 56% conversion and 100% selectivity for 1,2,3,4-THQ after 20 hours at 40 °C in water using 8 equivalents of NaBH$_4$ and when the number of equivalents of NaBH$_4$ was increased to 10, and the temperature raised to 60 °C the system gave 95% conversion and 100% selectivity for 1,2,3,4-THQ after 4 hours.[300]

4.2.4.6 Comparisons to a commercially available catalyst Pd/C

The activity of PdNP@PPh$_2$-PEGPIIL **4.5** and PdNP@PPh$_2$-*N*-decylPIIL **4.6** against a commercially available sample of Pd/C (10 wt%) at the same Pd loading was explored under the optimum conditions. The conversions achieved with the Pd/C catalyst are listed in Figure **4.12**, along with the results obtained using PdNP@PPh$_2$-PEGPIIL **4.5** and PdNP@PPh$_2$-*N*-decylPIIL **4.6**.
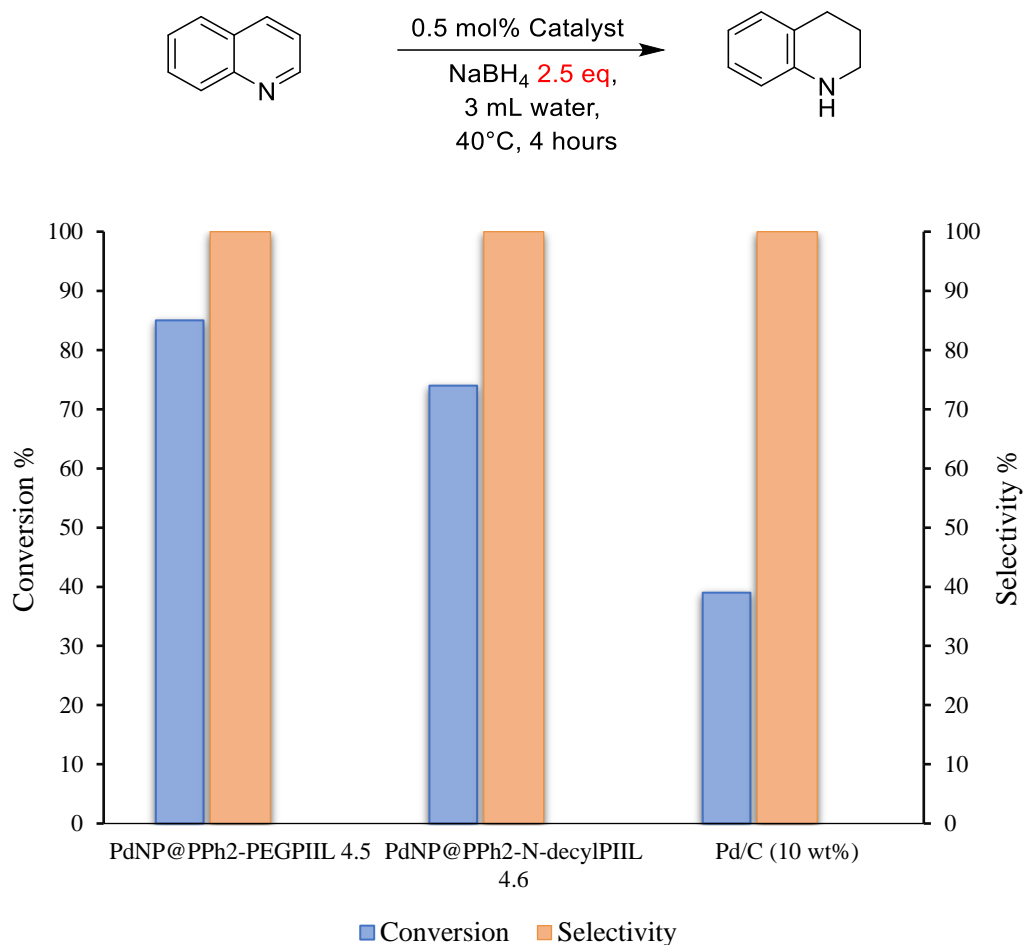
Figure 4.12: A comparison of the PdNP@PIIL systems to Pd/C.

Reaction conditions: 0.5 mol% catalyst (based on ICP), 3 mL H_2O and 2.5 mmol $NaBH_4$ were stirred for 5 minutes before adding 1 mmol quinoline, then heated at 40 °C for 4 hours. Conversion and selectivity were determined using ^{1}H NMR spectroscopy with 1,3-dinitrobenzene as the internal standard. Average of at least 3 runs.

Commercially available Pd/C gave 39% conversion with 100% selectivity for 1,2,3,4-THQ. Gratifyingly, The PdNP@PIIL systems outperform the commercially Pd/C (10 wt%) by a wide margin, as shown in Figure **4.12**.

Having investigated the use of sodium borohydride, we then repeated the study using an alternative reducing agent, the dimethylamine borane complex.

4.2.4.7 Dimethylamine Borane complex as a hydrogen source

4.2.4.7.1 Solvent optimisation

The effect of the reaction solvent on quinoline hydrogenation with dimethylamine borane complex as a hydrogen source was examined. Reactions in a range of polar solvents were performed under the optimum conditions to identify the ideal solvent and assess the performance of PdNP@PPh$_2$-PEGPIIL **4.5** and PdNP@PPh$_2$-N-decylPIIL **4.6** catalysts. The results in Table **4.8** show that varying the solvent considerably influences performance for both catalysts.

Table 4.6: Optimisation of reaction solvent for quinoline hydrogenation.
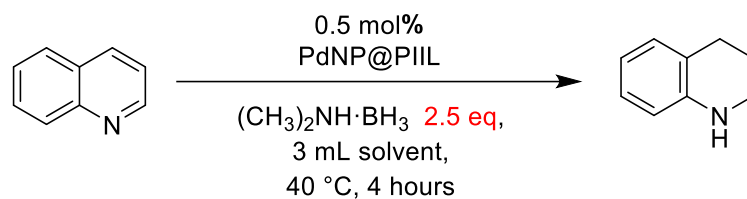
Entry	Catalyst	Solvent	Conversion[a][b] (%)	Selectivity % 1.2,3,4 THQ
1[a]	PdNP@PPh$_2$-PEGPIIL **4.5**	MeOH	55	100
2[a]	PdNP@PPh$_2$-N-decylPIIL **4.6**	MeOH	56	100
3[a]	PdNP@PPh$_2$-PEGPIIL **4.5**	EtOH	59	100
4[a]	PdNP@PPh$_2$-N-decylPIIL **4.6**	EtOH	62	100
5[a]	PdNP@PPh$_2$-PEGPIIL **4.5**	EtOH/H$_2$O (1:1)	82	100
6[a]	PdNP@PPh$_2$-N-decylPIIL **4.6**	EtOH/H$_2$O (1:1)	80	100
7[a]	PdNP@PPh$_2$-PEGPIIL **4.5**	H$_2$O	90	100
8[a]	PdNP@PPh$_2$-N-decylPIIL **4.6**	H$_2$O	100	100
9[c]	No catalyst	H$_2$O	0	0

[a]Reaction conditions: 0.5 mol% catalyst (based on ICP), 3 mL solvent and 2.5 mmol $(CH_3)_2NH \cdot BH_3$ were stirred for 5 minutes before adding 1 mmol quinoline, then heated at 40 °C for 4 hours.

[b]Conversion of quinoline and selectivity for 1,2,3,4-THQ were determined using ^{1}H NMR spectroscopy with 1,3-dinitrobenzene as the internal standard. Average of at least 3 runs.

[c]Reaction conditions: 3 mL H_2O and 2.5 mmol $(CH_3)_2NH \cdot BH_3$ were stirred for 5 minutes before adding 1 mmol quinoline then heated at 40 °C for 4 hours.

The conversions obtained in methanol with PdNP@PPh$_2$-PEGPIIL **4.5** and PdNP@PPh$_2$-*N*-decylPIIL **4.6** were 55% and 56%, respectively, with 100% selectivity for 1,2,3,4-THQ (Table **4.6,** entries 1 and 2). In the presence of ethanol, the conversion improved slightly to 59% and 62% with 100% selectivity for 1,2,3,4-THQ (Table **4.6**, entries 3 and 4). Furthermore, the combination of EtOH and water resulted in a dramatic increase to 82% and 80% conversion with 100% selectivity for 1,2,3,4-THQ (Table **4.6**, entries 5 and 6). Interestingly, the conversion was increased to 90% and 100%, respectively, and 100% selectivity for 1,2,3,4 -THQ with only water (Table **4.6**, entries 7 and 8). As we expected, the conversion was zero when the reaction was done in the absence of catalyst under identical conditions (Table **4.6**, entry 9). Hence water was deemed to be the optimum solvent for the remaining study.

4.2.4.7.2 Time profile and comparative test

Next, the hydrogenation of quinoline by using PdNP@PPh$_2$-PEGPIIL **4.5** and PdNP@PPh$_2$-*N*-decylPIIL **4.6** in the presence of dimethylamine borane complex $((CH_3)_2NH \cdot BH_3)$ as the reductant was studied under the optimum conditions to evaluate their activity compared to sodium borohydride (Figure **4.13**).
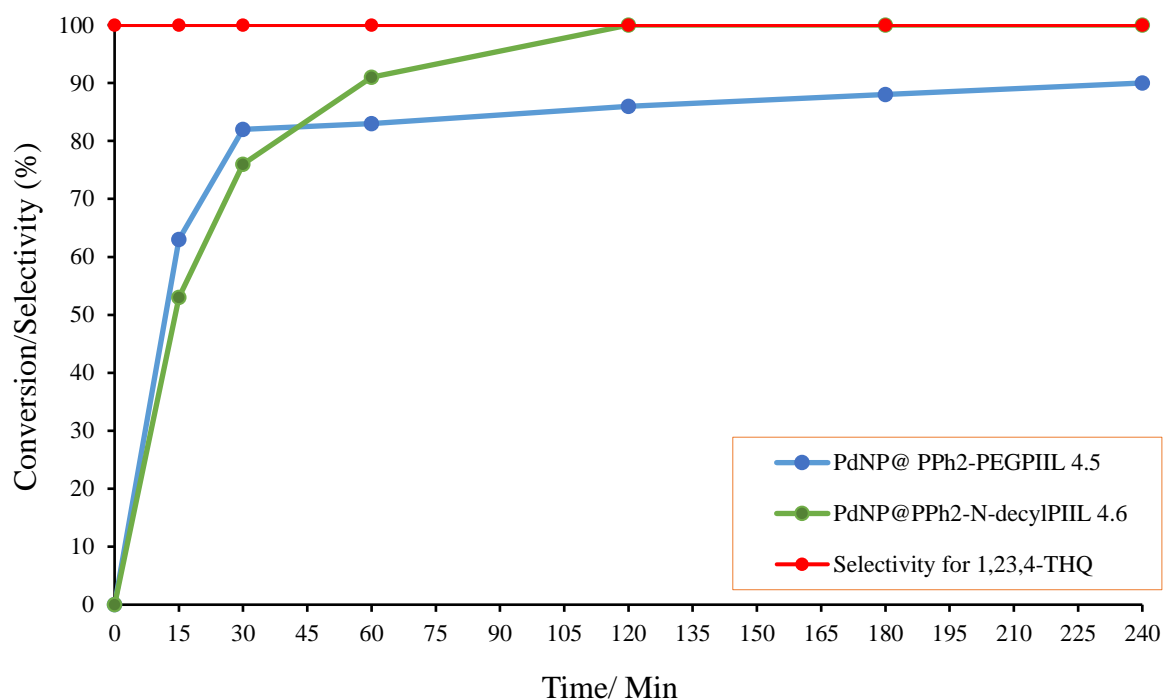
Figure 4.13: Time profile for quinoline hydrogenation to 1,2,3,4-THQ catalysed by PdNP@PPh$_2$-PEGPIIL **4.5** and PdNP@PPh$_2$-*N*-decylPIIL **4.6**. Reaction conditions: 0.5 mol% catalyst (based on ICP), 3 mL H$_2$O and 2.5 mmol (CH$_3$)$_2$NH·BH$_3$ were stirred for 5 minutes before adding 1 mmol quinoline, then heated at 40 °C for different intervals of time. Conversion of quinoline and selectivity for 1,2,3,4-THQ were determined using ^{1}H NMR spectroscopy with 1,3-dinitrobenzene as the internal standard. Average of at least 3 runs.

Surprisingly, PdNP@PPh$_2$-*N*-decylPIIL **4.6** gave 100% conversion and 100% selectivity for 1,2,3,4-THQ within 2 hours (Figure **4.13**). In contrast, PdNP@PPh$_2$-PEGPIIL **4.5** gave 90% conversion and 100% selectivity for 1,2,3,4-THQ after 4 hours. In principle, the more hydrophobic nature of the decyl-functionalised support material might lead to preferential interaction with the substrate and/or reductant and thus result in a higher effective concentration. But notably, PdNP@PPh$_2$-PEGPIIL **4.5** reached 82% within the first 30 minutes and therefore the initial reaction rate appears to be higher than PdNP@PPh$_2$-*N*-decylPIIL **4.6** which produced 76% conversion in the same time. Following the rapid initial conversion to 82%, subsequent reaction is then much slower, and reaches 90% after 4 hours. (Figure **4.13**). If saturation of the PdNP surface with the activated hydrogen occurs very rapidly, the reaction rate would be expected to directly depend on the available surface area of the PdNPs catalyst.[304]

The conversion/time profile reveals a significant improvement in reactivity of the catalysts compared to sodium borohydride.

4.2.4.7.3 Comparisons to a commercially available catalyst Pd/C

A comparative study between PdNP@PPh$_2$-PEGPIIL **4.5** and PdNP@PPh$_2$-*N*-decylPIIL **4.6** against a commercially available sample of Pd/C (10 wt%) was carried out using dimethylamine borane complex under the optimum conditions for 4 hours (Figure **4.14**).
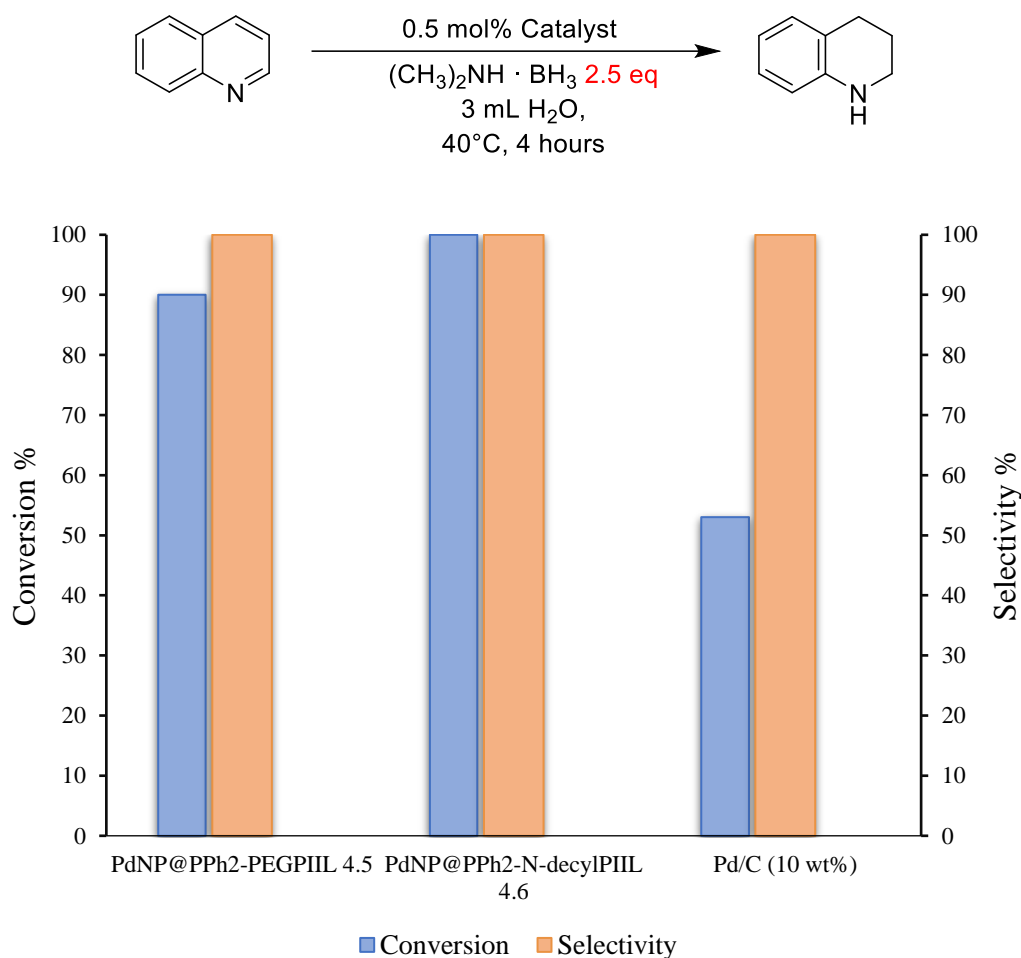
Figure 4.14: A comparison of PdNP@PPh$_2$-PEGPIIL **4.5** and PdNP@PPh$_2$-*N*-decylPIIL **4.6** to Pd/C.

Reaction conditions: 0.5 mol% catalyst (based on ICP), 3 mL solvent and 2.5 mmol (CH$_3$)$_2$NH·BH$_3$ were stirred for 5 minutes before adding 1 mmol quinoline, then heated at 40 °C for 4 hours. Conversion of quinoline and selectivity for 1,2,3,4-THQ were determined using ^{1}H NMR spectroscopy with 1,3-dinitrobenzene as the internal standard. Average of at least 3 runs.

Satisfyingly, the PdNP@PPh$_2$-PEGPIIL **4.5** and PdNP@PPh$_2$-*N*-decylPIIL **4.6** gave conversions of 90% and 100%, respectively, while the selectivity for both is 100% for 1,2,3,4-THQ. The PdNP@PIIL catalysts outperform the commercially available Pd/C (10 wt%) which produced 53% conversion and 100% selectivity for 1,2,3,4-THQ.

4.3 Conclusion

Palladium nanoparticle catalysts supported on two different phosphine-decorated polymers immobilised ionic liquids are highly efficient catalysts for quinoline hydrogenation in the presence of NaBH$_4$ and (CH$_3$)$_2$NH·BH$_3$ under mild conditions. PPh$_2$-*N*-decylPIIL **4.6** has been synthesised *via* free radical polymerisation and the solid-state ^{31}P NMR spectrum demonstrates one phosphorous containing species at δ -6.12 ppm. TGA analysis of PPh$_2$-*N*-decylPIIL **4.6** showed that the polymer is thermally stable above 250 °C which is required for liquid phase catalysis. SEM analysis of PPh$_2$-*N*-decylPIIL **4.6** has a smooth surface compared to PPh$_2$-PEGPIIL **3.8**.

The PIIL supports were impregnated with PdCl$_4^{2-}$ and reduced by NaBH$_4$ to give the corresponding PdNP@PIIL catalyst. The solid state ^{31}P NMR spectra were used to confirm the presence of Pd-P interactions, and most of the phosphine was coordinated to Pd. TEM analysis of PdNP@PPh$_2$-PEGPIIL **4.5** and PdNP@PPh$_2$-*N*-decylPIIL **4.6** revealed small near monodisperse nanoparticles with an average diameter of 1.4 ± 0.3 nm and 1.3 ± 0. 3 nm, respectively.

For quinoline reduction using either NaBH$_4$ or (CH$_3$)$_2$NH·BH$_3$ as hydrogen source, solvent optimisation studies demonstrated that the catalysts were most efficient in water delivering the highest conversion. Pre-formed generated PdNP catalyst showed higher catalytic activity than *in situ* generated PdNP for quinoline hydrogenation.

Quinoline hydrogenation performed in water under mild conditions and NaBH$_4$ as hydrogen source afford 100% selectivity toward 1,2,3,4-THQ and conversion (95% and 86%) were achieved with 0.5 mol% of PdNP@PPh$_2$-PEGPIIL **4.5** and PdNP@PPh$_2$-*N*-decylPIIL **4.6** after 5 hours at 40 °C. Interestingly, the use of (CH$_3$)$_2$NH·BH$_3$ as hydrogen source under identical conditions, resulted in a dramatic increase in the catalytic activity and achieved 90% conversion with PdNP@PPh$_2$-PEGPIIL **4.5** after 4 hours and 100% with PdNP@PPh$_2$-*N*-decylPIIL **4.6** after 2 hours while maintaining the 100% selectivity for 1,2,3,4-THQ. Comparative catalyst testing against

commercially available Pd/C (10 wt%), demonstrated that the catalysts outperformed Pd/C in the activity using both $NaBH_4$ and $(CH_3)_2NH \cdot BH_3$.

Having established that these phosphine-functionalised PIIL are effective supports for palladium nanoparticle catalysed transfer hydrogenation of quinoline using both $NaBH_4$ and $(CH_3)_2NH \cdot BH_3$ as hydrogen source, further studies will include:

- Increasing the equivalence of $NaBH_4$ and $(CH_3)_2NH \cdot BH_3$, to achieve 100% conversion in a short time.
- Investigation of the dependence of reaction rate on temperature in order to measure the activation energy (E_a) by Arrhenius plots.
- Exploration of the nature of the rate determining step by measuring kinetic isotopic effects using $NaBD_4$ and/or D_2O.
- Catalyst recycling studies including the importance of catalyst poisoning by adding 1,2,3,4-THQ to the reaction mixture.
- Substrate screening to functionalised quinolines with varying steric and electronic properties and additional potentially reducible groups (such as carbonyl, nitrile, halogen, nitro, alkene/alkyne) and other quinoline-like heterocycles (isoquinoline, quinoxaline, quinoline *N*-oxide, quinolinium salts)

Chapter 5. Platinum Nanoparticles Stabilised by PIIL for Evolution of Hydrogen from Hydrolysis of Sodium Borohydride

5.1   Introduction

The primary source of energy available currently is fossil fuels which are both limited and decreasing at an alarming rate.[305] In addition, the use of fossil fuels produces harmful byproducts for example, CO_2, CO, NO_x, $SO_{2,3}$, and H_2S the atmospheric concentration of all of which has increased in the last two decades.[306,307] As a result, fossil fuel use has a harmful effect on increasing the Earth's temperature, biodiversity, oceanic acidification of the environment and, of course, human health.[308–310]

Hydrogen has excellent potential as a clean and renewable energy carrier to ease the change from fossil fuels to renewable and environmentally friendly energy sources due to its high chemical energy per unit mass of hydrogen (142 MJ kg^{-1}) and the availability from different sources (e.g. H_2O, solar energy and biomass).[311–313] The use of solar energy to produce hydrogen as clean and renewable energy is currently among the hot topics among the scientific community. Not only because it is clean and renewable energy, but also has the beneficial aspect of producing CO_2-free energy and the only by-product formed during this process is water, which is beneficial and eco-friendly.[314–318] The issues associated with hydrogen are that it is dangerously flammable and possesses a low energy density per unit volume, therefore, efficient storage systems are required to handle and transport hydrogen safely. As a consequence, the use of hydrogen energy as an alternative to fossil fuel energy is quite challenging, especially in the automotive applications.[319–321] In order to apply this technology for commercial purposes, it is imperative to solve these potential issues. In this context, the identification or development of novel low molecular weight solid-state or hydrogen storage infrastructure materials has remained crucial since these materials have the capability of releasing hydrogen under normal conditions.[322–326]

Sodium borohydride ($NaBH_4$) is one of the most studied hydrogen storage materials because it has a high hydrogen capacity (up to 10.8 wt.%). In addition, it is very stable, non-hazardous, produces high purity hydrogen, cost-effective, lightweight, easily handled, water-soluble, and $NaBH_4$ solutions are non flammable.[312,313,322,327–329] The need for high temperatures to release hydrogen

from NaBH$_4$, limits its scope to some extent. However, NaBH$_4$ hydrolysis has been achieved with various catalysts under mild conditions (Equation **5.1**).

$$NaBH_4 + 4H_2O \longrightarrow NaB(OH)_4 + 4H_2$$

Equation 5.1: The reaction of NaBH$_4$ and H$_2$O to generate hydrogen.

Although the aqueous hydrolysis of NaBH$_4$ solution can be achieved by using homogeneous catalytic systems,[313,330–333] the use of heterogeneous catalysis has received increasing attention for several reasons. For instance, the morphology, uniform size, large surface area and catalyst-support interactions of supported metal nanoparticles can be fined tuned and controlled according to requirements.[306,334–336] The high catalytic efficiencies of these systems are due to the nanoparticles' small size which result in a high surface energy area/volume ratio and the quantum confinement effects. Nevertheless, the high surface energy and Van der Waals attraction between particles mean that NPs tend to aggregate to reduce the surface energy.[337–341] As described earlier in this thesis, to address this issue for catalytic hydrogen generation, the nanoparticles can be stabilised by using nanoporous materials such as carbon structures,[342–347] zeolites,[48,348–351] mesoporous organosilica,[329,352,353] organic polymers,[354,355] and metal-organic frameworks (MOFs).[344,356–358] In this regard, Astruc *et.al* reported that "click" dendrimers can be used as supports for noble metals-based nanoparticles and bimetallic nanoparticles-based catalytic systems for the production of hydrogen from NaBH$_4$ and NH$_3$BH$_3$. For instance, a dramatic synergy between platinum and cobalt stabilised by "click" dendrimers (Pt/CoNP@dendrimer) has been found and reported in the literature.[359–361]

In the course of examining, optimising and studying the use of platinum nanoparticles (PtNPs) supported on phosphine-decorated polymer immobilised ionic liquids as catalysts for quinoline hydrogenation mediated by NaBH$_4$, it was discovered that the competing production of hydrogen from the aqueous hydrolysis of NaBH$_4$ was found to be the reason for the observed lower conversions of quinoline (a similar observation was made in the case of the PdNPs used in Chapter 4). This prompted us to investigate the use of PIIL stabilised PtNPs as catalysts in hydrogen evolution from the hydrolysis of NaBH$_4$ under ambient conditions. We chose to compare the efficacy of phosphine-functionalised PIIL which differed in their hydrophilicity. This was explored using PIIL which incorporated either a more hydrophilic PEGylated- or a more hydrophobic *N-*

decyl-imidazolium-based backbone. Additionally, kinetic isotope experiments were conducted to probe the reaction mechanism.

5.2   Results and Discussion

5.2.1   Synthesis and Characterisation of the Tetrachloroplatinate (PtCl$_4$) Pre-catalysts and Nanoparticles

The general synthesis method and relative structure of the polymers, catalyst precursors, and corresponding PIIL stabilised PtNPs are shown in Scheme **5.1**. Using an ion-exchange procedure, the PPh$_2$-PEGPIIL **3.8** and PPh$_2$-*N*-decylPIIL **4.2** were impregnated with an appropriate quantity of potassium tetrachloroplatinate(II), *via* the addition of an aqueous solution of K$_2$[PtCl$_4$] to a suspension of the polymer in water to afford the precursors with a phosphine to metal in a stoichiometric ratio of 1:1. After overnight stirring at room temperature, PtCl$_4$@PPh$_2$-PEGPIIL **5.1** and PtCl$_4$@PPh$_2$-*N*-decylPIIL **5.2** were isolated by filtration then washed with water, ethanol, diethyl ether and dried under a high vacuum to afford the precursors as a red/brown powder in >90% yield.

PtNP@PPh$_2$-PEGPIIL **5.3** and PtNP@PPh$_2$-*N*-decylPIIL **5.4** were synthesised by reducing the Pt^{II} precursor with excess amount of sodium borohydride in ethanol. The red solution mixture was instantaneously changed to a black colour, signifying that reduction from Pt^{II} to Pt^0 was almost immediate. After overnight stirring at room temperature, the black mixture was filtered, washed with water to remove the excess salts, ethanol, and diethyl ether, then dried under high vacuum to give PtNP@PPh$_2$-PEGPIIL **5.3** and PtNP@PPh$_2$-*N*-decylPIIL **5.4** as grey/black powder in >78% yield.
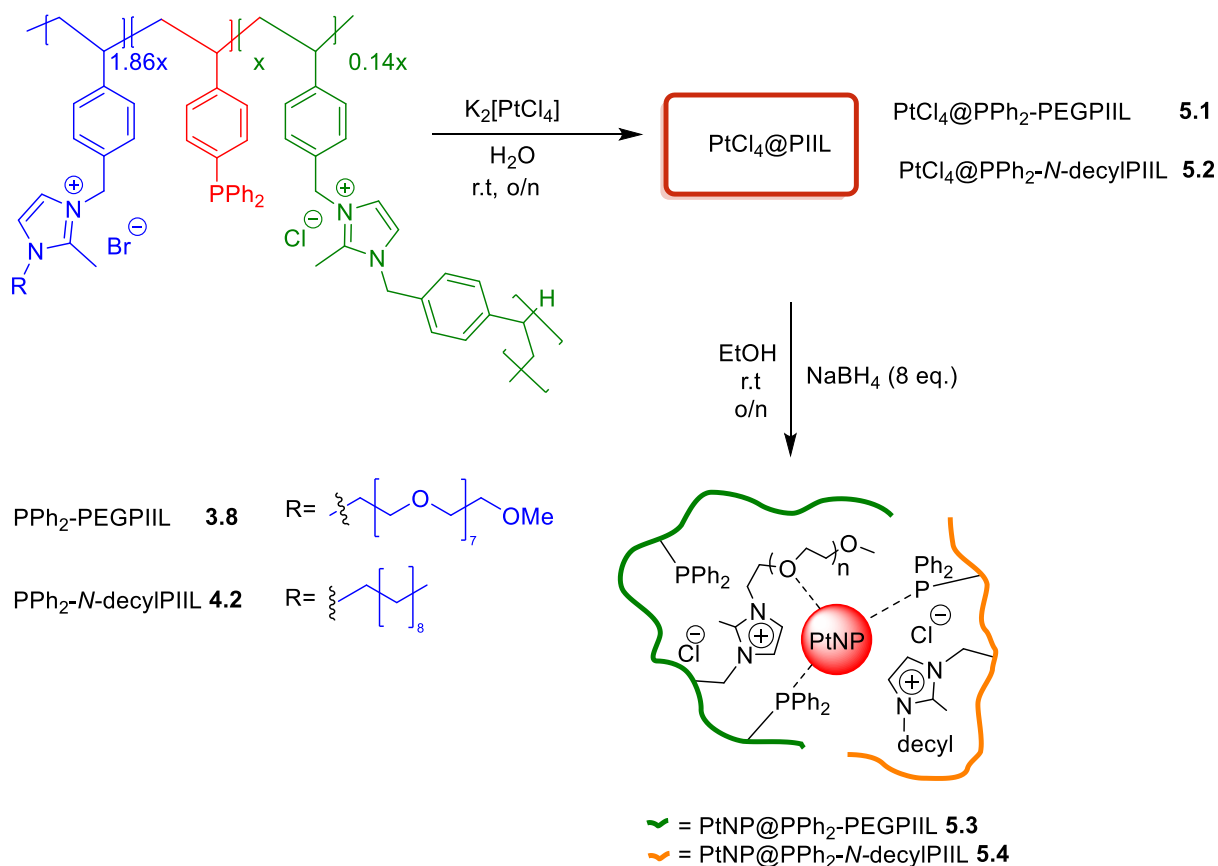
Scheme 5.1: Synthetic route used to impregnate the PIIL materials with $K_2[PdCl_4]$ and reduce to NP_S with $NaBH_4$ to give the corresponding PIIL-stabilised PtNPs.

5.2.1.1 ICP Optical Emission Spectrometry (ICP-OES)

ICP-OES analysis of $PtCl_4$@PPh_2-PEGPIIL **5.1**, $PtCl_4$@PPh_2-N-decylPIIL **5.2**, PtNP@PPh_2-PEGPIIL **5.3** and PtNP@PPh_2-N-decylPIIL **5.4** was used to determine their platinum content (Table **5.1**). Interestingly, platinum uptake was more efficient with the PPh_2-N-decylPIIL support in comparison with the PPh_2-PEGPIIL modified support. This might in principle be due to greater solvent/water retention in the PEG-functionalised material.

Table 5.1: Platinum content of PIIL catalysts and precursors as determined by ICP-OES.

Entry	Catalyst	mmol Pt/ g	Pt wt%
1	PtCl$_4$@ PPh$_2$-PEGPIIL **5.1**	0.43	8.52
2	PtCl$_4$@PPh$_2$-*N*-decylPIIL **5.2**	0.67	13.05
3	PtNP@ PPh$_2$-PEGPIIL **5.3**	0.36	7.10
4	PtNP@PPh$_2$-*N*-decylPIIL **5.4**	0.77	15.13

5.2.1.2 Solid-State Nuclear Magnetic Resonance (SSNMR)

As expected, all of the catalysts and precursors were of very low solubility in deuterated solvents, therefore solid-state NMR spectroscopy was utilised to determine any interactions between the donor modified supports and the metal surface.

The solid state ^{13}C NMR spectra of PtCl$_4$@PPh$_2$-PEGPIIL **5.1**, PtCl$_4$@PPh$_2$-*N*-decylPIIL **5.2**, PtNP@PPh$_2$-PEGPIIL **5.3** and PtNP@PPh$_2$-*N*-decylPIIL **5.4** displayed the expected signals corresponding to their structures (Figure **5.1**). For example, signals resonating around δ 123 ppm and δ 144 ppm were assigned for the carbon atoms of the imidazolium ring and the aromatic rings. The up-field signals resonating at δ 12-51 ppm were assigned to the methyl and methylene carbons on the imidazolium ring as well as the aliphatic carbon atoms of the polystyrene backbone. The characteristic strong signal resonating at δ 70 ppm, seen only for the PEGPIIL materials, and a relatively weaker signal resonating at δ 59 ppm was assigned to the carbon atoms and the terminal methoxy (OMe) group of the PEG chain of PtCl$_4$@PPh$_2$-PEGPIIL **5.1** and PtNP@PPh$_2$-PEGPIIL **5.3**.
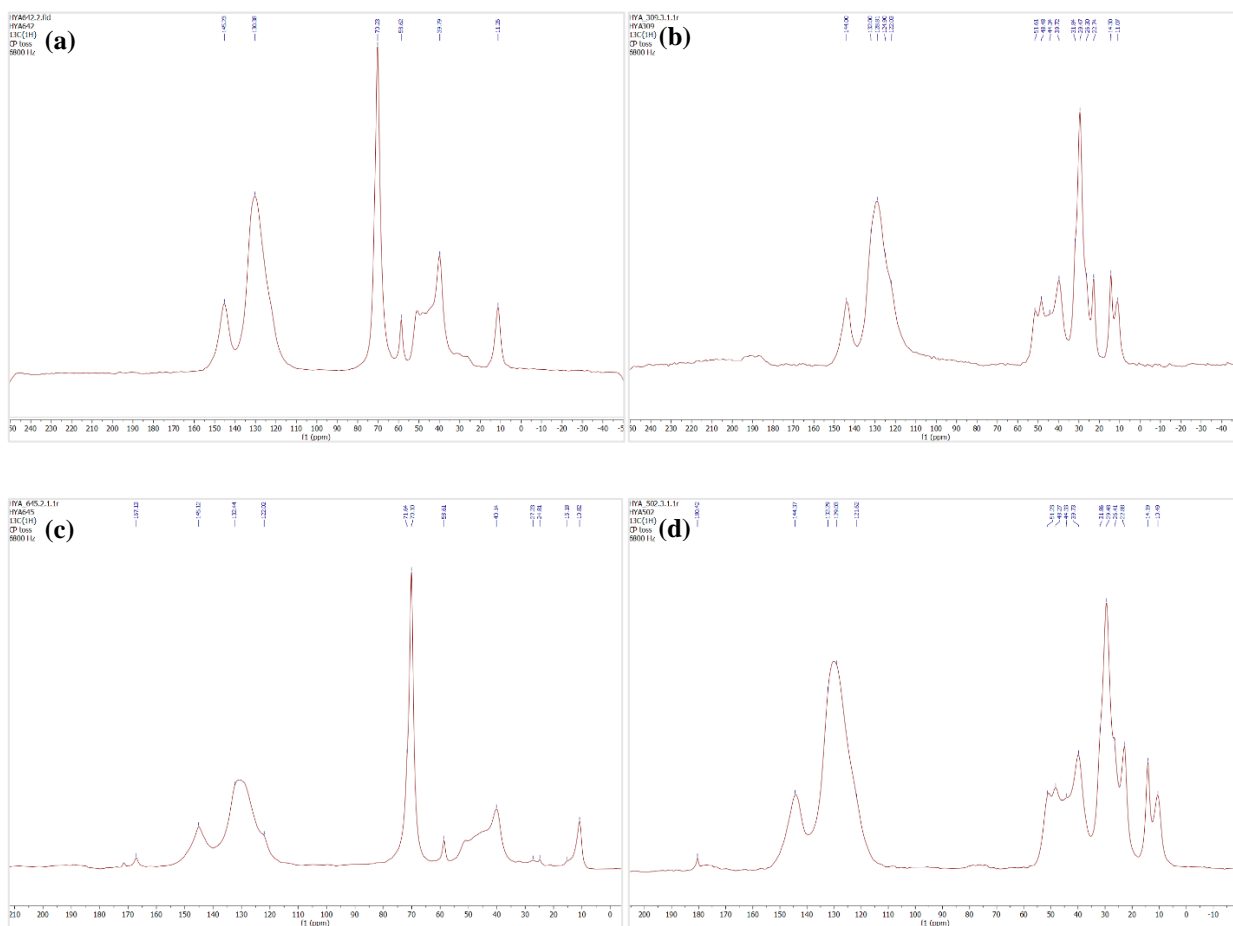
Figure 5.1: Solid state ^{13}C NMR spectrum of (a) PtCl$_4$@PPh$_2$-PEGPIIL **5.1**, (b) PtCl$_4$@PPh$_2$-*N*-decylPIIL **5.2**, (c) PtNP@PPh$_2$-PEGPIIL **5.3** and (d) PtNP@PPh$_2$-*N*-decylPIIL **5.4**.

The formation of PtCl$_4$@PPh$_2$-PEGPIIL **5.1**, PtCl$_4$@PPh$_2$-*N*-decylPIIL **5.2**, PtNP@PPh$_2$-PEGPIIL **5.3** and PtNP@PPh$_2$-*N*-decylPIIL **5.4** were further confirmed by performing solid state ^{31}P NMR spectroscopy (Figure **5.2**). The solid state ^{31}P NMR spectra showed signals consistent for the Pt---P interactions by displaying signals around δ 23 ppm and δ 18 ppm for PtCl$_4$@PPh$_2$-PEGPIIL **5.1** and PtCl$_4$@PPh$_2$-*N*-decylPIIL **5.2**, respectively. While the corresponding ^{31}P NMR signals for the polymers PPh$_2$-PEGPIIL **3.8** and PPh$_2$-*N*-decylPIIL **4.2** resonate at δ -6.7 and δ -6.6 ppm, respectively.[82,83,119,120] In addition, the ^{31}P NMR signals resonating around δ 25 ppm and δ 23 ppm observed for PtNP@PPh$_2$-PEGPIIL **5.3** and PtNP@PPh$_2$-*N*-decylPIIL **5.4** respectively, strongly infers incorporation of phosphine to the surface of the PtNPs. A similar ^{31}P NMR spectrum has been reported for triphenylphosphine-modified silica stabilised ultra-small PtNPs , with a chemical shift at δ 28.5 ppm, while the corresponding ^{31}P NMR signal for the triphenylphosphine-modified silica support was reported at δ -5.6 ppm.[362]
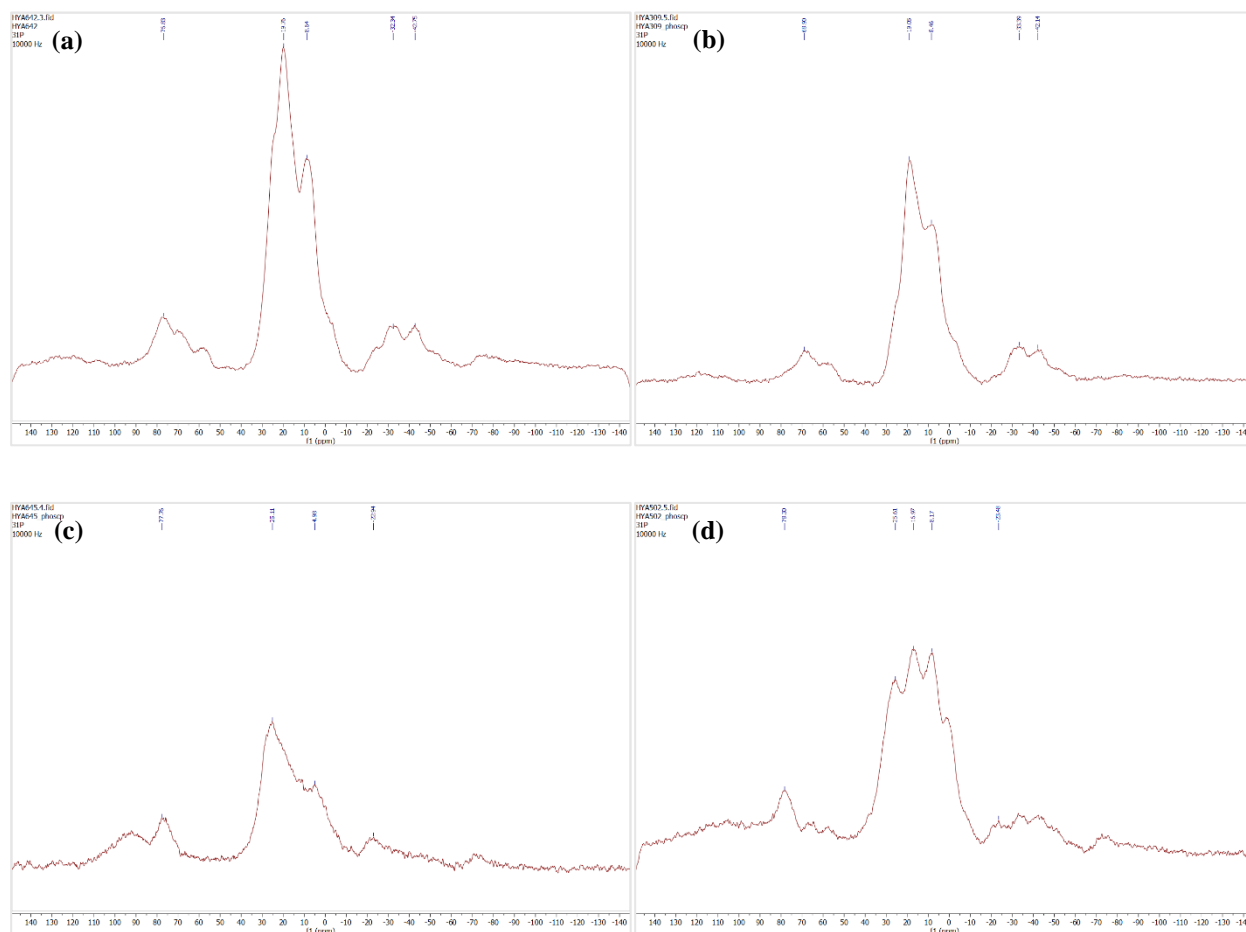
Figure 5.2:^{31}P solid state NMR spectrum of (a) PtCl$_4$@PPh$_2$-PEGPIIL **5.1**, (b) PtCl$_4$@PPh$_2$-*N*-decylPIIL **5.2**, (c) PtNP@PPh$_2$-PEGPIIL **5.3** and (d) PtNP@PPh$_2$-*N*-decylPIIL **5.4**.

5.2.1.3 X-ray Photoelectron Spectroscopy (XPS)

The surface of PtCl$_4$@PPh$_2$-PEGPIIL **5.1**, PtCl$_4$@PPh$_2$-*N*-decylPIIL **5.2,** PtNP@PPh$_2$-PEGPIIL **5.3** and PtNP@PPh$_2$-*N*-decylPIIL **5.4** was characterised by using X-ray photoelectron spectroscopy (XPS) to evaluate the chemical state and chemical composition of the sample (Figure **5.3**). A single Pt 4f electronic environment is expected to produce a 'doublet' in which the two peaks correspond to Pt 4f$_{7/2}$ and Pt 4f$_{5/2}$. In the case of PtCl$_4$@PPh$_2$-PEGPIIL **5.1**, two distinct Pt 4f electronic environments were indicated by the presence of two doublets in the XPS analysis. A binding energy of 72.7 eV and 73.8 eV was determined for the two Pt 4f$_{7/2}$ peaks of PtCl$_4$@PPh$_2$-PEGPIIL **5.1** and indicates the presence of both of Pt^0 and Pt^{2+} species, respectively. Likewise PtCl$_4$@PPh$_2$-*N*-decylPIIL **5.2** also produced two doublets, indicating two Pt 4f environments. A binding energy for the Pt 4f$_{7/2}$ peaks in this case, was found to be 72.3 eV and 74.8 eV, and supports presence of

both Pt^0 and Pt^{4+} species, respectively. The XPS analysis of PtNP@PPh$_2$-PEGPIIL **5.3** and PtNP@PPh$_2$-*N*-decylPIIL **5.4** each showed only a single Pt 4f$_{7/2}$ and Pt 4f$_{5/2}$ doublet. The corresponding binding energies were found at 72.6 eV and 75.9 eV respectively and supports presence of Pt^0 species only.[363] Spectral analysis, peak fitting and deconvolution were carried out using CasaXPS software.
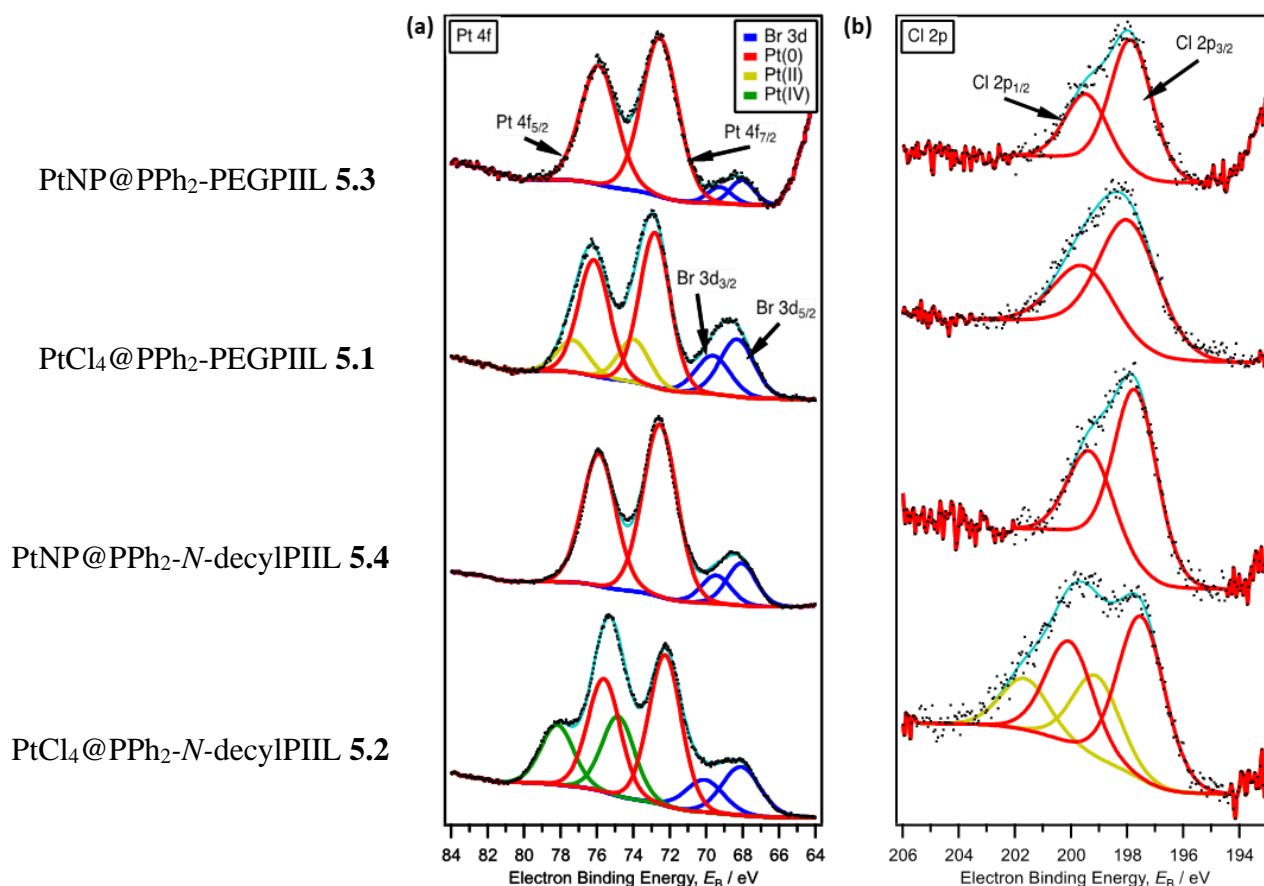
Figure 5.3: (a) Pt 4f core-level XPS spectra and (b) Cl 2p core-level spectra of (top-bottom) PtNP@PPh$_2$-PEGPIIL **5.3**, PtCl$_4$@PPh$_2$-PEGPIIL **5.1**, PtNP@PPh$_2$-*N*-decylPIIL **5.4** and PtCl$_4$@PPh$_2$-*N*-decylPIIL **5.2**, referenced to the Au 4f$_{7/2}$ peak at 84.0 eV.

5.2.1.4 Scanning Electron Microscopy (SEM)

SEM analysis was performed to examine the surface morphology of the freshly prepared PtCl$_4$@PPh$_2$-PEGPIIL **5.1**, PtCl$_4$@PPh$_2$-*N*-decylPIIL **5.2**, PtNP@PPh$_2$-PEGPIIL **5.3** and PtNP@PPh$_2$-*N*-decylPIIL **5.4** (Figure **5.4**). This showed that the surface of the precursor and the NPs are uneven and more granular compared to the polymers. This may be a result of the additional processing of the materials resulting in damage and fragmentation.
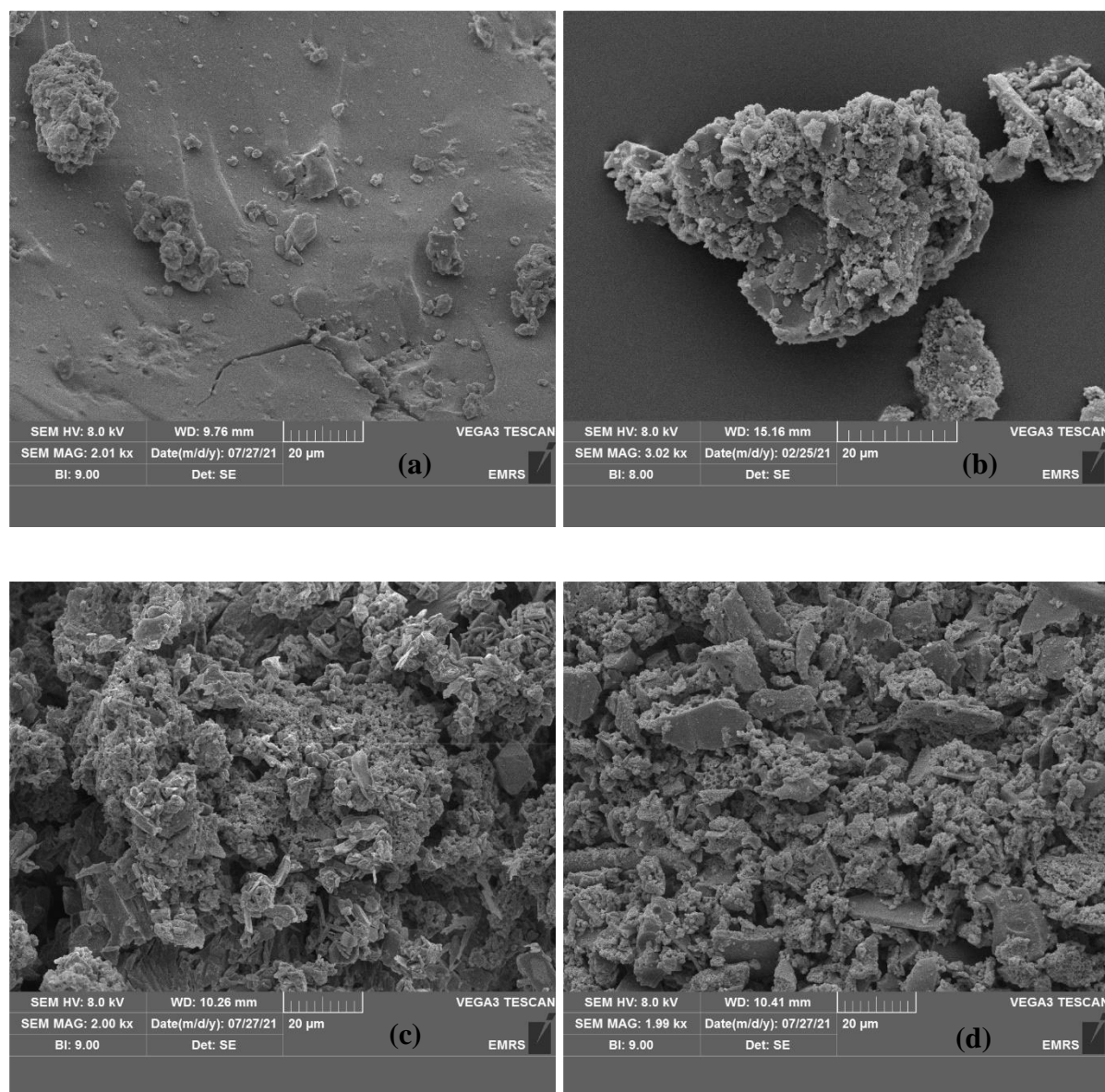
Figure 5.4: SEM image (a) PtCl$_4$@PPh$_2$-PEGPIIL **5.1**, (b) PtCl$_4$@PPh$_2$-*N*-decylPIIL **5.2**, (c) PtNP@PPh$_2$-PEGPIIL **5.3** and (d) PtNP@PPh$_2$-*N*-decylPIIL **5.4**.

5.2.1.5 Transmission Electron Microscopy (TEM)

Transmission Electron Microscopy (TEM) was used to assess the size and the shape of the PtNPs. The TEM images of PtNP@PPh$_2$-PEGPIIL **5.3** and PtNP@PPh$_2$-*N*-decylPIIL **5.4** showed spherical and near-monodisperse nanoparticles with an average diameter of 3.0 ± 0.8 nm and 2.7 ± 1.1 nm, respectively, as shown in Figure **5.5**.
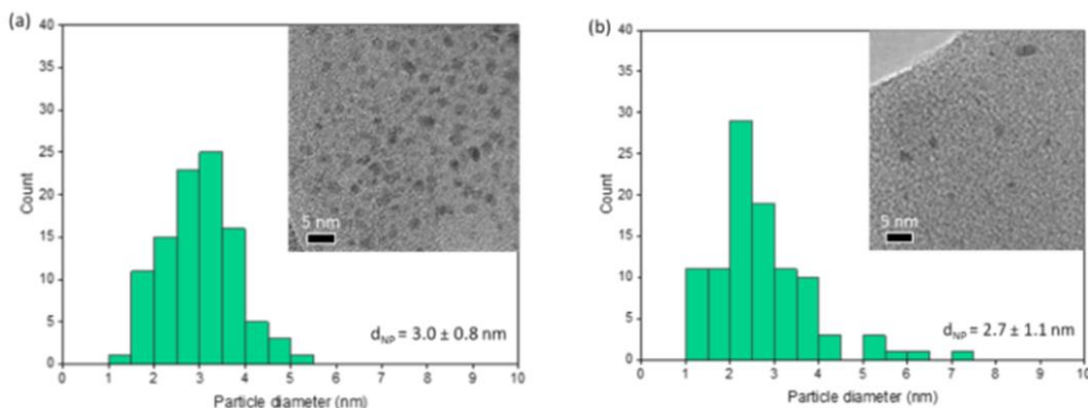
Figure 5.5: HRTEM images of (a) PtNP@PPh$_2$-PEGPIIL **5.3** and (b) PtNP@PPh$_2$-*N*-decylPIIL **5.4** along with the distribution histograms showing particle size distribution based on >100 particles.

In comparison, triphenylphosphine-modified silica-supported and stabilised PtNPs reported in the literature revealed an average diameter of 1 nm size and were smaller in comparison to unmodified silica-supported PtNPs.[362] In contrast, PtNPs embedded in ZIF-8 with an average diameter of 3.4 nm[356] or the first or second generation click dendrimers-stabilised PtNPs with an average diameter of 2.3 nm[361] were of similar size to PtNP@PPh$_2$-PEGPIIL **5.3** and PtNP@PPh$_2$-*N*-decylPIIL **5.4**.

5.2.2 PtNP-Catalysed Hydrolysis of NaBH$_4$

The generation of hydrogen gas *via* hydrolysis of a solution of NaBH$_4$ under ambient conditions was then measured as a function of time at different temperatures (21 to 40 °C). All the data collected was corrected by subtracting the background hydrogen gas produced without catalyst under identical reaction conditions. A typical procedure for the production of hydrogen gas was performed by hydrolysing a 0.27 M solution of NaBH$_4$ in the presence of 0.32 mol% of PtNP@PPh$_2$-PEGPIIL **5.3** and PtNP@PPh$_2$-*N*-decylPIIL **5.4** at 30 °C. The resulting hydrogen evolved was measured with respect to time and temperature as shown in Figure **5.6**. The reaction

progress was monitored by measuring the displacement of water inside a burette, which is directly proportion to the amount (volume) of hydrogen produced as a function of time. Under optimised reaction conditions, immediate hydrogen production without an induction period was observed, which agrees with platinum's metallic state. The hydrolysis of a solution of $NaBH_4$ in the presence of the non metal-loaded polymers PPh_2-PEGPIIL **3.8** and PPh_2-*N*-decylPIIL **4.2** showed that both polymers are catalytically inactive.
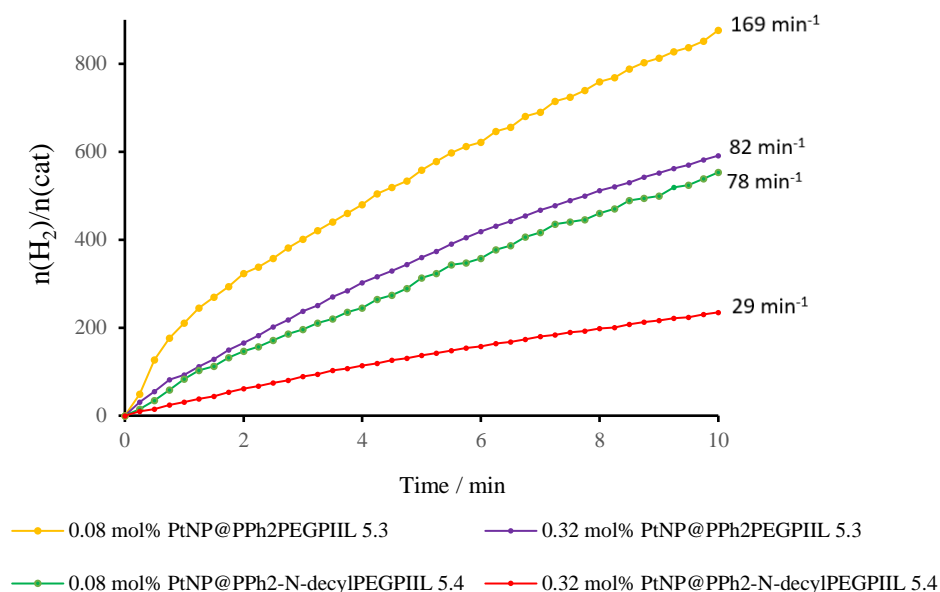
Figure 5.6: Comparison of H_2 evolution upon hydrolysis of $NaBH_4$ in water as a function of time at 30 °C catalysed by 0.32 mol% of PtNP@PPh_2-PEGPIIL **5.3**, 0.08 mol% PtNP@PPh_2-PEGPIIL **5.3**, 0.32 mol% of PtNP@PPh_2-*N*-decylPIIL **5.4,** 0.08 mol% of PtNP@PPh_2-*N*-decylPIIL **5.4** and the corresponding initial TOF value [(mol. H_2) (mol. cat)$^{-1}$min^{-1}].

The initial TOF values calculated showed a considerably higher TOF value of 82 mole$_{H2}$.mol$_{cat}$$^{-1}$.min^{-1} for PtNP@$PPh_2$-PEGPIIL **5.3** as compared to 29 mole$_{H2}$.mol$_{cat}$$^{-1}$.min^{-1} for PtNP@$PPh_2$-*N*-decylPIIL **5.4**. In contrast, a TOF of 6.09 mole$_{H2}$.mol$_{cat}$ $^{-1}$.min^{-1} has been reported when 1wt% Pt/C at 40 °C was used as catalyst for the hydrolysis of a dilute solution of $NaBH_4$.[364] Likewise, a TOF of 52 mole$_{H2}$.mol$_{cat}$$^{-1}$.min^{-1} was reported when the commercially available 5 wt% Pt/C was used.[365] The high TOFs obtained with the catalysts PtNP@PPh_2-PEGPIIL **5.3** and PtNP@PPh_2-*N*-decylPIIL **5.4** led us to screen a variety of reaction conditions. We found that the reaction with lower catalyst loadings (0.08 mol%) and more highly diluted $NaBH_4$ solution (10 mL of 0.054 M) improved the initial TOFs to 169 mole$_{H2}$.mol$_{cat}$$^{-1}$.min^{-1} for PtNP@$PPh_2$-PEGPIIL **5.3** and 78

mole$_{H2}$.mol$_{cat}$$^{-1}$.min^{-1} for PtNP@PPh$_2$-*N*-decylPIIL **5.4**. These improved TOF values are probably more representative of the intrinsic turnover rates of such catalytic systems, therefore, a comparative study with the literature protocols was carried out.

Although a conclusive comparison is hard to achieve *via* a direct comparison with the existing protocols reported for different Pt-based catalytic systems, because of the variations in the experimental conditions and different methodology adopted, a few selected examples with relatively similar conditions applied revealed that the TOF value of 169 mole$_{H2}$.mol$_{cat}$$^{-1}$.min^{-1} for PtNP@PPh$_2$-PEGPIIL **5.3** at 30 ºC is markedly higher than most of the reported methods in the literature.

For instance, a recent report showed a TOF of 133 mole$_{H2}$.molcat^{-1}.min^{-1} by using a PtNP@dendrimer as the catalyst.[359] Similarly, a TOF of 117 mole$_{H2}$.molcat^{-1}.min^{-1} at 80 °C has been reported when monodisperse PtNPs based on a mesoporous silicon nitrides support was used as the catalyst,[366,367] for PtNPs supported on multi-walled carbon nanotubes a TOF of 8.35 mole$_{H2}$.molcat^{-1}.min^{-1} was recorded,[368] 82.6 mole$_{H2}$.molcat^{-1}.min^{-1} TOF was calculated for PtNPs on a graphene support,[369] a TOF of 69 mole$_{H2}$.molcat^{-1}.min^{-1} for Pt clusters on a CeO$_2$-Co$_7$Ni$_2$O$_x$ support,[370] 53 mole$_{H2}$.molcat^{-1}.min^{-1} TOF was obtained when a flow reactor based on a monolithic PtNP/Al$_2$O$_3$/cordierite catalyst was used,[371] 41-60 mole$_{H2}$.molcat^{-1}.min^{-1} using PtNPs impregnated on a Si/Al/C/N framework.[372] Use of CoPtNPs supported on poly(3,4-ethylenedioxythiophene)/poly(styrenesulfonate) ((PEDOT:PSS)) functionalised CNTs gave a TOF of 60 mole$_{H2}$.molcat^{-1}.min^{-1},[373] 78 mole$_{H2}$.mol$_{cat}$$^{-1}$.min^{-1} was acquired at 80 ºC with PtNPs supported on a TiN/Si$_3$N$_4$ nanocomposite.[374] similar to that of 156 mole$_{H2}$.mol$_{cat}$$^{-1}$.min^{-1}, which was obtained at 70 ºC using PtNPs coated on fiber-shaped cobalt.[375] On the contrary, a TOF of 330 mole$_{H2}$.molcat^{-1}.min^{-1} was reported by using micro/mesoporous Pt-SiCN nanocomposites,[376] and a TOF of 780 mole$_{H2}$.molcat^{-1}.min^{-1}.min^{-1} (90,000 mL min^{-1}g^{-1} cat) by using the nonporous Pt catalysts;[377] both much higher than that of PtNP@PPh$_2$-PEGPIIL **5.3**, are indeed the most active catalysts known so far for the catalytic hydrolysis of NaBH$_4$ using noble metal nanoparticle-based catalytic systems.

5.2.3   Influence of NaOH

Several reports describe the beneficial effect of using NaOH as an additive along with metallic nanoparticles-based catalysts. For instance, for the hydrolysis of NaBH$_4$ and NH$_3$BH$_3$, coordination

of hydroxide to the surface of the metallic NPs has been proposed to play a significant role by enhancing the electron density around the nanoparticles, which ultimately results in a smooth oxidative addition of the O-H bond. In this context, improved hydrolysis rates were recorded for several noble transition metals such as RhNPs, RuNPs, PdNPs, AuNPs and NiNPs on click dendrimers,[359] embedded CoNPs and NiNPs on zeolitic imidazolate backbone of ZIF-8,[356,378] bimetallic nanoparticles such as CoPt and Ni_2Pt based nanoparticle systems,[357,361] nanoparticles derived from non-noble metals such as Cu-Co-Mo,[379] and Ni-Co-P on oxygen-doped porous carbon (OPC-300) .[342] Nevertheless the addition of NaOH has been reported to have a negative effect on the hydrolysis catalysed by nanoparticles based on Pt. Since Pt itself is electronically rich and is proposed to facilitate smooth oxidative addition of the O-H bond at the surface *via* an activated hydrogen-bonded adduct $[BH_3H^-]$---H-OH, no additional enhancement of electron density is required. In the case of Pt then, the additional OH^- occupies active sites on the nanoparticle surface and prevents coordination and activation of the desired substrate on the surface of the PtNPs and ultimately adversely affects the final outcome.[359,361,380]

In order to exploit any potential beneficial effect of NaOH addition on the hydrolysis of $NaBH_4$ by using the most active catalyst PtNP@PPh_2-PEGPIIL **5.3**, varying concentrations of NaOH between 0.035 - 1.12 mM were screened, and the initial TOFs obtained as a function of the quantity of NaOH added at 21 °C were recorded (Figure **5.7**). A slight increase in the initial TOF was observed as the concentration of NaOH was increased (optimum of 49 $mole_{H_2}.mol_{cat}^{-1}.min^{-1}$ in 0.14 mM), then the TOF started to decrease with increasing NaOH concentration further. It is worth mentioning that a TOF of 39 $mole_{H_2}.mol_{cat}^{-1}.min^{-1}$ was measured under similar reaction conditions in the absence of NaOH.
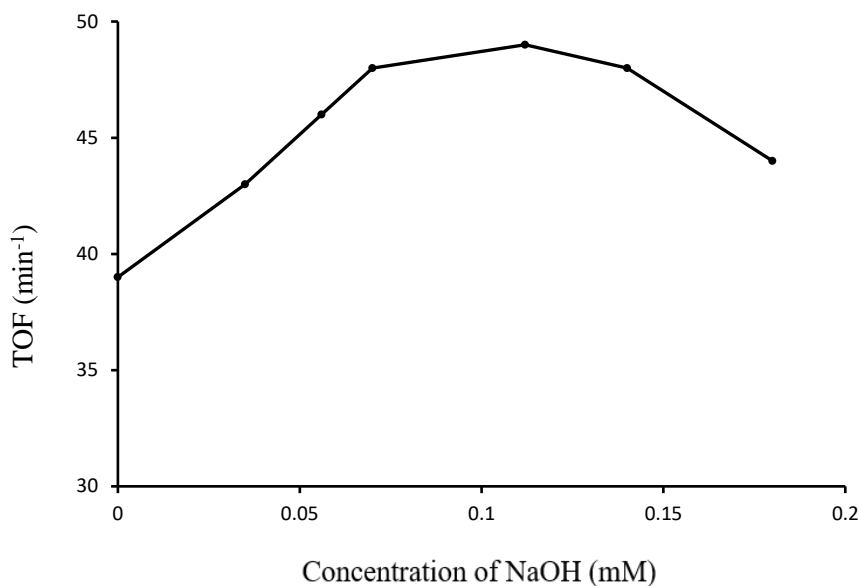
Figure 5.7: TOFs for 0.32 mol% PtNP@PPh$_2$-PEGPIIL **5.3** in the presence of various concentrations of sodium hydroxide and corresponding TOF value.

High concentrations of NaOH may indeed exert a negative effect *via* coordination to the PtNPs surface, as previously proposed. The slight enhancement of the initial TOF observed using low concentrations of NaOH is notable. The effect of catalyst dispersion on the hydrogenation reaction mixture was investigated by dynamic light scattering (DLS) (This experiment was done by Dr Thomas Chamberlain group at University of Leeds). DLS measurement revealed that the average hydrodynamic diameter index did not change as a function of NaOH, so this can be excluded as the reason for the marked change in TOF (Figure **5.8**).
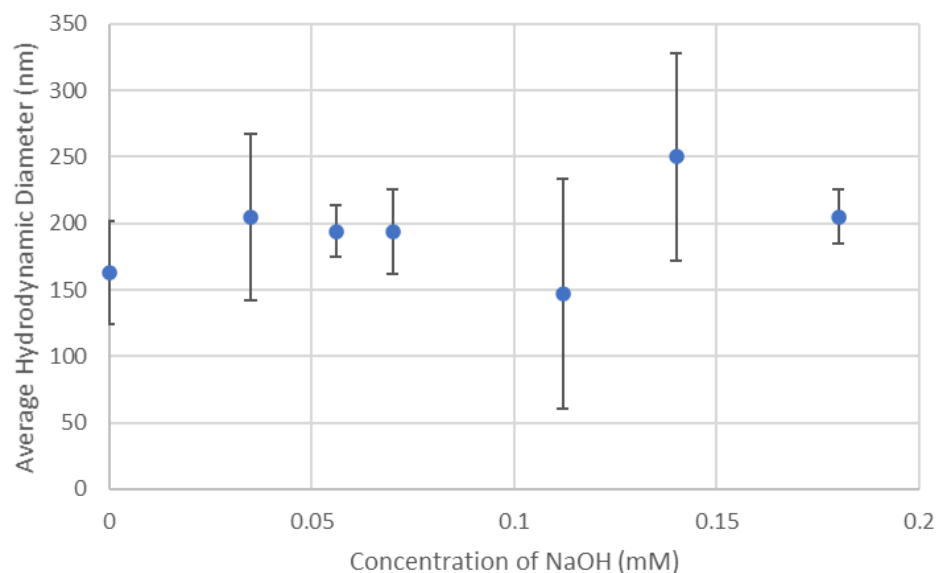
Figure 5.8: The average hydrodynamic diameter of PtNP@PPh$_2$-PEGPIIL **5.3** in the presence of various concentrations of sodium hydroxide at 21 °C while catalysing the degradation of NaBH$_4$.

5.2.4 A Comparative Kinetic Study

The difference in the catalytic activities of PtNP@PPh$_2$-PEGPIIL **5.3** and PtNP@PPh$_2$-*N*-decylPIIL **5.4** further prompted us to perform a comparative kinetic study by monitoring the dependency of rate on temperature. Furthermore, the impact of catalyst and NaBH$_4$ concentration on the rate of hydrolysis was also studied.

5.2.4.1 Temperature Study

The evolution of hydrogen as a function of time at temperatures between 294-313 K is summarised in Figure **5.9a-b** for the hydrolysis of a 0.27 M solution of NaBH$_4$ in the presence of 0.32 mol% of PtNP@PPh$_2$-PEGPIIL **5.3** and 0.69 mol% of PtNP@PPh$_2$-*N*-decylPIIL **5.4** respectively. The initial rates (k) were calculated from the linear portion of the graph. Arrhenius plots of ln k versus 1/T (ln k = ln A - Ea/RT) allowed calculation of the activation energies (Ea) of 23.9 kJ mol^{-1} and 35.6 kJ mol^{-1}, respectively (Figure **5.9c-d**). The Ea values obtained were quite similar to the activation energies reported for other catalytic systems based on noble metal nanoparticles. For example, for a nanoporous platinum based catalytic system synthesised by chemical etching, an activation energy of 32.1 kJ mol^{-1} has been reported.[374] Similarly, for a Pt/Co@dendrimer-based catalyst an Ea of 24.9 kJ mol^{-1},[359] for Pt atomic cluster on Co-NiO-CeO$_2$ an Ea of 47.4 kJ mol^{-1},[370] for a

polymer-derived silicon carbonitride supported PtNPs an Ea of 46.3 kJ mol^{-1},[373] for the homogenously dispersed PtNPs an Ea of 39.2 kJ mol^{-1},[381] for PtNPs supported on carbon an Ea of 36.0 kJ mol^{-1},[368] and for the RuNPs electrodeposited on nickel foams and RuNPs confined on zeolite support, Ea of 39.8 kJ mol^{-1},[382] and 32 kJ mol^{-1} [350] respectively, has been reported.
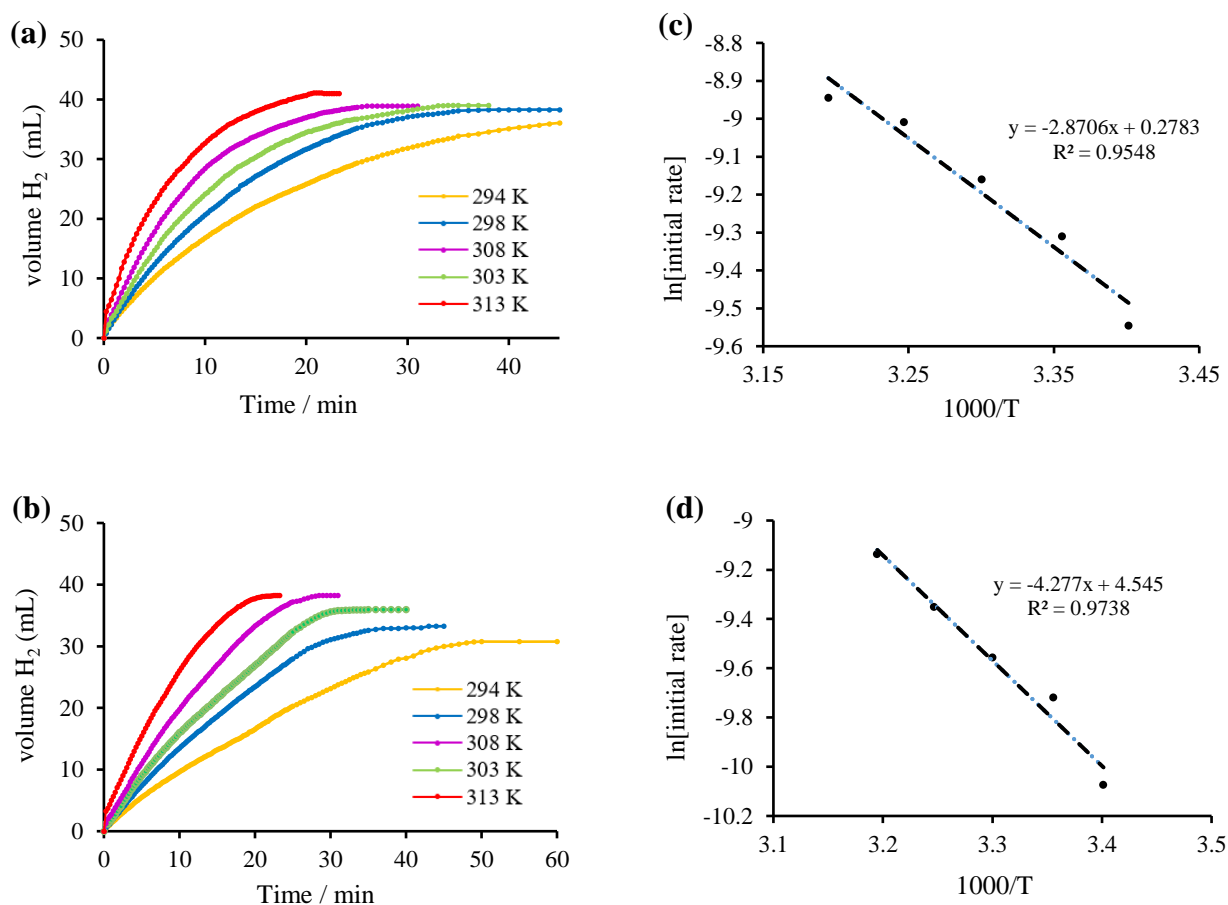
Figure 5.9: Volume of generated H$_2$ versus time obtained from the hydrolysis of 2 mL of 0.27 M NaBH$_4$ at different temperatures catalysed by (a) PtNP@PPh$_2$-PEGPIIL **5.3** and (b) PtNP@PPh$_2$-*N*-decylPIIL **5.4**; corresponding Arrhenius plots for the hydrolysis of NaBH$_4$ catalysed by (c) PtNP@PPh$_2$-PEGPIIL **5.3** and (d) PtNP@PPh$_2$-*N*-decylPIIL **5.4**.

The lower Ea observed for the catalyst PtNP@PPh$_2$-PEGPIIL **5.3** than PtNP@PPh$_2$-*N*-decylPIIL **5.4** might be due to the additional interactions generated between the catalyst and the support due to the PEG fragment. Another possible reason might be that the hydrophilic nature of the PEGylated support facilitates access of the substrate to reach the active sites of the catalyst. Thus, for an efficient NaBH$_4$ hydrolysis in the presence of a catalyst, a prompt penetration of the substrate into the polymer support followed by penetration of the BH$_4^-$ to the surface of the PtNPs is essential.

In this way the hydrophilicity of the PEGylated support might enable enhanced homogenous dispersion of catalyst in water. This in turn will create hydrophilic surroundings at the surface of the PtNPs and also allow an efficient interaction with the BH_4^-, resulting in the formation of a $[BH_3-H\text{---}H\text{-}OH]^-$ adduct and thereby enhancing oxidative addition *via* activation of water.

5.2.4.2 Catalyst concentration study

The activity of the catalysts PtNP@PPh$_2$-PEGPIIL **5.3** and PtNP@PPh$_2$-*N*-decylPIIL **5.4** for hydrogen production *via* hydrolysis of NaBH$_4$ as a function of catalyst concentration was then studied. For this, several catalyst loading experiments were performed by using 0.27 M NaBH$_4$ at 35 °C (Figure **5.10a-b**). The logarithmic plots for the rate of hydrogen production against the concentration of PtNPs are shown below in Figure **5.10c-d**. A straight line with slopes of 0.72 and 0.87 for the catalyst PtNP@PPh$_2$-PEGPIIL **5.3** and PtNP@PPh$_2$-*N*-decylPIIL **5.4**, respectively, suggested a first order rate of hydrolysis with respect to the concentration of catalyst. For comparison, a brief literature survey of the relevant catalytic systems was also performed. The results obtained with catalyst PtNP@PPh$_2$-PEGPIIL **5.3** and PtNP@PPh$_2$-*N*-decylPIIL **5.4** appear to be quite consistent with the literature reports describing hydrolysis of hydrogen-rich boron derivatives by using other noble and non-noble metallic NPs. For instance, a slope of 0.85 was reported for the hydrolysis of NaBH$_4$ or BH$_3$-NH$_3$ by using Pt/Co@dendrimer.[359,361] Similarly, slopes of 0.73, 0.94, 0.82, 0.98,0.83, 0.92, 0.88, 0.79, and 1.17 are reported for the hydrolysis of NaBH$_4$ or BH$_3$-NH$_3$ by using the zeolite-confined RuNPs,[350] RuNPs stabilised on PVP-supports,[383] Ni$_2$Pt@ZIF-8,[357] NiNP@ZIF-8,[356] PtNP@MWCNTs,[368] RuNP@dendrimer,[380] PtNP@dendrimer,[380] CoNP@dendrimer[380] and porphyrin-ring stabilised RuNPs, respectively.[384]
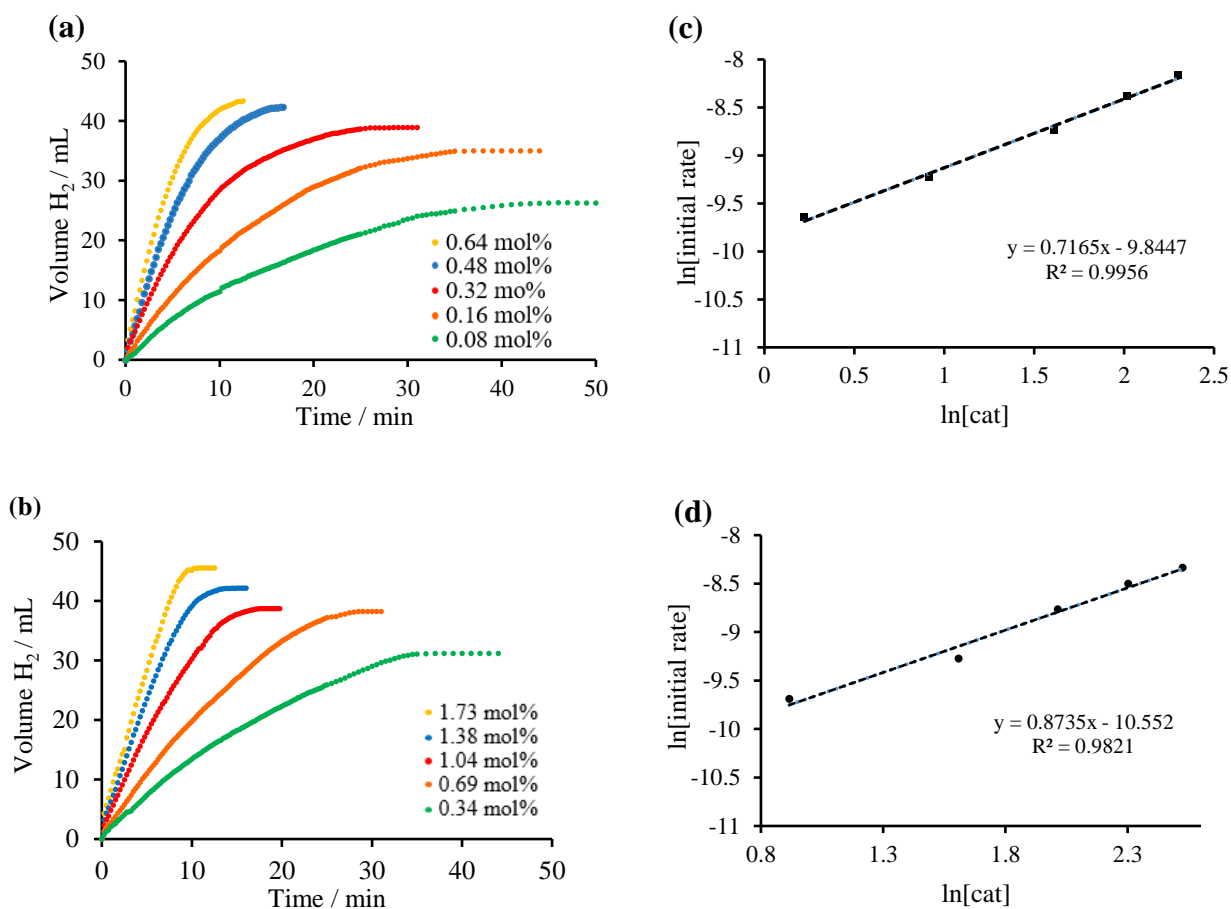
Figure 5.10: Volume of generated H_2 versus time for the hydrolysis of 2 mL of 0.27 M $NaBH_4$ at 35 °C catalysed by different concentrations of (a) PtNP@PPh$_2$-PEGPIIL **5.3** and (b) PtNP@PPh$_2$-*N*-decylPIIL **5.4**; the logarithmic plots for the rate of hydrogen production versus the concentration of (c) PtNP@PPh$_2$-PEGPIIL **5.3** and (d) PtNP@PPh$_2$-*N*-decylPIIL **5.4**.

5.2.4.3 NaBH$_4$ concentration study

The variation in the rate of hydrolysis of $NaBH_4$ with respect to concentration of the substrate was also studied by using the catalyst PtNP@PPh$_2$-PEGPIIL **5.3**. For this, varying initial concentrations of $NaBH_4$ ([$NaBH_4$]$_0$ = 0.13, 0.26, 0.39, 0.52, 0.65, 0.78 mM) were studied at 30 °C. These concentrations of $NaBH_4$ correspond to catalyst:substrate ratios from 1:1 to 1:6; the kinetic data are shown in Figure **5.11a**. The corresponding logarithmic plot of rate of hydrogen produced against the concentration of $NaBH_4$ used provided a straight line with a slope of 1.08 (Figure **5.11c**). These results suggest the catalytic hydrolysis of $NaBH_4$ to be first order with respect to substrate. A similar kinetic study by using PtNP@PPh$_2$-*N*-decylPIIL **5.4** as the catalyst under identical reaction conditions described above for PtNP@PPh$_2$-PEGPIIL **5.3** also suggested a first order

kinetics with respect to substrate (Figure **5.11b**). A slope of 1.16 for the logarithmic plot of the hydrogen produced versus $NaBH_4$ concentration was obtained for PtNP@PPh$_2$-*N*-decylPIIL **5.4** (Figure **5.11d**). All these experiments are consistent with rate-limiting activation of $NaBH_4$ in the catalytic hydrolysis of $NaBH_4$.
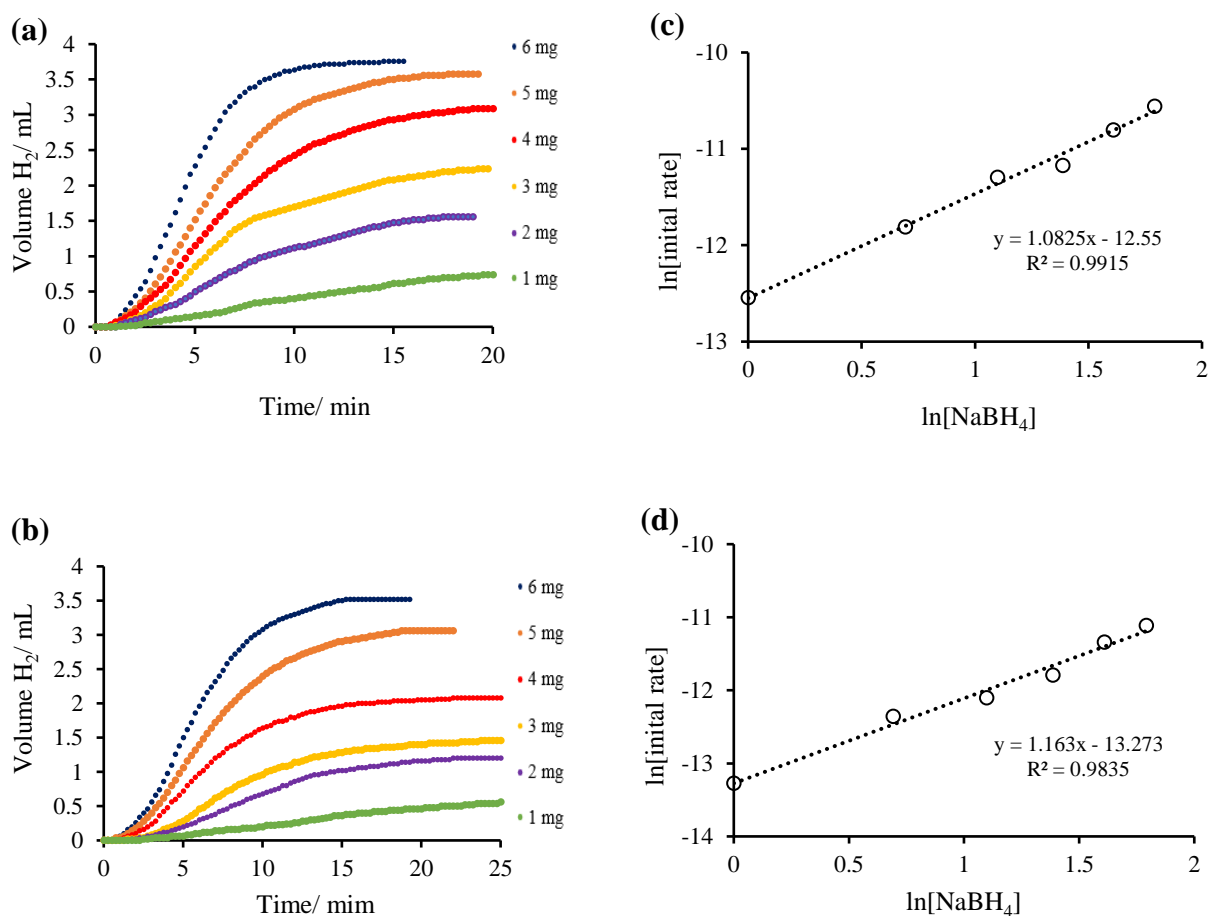
Figure 5.11: Volume of generated H_2 versus time for the hydrolytic dehydrogenation with different concentrations of $NaBH_4$ at 30 °C catalysed by (a) PtNP@PPh$_2$-PEGPIIL **5.3** (0.0725 g, 0.026 mmol) and (b) PtNP@PPh$_2$-*N*-decylPIIL **5.4** (0.0340 g, 0.026 mmol). The plots of H_2 generation rate against concentration of $NaBH_4$ in logarithmic scale for (c) PtNP@PPh$_2$-PEGPIIL **5.3** and (d) PtNP@PPh$_2$-*N*-decylPIIL **5.4**.

5.2.5 Kinetic Isotope Effect (KIE)

Several complications are anticipated when studying the kinetics of dehydrogenation of $NaBH_4$ *via* hydrolysis because the process of hydrolysis is dependent on several factors. For instance, the hydrolytic dehydrogenation is dependent on the catalyst nature, the catalyst support and also on the substrate concentration. Therefore, several plausible pathways have been reported.[297,325,365,385–387]

Nevertheless, the majority of studies suggest that one of the two H atoms of hydrogen is provided by $NaBH_4$ in the form of a hydride and other H atom comes from water in the form of a proton.[388] The reported primary kinetic isotope effects observed with D_2O are also consistent with the activation of one of the O-H bonds of water being involved in the rate determining step of this reaction.[359,378,389] The activation of the O-H bond of H_2O is proposed to proceed *via* an oxidative addition of the absorbed water on the surface of catalyst. This activation is further expedited *via* a hydrogen-bonding interaction from the water proton and the surface-coordinated borohydride $[H_3B-H---H-OH]^-$, by diminishing the electron density of the O-H bond. Finally, a molecule of hydrogen is released from the surface of the catalyst in either a reductive elimination step or *via* a σ-bond metathesis-type pathway. The reductive elimination pathway might proceed *via* bond formation between water- and borohydride-derived metal hydrides (Figure **5.12a**), while the σ-bond metathesis-type pathway proceeds *via* surface-coordinated-$[H_3B-H]$ and water-coordinated M-H [H-M-OH], conceivably aided by a surface hydroxide (Figure **5.12b**). The borohydride-derived metal hydrides may arise from hydrogen transfer onto the nanoparticle either through an oxidative addition pathway of B-H bond or through a hydride transfer pathway. The hydride transfer pathway is most likely for this process, since borohydride reagents are well known for their hydride transfer capabilities.[390] Nevertheless, the possibility of activation of the O-H bond of H_2O *via* a hydrogen bonding interaction pathway with a surface coordinated hydride, i.e. M-H---H-OH, cannot be excluded.
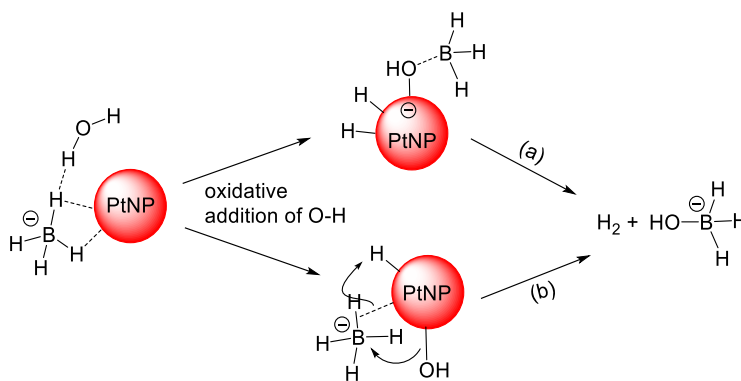
Figure 5.12: Suggested mechanism for $NaBH_4$ hydrolysis catalysed by PtNP@PIIL followed by either (a) reductive elimination or (b) a σ-bond metathesis-type process.

With this theoretical background knowledge, we then explored the role of H_2O in the hydrolysis of $NaBH_4$ by using PtNP@PPh_2-PEGPIIL **5.3** and PtNP@PPh_2-*N*-decylPIIL **5.4**. All the reactions

were therefore performed in both H_2O and D_2O at 35 °C in order to determine the catalytic efficiency of catalyst and to determine the kinetic isotope effect (KIE). The results obtained clearly demonstrate that the reaction is faster in H_2O as compared to D_2O. A primary KIE of (k_H/k_D) of 1.8 for PtNP@PPh$_2$-PEGPIIL **5.3** and 2.1 for PtNP@PPh$_2$-N-decylPIIL **5.4** was determined (Figure **5.13a-b**). These KIE values clearly suggest that the rate determining step of this reaction involves cleavage of one of the O-H bonds of H_2O. Furthermore, a KIE value of 1.8 was obtained by Guella and co-workers for aqueous hydrolysis of $NaBH_4$ by using 5 wt% Pt/C,[365] which also supports this pathway. In addition, a primary KIE (k_H/k_D) of 2.49 by using NiNP@ZIF-8,[390] 2.3 by using the dendrimer stabilised RhNPs,[380] 2.8 by using the dendrimer stabilised PdNPs,[380] and 2.4 for the PtCo@dendrimer have been reported very recently and were consistent with our observations.[361]

(a)

(b)
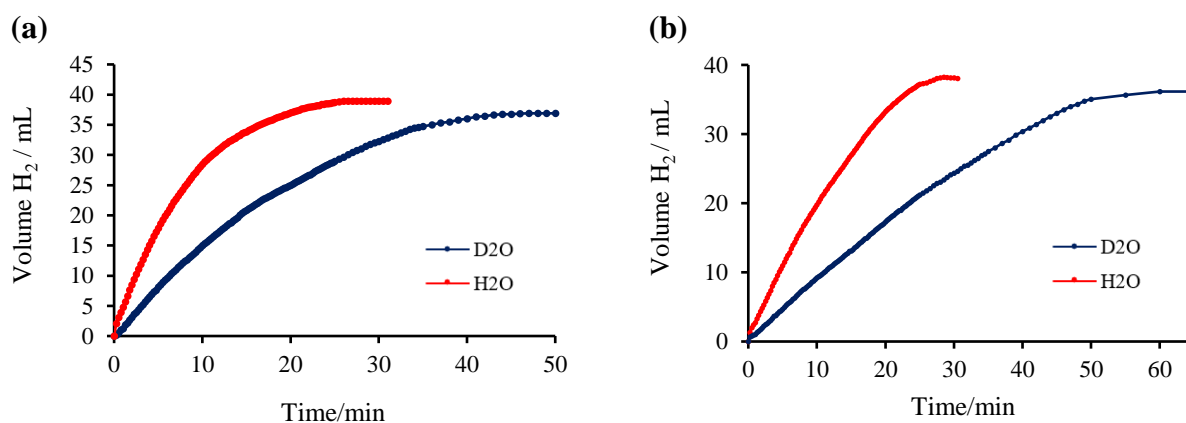
Figure 5.13: Comparison of hydrogen evolution from 0.27 M solution of $NaBH_4$ in H_2O and D_2O catalysed by (a) 0.32 mol% PtNP@PPh$_2$-PEGPIIL **5.3** and (b) 0.69 mol% PtNP@PPh$_2$-N-decylPIIL **5.4** performed at 35 °C.

Next, the efficiency of the catalysts PtNP@PPh$_2$-PEGPIIL **5.3** and PtNP@PPh$_2$-N-decylPIIL **5.4** for the aqueous hydrolysis of $NaBH_4$ and $NaBD_4$ was evaluated. Both the catalysts displayed a similar result by showing a very slight variation in the hydrogen evolution rate during hydrolysis. A KIE of 1.3 for PtNP@PPh$_2$-PEGPIIL **5.3** and 1.2 for PtNP@PPh$_2$-N-decylPIIL **5.4** was determined. This minor deviation in the KIEs from a value of 1, suggests that the rate determining step of this reaction does not proceed *via* the B-H(D) bond cleavage. Further support for this observation was obtained from the literature, where the aqueous hydrolysis of amine-borane complex and $NaBD_4$ by using NiNP@ZIF-8[356] and Pt/C[365] also showed a very small KIE values. Although, all the experiments performed fully support the mechanism of an oxidative addition pathway *via* rate limiting O-H bond activation, a pathway involving surface coordinated BH_4 and

a borohydride-derived Pt-H species cannot be excluded. Therefore, both the pathways might involve a surface-coordinated hydrogen bonded species, such as [H_3BH^-]---H-OH. The oxygen atoms of the PEG chain and the ionic liquid (IL) moiety are expected to enhance the hydrophilicity at the surface of the catalyst and may support H-transfer and/or O-H bond cleavage.

In order to get further evidence of the course of this reaction, a tandem reaction was then performed. For this, the hydrogen generated *in situ via* hydrolysis of $NaBH_4$ in D_2O in the presence of 0.32 mol% of catalyst PtNP@PPh$_2$-PEGPIIL **5.3** at 30 °C was used as the hydrogen source for the hydrogenation of 1,1-diphenylethene. The hydrogen produced inside the sealed reaction Schlenk flask after 1 hour was opened to another directly connected reaction Schlenk flask containing 1,1-diphenylethene solution in deuterated methanol and 0.5 mol% Pd/C. The reaction mixture was allowed to stir for 18 hours at 30 °C then the reaction mixture was analysed by ^{1}H NMR spectroscopy which showed a 100% conversion of 1,1-diphenylethene. The distribution of the product mixture formed was then analysed by using a combination of ^{1}H-, ^{2}H-, ^{13}C NMR spectroscopy and GC-MS. A detailed analysis of the product mixture indicated a total of 8 isotopologues, as shown in Scheme **5.2**.
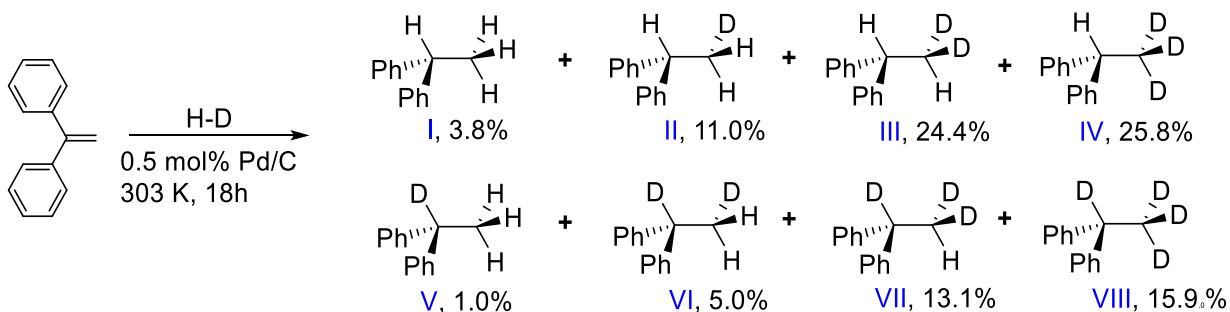
Scheme 5.2: The distribution of 8 isotopologues found and measured by ^{13}C NMR spectroscopy after 1,1-diphenylethene hydrogenation in deuterated methanol using HD produced by hydrolysis of $NaBH_4$ in D_2O catalysed by PtNP@PPh2-PEGPIIL **5.3**.

The ^{13}C NMR spectrum of reaction mixture revealed clear methine region signals with four distinct singlet signals resonating at δ 44.88, δ 44.81, δ 44.74, δ 44.66 ppm corresponding to the isotopologues **I**, **II**, **III** and **IV**, respectively. The assignment of these isotopologues is based on the chemical shift expected for a two bond ^{13}C-D shift of *ca.* 0.07 ppm. The four triplets (1:1:1) resonating at δ 44.46, δ 44.39, δ 44.31 and δ 44.24 ppm (J_{CD} =19.5 Hz) were assigned to the isotopologues **V**, **VI**, **VII**, **VIII** respectively. Each of them contains at least one deuterium on the

methine carbon and 0, 1, 2 or 3 D atoms on the methyl group. The stacked spectra of the reaction mixture is shown in Figure **5.14**.
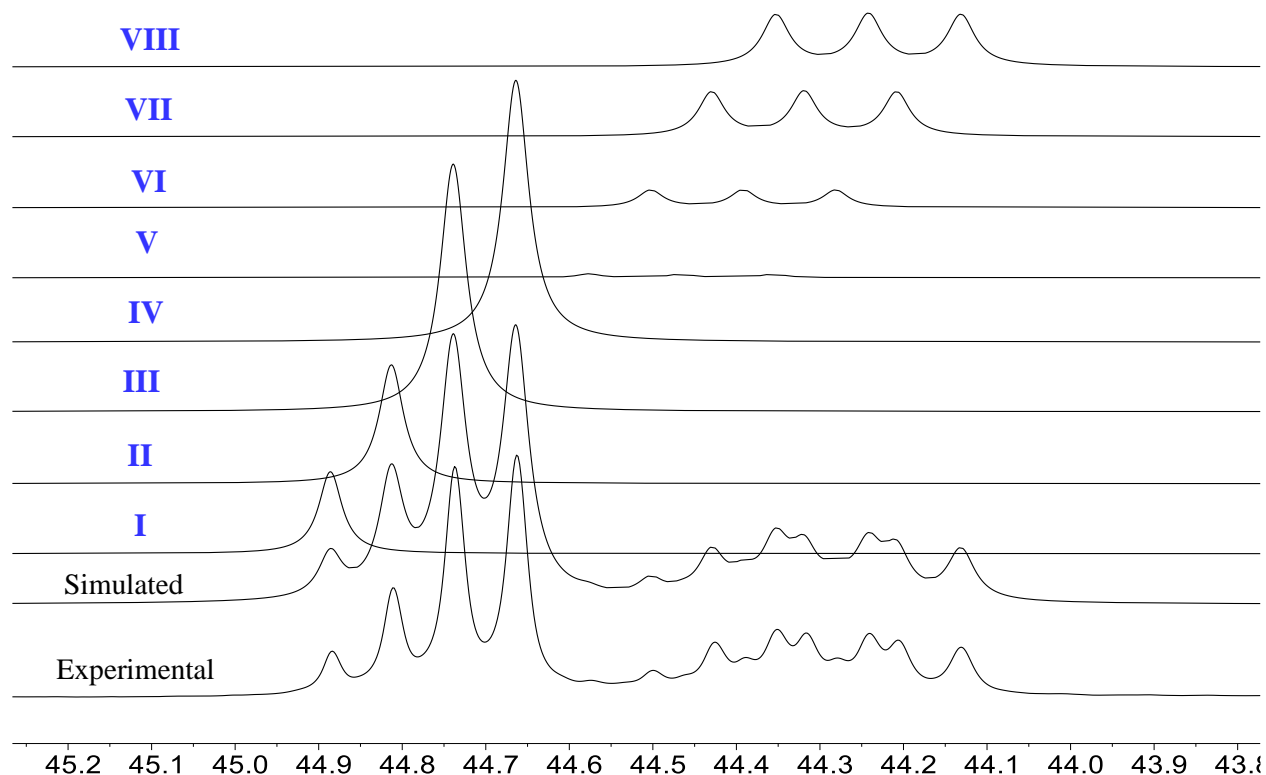
Figure 5.14: A stacked plot of ^{13}C NMR spectrum, displaying the separate simulated spectra in the methine region of the eight possible products.

Figure **5.14** displays the detailed simulated spectrum for every isotopologue individually including the simulated spectrum for all the isotopologues together and the observed spectrum of the reaction mixture obtained experimentally. The simulated spectrum is consistent with the assignments along with the respective integration of each isotopologue (Table **5.2).** The *J* values, isotopic chemical shifts, line width and the intensity of the signals are also in agreement with the assigned values. In addition, the ^{13}C-resonances of the methyl groups (ca. δ21 ppm) were also identified and were also in complete agreement with the corresponding simulated spectrum along with their relative integrations.

Table 5.2: Relative proportion of each of the isotopomers identified and quantified by assignment of the resonances in the methine region of the ^{13}C NMR spectrum. The hydrogen was generated from either $NaBH_4$ in D_2O, $NaBH_4$ in H_2O or $NaBD_4$ in D_2O and the hydrogenation was conducted in either d_4-methanol or toluene as indicated in row 1.

Isotopomer	$NaBH_4/D_2O$ d_4-methanol	$NaBH_4/H_2O$ d_4-methanol	$NaBH_4/D_2O$ toluene	$NaBD_4/D_2O$ toluene
I	3.8	29.8	38.2	19.4
II	11.0	22.3	30.5	24.4
III	24.4	11.5	14.2	20.5
IV	25.8	3.7	3.8	9.4
V	1.0	14.0	6	5.7
VI	5.0	10.2	4.5	9
VII	13.1	5.9	2.1	7.5
VIII	15.9	2.6	0.7	4.1

The interpretation of relative ratios of the experimental spectra was expected to show a total deuterium count of 1 across the isotopologues **II-VIII** for the hydrogen production *via* hydrolysis of aqueous sodium borohydride in D_2O due to combination of a hydride derived from the borohydride and a proton derived from D_2O. In contrast, a total deuterium count of 2.51 across the isotopologues **II-VIII** was actually determined by interpreting the relative ratios. This significant and unanticipated magnification of the total deuterium count might be due to generation of a D:H

ratio of >1:1 in the nanoparticle-catalysed hydrolysis phase. This might be possible by H/D exchange at the surface of the nanoparticle to produce a mixture of D_2 and HD with some of the $NaBH_4$ derived hydride 'leaking' away as HO^- or HOD rather than ending up as HD or H_2. If such an exchange pathway was possible, it would be expected to lead to loss of H relative to D due to the vastly greater amount of D_2O relative to $NaBH_4$. Another plausible reason might be due to the H/D exchange with the deuterated methanol on Pd/C surface during hydrogenation. Again, such a process would be expected to deplete the H relative to D due to the large amount of MeOD. Therefore, experiments to further investigate the behaviour of H/D exchange, hydrogenation of 1,1-diphenylethane in deuterated methanol was carried out by using hydrogen generated from $NaBH_4$ and H_2O. In this case, any exchange at the nanoparticle hydrolysis stage should not affect the H:D ratio, since H_2 is formed in this case and the expected total deuterium incorporation is 0. In contrast, any exchange at the Pd/C stage will lead to incorporation of some deuterium into the products. The analysis of the reaction mixture provided a total deuterium incorporation of 1.19, suggesting a rapid H/D exchange involving the solvent, on Pd/C surface. Next, the H/D exchange experiment at the surface of the nanoparticle in the presence of catalyst PtNP@PPh$_2$-PEGPIIL **5.3** was explored using $NaBH_4$ with D_2O for the hydrolysis phase and using toluene as the solvent in the Pd/C hydrogenation stage. A total deuterium incorporation of 0.94 was obtained for this, close to the expected deuterium count of 1. This suggests that H/D exchange does not occur with the D_2O solvent at the hydrolysis stage. A final possibility, that no exchange with the solvent occurs at either stage, but the outcome results from the availability of a large excess of HD and also that delivery of Pd-bound deuterium is simply faster than the delivery of hydrogen in the hydrogenation stage, i.e. a kinetic isotope effect favouring C-D formation over C-H formation ($k_D > k_H$), seems highly unlikely. Furthermore, the substantial quantities of isotopologues containing -CD_2H and -CD_3 (**III**, **IV**, **VII** and **VIII**) formation was noteworthy for this reaction. This observation was consistent with a facile scrambling *via* β-hydride elimination from the surface of the palladium in such a way that the Pd-CPh$_2$CH$_2$D species produces Ph$_2$C=CHD. A reinsertion into the Pd-D bond then delivers the corresponding M-CPh$_2$CHD$_2$ which is then followed by the reductive elimination step. This pathway is far more likely than a pathway involving any exchange of the diphenylethane reduction product, i.e. a σ-bond metathesis reaction between the Pd-D bond and the C-H bond of the methyl fragment in CPh$_2$HCH$_2$D. A similar observation with a higher value than the stoichiometric deuteration of phenylethylene by using tetrahydroxydiboron/D_2O-derived deuterium has been reported and is attributed to the olefin insertion/extrusion equilibrium involving

the metal-hydride/deuteride species.[307] Moreover, the scrambling effect was also observed for the hydrogenation reaction performed in toluene by using $NaBD_4$ and D_2O as a source of D_2. In this case, a total deuterium count of 1.65 was determined which was close to the expected value of 2.

5.2.6 Catalyst Recycling Studies

Catalyst recycling experiments were then studied using the catalyst $PtNP@PPh_2$-PEGPIIL **5.3** for $NaBH_4$ hydrolysis to assess the efficiency and lifetime of the catalyst, including its potential for deployment into a continuous flow system. For this, the protocol described previously for the reduction of nitroarenes using $PdNP@PPh_2$-PEGPIIL was followed.[119] Because of the difficulty associated with the recovery of small quantities of the catalyst, conventional filtration which might lead to the loss of the catalyst during the recycling was avoided. The experiments were thus performed by measuring the amount of gas produced till the completion of the reaction without isolating the catalyst. Then, an additional amount of $NaBH_4$ (0.021 g, 0.57 mmol) was added directly to the aqueous mixture and this sequence of reactions were repeated 5 times. The catalytic efficiency of the catalyst as a function of reaction time and reuse number was then plotted (Figure **5.15a**).
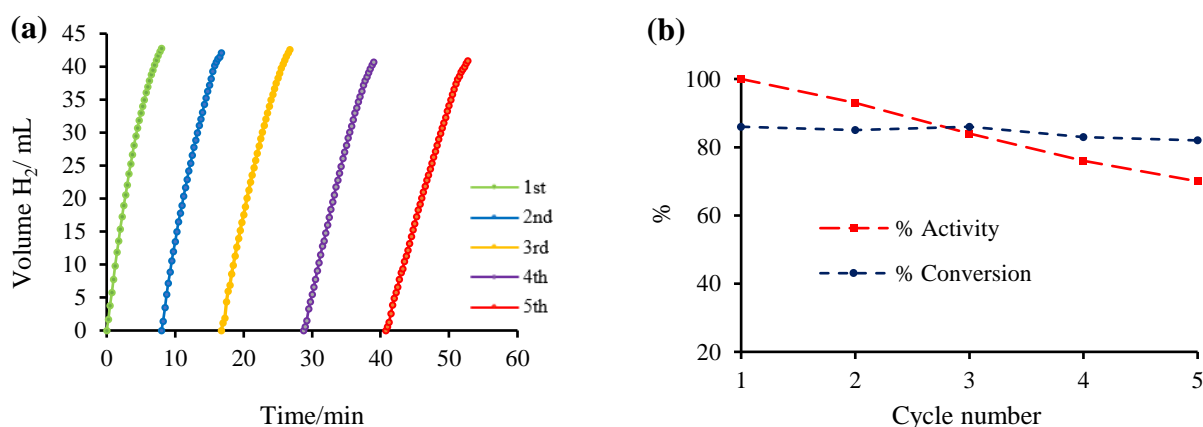
Figure 5.15: Plots of the hydrogen volume versus time for $NaBH_4$ hydrolysis catalysed by 2 mol% of $PtNP@PPh_2$-PEGPIIL **5.3** at 30 °C. (b) Conversion and percentage of initial activity achieved in each run after consecutive recycles.

Initially, high conversions were observed across 5 cycles. It is noteworthy to mention that to attain an analogous conversion to the first cycle, the successive cycles were allowed to stir for longer reaction time for each run (Table **5.3**). For instance, the conversion 85% after 8 min of the 2nd cycle decreased to 82% in the 5th cycle after 12 min. The loss of catalytic efficiency of the catalyst in the

successive cycles is shown in Figure **5.15b** and the % decrease in the initial rates of each run is based on the slope of the linear portion of the plots in Figure **5.15a**. Figure **5.15b** clearly demonstrates that the catalytic activity of PtNP@PPh$_2$-PEGPIIL **5.3** is retained to a level of about 70% across the 5th cycle. For comparison, catalytic recycling studies by using the dendrimer-stabilised PtCo-NPs, RhNPs and PtNPs,[359,361,380] embedded amine functionalised MIL-53(A1) stabilised RuNPs,[391] zeolite confined RuNPs and polyvinylpyrollidine stabilised RuNPs,[350,383,391] zeolitic imidazolate framework of ZIF-8 based NiNPs,[356] and β-cyclodextrin derived highly dispersed PtNPs,[381] also showed a comparable recycling pattern and conversions in the range of 61-75% up to the 5th cycle.

Table 5.3: Conversion as function of time for the recycle of PtNP@PPh$_2$-PEGPIIL **5.3**.

Run	Conversion	Time (min)
1	86	8
2	85	8.75
3	86	10
4	83	10.25
5	82	12

The rapid loss of the catalytic activity after the 5th cycle led us to analyse the aqueous phase after the 5th cycle by using ICP-OES to measure the Pt content. The result showed that the Pt content ($<$ 0.1 mg L^{-1}) is too low to be detected. This observation suggests that the loss of catalyst activity is not due to the leaching of Pt-metal to produce homogeneous species. The Energy Dispersive X-Ray Spectroscopy (EDX) analysis of the catalyst after 5th cycle showed the presence of substantial quantities of boron accumulating on the catalyst (0.48 boron:1.00 platinum), which might be the major reason for the loss of catalytic activity. Therefore, a hot filtration study was used to

investigate the heterogeneous nature of the active species. For this, the hydrolysis of $NaBH_4$ in the presence of 0.32 mol% PtNP@PPh$_2$-PEGPIIL **5.3** was allowed to progress until complete consumption. After that, a micro syringe filter was used to filter the reaction mixture, then an additional amount (0.021 g, 0.57 mmol) of $NaBH_4$ was added to the filtrate. The resulting hydrogen gas produced corresponds to the background hydrolysis only, further confirming that the active Pt-species has been removed by filtration. In an analogous hot filtration experiment, the hydrolytic reaction mixture was filtered using a micro syringe filter to remove the catalyst PtNP@PPh$_2$-PEGPIIL **5.3** from the reaction mixture when the reaction had reached *ca.* 50% conversion after 8 minutes. The resulting hydrogen produced was then quantified which showed again the background hydrolysis only (Figure **5.16**).
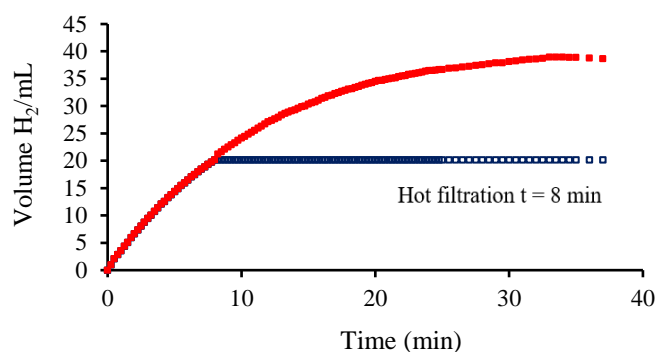
Figure 5.16: Hot filtration study for for $NaBH_4$ hydrolysis catalysed by 0.32 mol% PtNP@PPh$_2$-PEGPIIL **5.3** displaying that turnover has been totally stopped after filtration of the catalyst at t = 8 minutes (Blue line). Red line - reaction with catalyst PtNP@PPh$_2$-PEGPIIL **5.3**.

This supports the conclusion that the active catalyst for this reaction is heterogeneous in nature. Nevertheless, the ICP analysis and the hot filtration test cannot distinguish between heterogeneous catalysis occurring at defect sites on the nanoparticle surface and homogeneous reactions in which leaching and fast re-deposition of the metal occurs.

TEM analysis was carried out by isolating PtNP@PPh$_2$-PEGPIIL **5.3** after the 5th cycle. The TEM analysis showed that the NPs remained monodisperse with an average diameter of 2.6 ± 0.7 nm compared to 3.0 ± 0.8 nm for the freshly prepared PtNPs (Figure **5.17**).
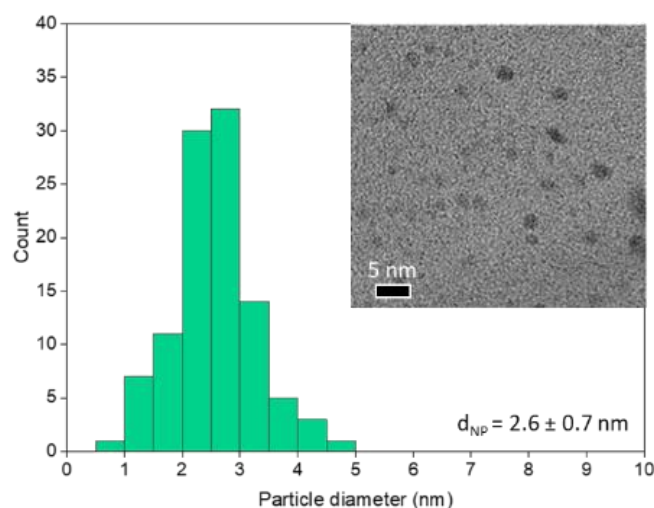
Figure 5.17: HRTEM image and nanoparticles size after 5 experimental cycles of PtNP@PPh$_2$-PEGPIIL **5.3**.

5.2.7 Poisoning Study

Agglomeration was ruled out for the rapid drop in conversion in the successive cycles, nonetheless, formation of the sodium metaborate (NaBO$_2$) hydrolysis product might be responsible for this. There are several reports describing deactivation of the catalyst due to the formation of NaBO$_2$ and its adsorption on the surface of nanoparticles.[307,329,361,391] In order to address this behaviour, several experiments were performed by pre-stirring an aqueous solution of PtNP@PPh$_2$-PEGPIIL **5.3** with NaBO$_2$ (1.0 eq.) before the addition of NaBH$_4$. The catalytic activity was then measured as a function of pre-stirring time in the presence and absence of NaBO$_2$. The plot of the activity against the pre-stirring time suggests NaBO$_2$ poisoning and hence deactivation of the catalyst (Figure **5.18a**). Figure **5.18b** further shows that NaBO$_2$ poisoning is immediate and leads to a significant decline in the conversion rates. A conversion of 86% in the absence of NaBO$_2$ can be achieved while the corresponding conversion of 63% was observed upon the direct addition of NaBO$_2$ even with no pre-stirring. The drop in conversion was clearly correlated to the pre-stirring time. For instance, a conversion of 39% was obtained when the reaction was allowed for 60 min pre-stirring and dropped down to 32% after the pre-stirring time was raised to 18 hours. These stirring time-conversion experiments apparently show the kinetics of the adsorption of NaBO$_2$ on the surface of the NPs.
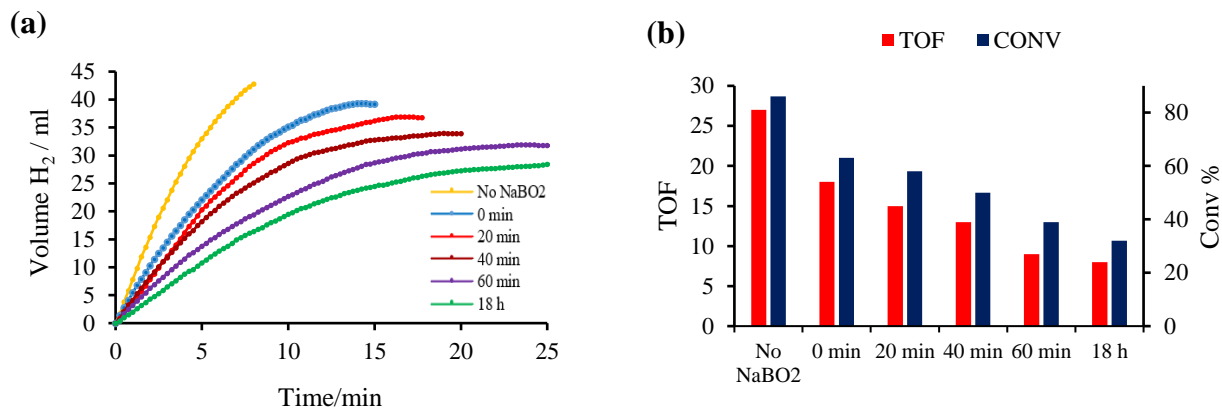
Figure 5.18: Plots of the hydrogen volume versus time for NaBH$_4$ hydrolysis catalysed by 2 mol% PtNP@PPh$_2$-PEGPIIL **5.3** (b) the corresponding conversions and TOFs as a function of NaBO$_2$ pre-stirring time.

Finally, experiments for the stability of the catalyst in the reaction medium were performed. For this, a baseline experiment was set up for the catalyst PtNP@PPh$_2$-PEGPIIL **5.3** and allowed to stir for 18 hours in an aqueous solution before adding NaBH$_4$. Analogously, another experiment was performed by adding NaBH$_4$ to a freshly prepared PtNP catalyst. Both experiments provided a similar initial TOF and conversion profile indicating that stirring the catalyst in aqueous solution alone, does not adversely affect the catalytic activity. This suggests that the immediate reduction in the conversion rate after 18 hours of pre-stirring with NaBO$_2$ was due to adsorption of the hydrolysis product i.e., NaBO$_2$ on the support and/or on the surface of the NPs. In addition, the trivial growth in the size of the PtNPs and also the slight increase in the viscosity of the reaction mixture might also limit the diffusion of the substrate and hence contribute to the observed deactivation.[391]

5.3   Conclusion

Polymer immobilised ionic liquid (PIIL) stabilised PtNPs catalyse the aqueous hydrolysis of NaBH$_4$ to produce hydrogen. The hydrolysis proceeds efficiently in the presence of catalyst derived from PtNP@PPh$_2$-PEGPIIL **5.3** which was found to be more efficient than PtNP@PPh$_2$-*N*-decylPIIL **5.4**.

The PIIL were loaded with Pt^{II} by anion exchange using an aqueous solution of K$_2$[PtCl$_4$] to afford PtCl$_4$@PIIL. Reduction of PtCl$_4$@PIIL by NaBH$_4$ gave the corresponding PIIL stabilised PtNPs. Analysis of the materials by solid state ^{31}P NMR spectroscopy confirmed the presence of a Pt---P interaction and that all the phosphine was coordinated to Pt. XPS analysis showed complete reduction of the Pd^{II} precursor to Pt^0 for both catalysts. TEM analysis of PtNP@PPh$_2$-PEGPIIL **5.3** and PtNP@PPh$_2$-*N*-decylPIIL **5.4** showed near-monodisperse distribution with an average diameter of 3.0 ± 0.8 nm and 2.7 ± 1.1 nm, respectively.

An initial TOF of 169 mole$_{H_2}$.mol$_{cat}^{-1}$.min^{-1} with PtNP@PPh$_2$-PEGPIIL **5.3** is one of the highest TOF obtained for any PtNP-based catalyst to date. The reaction follows first order reaction kinetics with respect to both catalyst and NaBH$_4$. An activation energy of 23.9 kJ mol^{-1} for PtNP@PPh$_2$-PEGPIIL **5.3** and 35.6 kJ mol^{-1} for PtNP@PPh$_2$-*N*-decylPIIL **5.4**, was also determined during the kinetic studies. Albeit the primary function of the PIIL support is to provide stability to the metal NPs, the better catalytic efficiency of the catalyst due to introduction of the *N*-PEGylated imidazolium chain as compared to its *N*-decyl analogue might be due to the dramatic change in the hydrophilicity/hydrophobicity balance. This change might be responsible for improved homogenous dispersion of the catalyst on the surface and facilitate access to more active sites. Also, it might alter the catalyst-support interactions in order to provide a better substrate activation and better interaction with the borohydride by forming surface bound hydrogen-bonded [BH$_3$-H---H-OH]$^-$ species and also facilitate activation of H$_2$O to undergo a facile oxidative addition.

Addition of NaOH to the hydrolysis of NaBH$_4$ by PtNP@PPh$_2$-PEGPIIL **5.3** leads to a slight increase in initial TOF as the concentration of NaOH was increased and the TOF reached a maximum of 49 mole$_{H_2}$.molcat^{-1}.min^{-1} in 0.14 mM NaOH, increasing the NaOH concentration further then leads to a decline in the TOF. A TOF of 39 mole$_{H2}$.mol$_{cat}^{-1}$.min^{-1} was measured under similar reaction conditions in the absence of NaOH.

Primary kinetic isotopic labelling experiments revealed a KIE (k_H/k_D) 1.8 for PtNP@PPh$_2$-PEGPIIL **5.3** and 2.1 for PtNP@PPh$_2$-*N*-decylPIIL **5.4** in D$_2$O indicating the O-H bond cleavage of H$_2$O to be involved in the rate determining step. This O-H bond cleavage is likely to be facilitated *via* hydrogen bonding with a hydridic B-H bond of surface bound borohydride.

PtNP@PPh$_2$-PEGPIIL **5.3** recycling experiments revealed a retention of 70% of the catalytic activity up to 5 cycles and TEM analysis after 5 cycles indicated that the average size of the nanoparticles remained unchanged. The EDX analysis showed a substantial amount of boron accumulating on the catalyst, which has been proposed as the cause of the catalyst's decreased activity. Catalytic poisoning experiments suggested that the loss of the catalytic activity was due to the formation of sodium metaborate and deactivation due to adsorption at the surface of the catalyst.

Hydrogenation of 1,1-diphenylethene was performed with the hydrogen produced from NaBH$_4$ hydroysis in D$_2$O, and the products was analysed by ^{13}C NMR. The result shows that the product is formed a mixture of 8 isotopologues and further studied indicated that H/D scrambling occurs on the surface of the Pd/C catalyst at the hydrogenation stage and not at the nanoparticle surface during borohydride hydrolysis.

Having demonstrated that these Pt PIIL systems are highly effective catalysts for hydrogen generation by hydrolysis of NaBH$_4$, further investigation into the use of other hydrogen carriers remains to be explored. We plan to study the efficiency of PtNPs derived from PtNP@PPh$_2$-PEGPIIL **5.3** and PtNP@PPh$_2$-*N*-decylPIIL **5.4** as catalysts for evolution of hydrogen from hydrolysis of NH$_3$BH$_3$ and (CH$_3$)$_2$NH·BH$_3$.

Chapter 6. Experimental

- General comments

All manipulations involving air-sensitive compounds were carried out using standard Schlenk line techniques under an atmosphere of N_2 in oven-dried glassware. All reaction solvents were distilled before use; toluene, dichloromethane and chloroform were dried over calcium hydride; diethyl ether and tetrahydrofuran were dried over sodium wire in the presence of benzophenone; methanol and ethanol from magnesium; acetonitrile from potassium carbonate; dimethyl formamide was dried over molecular sieves. All chemicals were purchased from commercial suppliers and used as received without further purification. ^{1}H, ^{13}C and ^{31}P spectra were recorded on either JEOL ECS-400 MHz, JEOL ECS-500 MHz, Bruker Avance III 300 MHz, or Bruker Ascend 700 MHz spectrometer. FT-IR spectroscopy was performed using Perkin Elmer spectrum two with the UATR accessory spectrometer scanning from 6000-550 cm^{-1}.

The (SEM/ EDS) analysis was taken using high-resolution imaging of surfaces by a Tescan Vega 3LMU scanning electron microscope fitted with a detector (Bruker XFlash® 6 | 30). Mass spectrometry analysis was performed using a Micromass LCT premier Mass Spectrometer in Electro Spray (ES) mode by the National Mass Spectrometry Facility (NMSF) Swansea. XPS measurements were carried out using a Theta Probe system (Thermo Scientific, UK) equipped with a micro-focused monochromatic AlKα source. For transmission electron microscopy (TEM), samples were dispersed in ethanol using an ultrasonic bath and deposited on lacey carbon film-coated copper grids. TEM images were acquired on a FEI Tecnai TF20 field emission gun microscope operating at 200 kV. NP size distribution histograms were obtained from measurements of at least 100 different NPs assuming a spherical shape and with random distribution. EDX spectra were taken using a field emission SEM FEI Nova 450, EDAX TEAM software and a voltage of 18 kV. Inductively coupled plasma (ICP-OES) analysis to calculate metal loadings was conducted using a Perkin-Elmer Optima 4300.

6.1 Chapter 2 experimental.

6.1.1 General Procedure for the Iridium-Catalysed Borylation of Diethyl Phenylphosphonate with B$_2$pin$_2$.[221]

An oven dried Schlenk flask under N$_2$ was charged with iridium precursor (2.5 mol%), ligand (2.5 mol%) and bis(pinacolato)diboron (0.06 g, 0.28 mmol) or pinacolborane (0.09 g, 0.74 mmol). Diethyl phenylphosphonate (0.09 g, 0.08 mL, 0.37 mmol) and dry solvent (4 mL) were added, and the reaction mixture was stirred for the allocated time at the specified temperature. After this time, the resulting solution was left to cool to room temperature, diluted by adding acetonitrile (2 mL). The resulting solution was passed through a silica plug and the solvent was removed under reduced pressure. The crude product was dissolved in CDCl$_3$ and analysed by ^{31}P and ^{1}H NMR spectroscopy to quantify the composition and determine the selectivity profile.

6.1.2 General Procedure for the Iridium-catalysed Borylation of Diethyl Phenylphosphonate with HBpin.[221]

Addition of tmphen before HBpin: An oven dried Schlenk flask under N_2 was charged with [Ir(COD)(OMe)]$_2$ (0.006 g, 0.009 mmol, 2.5 mol%), tmphen (0.004 g 0.018 mmol, 5 mol%) and dry hexane (4 mL). After stirring for two minutes, pinacolborane (0.09 g, 0.74 mmol) was added followed by diethyl phenylphosphonate (0.09 g, 0.08 mL, 0.37 mmol) and the reaction mixture was stirred for the allocated time at the specified temperature. After this time, the resulting solution was left to cool to room temperature, diluted by the addition of acetonitrile (2 mL), the resulting solution was passed through a silica plug and the solvent was removed under reduced pressure. The crude product was dissolved in CDCl$_3$ and analysed by ^{31}P and ^{1}H NMR spectroscopy to quantify the composition and determine the selectivity profile.

Addition of HBpin before tmphen: An oven dried Schlenk flask under N_2 was charged with [Ir(COD) (OMe)]$_2$ (0.006 g, 0.009 mmol, 2.5 mol%), pinacolborane (0.09 g, 0.74 mmol) and dry hexane (4 mL). After stirring for two minutes, tmphen (0.004 g 0.018 mmol, 5 mol%) was added followed immediately by diethyl phenylphosphonate (0.09 g, 0.08 mL, 0.37 mmol) and the reaction mixture was stirred for the allocated time at the specified temperature. After this time, the resulting solution was left to cool to room temperature, diluted by the addition of acetonitrile (2 mL), the resulting solution was passed through a silica plug and the solvent was removed under reduced pressure. The crude product was dissolved in CDCl$_3$ and analysed by ^{31}P and ^{1}H NMR spectroscopy to quantify the composition and determine the selectivity profile

6.2 Chapter 3 experimental.

6.2.1 Synthesis of PEG-chloride (3.1).
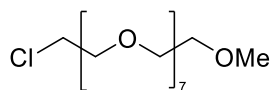
An oven dried Schlenk flask under N_2 was charged with polyethylene glycol monomethyl ether (7.00 g, 20.0 mmol), pyridine (3.16 g, 40.0 mmol) and dry toluene (40 mL). The mixture was stirred, heated slowly to 80 °C and then thionyl chloride (4.74 g, 40.0 mmol) was added over 20 minutes. The mixture was stirred for two days under reflux. After this time, the reaction mixture was cooled to room temperature, and then water (10 mL) was added to quench the excess of thionyl chloride. The mixture was extracted with toluene (3 x 30 mL), the organic fractions were combined and dried over $MgSO_4$, filtered and the solvent was removed under reduced pressure. The oily product was dissolved in dichloromethane (40 mL) and washed with water (4 x 30 mL). The organic layer was dried over $MgSO_4$, filtered and the solvent was removed under reduced pressure to afford PEG-chloride **3.1** as a red oil (6.37 g, 85%). ^{1}H NMR (300 MHz, CDCl$_3$) δ 3.69 (t, J = 5.5 Hz, 2H), 3.63 – 3.55 (m, 28H), 3.50 – 3.46 (m, 2H), 3.31 (s, 3H); ^{13}C NMR (75 MHz, CDCl$_3$) δ 71.79, 71.88, 70.60, 70.53, 70.45, 58.96, 42.69.

This is consistent with data reported in the literature.[120]

6.2.2 Synthesis of 2-methyl-1-PEG-imidazole (3.2).

An oven dried Schlenk flask under N_2 was charged with sodium hydride (1.41 g, 60% dispersion in mineral oil, 58.7 mmol) which was washed with dry hexane (3 x 15 mL) to remove the mineral oil. The resultant was suspended in dry tetrahydrofuran (70 mL). The mixture was cooled to 0 °C, then 2-methylimidazole (1.93 g, 23.5 mmol) was added dropwise, resulting in the liberation of hydrogen gas. Once the exotherm had subsided, PEG-chloride **3.1** (10.5 g, 28.2 mmol) was added dropwise. The mixture was heated overnight at 75 °C. After this time, the mixture was cooled to room temperature and water (2 mL) was added to quench the excess of sodium hydride. The solvent was removed using an external trap and the residue was washed with diethyl ether (4 x 40 mL), the ether fractions were combined, and the solvent was removed under reduced pressure to afford 2-methyl-1-PEG-imidazole **3.2** as a red oil (9.49 g, 90%). ^{1}H NMR (400 MHz, CDCl$_3$) δ 6.78 (d, J = 1.3 Hz, 1H), 6.75 (d, J = 1.3 Hz, 1H), 3.90 (t, J = 5.5 Hz, 2H), 3.66 – 3.37 (m, 30H), 3.25 (s, 3H), 2.27 (s, 3H); ^{13}C NMR (101 MHz, CDCl$_3$) δ 144.59, 126.84, 119.39, 71.76, 70.59, 70.41, 70.32, 58.82, 45.87, 12.97.

This is consistent with data reported in the literature.[120]

6.2.3   Synthesis of 4 vinylbenzyl bromide (3.3).
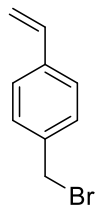
An oven dried Schlenk flask under N_2 was charged with 4-vinylbenzyl chloride (5.72 g, 37.5 mmol), sodium bromide (15.4 g, 150 mmol) and dry acetonitrile (50 mL). The reaction mixture was heated overnight at 85 °C. After this time, the mixture was allowed to cool to room temperature, filtered then the solvent was removed under reduced pressure to afford 4 vinylbenzyl bromide **3.3** as a yellow oil (6.37 g, 86%). ^{1}H NMR (400 MHz, CDCl$_3$) δ 7.43 – 7.33 (m, 4H), 6.71 (dd, J = 17.6, 10.9 Hz, 1H), 5.77 (d, J = 17.5 Hz, 1H), 5.28 (d, J = 10.9 Hz, 1H), 4.50 (s, 2H). ^{13}C NMR (101 MHz, CDCl$_3$) δ 137.80, 137.29, 136.24, 129.35, 126.67, 114.71, 33.52.

This is consistent with data reported in the literature.[242]

6.2.4   Synthesis of 2-methyl-1-PEG-3-(4-vinlbenzyl) imidazolium bromide (3.4).
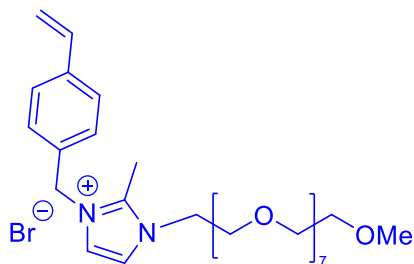
An oven dried Schlenk flask under N_2 was charged with 4-vinylbenzyl bromide **3.3** (7.40 g, 34.7 mmol), 2-methyl-1-PEG-imidazole **3.2** (12.0 g, 28.9 mmol) and dry dichloromethane (200 mL). The mixture was stirred overnight at 35 °C. The solvent was removed under reduced pressure, the resultant residue was triturated with diethyl ether (5 x 50 mL) and dried under high vacuum to afford 2-methyl-1-PEG-3-(4-vinlbenzyl) imidazolium bromide **3.4** as a yellow oil (16.6 g, 89%). ^{1}H NMR (400 MHz, CDCl$_3$) δ 7.82 (s, 1H), 7.45 (s, 1H), 7.35 (d, J = 8.0 Hz, 2H), 7.21 (d, J = 7.9 Hz, 2H), 6.60 (dd, J = 17.6, 10.9 Hz, 1H), 5.70 (d, J = 17.6 Hz, 1H), 5.45 (s, 2H), 5.23 (d, J = 10.9 Hz, 1H), 4.46 (t, J = 4.8 Hz, 2H), 3.83 (t, J = 4.7 Hz, 2H), 3.63 – 3.38 (m, 28H), 3.34 – 3.23 (m, 3H), 2.73 (s, 3H);^{13}C NMR (75 MHz, CDCl$_3$) δ 144.57, 137.66, 135.73, 132.99, 128.18, 126.72, 121.90, 121.62, 114.78, 71.58, 71.47, 70.19, 70.14, 70.07, 68.99, 58.66, 53.70, 51.46, 48.84, 10.66.

This is consistent with data reported in the literature.[120]

6.2.5   Synthesis of diphenyl(4-vinylphenyl)phosphine (3.5).

An oven dried two necked round bottom flask under N_2 was charged with Mg turnings (3.75 g, 154 mmol) and dry tetrahydrofuran (40 mL). A crystal of iodine was added to the mixture, which was cooled to 0 °C. 4-Bromostyrene (14.4 g, 78.6 mmol) was dissolved in dry tetrahydrofuran (35 mL) in a dropping funnel and the solution was added dropwise to the Mg turnings to start Grignard formation. Then the mixture was stirred and heated at 65 °C for 4 hours. Another round bottom flask was charged with chlorodiphenylphosphine (12.9 g, 58.5 mmol) dissolved in dry tetrahydrofuran (40 mL). The solution was cooled to 0 °C, the Grignard solution was filtered and transfer by cannula into the chlorodiphenylphosphine solution and the resultant mixture was left to stir overnight at room temperature. The reaction was quenched with degassed water (100 mL) and extracted with dry diethyl ether (3 x 150 mL). The organic fractions were combined and dried over $MgSO_4$, filtered and the solvent was removed by an external trap. Diphenyl(4-vinylphenyl) phosphine **3.5** was obtained as a white powder (10.8 g, 64%) and stored under nitrogen. ^{1}H NMR (300 MHz, CDCl$_3$) δ 7.48 – 7.24 (m, 14H), 6.71 (dd, *J* = 17.6, 10.9 Hz, 1H), 5.79 (d, *J* = 17.6 Hz, 1H), 5.28 (d, *J* = 10.9 Hz, 1H); ^{13}C NMR (75 MHz, CDCl$_3$) δ 137.95, 137.23, 137.09, 136.4, 134.09, 133.86, 133.83, 133.60, 128.75, 126.35; ^{31}P NMR (121 MHz, CDCl$_3$) δ -5.74 ppm.

This is consistent with data reported in the literature.[244]

6.2.6 Synthesis of 2-methyl-1-(4-vinylbenzyl)-1*H*-imidazole (3.6).
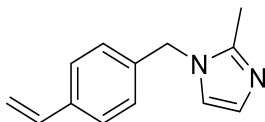
An oven dried Schlenk flask under N_2 was charged with sodium hydride (1.22 g, 60% dispersion in mineral oil, 50.8 mmol) in dry dimethylformamide (20 mL). The mixture was stirred and cooled in an ice bath to 0 °C. 2-Methylimidazole (3.00 g, 36.5 mmol) was added portion wise, resulting in the liberation of hydrogen gas. Once the exotherm had subsided, then 4-vinylbenzyl chloride (4.65 g, 30.4 mmol) was added to the mixture. The reaction mixture was heated for 1 hour at 75 °C. Then the mixture was poured onto water (250 mL) and extracted with ethyl acetate (2 x 100 mL). The combined organic extracts were washed with water (180 mL), brine (50 mL) and then extracted with 6N HCl (2 x 25 mL). The aqueous layer was washed with diethyl ether (20 mL) and basified through addition of 1M NaOH solution until pH 12. Then, the product was extracted with diethyl ether (3 x 50 mL), dried over MgSO$_4$, filtered and the solvent was removed under reduced pressure to afford 2-methyl-1-(4-vinylbenzyl)-1*H*-imidazole **3.6** as a yellow oil (5.73 g, 95%). ^{1}H NMR (300 MHz, CDCl$_3$) δ 7.30 (d, *J* = 8.2 Hz, 2H), 6.94 (d, *J* = 8.3 Hz, 2H), 6.88 (d, *J* = 1.3 Hz, 1H), 6.76 (d, *J* = 1.3 Hz, 1H), 6.62 (dd, *J* = 17.6, 10.9 Hz, 1H), 5.67 (d, *J* = 17.6 Hz, 1H), 5.19 (d, *J* = 10.9 Hz, 1H), 4.96 (s, 2H), 2.27 (s, 3H); ^{13}C NMR (75 MHz, CDCl$_3$) δ 144.77, 137.14, 135.98, 135.77, 126.96, 126.81, 126.60, 119.83, 114.32, 49.30, 12.85; FT-IR (neat, cm^{-1}): ṽ = 3350, 3005, 2932, 2360, 1630, 1510, 1495, 1420, 1407, 1282, 1133, 988, 914, 825, 735, 675.

This is consistent with data reported in the literature.[245]

6.2.7 Synthesis of 2-methyl-1,3-bis(4-vinylbenzyl)-1*H*-imidazol-3-ium chloride (3.7).
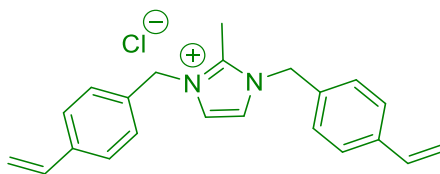
An oven dried Schlenk flask under N_2 was charged with 2-methyl-1-(4-vinylbenzyl)-1*H*-imidazole **3.6** (2.40 g, 12.1 mmol), 4-vinylbenzyl chloride (2.21 g, 14.5 mmol) and dry chloroform (50 mL). The reaction mixture was stirred overnight at 50 °C. The solvent was removed under reduced pressure, the resulting residue was washed with ethyl acetate, then dissolved in the minimum amount of dichloromethane and added dropwise to diethyl ether (250 mL) with stirring. After 60 minutes of stirring, the product was allowed to settle then filtered, washed with diethyl ether (50 mL) and dried under high vacuum to afford 2-methyl-1,3-bis(4-vinylbenzyl)-1*H*-imidazol-3-ium chloride **3.7** as white powder (4.20 g, 98%). ^{1}H NMR (300 MHz, CDCl$_3$) δ 7.55 (s, 2H), 7.42 (d, *J* = 8.2 Hz, 4H), 7.30 (d, *J* = 7.5 Hz, 4H), 6.69 (dd, *J* = 17.6, 10.9 Hz, 2H), 5.77 (d, *J* = 18.2 Hz, 2H), 5.53 (s, 4H), 5.32 (d, *J* = 10.9 Hz, 2H), 2.82 (s, 3H); ^{13}C NMR (75 MHz, CDCl$_3$) δ ^{13}C NMR (75 MHz, CDCl$_3$) δ 144.37, 138.46, 135.77, 132.09, 128.51, 127.14, 121.93, 115.35, 52.18, 11.35.; mp = 115– 117 °C; FT-IR (neat, cm^{-1}): ṽ = 3379, 3110, 3070, 2970, 1635, 1580, 1525, 1513, 1409, 1170, 985, 910, 829, 785, 715.

This is consistent with data reported in the literature.[245]

6.2.8 Synthesis of PPh₂-PEGPIIL (3.8).

An oven dried Schlenk flask under N₂ was charged 2-methyl-1-PEG-3-(4-vinylbenzyl)imidazolium bromide **3.4** (7.91 g, 12.9 mmol), diphenyl(4-vinylphenyl)phosphine **3.5** (2.00 g, 6.93 mmol), 2-methyl-1,3-bis(4-vinylbenzyl)-1*H*-imidazol-3-ium chloride **3.7** (0.34 g, 0.97 mmol), AIBN (0.05 g, 0.34 mmol, 5 mol%), dry ethanol (40 mL) and dry tetrahydrofuran (40 mL). The mixture was degassed using the freeze-pump-thaw method six times before being heated for four days at 80 °C. After this time, an additional equivalence of AIBN (0.05 g, 0.34 mmol, 5 mol%) was added, the degassing procedure was repeated and then the mixture was heated for 24 hours at 80 °C. The solvent was removed under reduced pressure, the resulting residue was dissolved in dichloromethane (10 mL /g polymer) and added dropwise to diethyl ether (350 mL) with stirring. After 60 minutes of stirring, the product was allowed to settle, filtered, washed with diethyl ether, and dried under high vacuum to afford PPh₂-PEGPIIL **3.8** as a white powder (8.70 g, 85%). ³¹P NMR (162 MHz CDCl₃) δ -6.68; FT-IR (neat, cm⁻¹): ṽ = 3401, 2869, 1584, 1514, 1436, 1349, 1248, 1188, 1093, 943, 848, 753, 721, 701, 672, 539.

This is consistent with data reported in the literature.[120]

6.2.9   Attempted Synthesis of [AuCl₄]@PPh₂-PEGPIIL (3.9).

An oven dried Schlenk flask under N_2 was charged with PPh$_2$-PEGPIIL **3.8** (2.50 g, 1.66 mmol), KAuCl$_4$ (0.63 g, 1.66 mmol) and water (40 mL). The reaction mixture was stirred overnight at room temperature. The solvent was removed under reduced pressure and the resulting residue was dissolved in dichloromethane (10 mL /g polymer) and added dropwise to a large volume of diethyl ether (350 mL) and stirred for 60 min. After this time, the mixture was allowed to settle and the product was filtered through a frit, washed with water (2 x 10 mL), ethanol (2 x 10 mL) and diethyl ether (2 x 30 mL) to give what was expected to be [AuCl$_4$]@PPh$_2$-PEGPIIL adduct **3.9** as an orange powder (2.20 g, 80%). ^{31}P NMR (202 MHz, CDCl$_3$) δ 29.46; FT-IR (neat, cm^{-1}): ṽ = 3355, 2871, 1585, 1513., 1437, 1349, 1250, 1185, 1093, 943, 830, 752, 722, 704, 539. ICP-OES data: 8.61 wt% gold corresponding to a gold loading of 0.43 mmol g^{-1}.

This is consistent with data reported in the literature[83] but note that the ^{31}P NMR chemical shift indicates that, in fact, the phosphine oxide may be formed along with concomitant reduction of the Au(III).

6.2.10 Synthesis of Ph₃=O (3.10).
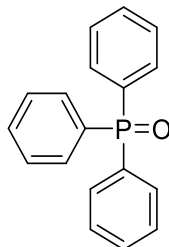
An oven dried Schlenk flask under N_2 was charged with triphenylphosphine (1.00 g, 3.81 mmol), and dichloromethane (5 mL), and a solution of hydrogen peroxide (30% w/w in water, 4 mL) and water (45 mL). The mixture was vigorously stirred for 5 hours at room temperature. After this time, the two layers were separated, and the organic layer was dried over $MgSO_4$, filtered, and the solvent was removed under reduced pressure to afford $Ph_3P=O$ **3.10** as a white powder (1.00 g, 94%). ^{31}P NMR (121 MHz, $CDCl_3$) δ 29.4 ppm.

This is consistent with data reported in the literature.[247]

6.2.11 Synthesis of Au^{I}(THT)Cl (3.11).
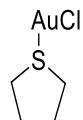
An oven dried Schlenk flask under N_2 was charged with $KAuCl_4$ (2.04 g, 5.30 mmol), ethanol (50 mL) and water (10 mL). Tetrahydrothiophene (1.17 g, 13.2 mmol) was added dropwise which resulted in the formation of a yellow precipitate which changed into a white solid. Ethanol (10 mL) was added to the mixture to ensure efficient mixing. The reaction mixture was stirred for 40 min at room temperature. The white precipitate was filtered, washed with ethanol, diethyl ether and dried under high vacuum to get Au^{I}(THT)Cl **3.11** as a fine white powder (1.50 g, 88%), which was stored in the freezer. ^{1}H NMR (400 MHz, CDCl$_3$) δ 3.48 – 3.27 (m, 4H,), 2.08 – 1.91 (m, 4H); ^{13}C NMR (101 MHz, CDCl$_3$) δ 31.10, 31.11, 28.08, 28.0.

This is consistent with data reported in the literature.[392]

6.2.12 Synthesis of Au^I(PPh$_3$)Cl (3.12).
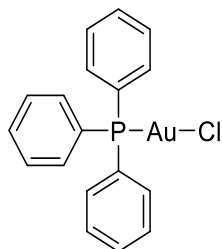
An oven dried Schlenk flask under N$_2$ was charged with Au^I(THT)Cl **3.11** (0.38 g, 1.20 mmol), triphenylphosphine (0.31 g, 1.20 mmol) and dichloromethane (50 mL). The reaction mixture was stirred overnight at room temperature. The white precipitate was filtered and washed with ethanol, diethyl ether and dried under high vacuum. Then, the white precipitate was recrystallised (chloroform:hexane 1:3) to give Au^I(PPh$_3$)Cl **3.12** as a white crystalline solid (0.42 g, 71%). ^{1}H NMR (400 MHz, CDCl$_3$) δ 7.49-7.44 (m, 6H); 7.44-7.37 (m, 9H); ^{13}C NMR (121 MHz, CDCl$_3$) δ 134.17, 132.01, 129.25, 128.42; ^{31}P NMR (162 MHz, CDCl$_3$) δ 33.20 ppm.

This is consistent with data reported in the literature.[251]

6.2.13 Synthesis of Au^{III}(PPh$_3$)Cl$_3$ (3.13).
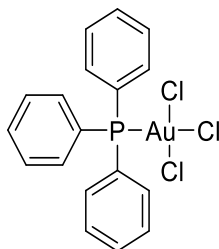
This experiment was performed in a well-ventilated fume hood. Chlorine gas was generated by adding concentrated HCl dropwise to potassium permanganate. The gas released was bubbled through H_2SO_4 to remove any HCl gas, then through the reaction mixture, then through sodium hydroxide solution pH 14 to destroy any unreacted chlorine.

Chlorine gas was gently bubbled through a chloroform (20 mL) solution containing Au^I(PPh$_3$)Cl **3.12** (0.15 g 0.30 mmol) while the solution was stirring. The solution turned from colourless to bright yellow within few seconds. The solvent was removed under reduced pressure and the resulting solid was washed with hexane, diethyl ether and dried under high vacuum to give Au^{III}(PPh$_3$)Cl$_3$ **3.13** as a yellow solid (0.14 g, 82%). The product was stored in the freezer and covered with aluminium foil. ^{1}H NMR (400 MHz, CDCl$_3$) δ 7.66-7.75 (m, 9H), 7.54-7.60 (m, 6H); ^{31}P NMR (121 MHz, CDCl$_3$) δ 43.59 ppm.

This is consistent with data reported in the literature.[249]

6.2.14 Synthesis of [AuCl]@PPh₂-PEGPIIL (3.14).
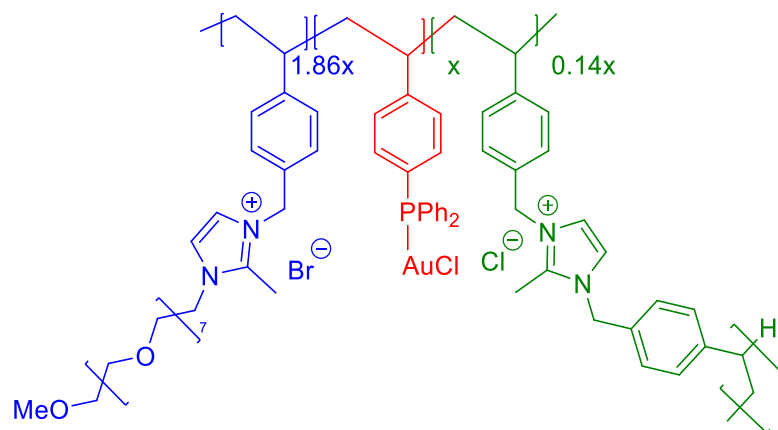
According to an adapted literature procedure,[83] an oven dried Schlenk flask under N_2 was charged with PPh₂-PEGPIIL **3.8** (2.00 g, 1.33 mmol), Au^I(THT)Cl **3.11** (0.42 g, 1.33 mmol), water (35 mL) and dichloromethane (10 mL). The reaction mixture was stirred overnight at room temperature. The solvent was removed under reduced pressure and the resulting residue was dissolved in dichloromethane (10 mL /g polymer), added dropwise to a large volume of diethyl ether (400 mL) and stirred for 60 min. After this time, the product was allowed to settle and filtered through a frit, washed with water (2 x 10 mL), ethanol (2 x 10 mL), and diethyl ether (2 x 30 mL) to give [AuCl]@PPh₂-PEGPIIL **3.14** as a white powder (2.00 g, 95%). ^{31}P NMR (202 MHz, CDCl₃) δ 33.47; FT-IR (neat, cm^{-1}): υ = 3353, 2871, 1585, 1514, 1436, 1349, 1184, 1099, 945, 847, 751, 695, 667, 610, 540, 509. ICP-OES data: 8.94 wt% gold corresponding to a gold loading of 0.45 mmol g^{-1}.

6.2.15 Attempted synthesis of [AuCl$_4$]@PPh$_2$-PEGPIIL (3.15).
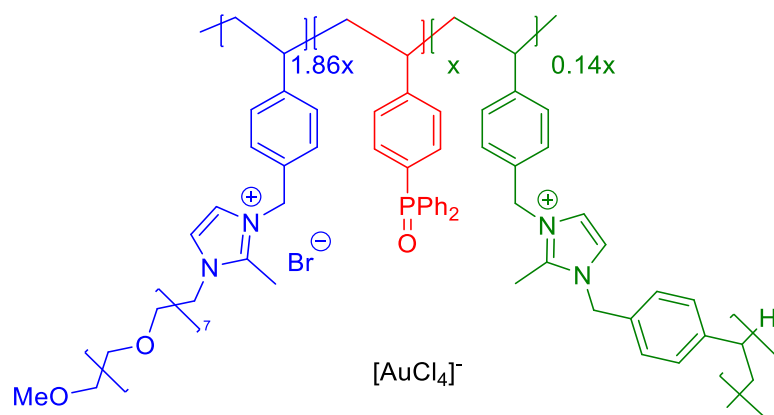
According to an adapted literature procedure,[249] chlorine gas was gently bubbled through chloroform (50 mL) solution containing [AuCl]@PPh$_2$-PEGPIIL **3.14** (0.10 g 0.06 mmol) while the solution was stirring. The solution turned from colourless to bright yellow within a few seconds. The solvent was removed under reduced pressure and the resulting solid was washed with hexane, diethyl ether and dried under high vacuum to give [AuCl$_4$]@PPh$_2$-PEGPIIL **3.15** as a yellow solid (0.09 g, 90%). ^{31}P NMR (283 MHz, CDCl$_3$) indicated a mixture of the Au^{III} δ 43.59 and P=O δ 28.95. The product mixture was stored in the freezer and covered with aluminium foil. The next day, ^{31}P NMR showed that further decomposition to phosphine oxide had occurred.

6.2.16 Synthesis of O=PPh₂-PEGPIIL (3.16).

According to an adapted literature procedure,[120] an oven dried Schlenk flask was charged with PPh₂-PEGPIIL **3.8** (1.50 g, 1.00 mmol), dichloromethane (50 mL) and H_2O_2 (35% w/w, 1.70 mL, 15.0 mmol), dissolved in water (2 mL) and stirred vigorously overnight at room temperature. The organic layer was separated, dried over $MgSO_4$, filtered and the solvent was removed under reduced pressure to afford O=PPh₂-PEGPIIL **3.16** as a white powder (1.40 g, 90%). ^{31}P NMR (162 MHz, CDCl₃) δ 29.26; FT-IR (neat, cm^{-1}): $\check{\upsilon}$ = 3340, 2921, 2861, 1911, 1585, 1529, 1511, 1436, 1420, 1400, 1355, 1300, 1257, 1185, 1113, 1093, 1027, 1001, 946, 820, 756, 722, 703. 673, 531.

6.2.17 Synthesis of [AuCl₄]@O=PPh₂-PEGPIIL (3.17).

According to an adapted literature procedure,[83] an oven dried Schlenk flask under N_2 was charged with O=PPh₂-PEGPIIL **3.16** (1.18 g, 0.78 mmol), KAuCl₄ (0.29 g, 0.78 mmol) and water (25 mL). The reaction mixture was stirred overnight at room temperature. The solvent was removed under reduced pressure and the resulting residue was dissolved in dichloromethane (10 mL /g polymer), added dropwise to a large volume of diethyl ether (350 mL), and stirred for 60 min. After this time, the mixture was allowed to settle and the product was filtered through a frit, washed with water (2 x 10 mL), ethanol (2 x 10 mL) and diethyl ether (2 x 30 mL) to give [AuCl₄]@O=PPh₂-PEGPIIL **3.17** as an orange powder (1.10 g, 92%); ^{31}P NMR (202 MHz, CDCl₃) δ 29.45; FT-IR (neat, cm^{-1}): ṽ = 3346, 3130, 2871, 1642, 1586, 1514, 1436, 1349, 1250, 1174, 1116, 941, 824, 752, 722, 703, 605, 538. ICP-OES data: 8.15 wt% gold corresponding to a gold loading of 0.41 mmol g^{-1}.

6.2.18 ICP gold sample preparation

The amount of gold sample needed for approximately 80 ppm Au in 100 mL (assumed 100% loading) was calculated, accurately weighed out, and added to a test tube. Aqua regia (2 mL) and a stirrer bar were added to the test tube. Layers of parafilm were used to cover the top of the test tube before being heated at 90 °C and stirred for two days. The test tube contents were then transferred to a 100 mL volumetric flask made up to 100 mL with distilled water. A standard solution of 100 ppm Au in 2% aqueous aqua regia was prepared. This stock solution was then used to prepare standards of 20, 40, 60 and 80 ppm Au by dilution. The samples were then filtered through a syringe filter (0.45 µm) and submitted for ICP-OES analysis in a screw-top vial.

6.2.19 General procedure for the selective reduction of nitrobenzene to *N*-phenyl hydroxylamine.[83]

An oven dried Schlenk flask under N_2 was charged with catalyst (0.05 mol% based on the gold content determined by ICP-OES) and $NaBH_4$ or $(CH_3)_2NH \cdot BH_3$ (2.5 mmol) and water (2.5 mL) was added immediately. The mixture was stirred for 5 min at room temperature. Then nitrobenzene (1 mmol) was added, and the mixture was stirred for the appropriate time at room temperature. After this time, the reaction was quenched by addition of water (5 mL), the product was extracted with ethyl acetate (20 mL) and the solvent was removed under reduced pressure. The resulting residue was analysed by ^{1}H NMR spectroscopy using 1,4-dioxane as the internal standard to measure the composition of the starting material and the product, determine the selectivity and conversion.

6.2.20 General procedure for the selective reduction of nitrobenzene to azoxybenzene.[83]

An oven dried Schlenk flask under N_2 was charged with catalyst (0.05 mol% based on the gold content determined by ICP-OES) and $NaBH_4$ or $(CH_3)_2NH \cdot BH_3$ (2.5 mmol) and ethanol (2 mL) was added immediately. The mixture was stirred for 5 min at room temperature. Then nitrobenzene (1 mmol) was added and the mixture was stirred for the appropriate time at room temperature. After this time, 1,4 dioxane (85 µL, 1 mmol) was added as the internal reference and a 0.05 mL of solution was taken and diluted with $CDCl_3$. The resulting solution was analysed by ^1H NMR spectroscopy to measure the composition of the starting material and the product, determine the selectivity and conversion.

6.2.21 General procedure for the selective reduction of nitrobenzene to aniline.[83]

An oven dried Schlenk flask under N_2 was charged with catalyst (0.05 mol% based on the gold content determined by ICP-OES) and $NaBH_4$ (5 mmol) and water (2 mL) was added immediately. The mixture was stirred for 5 min at 60 °C Then nitrobenzene (1 mmol) was added and the mixture was stirred for the appropriate time at 60 °C. After this time, 1,4 dioxane (85 µL, 1 mmol) was added as the internal reference and a 0.05 mL of solution was taken and diluted with $CDCl_3$. The resulting solution was analysed by ^1H NMR spectroscopy to measure the composition of the starting material and the product, determine the selectivity and conversion.

6.3   Chapter 4 experimental

6.3.1   Synthesis of 1-decyl-2-methyl-3-(4-vinylbenzyl)-1*H*-imidazol-3-ium bromide (4.1).
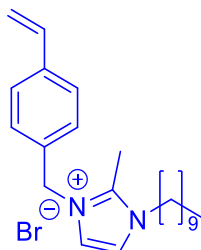
An oven dried Schlenk flask under N_2 was charged with 1-decyl-2-methylimidazole (1.00 g, 4.49 mmol) and 4-vinylbenzyl bromide **3.3** (1.15 g, 5.84 mmol) and dry dichloromethane (20 mL). The mixture was stirred overnight at 35 °C. The solvent was removed under reduced pressure and the resultant residue was triturated with diethyl ether (3 x 10 mL) and dried under high vacuum to afford the product 1-decyl-2-methyl-3-(4-vinylbenzyl)-1*H*-imidazol-3-ium bromide **4.1** as a fine white powder (1.43 g, 94%).^{1}H NMR (300 MHz, CDCl$_3$) δ 7.59 (d, *J* = 2.0 Hz, 1H), 7.44 – 7.30 (m, 5H), 6.68 (dd, *J* = 17.6, 10.9 Hz, 1H), 5.76 (d, *J* = 17.6 Hz, 1H), 5.59 (s, 2H), 5.30 (d, *J* = 11.5 Hz, 1H), 4.15 (t, *J* = 7.2 Hz, 2H), 2.80 (s, 3H), 1.81 (t, *J* = 7.6 Hz, 2H), 1.41 – 1.14 (m, 14H), 0.86 (t, *J* = 6.7 Hz, 3H) ; ^{13}C NMR (75 MHz, CDCl$_3$) δ 143.68, 138.32, 135.80, 132.35, 128.66, 127.03, 122.32, 121.21, 115.24, 52.18, 48.99, 31.81, 29.82, 29.42, 29.35, 29.21, 29.00, 26.36, 22.63, 14.09, 11.38; Mp: 88-90 °C; IR (neat, cm^{-1}): ʊ = 3086, 2923, 285.3, 1631, 1582, 1525, 1513, 1467, 1424, 1366, 1168, 992, 902, 830, 783, 767, 715, 671, 472. Found [M-Br]$^+$; 339.2791 C$_{23}$H$_{35}$N$_2$Br: requires [M-Br]$^+$; 339.2795.

6.3.2 Synthesis of PPh₂-*N*-decylPIIL (4.2).
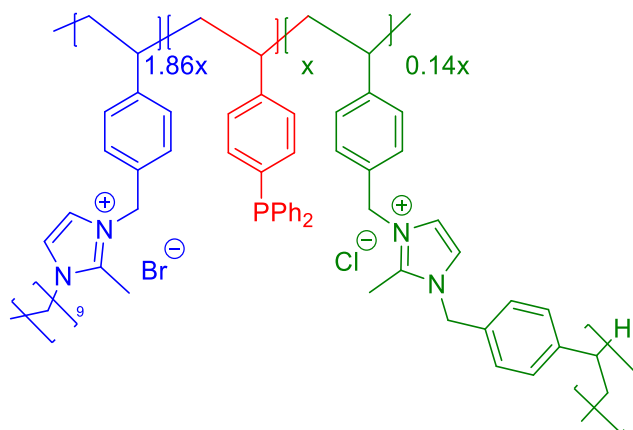
According to an adapted literature procedure,[120] an oven dried Schlenk flask under N_2 was charged with 1-decyl-2-methyl-3-(4-vinylbenzyl)-1*H*-imidazol-3-ium bromide **4.1** (5.00 g, 11.9 mmol), diphenyl(4-vinylphenyl) phosphine **3.5** (1.85 g, 6.42 mmol) , 2-methyl-1,3-bis(4-vinylbenzyl)-1*H*-imidazol-3-ium chloride **3.7** (0.31 g, 0.89 mmol), AIBN (0.05 g, 0.32 mmol, 5 mol%), dry ethanol (30 mL) and dry tetrahydrofuran (30 mL). The mixture was degassed using the freeze-pump-thaw method six times before being heated for four days at 80 °C. After this time, an additional equivalence of AIBN (0.05 g, 0.32 mmol, 5 mol%) was added and the degassing procedure was repeated six times, and then heated for 24 hours at 80 °C. The mixture was allowed to cool to room temperature and the solvent was removed under reduced pressure and the resulting residue was dissolved in dichloromethane (10 mL /g polymer) and added dropwise to diethyl ether (350 mL) with stirring. After 60 minutes of stirring, the product was allowed to settle, filtered, washed with diethyl ether, and dried under high vacuum to afford the product PPh₂-*N*-decylPIIL **4.2** as a white powder (6.50 g, 91%). ^{31}P NMR (121 MHz, CDCl₃) δ -6.61; FT-IR (neat, cm^{-1}): ʋ = 3413, 2923, 2853, 1581, 1513, 1527, 1465, 1455, 1433, 1425, 1358, 1262, 1184, 1091, 1018, 822, 773, 744, 721, 697, 669, 639, 610, 558, 504, 475, 461, 452, 438, 425, 411.

6.3.3   Synthesis of PdCl$_4$@PPh$_2$-PEGPIIL (4.3).
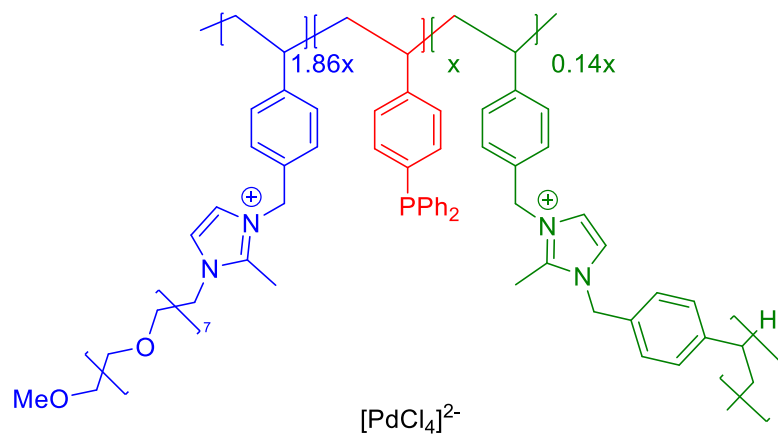
A round-bottomed flask was charged with PPh$_2$-PEGPIIL **3.8** (5.00 g, 3.33 mmol) and water (60 mL) and stirred vigorously while adding a solution of Na$_2$[PdCl$_4$] (0.98 g, 3.33 mmol) in water (5 mL). The resulting orange mixture was stirred overnight at room temperature. The solvent was removed under reduced pressure, the resulting residue was dissolved in a minimum amount of dichloromethane and added dropwise to a large amount of diethyl ether with stirring. After 60 minutes of stirring, the product was allowed to settle, filtered, washed with water (3 x 15 mL), ethanol (3 x 20 mL) and diethyl ether (3 x 20 mL) to afford PdCl$_4$@PPh$_2$-PEGPIIL **4.3** as a brown powder (2.42 g, 46.5%). ICP-OES data: 6.8 wt% palladium corresponding to a palladium loading of 0.63 mmol g^{-1}.

This is consistent with data reported in the literature.[120]

6.3.4 Synthesis of [PdCl$_4$]@PPh$_2$-*N*-decylPIIL (4.4).
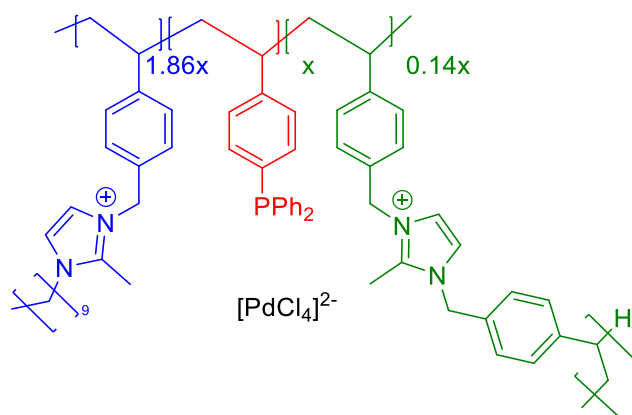
According to an adapted literature procedure,[120] a round-bottomed flask was charged with PPh$_2$-PPh$_2$-*N*-decylPIIL **4.2** (3.20 g, 2.85 mmol), water (45 mL) and stirred vigorously while adding a solution of Na$_2$[PdCl$_4$] (0.84 g, 2.85 mmol) in water (5 mL). The resulting red mixture was stirred overnight at room temperature. The solvent was removed under reduced pressure, the resulting residue was dissolved in a minimum amount of dichloromethane and added dropwise to a large amount of diethyl ether with stirring. After 60 minutes of stirring, the product was allowed to settle, filtered, washed with water (3 x 15 mL), ethanol (3 x 20 mL) and diethyl ether (3 x 20 mL) to afford [PdCl$_4$]@PPh$_2$-*N*-decylPIIL **4.4** as a brown powder yield (3.00 g, 89%). ICP-OES data: 7.6 wt% palladium corresponding to a palladium loading of 0.72 mmol g^{-1}.

6.3.5   Synthesis of PdNP@PPh$_2$-PEGPIIL (4.5).
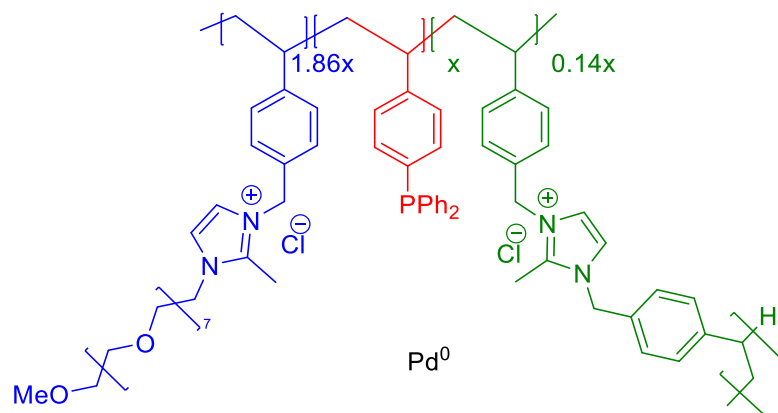
A round bottom flask was charged with PdCl$_4$@PPh$_2$-PEGPIIL **4.3** (2.22 g, 1.42 mmol) and ethanol (30 mL) and the resulting suspension was treated dropwise with a solution of NaBH$_4$ (0.43 g, 11.3 mmol) in water (3 mL). The solution immediately turned from orange to black. After stirring overnight at room temperature, the solvent was removed under reduced pressure and the resulting solid was triturated with acetone (20 mL), then transferred to a sintered glass frit and washed with water (2 x 20 mL), ethanol (3 x 20 mL) and diethyl ether (3 x 20 mL) and dried under high vacuum to afford PdNP@PPh$_2$-PEGPIIL **4.5** as a black solid (0.69 g, 48%). ICP-OES data: 5.4 wt% palladium and a palladium loading of 0.51 mmol g^{-1}.

This is consistent with data reported in the literature.[120]

6.3.6 Synthesis of PdNP@PPh₂-*N*-decylPIIL (4.6).
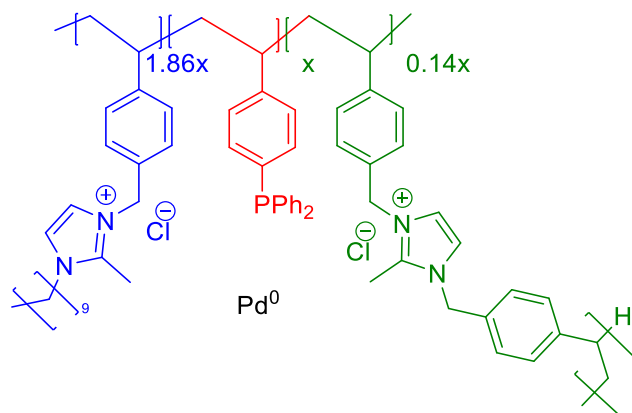
According to an adapted literature procedure,[120] a round bottom flask was charged with PdCl$_4$@ PPh$_2$-*N*-decylPIIL **4.4** (2.50 g, 2.11 mmol), ethanol (50 mL) and the resulting suspension was treated dropwise with a solution of NaBH$_4$ (0.63 g, 16.5 mmol) in water (4 mL). The solution immediately turned from orange to black. After stirring overnight at room temperature, the solvent was removed under reduced pressure and the resulting solid was triturated with acetone (20 mL), then transferred to a sintered glass frit and washed with water (3 x 20 mL), ethanol (3 x 20 mL) and diethyl ether (3 x 20 mL) and dried under high vacuum to afford PdNP@PPh$_2$-*N*-decylPIIL **4.6** as a dark grey solid (1.68 g, 72%). ICP-OES data: 11 wt% palladium and a palladium loading of 1.06 mmol g^{-1}.

6.3.7   ICP palladium sample preparation

The amount of palladium sample needed for approximately 80 ppm Pd in 100 mL (assumed 100% loading) was calculated, accurately weighed out, and added to a quartz vial. The quartz vial was secured in metal tongs and held over a Bunsen flame for approximately 10 minutes until the sample turned to ash. The quartz vial was cooled to room temperature and transferred to a boiling tube. To the quartz vial, conc. HCl (2 mL) was added together with a stirring bar. Layers of parafilm were used to cover the top of the test tube before being heated to 90 ^{0}C and stirred for two days. The boiling tube mixture was then transferred to a 100 mL volumetric flask, washing with distilled water and made up to 100 mL with distilled water. A standard solution of 100 ppm Pd in 2% HCl was prepared. This stock solution was then used to prepare standards of 20, 40, 60 and 80 ppm Pd by dilution. The samples were then filtered through a syringe filter (0.45 µm) and submitted for ICP-OES analysis in a screw-top vial.

6.3.8 General procedure for the selective reduction of quinoline to 1,2,3,4-tetrahydroquinolines.

An oven dried Schlenk flask under N_2 was charged with catalyst (0.5 mol%) based on the palladium content determined by ICP-OES and $NaBH_4$ (2.5 mmol) or $(CH_3)_2NH\cdot BH_3$ (2.5 mmol) and water (3 mL) was added immediately. The mixture was stirred for 5 min at 40 °C. Then, quinoline (1 mmol) was added and the mixture was stirred for the appropriate time at 40 °C. The reaction was quenched by addition of water (10 mL), the product was extracted with ethyl acetate (20 mL) and the solvent was removed under reduced pressure. The resulting product mixture was analysed by ^{1}H NMR spectroscopy using 1,3-dinitrobenzene (1 mmol) as the internal standard to measure the composition of the starting material and the product, determine the selectivity and conversion.

6.4   Chapter 5 experimental

6.4.1   Synthesis of PtCl₄@PPh₂-PEGPIIL (5.1).
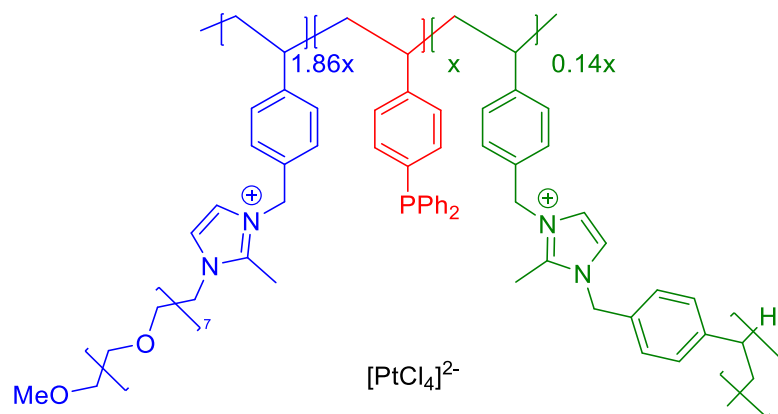
According to an adapted literature procedure,[120] a round-bottomed flask was charged with PPh₂-PEGPIIL **3.8** (3.04 g, 2.02 mmol), water (45 mL) and stirred vigorously while adding a solution of K₂[PtCl₄] (0.84 g, 2.02 mmol) in water (5 mL). The resulting orange mixture was stirred overnight at room temperature. The solvent was removed under reduced pressure and the resulting residue was dissolved in a minimum amount of dichloromethane and added dropwise to a large amount of diethyl ether with stirring. After 60 minutes of stirring, the product was allowed to settle, filtered, washed with water (3 x 15 mL), ethanol (3 x 20 mL) and diethyl ether (3 x 20 mL) to afford PtCl₄@PPh₂-PEGPIIL **5.1** as a brown powder (2.80 g, 80%). ICP-OES data: 8.5 wt% platinum corresponding to a platinum loading of 0.43 mmol g⁻¹.

6.4.2 Synthesis of PtCl$_4$@PPh$_2$-*N*-decylPIIL (5.2).
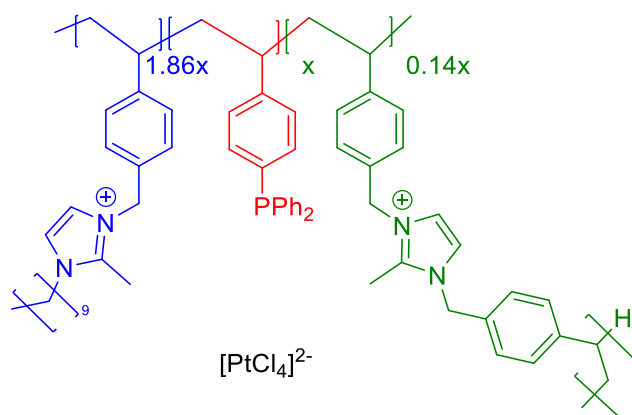
According to an adapted literature procedure,[120] a round-bottomed flask was charged with PPh$_2$-*N*-decylPIIL **4.2** (5.00 g, 4.48 mmol) and water (65 mL) and stirred vigorously while adding a solution of K$_2$[PtCl$_4$] (1.86 g, 4.48 mmol) in water (5 mL). The resulting red mixture was stirred overnight at room temperature. 50 mL of water was removed under reduced pressure and the resulting precipitate was collected by filtration through a frit and the resultant red solid was washed with water (3 x 20 mL), ethanol (3 x 20 mL) and diethyl ether (3 x 20 mL) to afford PtCl$_4$@PPh$_2$-*N*-decylPIIL **5.2** as a red powder (5.50 g, 92%). ICP-OES data: 13 wt% platinum corresponding to a platinum loading of 0.66 mmol g^{-1}.

6.4.3 Synthesis of PtNP@PPh₂-PEGPIIL (5.3).
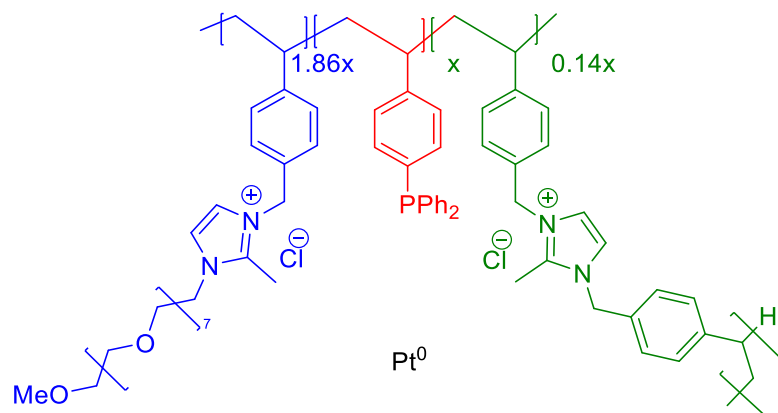
According to an adapted literature procedure,[120] a round bottom flask was charged with PtCl₄@PPh₂-PEGPIIL **5.1** (2.50 g, 1.45 mmol) and ethanol (50 mL) and the resulting suspension was treated dropwise with a solution of NaBH₄ (0.43 g, 11.6 mmol) in water (3 mL). The solution immediately turned from orange to black. After stirring overnight at room temperature, the solvent was removed under reduced pressure and the resulting solid was triturated with acetone (20 mL), then transferred to a sintered glass frit and washed with water (2 x 20 mL), ethanol (3 x 20 mL) and diethyl ether (3 x 20 mL) and dried under high vacuum to afford PtNP@PPh₂-PEGPIIL **5.3** as a black solid (1.80 g, 78%). ICP-OES data: 7.1 wt% palladium and a palladium loading of 0.36 mmol g^{-1}.

6.4.4 Synthesis of PtNP@PPh₂-*N*-decylPIIL (5.4).
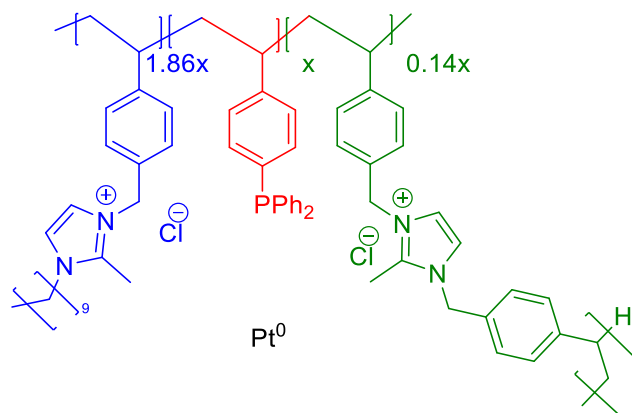
According to an adapted literature procedure,[120] a round bottom flask was charged with PtCl$_4$@ PPh$_2$-*N*-decylPIIL **5.2** (3.58 g, 2.67 mmol) and ethanol (60 mL) and the resulting suspension was treated dropwise with a solution of NaBH$_4$ (0.80 g, 21.3 mmol) in water (5 mL). The solution immediately turned from red to black. After stirring overnight at room temperature, the solvent was removed under vacuum and the resulting solid was triturated with acetone (20 mL), then transferred to a sintered glass frit and washed with water (3 x 20 mL), ethanol (3 x 20 mL) and diethyl ether (3 x 20 mL) and dried under high vacuum to afford PtNP@PPh$_2$-*N*-decylPIIL **5.4** as a dark grey solid (2.60 g, 81%). ICP-OES data: 15 wt% platinum and a platinum loading of 0.77 mmol g^{-1}.

6.4.5   ICP platinum sample preparation

The amount of platinum sample needed for approximately 80 ppm Pt in 100 mL (assumed 100% loading) was calculated and accurately weighed out. To a quartz vial, the Pt sample and sodium carbonate in a 1:2 weight ratio were added. The quartz vial was secured in metal tongs and held over a Bunsen flame for approximately 10 mins until the sample turned to ash. The quartz vial was cool to room temperature and transferred to a boiling tube. To the quartz vial, aqua regia (2 mL) was added together with a stirring bar. Layers of parafilm were used to cover the top of the test tube before being heated to 90 ^{0}C and stirred for two days. The boiling tube mixture was then transferred to a 100 mL volumetric flask, washing with distilled water and made up to 100 mL with distilled water. A standard solution of 100 ppm Pt in 2% aqueous aqua regia was prepared. This stock solution was then used to prepare standards of 20, 40, 60 and 80 ppm Pt by dilution. The samples were then filtered through a syringe filter (0.45 µm) and submitted for ICP-OES analysis in a screw-top vial.

6.4.6 Platinum Nanoparticle Catalysed Hydrolysis of Sodium Borohydride.[84]

Catalytic hydrolysis reactions were conducted in water at the appropriate temperature in a 50 mL round bottom flask. The flask was charged with a stir bar, an appropriate quantity of catalyst (0.32 mol%, 0.0050 g PtNP@PPh$_2$-PEGPIIL **5.3**; 0.32 mol% 0.0026 g PtNP@PPh$_2$-N-decylPIIL **5.4**) and NaBH$_4$ (0.02 g, 0.57 mmol) and fitted with a gas outlet which was connected to the top of an inverted water-filled burette. The reaction was initiated by adding water (2 mL), immediately sealing the system by replacing the gas outlet, opening the tap of the water filled burette and recording the time zero volume. Gas evolution began immediately, and the progress of the reaction was monitored by measuring the amount of gas generated by recording the volume of water displaced from the burette at regular time intervals (15 sec). The optimum turnover frequency for each catalyst was determined by conducting a series of experiments with catalyst loadings ranging from 0.08 – 0.32 mol% at 30 °C and measuring the hydrogen generated, as described above.

Kinetic studies were also conducted as described above using 0.32 mol%, 0.0050 g PtNP@PPh$_2$-PEGPIIL **5.3** and 0.69 mol%, 0.0050 g PtNP@PPh$_2$-N-decylPIIL **5.4** across a range of temperatures (21 °C, 25 °C, 30 °C, 35 °C and 40 °C) to determine the activation energy (E$_a$).

6.4.7 Determination of the Reaction Order for the PtNP Catalysed Hydrolysis of Sodium Borohydride.[84]

The rate law was investigated by conducting the catalytic hydrolysis reactions at 35 °C with a constant concentration of $NaBH_4$ (0.28 M, 0.02 g in water (2 mL)) across a range of catalyst concentrations from 0.08 mol% to 0.64 mol% for PtNP@PPh$_2$-PEGPIIL **5.3** and 0.34 mol% to 1.73 mol% for PtNP@PPh$_2$-*N*-decylPIIL **5.4**.

The influence of sodium borohydride concentration on the rate of hydrolysis was determined by conducting reactions at 25 °C in water (200 mL) with 26.5 µmole of catalyst PtNP@PPh$_2$-PEGPIIL **5.3** and PtNP@PPh$_2$-*N*-decylPIIL **5.4** and varying the quantity of $NaBH_4$ from 26.5 µmmol to 158 µmmol ($[NaBH_4]_0 = 0.13, 0.26, 0.39, 0.52, 0.65, 0.78$ mM), which corresponds to catalyst: $NaBH_4$ ratios between 1:1 and 1:6.

6.4.8 Catalyst Recycle Studies for the Hydrolysis of Sodium Borohydride.[84]

Recycle studies were conducted at 30 °C as described above using 2 mol%, 0.03 g PtNP@PPh$_2$-PEGPIIL **5.3** to catalyse the hydrolysis of NaBH$_4$ (0.02 g, 0.57 mmol in water (20 mL). After gas evolution had ceased, the flask was recharged with a fresh portion of NaBH$_4$ (0.02 g, 0.57 mmol). The gas evolution was monitored by recording the volume of water displaced from the burette at regular time intervals; this procedure was repeated five times.

6.4.9 Hot Filtration Tests.[84]

Hot filtration studies were conducted at 30 °C following the protocol described above using 0.32 mol%, 0.0050 g PtNP@PPh$_2$-PEGPIIL **5.3** to catalyse the hydrolysis of NaBH$_4$ (0.02 g, 0.57 mmol in water (2 mL)). The reaction was monitored by periodically measuring the amount of gas generated. After 8 min, when the reaction had reached about 50% conversion, the reaction mixture was quickly filtered through a 0.45 µm pore-size syringe filter. The gas generated was monitored for a further 30 min. In an alternative procedure, a catalytic hydrolysis of NaBH$_4$ (0.02 g, 0.57 mmol in water (20 mL)) using 0.32 mol%, 0.0050 g PtNP@PPh$_2$-PEGPIIL **5.3** was allowed to reach completion after which the reaction mixture was filtered through a 0.45 µm pore-size syringe filter, a further portion of NaBH$_4$ added (0.02 g, 0.57 mmol mmol) and the amount of gas evolved measured.

6.4.10 Catalyst Poisoning Study.[84]

A 50 mL round bottom flask was charged with a stir bar, an appropriate quantity of catalyst (2 mol%, 0.03 g PtNP@PPh$_2$-PEGPIIL **5.3**), water (20 mL) and NaBO$_2$ (0.07 g, 0.57 mmol) and the mixture stirred for the allocated time (t = 0 min, 20 min, 40 min, 60 min 18 h) to explore the effect of poisoning time on catalyst efficacy. The reaction was initiated by adding NaBH$_4$ (0.02 g, 0.57 mmol) and the progress of the reaction was monitored by periodically measuring the amount of gas generated, according to the procedure described above.

6.4.11 Tandem Reaction for the Hydrogenationof 1,1-Diphenylethene.[84]

Tandem reactions were conducted in a double Schlenk flask system connected by tubing. One flask was charged with a stir bar, NaBH$_4$ (0.04 g, 1.11 mmol) or NaBD$_4$ (0.04 g, 1.11 mol), PtNP@PPh$_2$-PEGPIIL **5.3** (0.0050 g, 0.32 mol%). The hydrolysis was initiated by adding deuterium oxide (2 mL) or water (2 mL) and the reaction flask was sealed with a stopper and isolated from the second flask. Meanwhile the second flask was charged with a stir bar, 1,1-diphenylethene (0.18 g, 1.00 mmol), Pd/C (0.0053 g, 10 wt%, 0.5 mol%) and methanol (2 mL) or deuterated methanol (2 mL). The hydrolysis was left for 30 mins after which time the second flask was evacuated briefly, and the connector opened. The hydrogenation mixture was stirred at 30 °C for 18 h, after which time the solvent was removed under vacuum and the resulting residue analysed by ^{13}C spectroscopy and GC-MS to determine the composition and the distribution of isotopologues.

References

(1) Schlögl, R. Heterogeneous Catalysis. *Angew. Chem. Int. Ed.* **2015**, *54* (11), 3465–3520. https://doi.org/10.1002/anie.201410738.

(2) Chorkendorff, I.; Niemantsverdriet, J. W. *Concepts of Modern Catalysis and Kinetics*; John Wiley & Sons, 2017.

(3) Anslyn, E. V.; Dougherty, D. A. *Modern Physical Organic Chemistry*; University Science Books, 2006.

(4) Bertini, I. *Inorganic and Bio-Inorganic Chemistry - Volume II*; EOLSS Publications, 2009.

(5) Vries, J. G. de; David Jackson, S. Homogeneous and Heterogeneous Catalysis in Industry. *Catal. Sci. Technol.* **2012**, *2* (10), 2009–2009. https://doi.org/10.1039/C2CY90039D.

(6) Astruc, D.; Lu, F.; Aranzaes, J. R. Nanoparticles as Recyclable Catalysts: The Frontier between Homogeneous and Heterogeneous Catalysis. *Angew. Chem. Int. Ed.* **2005**, *44* (48), 7852–7872. https://doi.org/10.1002/anie.200500766.

(7) Lei, Z.; Chen, B.; Koo, Y.-M.; MacFarlane, D. R. Introduction: Ionic Liquids. *Chem. Rev.* **2017**, *117* (10), 6633–6635. https://doi.org/10.1021/acs.chemrev.7b00246.

(8) Rogers, R. D.; Sheldon, R.; Doherty, S.; Muldoon, M.; Wasserscheid, P.; Claus, P.; Spivey, J. J. *Catalysis in Ionic Liquids: Catalysts Synthesis to Application*; Hardacre, C., Parvulescu, V. I., Eds.; Royal Society of Chemistry: Cambridge, 2014.

(9) Koel, M. *Ionic Liquids in Chemical Analysis*; CRC Press, 2008.

(10) Ma, Z.; Yu, J.; Dai, S. Preparation of Inorganic Materials Using Ionic Liquids. *Adv. Mater.* **2010**, *22* (2), 261–285. https://doi.org/10.1002/adma.200900603.

(11) Burguete, M. I.; Galindo, F.; García-Verdugo, E.; Karbass, N.; Luis, S. V. Polymer Supported Ionic Liquid Phases (SILPs) versus Ionic Liquids (ILs): How Much Do They Look Alike. *Chem. Commun.* **2007**, No. 29, 3086–3088. https://doi.org/10.1039/B704611A.

(12) Xiao, J.-C.; Twamley, B.; Shreeve, J. M. An Ionic Liquid-Coordinated Palladium Complex: A Highly Efficient and Recyclable Catalyst for the Heck Reaction. *Org. Lett.* **2004**, *6* (21), 3845–3847. https://doi.org/10.1021/ol048327i.

(13) Bargon, J.; Kuhn, L. T. *In Situ NMR Methods in Catalysis*; Springer, 2007.

(14) Olivier-Bourbigou, H.; Magna, L.; Morvan, D. Ionic Liquids and Catalysis: Recent Progress from Knowledge to Applications. *Appl. Catal. A: Gen.* **2010**, *373* (1), 1–56. https://doi.org/10.1016/j.apcata.2009.10.008.

(15)   Chen, H.; Chen, X.; Deng, J.; Zheng, J. Isotropic Ordering of Ions in Ionic Liquids on the Sub-Nanometer Scale. *Chem. Sci.* **2018**, *9* (6), 1464–1472. https://doi.org/10.1039/C7SC05184K.

(16)   Rogers, R. D.; Voth, G. A. Ionic Liquids. *Acc. Chem. Res.* **2007**, *40* (11), 1077–1078. https://doi.org/10.1021/ar700221n.

(17)   Mele, A.; Romanò, G.; Giannone, M.; Ragg, E.; Fronza, G.; Raos, G.; Marcon, V. The Local Structure of Ionic Liquids: Cation–Cation NOE Interactions and Internuclear Distances in Neat [BMIM][BF$_4$] and [BDMIM][BF$_4$]. *Angew. Chem. Int. Ed.* **2006**, *45* (7), 1123–1126. https://doi.org/10.1002/anie.200503745.

(18)   Wasserscheid, P.; Welton, T. *Ionic Liquids in Synthesis*; John Wiley & Sons, 2008.

(19)   Zhao, D.; Wu, M.; Kou, Y.; Min, E. Ionic Liquids: Applications in Catalysis. *Catal. Today* **2002**, *74* (1), 157–189. https://doi.org/10.1016/S0920-5861(01)00541-7.

(20)   Smiglak, M.; D. Holbrey, J.; T. Griffin, S.; Matthew Reichert, W.; P. Swatloski, R.; R. Katritzky, A.; Yang, H.; Zhang, D.; Kirichenko, K.; D. Rogers, R. Ionic Liquids *via* Reaction of the Zwitterionic 1,3-Dimethylimidazolium-2-Carboxylate with Protic Acids. Overcoming Synthetic Limitations and Establishing New Halide Free Protocols for the Formation of ILs. *Green Chem.* **2007**, *9* (1), 90–98. https://doi.org/10.1039/B610421E.

(21)   Wilkes, J. S.; Levisky, J. A.; Wilson, R. A.; Hussey, C. L. Dialkylimidazolium Chloroaluminate Melts: A New Class of Room-Temperature Ionic Liquids for Electrochemistry, Spectroscopy and Synthesis. *Inorg. Chem.* **1982**, *21* (3), 1263–1264. https://doi.org/10.1021/ic00133a078.

(22)   S. Wilkes, J.; J. Zaworotko, M. Air and Water Stable 1-Ethyl-3-Methylimidazolium Based Ionic Liquids. *J. Chem. Soc., Chem. Commun.* **1992**, *0* (13), 965–967. https://doi.org/10.1039/C39920000965.

(23)   Steinrück, H.-P.; Wasserscheid, P. Ionic Liquids in Catalysis. *Catal. Lett.* **2015**, *145* (1), 380–397. https://doi.org/10.1007/s10562-014-1435-x.

(24)   Camper, D.; Becker, C.; Koval, C.; Noble, R. Diffusion and Solubility Measurements in Room Temperature Ionic Liquids. *Ind. Eng. Chem. Res.* **2006**, *45* (1), 445–450. https://doi.org/10.1021/ie0506668.

(25)   Werner, S.; Haumann, M.; Wasserscheid, P. Ionic Liquids in Chemical Engineering. *Annu. Rev. Chem. Biomol. Eng.* **2010**, *1* (1), 203–230. https://doi.org/10.1146/annurev-chembioeng-073009-100915.

(26) Haumann, M.; Wasserscheid, P. CHAPTER 7:SILP and SCILL Catalysis. In *Catalysis in Ionic Liquids*; RSC Publishing: Cambridge, UK, 2014; pp 410–432. https://doi.org/10.1039/9781849737210-00410.

(27) Estager, J.; Holbrey, J. D.; Swadźba-Kwaśny, M. Halometallate Ionic Liquids – Revisited. *Chem. Soc. Rev.* **2014**, *43* (3), 847–886. https://doi.org/10.1039/C3CS60310E.

(28) Wang, Y.; Gong, X.; Wang, Z.; Dai, L. SO_3H-Functionalized Ionic Liquids as Efficient and Recyclable Catalysts for the Synthesis of Pentaerythritol Diacetals and Diketals. *J. Mol. Catal. A: Chem.* **2010**, *322* (1), 7–16. https://doi.org/10.1016/j.molcata.2010.01.011.

(29) Noel, M. A. M.; Trulove, P. C.; Osteryoung, R. A. Removal of Protons from Ambient-Temperature Chloroaluminate Ionic Liquids. *Anal. Chem.* **1991**, *63* (24), 2892–2895.

(30) Smith, G. P.; Dworkin, A. S.; Pagni, R. M.; Zingg, S. P. Quantitative Study of the Acidity of Hydrogen Chloride in a Molten Chloroaluminate System (Aluminum Chloride/1-Ethyl-3-Methyl-1*H*-Imidazolium Chloride) as a Function of HCl Pressure and Melt Composition (51.0-66.4 Mol% $AlCl_3$). *J. Am. Chem. Soc.* **1989**, *111* (14), 5075–5077. https://doi.org/10.1021/ja00196a009.

(31) Brausch, N.; Metlen, A.; Wasserscheid, P. New, Highly Acidic Ionic Liquid Systems and Their Application in the Carbonylation of Toluene. *Chem. Commun.* **2004**, No. 13, 1552–1553. https://doi.org/10.1039/B403464C.

(32) Earle, M. J.; Seddon, K. R.; Adams, C. J.; Roberts, G. Friedel–Crafts Reactions in Room Temperature Ionic Liquids. *Chem. Commun.* **1998**, No. 19, 2097–2098. https://doi.org/10.1039/A805599H.

(33) Joni, J.; Schmitt, D.; Schulz, P. S.; Lotz, T. J.; Wasserscheid, P. Detailed Kinetic Study of Cumene Isopropylation in a Liquid–Liquid Biphasic System Using Acidic Chloroaluminate Ionic Liquids. *J. Catal.* **2008**, *258* (2), 401–409. https://doi.org/10.1016/j.jcat.2008.06.018.

(34) Aschauer, S.; Schilder, L.; Korth, W.; Fritschi, S.; Jess, A. Liquid-Phase Isobutane/Butene-Alkylation Using Promoted Lewis-Acidic IL-Catalysts. *Catal. Lett.* **2011**, *141* (10), 1405. https://doi.org/10.1007/s10562-011-0675-2.

(35) Xiao, L.; Johnson, K. E.; Treble, R. G. Alkane Cracking, Alkene Polymerization, and Friedel–Crafts Alkylation in Liquids Containing the Acidic Anions HX_2^-, $XH(AlX_4)^-$, $XH(Al_2X_7)^-$, and $Al_2X_7^-$ (X = Chlorine, Bromine). *J. Mol. Catal. A Chem.* **2004**, *214* (1), 121–127. https://doi.org/10.1016/j.molcata.2003.12.030.

(36) Stenzel, O.; Brüll, R.; Wahner, U. M.; Sanderson, R. D.; Raubenheimer, H. G. Oligomerization of Olefins in a Chloroaluminate Ionic Liquid. *J. Mol. Catal. A: Chem.* **2003**, *192* (1), 217–222. https://doi.org/10.1016/S1381-1169(02)00450-8.

(37) Hallett, J. P.; Welton, T. Room-Temperature Ionic Liquids: Solvents for Synthesis and Catalysis. 2. *Chem. Rev.* **2011**, *111* (5), 3508–3576. https://doi.org/10.1021/cr1003248.

(38) Keith, A.; Kosik, S.; Tillekeratne, L.; Mason, M. Ion-Tagged Phosphines as Ligands for Suzuki Coupling of Aryl Halides in a Phosphonium Ionic Liquid. *Synlett* **2014**, *25* (07), 977–982. https://doi.org/10.1055/s-0033-1340846.

(39) Autenrieth, B.; Willig, F.; Pursley, D.; Naumann, S.; Buchmeiser, M. R. Ionically Tagged Ru–Alkylidenes for Metathesis Reactions under Biphasic Liquid–Liquid Conditions. *ChemCatChem* **2013**, *5* (10), 3033–3040. https://doi.org/10.1002/cctc.201300199.

(40) Scholten, J. D.; Leal, B. C.; Dupont, J. Transition Metal Nanoparticle Catalysis in Ionic Liquids. *ACS Catal.* **2012**, *2* (1), 184–200. https://doi.org/10.1021/cs200525e.

(41) Antonietti, M.; Kuang, D.; Smarsly, B.; Zhou, Y. Ionic Liquids for the Convenient Synthesis of Functional Nanoparticles and Other Inorganic Nanostructures. *Angew. Chem. Int.* **2004**, *43* (38), 4988–4992. https://doi.org/10.1002/anie.200460091.

(42) S. Campbell, P.; H.G. Prechtl, M.; C. Santini, C.; Haumesser, P.-H. Ruthenium Nanoparticles in Ionic Liquids – A Saga. *Curr. Org. Chem.* **2013**, *17* (4), 414–429.

(43) Ghandi, K. A Review of Ionic Liquids, Their Limits and Applications. *Curr. Opin. Green Sustain. Chem.* **2014**, *2014*. https://doi.org/10.4236/gsc.2014.41008.

(44) Zhang, L.; Zhu, Y.; Nie, Z.; Li, Z.; Ye, Y.; Li, L.; Hong, J.; Bi, Z.; Zhou, Y.; Hu, G. Co/MoC Nanoparticles Embedded in Carbon Nanoboxes as Robust Trifunctional Electrocatalysts for a Zn–Air Battery and Water Electrocatalysis. *ACS Nano* **2021**, *15* (8), 13399–13414. https://doi.org/10.1021/acsnano.1c03766.

(45) Xu, W.; He, W.; Du, Z.; Zhu, L.; Huang, K.; Lu, Y.; Luo, Y. Functional Nucleic Acid Nanomaterials: Development, Properties, and Applications. *Angew. Chem. Int. Ed.* **2021**, *60* (13), 6890–6918. https://doi.org/10.1002/anie.201909927.

(46) Mitchell, M. J.; Billingsley, M. M.; Haley, R. M.; Wechsler, M. E.; Peppas, N. A.; Langer, R. Engineering Precision Nanoparticles for Drug Delivery. *Nat. Rev. Drug Discov.* **2021**, *20* (2), 101–124. https://doi.org/10.1038/s41573-020-0090-8.

(47) Kakaei, K.; Rahnavardi, M. Synthesis of Nitrogen-Doped Reduced Graphene Oxide and Its Decoration with High Efficiency Palladium Nanoparticles for Direct Ethanol Fuel Cell. *Renew. Energy* **2021**, *163*, 1277–1286. https://doi.org/10.1016/j.renene.2020.09.043.

(48) Zahmakıran, M.; Özkar, S. Metal Nanoparticles in Liquid Phase Catalysis; from Recent Advances to Future Goals. *Nanoscale* **2011**, *3* (9), 3462–3481. https://doi.org/10.1039/C1NR10201J.

(49) Ostwald, W. Blocking of Ostwald Ripening Allowing Long-Term Stabilization. *Phys. Chem.* **1901**, *37*, 385.

(50) Cao, G. *Nanostructures & Nanomaterials: Synthesis, Properties & Applications*; Imperial College Press, 2004.

(51) Nalwa, H. S. *Nanostructured Materials and Nanotechnology: Concise Edition*; Elsevier, 2001.

(52) Sharma, S.; S. Pande, S.; Swaminathan, P. Top-down Synthesis of Zinc Oxide Based Inks for Inkjet Printing. *RSC Adv.* **2017**, *7* (63), 39411–39419. https://doi.org/10.1039/C7RA07150G.

(53) da Silva, F. P.; Fiorio, J. L.; Rossi, L. M. Tuning the Catalytic Activity and Selectivity of Pd Nanoparticles Using Ligand-Modified Supports and Surfaces. *ACS Omega* **2017**, *2* (9), 6014–6022. https://doi.org/10.1021/acsomega.7b00836.

(54) Schmid, K.; Riediker, M. Use of Nanoparticles in Swiss Industry: A Targeted Survey. *Environ. Sci. Technol.* **2008**, *42* (7), 2253–2260. https://doi.org/10.1021/es071818o.

(55) Lei, Y.; Chen, Z.; Lan, G.; Wang, R.; Zhou, X.-Y. Pd Nanoparticles Stabilized with Phosphine-Functionalized Porous Ionic Polymer for Efficient Catalytic Hydrogenation of Nitroarenes in Water. *New J. Chem.* **2020**, *44* (9), 3681–3689. https://doi.org/10.1039/C9NJ05734J.

(56) Chen, C. Designing Catalysts for Olefin Polymerization and Copolymerization: Beyond Electronic and Steric Tuning. *Nat. Rev. Chem.* **2018**, *2* (5), 6–14. https://doi.org/10.1038/s41570-018-0003-0.

(57) Wu, Q.; Qiu, L.; Zhang, L.; Liu, H.; Ma, R.; Xie, P.; Liu, R.; Hou, P.; Ding, F.; Liu, C.; He, M. Temperature-Dependent Selective Nucleation of Single-Walled Carbon Nanotubes from Stabilized Catalyst Nanoparticles. *Chem. Eng. J.* **2022**, *431*, 133487. https://doi.org/10.1016/j.cej.2021.133487.

(58) R. Thawarkar, S.; Thombare, B.; S. Munde, B.; D. Khupse, N. Kinetic Investigation for the Catalytic Reduction of Nitrophenol Using Ionic Liquid Stabilized Gold Nanoparticles. *RSC Adv.* **2018**, *8* (67), 38384–38390. https://doi.org/10.1039/C8RA07404F.

(59) Wang, Y.; A. Weinstock, I. Polyoxometalate-Decorated Nanoparticles. *Chem. Soc. Rev.* **2012**, *41* (22), 7479–7496. https://doi.org/10.1039/C2CS35126A.

(60) Li, G.; Zhao, S.; Zhang, Y.; Tang, Z. Metal–Organic Frameworks Encapsulating Active Nanoparticles as Emerging Composites for Catalysis: Recent Progress and Perspectives. *Adv. Mater.* **2018**, *30* (51), 1800702. https://doi.org/10.1002/adma.201800702.

(61) Lyklema, J.; van Leeuwen, H. P.; Minor, M. DLVO-Theory, a Dynamic Re-Interpretation. *Adv. Colloid Interface Sci.* **1999**, *83* (1), 33–69. https://doi.org/10.1016/S0001-8686(99)00011-1.

(62) Ding, S.; Guo, Y.; Hülsey, M. J.; Zhang, B.; Asakura, H.; Liu, L.; Han, Y.; Gao, M.; Hasegawa, J.; Qiao, B.; Zhang, T.; Yan, N. Electrostatic Stabilization of Single-Atom Catalysts by Ionic Liquids. *Chem.* **2019**, *5* (12), 3207–3219. https://doi.org/10.1016/j.chempr.2019.10.007.

(63) Yan, N.; Xiao, C.; Kou, Y. Transition Metal Nanoparticle Catalysis in Green Solvents. *Coord. Chem. Rev.* **2010**, *254* (9), 1179–1218. https://doi.org/10.1016/j.ccr.2010.02.015.

(64) Dupont, J.; Scholten, J. D. On the Structural and Surface Properties of Transition-Metal Nanoparticles in Ionic Liquids. *Chem. Soc. Rev.* **2010**, *39* (5), 1780–1804. https://doi.org/10.1039/B822551F.

(65) Kim, K.-S.; Demberelnyamba, D.; Lee, H. Size-Selective Synthesis of Gold and Platinum Nanoparticles Using Novel Thiol-Functionalized Ionic Liquids. *Langmuir* **2004**, *20* (3), 556–560. https://doi.org/10.1021/la0355848.

(66) Verma, C.; Ebenso, E. E.; Quraishi, M. A. Transition Metal Nanoparticles in Ionic Liquids: Synthesis and Stabilization. *J. Mol. Liq.* **2019**, *276*, 826–849. https://doi.org/10.1016/j.molliq.2018.12.063.

(67) Tatumi, R.; Fujihara, H. Remarkably Stable Gold Nanoparticles Functionalized with a Zwitterionic Liquid Based on Imidazolium Sulfonate in a High Concentration of Aqueous Electrolyte and Ionic Liquid. *Chem. Commun.* **2005**, *0* (1), 83–85. https://doi.org/10.1039/B413385D.

(68) Napper, D. H. Steric Stabilization. *J. Colloid Interface Sci.* **1977**, *58* (2), 390–407. https://doi.org/10.1016/0021-9797(77)90150-3.

(69) Zhulina, E. B.; Borisov, O. V.; Priamitsyn, V. A. Theory of Steric Stabilization of Colloid Dispersions by Grafted Polymers. *J. Colloid Interface Sci.* **1990**, *137* (2), 495–511. https://doi.org/10.1016/0021-9797(90)90423-L.

(70) Hooper, J. B.; Schweizer, K. S. Contact Aggregation, Bridging, and Steric Stabilization in Dense Polymer−Particle Mixtures. *Macromolecules* **2005**, *38* (21), 8858–8869. https://doi.org/10.1021/ma051318k.

(71) Kraynov, A.; Müller, T. E. *Concepts for the Stabilization of Metal Nanoparticles in Ionic Liquids*; IntechOpen, 2011. https://doi.org/10.5772/22111.

(72) Temirov, R.; Soubatch, S.; Luican, A.; Tautz, F. S. Free-Electron-like Dispersion in an Organic Monolayer Film on a Metal Substrate. *Nature* **2006**, *444* (7117), 350–353. https://doi.org/10.1038/nature05270.

(73) Henze, S. K. M.; Bauer, O.; Lee, T.-L.; Sokolowski, M.; Tautz, F. S. Vertical Bonding Distances of PTCDA on Au(111) and Ag(111): Relation to the Bonding Type. *Surf. Sci.* **2007**, *601* (6), 1566–1573. https://doi.org/10.1016/j.susc.2007.01.020.

(74) Wang, J.; Kondrat, S. A.; Wang, Y.; Brett, G. L.; Giles, C.; Bartley, J. K.; Lu, L.; Liu, Q.; Kiely, C. J.; Hutchings, G. J. Au–Pd Nanoparticles Dispersed on Composite Titania/Graphene Oxide-Supports as a Highly Active Oxidation Catalyst. *ACS Catal.* **2015**, *5* (6), 3575–3587. https://doi.org/10.1021/acscatal.5b00480.

(75) Sanders, C. A.; George, S. R.; Deeter, G. A.; Campbell, J. D.; Reck, B.; Cunningham, M. F. Amphiphilic Block-Random Copolymers: Self-Folding Behavior and Stabilizers in Emulsion Polymerization. *Macromolecules* **2019**, *52* (12), 4510–4519. https://doi.org/10.1021/acs.macromol.9b00519.

(76) Wu, L.; Ge, Y.; Zhang, L.; Yu, D.; Wu, M.; Ni, H. Enhanced Electrical Conductivity and Competent Mechanical Properties of Polyaniline/Polyacrylate (PANI/PA) Composites for Antistatic Finishing Prepared at the Aid of Polymeric Stabilizer. *Prog. Org. Coat.* **2018**, *125*, 99–108. https://doi.org/10.1016/j.porgcoat.2018.09.002.

(77) Joo, S. H.; Zhao, D. Environmental Dynamics of Metal Oxide Nanoparticles in Heterogeneous Systems: A Review. *J. Hazard. Mater.* **2017**, *322*, 29–47. https://doi.org/10.1016/j.jhazmat.2016.02.068.

(78) Vollmer, C.; Janiak, C. Naked Metal Nanoparticles from Metal Carbonyls in Ionic Liquids: Easy Synthesis and Stabilization. *Coord. Chem. Rev.* **2011**, *255* (17), 2039–2057. https://doi.org/10.1016/j.ccr.2011.03.005.

(79) Fonseca, G. S.; Umpierre, A. P.; Fichtner, P. F. P.; Teixeira, S. R.; Dupont, J. The Use of Imidazolium Ionic Liquids for the Formation and Stabilization of Ir^0 and Rh^0 Nanoparticles: Efficient Catalysts for the Hydrogenation of Arenes. *Chem. Eur. J.* **2003**, *9* (14), 3263–3269. https://doi.org/10.1002/chem.200304753.

(80) Vijayakrishna, K.; Charan, K. T. P.; Manojkumar, K.; Venkatesh, S.; Pothanagandhi, N.; Sivaramakrishna, A.; Mayuri, P.; Kumar, A. S.; Sreedhar, B. Ni Nanoparticles Stabilized by Poly(Ionic Liquids) as Chemoselective and Magnetically Recoverable Catalysts for Transfer Hydrogenation Reactions of Carbonyl Compounds. *ChemCatChem* **2016**, *8* (6), 1139–1145. https://doi.org/10.1002/cctc.201501313.

(81) Prabhu Charan, K. T.; Pothanagandhi, N.; Vijayakrishna, K.; Sivaramakrishna, A.; Mecerreyes, D.; Sreedhar, B. Poly(Ionic Liquids) as "Smart" Stabilizers for Metal Nanoparticles. *Eur. Polym. J.* **2014**, *60*, 114–122. https://doi.org/10.1016/j.eurpolymj.2014.09.004.

(82) Doherty, S.; Knight, J. G.; Backhouse, T.; Abood, E.; Al-shaikh, H.; Clemmet, A. R.; Ellison, J. R.; Bourne, R. A.; Chamberlain, T. W.; Stones, R.; Warren, N. J.; Fairlamb, I. J. S.; Lovelock, K. R. J. Heteroatom Donor-Decorated Polymer-Immobilized Ionic Liquid Stabilized Palladium Nanoparticles: Efficient Catalysts for Room-Temperature Suzuki-Miyaura Cross-Coupling in Aqueous Media. *Adv. Synth. Catal.* **2018**, *360* (19), 3716–3731. https://doi.org/10.1002/adsc.201800561.

(83) Doherty, S.; Knight, J. G.; Backhouse, T.; Summers, R. J.; Abood, E.; Simpson, W.; Paget, W.; Bourne, R. A.; Chamberlain, T. W.; Stones, R.; Lovelock, K. R. J.; Seymour, J. M.; Isaacs, M. A.; Hardacre, C.; Daly, H.; Rees, N. H. Highly Selective and Solvent-Dependent Reduction of Nitrobenzene to *N*-Phenylhydroxylamine, Azoxybenzene, and Aniline Catalyzed by Phosphino-Modified Polymer Immobilized Ionic Liquid-Stabilized AuNPs. *ACS Catal.* **2019**, *9* (6), 4777–4791. https://doi.org/10.1021/acscatal.9b00347.

(84) Doherty, S.; Knight, J. G.; Alharbi, H. Y.; Paterson, R.; Wills, C.; Dixon, C.; Šiller, L.; Chamberlain, T. W.; Griffiths, A.; Collins, S. M.; Wu, K.; Simmons, M. D.; Bourne, R. A.; Lovelock, K. R. J.; Seymour, J. Efficient Hydrolytic Hydrogen Evolution from Sodium Borohydride Catalyzed by Polymer Immobilized Ionic Liquid-Stabilized Platinum Nanoparticles. *ChemCatChem* **2022**, *14* (4), e202101752. https://doi.org/10.1002/cctc.202101752.

(85) Zhang, Q.; Zhang, S.; Deng, Y. Recent Advances in Ionic Liquid Catalysis. *Green Chem.* **2011**, *13* (10), 2619–2637. https://doi.org/10.1039/C1GC15334J.

(86) Mehnert, C. P. Supported Ionic Liquid Catalysis. *Chem. Eur. J.* **2005**, *11* (1), 50–56. https://doi.org/10.1002/chem.200400683.

(87) Doorslaer, C. V.; Wahlen, J.; Mertens, P.; Binnemans, K.; Vos, D. D. Immobilization of Molecular Catalysts in Supported Ionic Liquid Phases. *Dalton Trans.* **2010**, *39* (36), 8377–8390. https://doi.org/10.1039/C001285H.

(88) Corma, A.; García, H.; Leyva, A. An Imidazolium Ionic Liquid Having Covalently Attached an Oxime Carbapalladacycle Complex as Ionophilic Heterogeneous Catalysts for the Heck and Suzuki–Miyaura Cross-Coupling. *Tetrahedron* **2004**, *60* (38), 8553–8560. https://doi.org/10.1016/j.tet.2004.06.121.

(89) Rosli, N. A. H.; Loh, K. S.; Wong, W. Y.; Yunus, R. M.; Lee, T. K.; Ahmad, A.; Chong, S. T. Review of Chitosan-Based Polymers as Proton Exchange Membranes and Roles of Chitosan-Supported Ionic Liquids. *Int. J. Mol. Sci.* **2020**, *21* (2), 632. https://doi.org/10.3390/ijms21020632.

(90) Lozano, L. J.; Godínez, C.; de los Ríos, A. P.; Hernández-Fernández, F. J.; Sánchez-Segado, S.; Alguacil, F. J. Recent Advances in Supported Ionic Liquid Membrane Technology. *J. Membr. Sci.* **2011**, *376* (1), 1–14. https://doi.org/10.1016/j.memsci.2011.03.036.

(91) Ruta, M.; Yuranov, I.; Dyson, P. J.; Laurenczy, G.; Kiwi-Minsker, L. Structured Fiber Supports for Ionic Liquid-Phase Catalysis Used in Gas-Phase Continuous Hydrogenation. *J. Catal.* **2007**, *247* (2), 269–276. https://doi.org/10.1016/j.jcat.2007.02.012.

(92) Gu, Y.; Li, G. Ionic Liquids-Based Catalysis with Solids: State of the Art. *Adv. Synth. Catal.* **2009**, *351* (6), 817–847. https://doi.org/10.1002/adsc.200900043.

(93) Ziarani, G. M.; Rohani, S.; Ziarati, A.; Badiei, A. Applications of SBA-15 Supported Pd Metal Catalysts as Nanoreactors in C–C Coupling Reactions. *RSC Adv.* **2018**, *8* (71), 41048–41100. https://doi.org/10.1039/C8RA09038F.

(94) Sievers, C.; Jimenez, O.; Müller, T. E.; Steuernagel, S.; Lercher, J. A. Formation of Solvent Cages around Organometallic Complexes in Thin Films of Supported Ionic Liquid. *J. Am. Chem. Soc.* **2006**, *128* (43), 13990–13991. https://doi.org/10.1021/ja064204c.

(95) Castillo, M. R.; Fousse, L.; Fraile, J. M.; García, J. I.; Mayoral, J. A. Supported Ionic-Liquid Films (SILF) as Two-Dimensional Nanoreactors for Enantioselective Reactions: Surface-

Mediated Selectivity Modulation (SMSM). *Chem. Eur. J.* **2007**, *13* (1), 287–291. https://doi.org/10.1002/chem.200600557.

(96) Valkenberg, M. H.; deCastro, C.; Hölderich, W. F. Immobilisation of Ionic Liquids on Solid Supports. *Green Chem.* **2002**, *4* (2), 88–93. https://doi.org/10.1039/B107946H.

(97) Gruttadauria, M.; Riela, S.; Aprile, C.; Meo, P. L.; D'Anna, F.; Noto, R. Supported Ionic Liquids. New Recyclable Materials for the L-Proline-Catalyzed Aldol Reaction. *Adv. Synth. Catal.* **2006**, *348* (1–2), 82–92. https://doi.org/10.1002/adsc.200505227.

(98) Lou, L.-L.; Yu, K.; Ding, F.; Zhou, W.; Peng, X.; Liu, S. An Effective Approach for the Immobilization of Chiral Mn(III) Salen Complexes through a Supported Ionic Liquid Phase. *Tetrahedron Lett.* **2006**, *47* (37), 6513–6516. https://doi.org/10.1016/j.tetlet.2006.07.048.

(99) Rodríguez-Pérez, L.; Teuma, E.; Falqui, A.; Gómez, M.; Serp, P. Supported Ionic Liquid Phase Catalysis on Functionalized Carbon Nanotubes. *Chem. Commun.* **2008**, No. 35, 4201–4203. https://doi.org/10.1039/B804969F.

(100) Karimi, B.; Enders, D. New N-Heterocyclic Carbene Palladium Complex/Ionic Liquid Matrix Immobilized on Silica: Application as Recoverable Catalyst for the Heck Reaction. *Org. Lett.* **2006**, *8* (6), 1237–1240. https://doi.org/10.1021/ol060129z.

(101) Bridging the Gap in Catalysis *via* Multidisciplinary Approaches. *Dalton Trans.* **2010**, *39* (36), 8354–8354. https://doi.org/10.1039/C0DT90044C.

(102) Gu, Y.; Ogawa, C.; Kobayashi, J.; Mori, Y.; Kobayashi, S. A Heterogeneous Silica-Supported Scandium/Ionic Liquid Catalyst System for Organic Reactions in Water. *Angew. Chem. Int. Ed.* **2006**, *118* (43), 7375–7378. https://doi.org/10.1002/ange.200603070.

(103) Kernchen, U.; Etzold, B.; Korth, W.; Jess, A. Solid Catalyst with Ionic Liquid Layer (SCILL) – A New Concept to Improve Selectivity Illustrated by Hydrogenation of Cyclooctadiene. *Chem. Eng. Technol.* **2007**, *30* (8), 985–994. https://doi.org/10.1002/ceat.200700050.

(104) Zhao, J.; Yu, Y.; Xu, X.; Di, S.; Wang, B.; Xu, H.; Ni, J.; Guo, L.; Pan, Z.; Li, X. Stabilizing Au(III) in Supported-Ionic-Liquid-Phase (SILP) Catalyst Using $CuCl_2$ *via* a Redox Mechanism. *Appl. Catal. B: Environ.* **2017**, *206*, 175–183. https://doi.org/10.1016/j.apcatb.2017.01.026.

(105) Bauer, T.; Stepic, R.; Wolf, P.; Kollhoff, F.; Karawacka, W.; R. Wick, C.; Haumann, M.; Wasserscheid, P.; M. Smith, D.; Smith, A.-S.; Libuda, J. Dynamic Equilibria in Supported Ionic Liquid Phase (SILP) Catalysis: In Situ IR Spectroscopy Identifies $[Ru(CO)_xCl_y]_n$

Species in Water Gas Shift Catalysis. *Catal. Sci. Technol.* **2018**, *8* (1), 344–357. https://doi.org/10.1039/C7CY02199B.

(106) Avdibegović, D.; Regadío, M.; Binnemans, K. Recovery of Scandium(III) from Diluted Aqueous Solutions by a Supported Ionic Liquid Phase (SILP). *RSC Adv.* **2017**, *7* (78), 49664–49674. https://doi.org/10.1039/C7RA07957E.

(107) Riisager, A.; Fehrmann, R.; Haumann, M.; Wasserscheid, P. Catalytic SILP Materials. In *Regulated Systems for Multiphase Catalysis*; Leitner, W., Hölscher, M., Eds.; Topics in Organometallic Chemistry; Springer: Berlin, Heidelberg, 2008; pp 149–161. https://doi.org/10.1007/3418_042.

(108) Haumann, M. Continuous Catalytic Processes with Supported Ionic Liquid Phase (SILP) Materials. In *Commercial Applications of Ionic Liquids*; Shiflett, M. B., Ed.; Green Chemistry and Sustainable Technology; Springer International Publishing: Cham, 2020; pp 49–67. https://doi.org/10.1007/978-3-030-35245-5_3.

(109) Qian, W.; Texter, J.; Yan, F. Frontiers in Poly(Ionic Liquid)s: Syntheses and Applications. *Chem. Soc. Rev.* **2017**, *46* (4), 1124–1159. https://doi.org/10.1039/C6CS00620E.

(110) Corain, B.; Zecca, M.; Jerabek, K. Catalysis and Polymer Networks: The Role of Morphology and Molecular Accessibility. *J. mol. catal. A Chem.*; 2001; Vol. 177, pp 3–20.

(111) Venugopal, J.; Ramakrishna, S. Applications of Polymer Nanofibers in Biomedicine and Biotechnology. *Appl. Biochem. Biotechnol.* **2005**, *125* (3), 147–157. https://doi.org/10.1385/ABAB:125:3:147.

(112) Liu, S.; Zhou, L.; Wang, P.; Zhang, F.; Yu, S.; Shao, Z.; Yi, B. Ionic-Liquid-Based Proton Conducting Membranes for Anhydrous H_2/Cl_2 Fuel-Cell Applications. *ACS Appl. Mater. Interfaces* **2014**, *6* (5), 3195–3200. https://doi.org/10.1021/am404645c.

(113) Ajjan, F. N.; Ambrogi, M.; Tiruye, G. A.; Cordella, D.; Fernandes, A. M.; Grygiel, K.; Isik, M.; Patil, N.; Porcarelli, L.; Rocasalbas, G.; Vendramientto, G.; Zeglio, E.; Antonietti, M.; Detrembleur, C.; Inganäs, O.; Jérôme, C.; Marcilla, R.; Mecerreyes, D.; Moreno, M.; Taton, D.; Solin, N.; Yuan, J. Innovative Polyelectrolytes/Poly(Ionic Liquid)s for Energy and the Environment. *Polym. Int.* **2017**, *66* (8), 1119–1128. https://doi.org/10.1002/pi.5340.

(114) Omedes Pujol, M.; Coleman, D. J. L.; Allen, C. D.; Heidenreich, O.; Fulton, D. A. Determination of Key Structure–Activity Relationships in SiRNA Delivery with a Mixed Micelle System. *J. Control. Release* **2013**, *172* (3), 939–945. https://doi.org/10.1016/j.jconrel.2013.10.013.

(115) Manojkumar, K.; Sivaramakrishna, A.; Vijayakrishna, K. A Short Review on Stable Metal Nanoparticles Using Ionic Liquids, Supported Ionic Liquids, and Poly(Ionic Liquids). *J. Nanoparticle Res.* **2016**, *18* (4), 103. https://doi.org/10.1007/s11051-016-3409-y.

(116) Mahouche-Chergui, S.; Guerrouache, M.; Carbonnier, B.; Chehimi, M. M. Polymer-Immobilized Nanoparticles. *Colloids Surf. A Physicochem. Eng. Asp.* **2013**, *439*, 43–68. https://doi.org/10.1016/j.colsurfa.2013.04.013.

(117) Zhu, W.; Yu, Y.; Yang, H.; Hua, L.; Qiao, Y.; Zhao, X.; Hou, Z. Cooperative Effects in Catalytic Hydrogenation Regulated by Both the Cation and Anion of an Ionic Liquid. *Chem. Eur. J.* **2013**, *19* (6), 2059–2066. https://doi.org/10.1002/chem.201202707.

(118) Doherty, S.; Knight, J. G.; Ellison, J. R.; Weekes, D.; Harrington, R. W.; Hardacre, C.; Manyar, H. An Efficient Recyclable Peroxometalate-Based Polymer-Immobilised Ionic Liquid Phase (PIILP) Catalyst for Hydrogen Peroxide-Mediated Oxidation. *Green Chem.* **2012**, *14* (4), 925–929. https://doi.org/10.1039/C2GC16679H.

(119) Doherty, S.; Knight, J. G.; Backhouse, T.; Bradford, A.; Saunders, F.; Bourne, R. A.; Chamberlain, T. W.; Stones, R.; Clayton, A.; Lovelock, K. Highly Efficient Aqueous Phase Reduction of Nitroarenes Catalyzed by Phosphine-Decorated Polymer Immobilized Ionic Liquid Stabilized PdNPs. *Catal. Sci. Technol.* **2018**, *8* (5), 1454–1467. https://doi.org/10.1039/C7CY02557B.

(120) Doherty, S.; Knight, J. G.; Backhouse, T.; Abood, E.; Alshaikh, H.; Fairlamb, I. J. S.; Bourne, R. A.; Chamberlain, T. W.; Stones, R. Highly Efficient Aqueous Phase Chemoselective Hydrogenation of *α,β*-Unsaturated Aldehydes Catalysed by Phosphine-Decorated Polymer Immobilized IL-Stabilized PdNPs. *Green Chem.* **2017**, *19* (7), 1635–1641. https://doi.org/10.1039/C6GC03528K.

(121) Young, R. J.; Lovell, P. A. *Introduction to Polymers*; CRC Press, 2011.

(122) Urban, M. W. *Stimuli-Responsive Materials: From Molecules to Nature Mimicking Materials Design*; RSC, 2019.

(123) Veale, C. A.; Bernstein, P. R.; Bryant, C.; Ceccarelli, C.; Damewood, J. R. Jr.; Earley, R.; Feeney, S. W.; Gomes, B.; Kosmider, B. J. Nonpeptidic Inhibitors of Human Leukocyte Elastase. 5. Design, Synthesis, and x-Ray Crystallography of a Series of Orally Active 5-Aminopyrimidin-6-One-Containing Trifluoromethyl Ketones. *J. Med. Chem.* **1995**, *38* (1), 98–108. https://doi.org/10.1021/jm00001a015.

(124) Ortwine, D. F.; Malone, T. C.; Bigge, C. F.; Drummond, J. T.; Humblet, C.; Johnson, G.; Pinter, G. W. Generation of *N*-Methyl-D-Aspartate Agonist and Competitive Antagonist Pharmacophore Models. Design and Synthesis of Phosphonoalkyl-Substituted Tetrahydroisoquinolines as Novel Antagonists. *J. Med. Chem.* **1992**, *35* (8), 1345–1370. https://doi.org/10.1021/jm00086a004.

(125) Huang, W.-S.; Liu, S.; Zou, D.; Thomas, M.; Wang, Y.; Zhou, T.; Romero, J.; Kohlmann, A.; Li, F.; Qi, J.; Cai, L.; Dwight, T. A.; Xu, Y.; Xu, R.; Dodd, R.; Toms, A.; Parillon, L.; Lu, X.; Anjum, R.; Zhang, S.; Wang, F.; Keats, J.; Wardwell, S. D.; Ning, Y.; Xu, Q.; Moran, L. E.; Mohemmad, Q. K.; Jang, H. G.; Clackson, T.; Narasimhan, N. I.; Rivera, V. M.; Zhu, X.; Dalgarno, D.; Shakespeare, W. C. Discovery of Brigatinib (AP26113), a Phosphine Oxide-Containing, Potent, Orally Active Inhibitor of Anaplastic Lymphoma Kinase. *J. Med. Chem.* **2016**, *59* (10), 4948–4964. https://doi.org/10.1021/acs.jmedchem.6b00306.

(126) Dang, Q.; Liu, Y.; Cashion, D. K.; Kasibhatla, S. R.; Jiang, T.; Taplin, F.; Jacintho, J. D.; Li, H.; Sun, Z.; Fan, Y.; DaRe, J.; Tian, F.; Li, W.; Gibson, T.; Lemus, R.; van Poelje, P. D.; Potter, S. C.; Erion, M. D. Discovery of a Series of Phosphonic Acid-Containing Thiazoles and Orally Bioavailable Diamide Prodrugs That Lower Glucose in Diabetic Animals Through Inhibition of Fructose-1,6-Bisphosphatase. *J. Med. Chem.* **2011**, *54* (1), 153–165. https://doi.org/10.1021/jm101035x.

(127) Wydysh, E. A.; Medghalchi, S. M.; Vadlamudi, A.; Townsend, C. A. Design and Synthesis of Small Molecule Glycerol 3-Phosphate Acyltransferase Inhibitors. *J. Med. Chem.* **2009**, *52* (10), 3317–3327. https://doi.org/10.1021/jm900251a.

(128) Kamer, P. C. J.; Leeuwen, P. W. N. M. van. *Phosphorus(III)Ligands in Homogeneous Catalysis: Design and Synthesis*; John Wiley & Sons, 2012.

(129) Allcock, H. R.; Hofmann, M. A.; Ambler, C. M.; Morford, R. V. Phenylphosphonic Acid Functionalized Poly[Aryloxyphosphazenes]. *Macromolecules* **2002**, *35* (9), 3484–3489. https://doi.org/10.1021/ma0116295.

(130) Queffélec, C.; Petit, M.; Janvier, P.; Knight, D. A.; Bujoli, B. Surface Modification Using Phosphonic Acids and Esters. *Chem. Rev.* **2012**, *112* (7), 3777–3807. https://doi.org/10.1021/cr2004212.

(131) Troev, K. D. *Chemistry and Application of H-Phosphonates*; Elsevier, 2006.

(132) Chou, H.-H.; Cheng, C.-H. A Highly Efficient Universal Bipolar Host for Blue, Green, and Red Phosphorescent OLEDs. *Adv. Mater.* **2010**, *22* (22), 2468–2471. https://doi.org/10.1002/adma.201000061.

(133) Hsu, F.-M.; Chien, C.-H.; Shu, C.-F.; Lai, C.-H.; Hsieh, C.-C.; Wang, K.-W.; Chou, P.-T. A Bipolar Host Material Containing Triphenylamine and Diphenylphosphoryl-Substituted Fluorene Units for Highly Efficient Blue Electrophosphorescence. *Adv. Funct. Mater.* **2009**, *19* (17), 2834–2843. https://doi.org/10.1002/adfm.200900703.

(134) Gelman, D.; Jiang, L.; Buchwald, S. L. Copper-Catalyzed C−P Bond Construction *via* Direct Coupling of Secondary Phosphines and Phosphites with Aryl and Vinyl Halides. *Org. Lett.* **2003**, *5* (13), 2315–2318. https://doi.org/10.1021/ol0346640.

(135) Hirao, T.; Masunaga, T.; Ohshiro, Y.; Agawa, T. Stereoselective Synthesis of Vinylphosphonate. *Tetrahedron Lett.* **1980**, *21* (37), 3595–3598. https://doi.org/10.1016/0040-4039(80)80245-0.

(136) Hirao, T.; Masunaga, T.; Yamada, N.; Ohshiro, Y.; Agawa, T. Palladium-Catalyzed New Carbon-Phosphorus Bond Formation. *Bull. Chem. Soc. Jpn.* **1982**, *55* (3), 909–913. https://doi.org/10.1246/bcsj.55.909.

(137) Montchamp, J.-L.; Dumond, Y. R. Synthesis of Monosubstituted Phosphinic Acids: Palladium-Catalyzed Cross-Coupling Reactions of Anilinium Hypophosphite. *J. Am. Chem. Soc.* **2001**, *123* (3), 510–511. https://doi.org/10.1021/ja005721c.

(138) Peng, H.; Cai, R.; Xu, C.; Chen, H.; Shi, X. Nucleophile Promoted Gold Redox Catalysis with Diazonium Salts: C–Br, C–S and C–P Bond Formation through Catalytic Sandmeyer Coupling. *Chem. Sci. J.* **2016**, *7* (9), 6190–6196. https://doi.org/10.1039/C6SC01742H.

(139) Kalek, M.; Ziadi, A.; Stawinski, J. Microwave-Assisted Palladium-Catalyzed Cross-Coupling of Aryl and Vinyl Halides with H-Phosphonate Diesters. *Org. Lett.* **2008**, *10* (20), 4637–4640. https://doi.org/10.1021/ol801935r.

(140) Deal, E. L.; Petit, C.; Montchamp, J.-L. Palladium-Catalyzed Cross-Coupling of H-Phosphinate Esters with Chloroarenes. *Org. Lett.* **2011**, *13* (12), 3270–3273. https://doi.org/10.1021/ol201222n.

(141) Fu, W. C.; So, C. M.; Kwong, F. Y. Palladium-Catalyzed Phosphorylation of Aryl Mesylates and Tosylates. *Org. Lett.* **2015**, *17* (23), 5906–5909. https://doi.org/10.1021/acs.orglett.5b03104.

(142) Xu, K.; Yang, F.; Zhang, G.; Wu, Y. ChemInform Abstract: Palladacycle-Catalyzed Phosphonation of Aryl Halides in Neat Water. *Green Chem.* **2013**, *15*, 1055. https://doi.org/10.1039/c3gc00030c.

(143) Bloomfield, A. J.; Herzon, S. B. Room Temperature, Palladium-Mediated P–Arylation of Secondary Phosphine Oxides. *Org. Lett.* **2012**, *14* (17), 4370–4373. https://doi.org/10.1021/ol301831k.

(144) Ramírez-López, P.; Ros, A.; Estepa, B.; Fernández, R.; Fiser, B.; Gómez-Bengoa, E.; Lassaletta, J. M. A Dynamic Kinetic C–P Cross–Coupling for the Asymmetric Synthesis of Axially Chiral P,N Ligands. *ACS Catal.* **2016**, *6* (6), 3955–3964. https://doi.org/10.1021/acscatal.6b00784.

(145) Bonnaventure, I.; Charette, A. B. Probing the Importance of the Hemilabile Site of Bis(Phosphine) Monoxide Ligands in the Copper-Catalyzed Addition of Diethylzinc to *N*-Phosphinoylimines: Discovery of New Effective Chiral Ligands. *J. Org. Chem.* **2008**, *73* (16), 6330–6340. https://doi.org/10.1021/jo800969x.

(146) Zhuang, R.; Xu, J.; Cai, Z.; Tang, G.; Fang, M.; Zhao, Y. Copper-Catalyzed C−P Bond Construction *via* Direct Coupling of Phenylboronic Acids with H-Phosphonate Diesters. *Org. Lett.* **2011**, *13* (8), 2110–2113. https://doi.org/10.1021/ol200465z.

(147) Hu, G.; Chen, W.; Fu, T.; Peng, Z.; Qiao, H.; Gao, Y.; Zhao, Y. Nickel-Catalyzed C–P Cross-Coupling of Arylboronic Acids with P(O)H Compounds. *Org. Lett.* **2013**, *15* (20), 5362–5365. https://doi.org/10.1021/ol402672e.

(148) Chen, T.-H.; Mallikarjuna Reddy, D.; Lee, C.-F. A Palladium-Catalyzed Oxidative Cross-Coupling Reaction between Aryl Pinacol Boronates and H -Phosphonates in Ethanol. *RSC Adv.* **2017**, *7* (48), 30214–30220. https://doi.org/10.1039/C7RA04619G.

(149) Andaloussi, M.; Lindh, J.; Sävmarker, J.; J. R. Sjöberg, P.; Larhed, M. Microwave-Promoted Palladium(II)-Catalyzed C-P Bond Formation by Using Arylboronic Acids or Aryltrifluoroborates. *Chem. Eur. J.* **2009**, *15* (47), 13069–13074. https://doi.org/10.1002/chem.200901473.

(150) Fu, T.; Qiao, H.; Peng, Z.; Hu, G.; Wu, X.; Gao, Y.; Zhao, Y. Palladium-Catalyzed Air-Based Oxidative Coupling of Arylboronic Acids with H-Phosphine Oxides Leading to Aryl Phosphine Oxides. *Org. Biomol. Chem.* **2014**, *12* (18), 2895–2902. https://doi.org/10.1039/c3ob42470g.

(151) Luo, H.; Liu, H.; Chen, X.; Wang, K.; Luo, X.; Wang, K. Ar-P Bond Construction by the Pd-Catalyzed Oxidative Cross-Coupling of Arylsilanes with H-Phosphonates *via* C-Si Bond Cleavage. *Chem. Commun. (Camb)* **2017**, *53* (5), 956–958. https://doi.org/10.1039/c6cc08408g.

(152) Isshiki, R.; Muto, K.; Yamaguchi, J. Decarbonylative C–P Bond Formation Using Aromatic Esters and Organophosphorus Compounds. *Org. Lett.* **2018**, *20* (4), 1150–1153. https://doi.org/10.1021/acs.orglett.8b00080.

(153) Dong, J.; Liu, L.; Ji, X.; Shang, Q.; Liu, L.; Su, L.; Chen, B.; Kan, R.; Zhou, Y.; Yin, S.-F.; Han, L.-B. General Oxidative Aryl C–P Bond Formation through Palladium-Catalyzed Decarbonylative Coupling of Aroylhydrazides with P(O)H Compounds. *Org. Lett.* **2019**, *21* (9), 3198–3203. https://doi.org/10.1021/acs.orglett.9b00922.

(154) Liu, C.; Szostak, M. Decarbonylative Phosphorylation of Amides by Palladium and Nickel Catalysis: The Hirao Cross-Coupling of Amide Derivatives. *Angew. Chem. Int. Ed.* **2017**, *56* (41), 12718–12722. https://doi.org/10.1002/anie.201707102.

(155) Xu, J.; Zhang, P.; Gao, Y.; Chen, Y.; Tang, G.; Zhao, Y. Copper-Catalyzed P-Arylation *via* Direct Coupling of Diaryliodonium Salts with Phosphorus Nucleophiles at Room Temperature. *J. Org. Chem.* **2013**, *78* (16), 8176–8183. https://doi.org/10.1021/jo4012199.

(156) Feng, C.-G.; Ye, M.; Xiao, K.-J.; Li, S.; Yu, J.-Q. Pd(II)-Catalyzed Phosphorylation of Aryl C–H Bonds. *J. Am. Chem. Soc.* **2013**, *135* (25), 9322–9325. https://doi.org/10.1021/ja404526x.

(157) Hou, C.; Ren, Y.; Lang, R.; Hu, X.; Xia, C.; Li, F. Palladium-Catalyzed Direct Phosphonation of Azoles with Dialkyl Phosphites. *Chem.Comm.* **2012**.

(158) Khrizanforov, M.; Strekalova, S.; Khrizanforova, V.; Dobrynin, A.; Kholin, K.; Gryaznova, T.; Grinenko, V.; Gubaidullin, A.; Kadirov, M. K.; Budnikova, Y. Cobalt-Catalyzed Green Cross-Dehydrogenative C(Sp^2)-H/P-H Coupling Reactions. *Top. Catal.* **2018**, *61* (18), 1949–1956. https://doi.org/10.1007/s11244-018-1014-2.

(159) Shaikh, R. S.; Ghosh, I.; König, B. Direct C−H Phosphonylation of Electron-Rich Arenes and Heteroarenes by Visible-Light Photoredox Catalysis. *Chem. Eur. J.* **2017**, *23* (50), 12120–12124. https://doi.org/10.1002/chem.201701283.

(160) Hu, R.-B.; Wang, H.-L.; Zhang, H.-Y.; Zhang, H.; Ma, Y.-N.; Yang, S. P(O)R$_2$-Directed Pd-Catalyzed C–H Functionalization of Biaryl Derivatives to Synthesize Chiral Phosphorous

Ligands. *Beilstein J. Org. Chem.* **2014**, *10* (1), 2071–2076. https://doi.org/10.3762/bjoc.10.215.

(161) Wang, S.; Guo, R.; Wang, G.; Chen, S.-Y.; Yu, X.-Q. Copper-Catalyzed Phosphorylation of Sp$^{(2)}$ C-H Bonds. *Chem. Commun. (Camb)* **2014**, *50* (84), 12718–12721. https://doi.org/10.1039/c4cc06246a.

(162) Li, C.; Yano, T.; Ishida, N.; Murakami, M. Pyridine-Directed Palladium-Catalyzed Phosphonation of C(Sp^2)-H Bonds. *Angew. Chem.* **2013**, *125* (37), 9983–9986. https://doi.org/10.1002/ange.201305202.

(163) Zhang, Z.; Dixneuf, P. H.; Soulé, J.-F. Late Stage Modifications of P-Containing Ligands Using Transition-Metal-Catalysed C–H Bond Functionalisation. *Chem.Comm.* **2018**.

(164) Zhang, H.; Hu, R.-B.; Zhang, X.-Y.; Li, S.-X.; Yang, S.-D. Palladium-Catalyzed R$_2$(O)P Directed C(Sp^2)-H Acetoxylation. *Chem. Commun. (Camb)* **2014**, *50* (36), 4686–4689. https://doi.org/10.1039/c4cc01238k.

(165) Zhao, D.; Nimphius, C.; Lindale, M.; Glorius, F. Phosphoryl-Related Directing Groups in Rhodium(III) Catalysis: A General Strategy to Diverse P-Containing Frameworks. *Org. Lett.* **2013**, *15* (17), 4504–4507. https://doi.org/10.1021/ol402053n.

(166) Kuninobu, Y.; Yoshida, T.; Takai, K. Palladium-Catalyzed Synthesis of Dibenzophosphole Oxides *via* Intramolecular Dehydrogenative Cyclization. *J. Org. Chem.* **2011**, *76* (18), 7370–7376. https://doi.org/10.1021/jo201030j.

(167) Ma, Y.-N.; Zhang, H.-Y.; Yang, S.-D. Pd(II)-Catalyzed P(O)R^{1}R^2-Directed Asymmetric C–H Activation and Dynamic Kinetic Resolution for the Synthesis of Chiral Biaryl Phosphates. *Org. Lett.* **2015**, *17* (8), 2034–2037. https://doi.org/10.1021/acs.orglett.5b00844.

(168) Hu, R.-B.; Zhang, H.; Zhang, X.-Y.; Yang, S.-D. Palladium-Catalyzed P(O)R$_2$ Directed C-H Arylation to Synthesize Electron-Rich Polyaromatic Monophosphorus Ligands. *Chem. Commun. (Camb)* **2014**, *50* (17), 2193–2195. https://doi.org/10.1039/c3cc49050e.

(169) Zhang, H.-Y.; Yi, H.-M.; Wang, G.-W.; Yang, B.; Yang, S.-D. Pd(II)-Catalyzed C(Sp^2)–H Hydroxylation with R$_2$(O)P-Coordinating Group. *Org. Lett.* **2013**, *15* (24), 6186–6189. https://doi.org/10.1021/ol403028a.

(170) Luo, X.; Yuan, J.; Yue, C.-D.; Zhang, Z.-Y.; Chen, J.; Yu, G.-A.; Che, C.-M. Synthesis of Peri-Substituted (Naphthalen-1-Yl)Phosphine Ligands by Rhodium(I)-Catalyzed Phosphine-Directed C–H Arylation. *Org. Lett.* **2018**, *20* (7), 1810–1814. https://doi.org/10.1021/acs.orglett.8b00305.

(171) Li, S.-X.; Ma, Y.-N.; Yang, S.-D. P(O)R$_2$-Directed Enantioselective C–H Olefination toward Chiral Atropoisomeric Phosphine–Olefin Compounds. *Org. Lett.* **2017**, *19* (7), 1842–1845. https://doi.org/10.1021/acs.orglett.7b00608.

(172) Jj, Y.; Sl, B. A Catalytic Asymmetric Suzuki Coupling for the Synthesis of Axially Chiral Biaryl Compounds. *J. Am. Chem. Soc.* **2000**, *122* (48), 12051–12052.

(173) Kinzel, T.; Zhang, Y.; Buchwald, S. L. A New Palladium Precatalyst Allows for the Fast Suzuki−Miyaura Coupling Reactions of Unstable Polyfluorophenyl and 2-Heteroaryl Boronic Acids. *J. Am. Chem. Soc.* **2010**, *132* (40), 14073–14075. https://doi.org/10.1021/ja1073799.

(174) Tang, W.; Patel, N. D.; Xu, G.; Xu, X.; Savoie, J.; Ma, S.; Hao, M.-H.; Keshipeddy, S.; Capacci, A. G.; Wei, X.; Zhang, Y.; Gao, J. J.; Li, W.; Rodriguez, S.; Lu, B. Z.; Yee, N. K.; Senanayake, C. H. Efficient Chiral Monophosphorus Ligands for Asymmetric Suzuki–Miyaura Coupling Reactions. *Org. Lett.* **2012**, *14* (9), 2258–2261. https://doi.org/10.1021/ol300659d.

(175) Wu, W.; Wang, S.; Zhou, Y.; He, Y.; Zhuang, Y.; Li, L.; Wan, P.; Wang, L.; Zhou, Z.; Qiu, L. Highly Diastereoselective Synthesis of Atropisomeric Bridged P,*N*-Ligands and Their Applications in Asymmetric Suzuki–Miyaura Coupling Reaction. *Adv. Synth. Catal.* **2012**, *354* (13), 2395–2402. https://doi.org/10.1002/adsc.201200095.

(176) Yamamoto, T.; Akai, Y.; Nagata, Y.; Suginome, M. Highly Enantioselective Synthesis of Axially Chiral Biarylphosphonates: Asymmetric Suzuki–Miyaura Coupling Using High-Molecular-Weight, Helically Chiral Polyquinoxaline-Based Phosphines. *Angew. Chem. Int. Ed.* **2011**, *50* (38), 8844–8847. https://doi.org/10.1002/anie.201103792.

(177) Wang, S.; Li, J.; Miao, T.; Wu, W.; Li, Q.; Zhuang, Y.; Zhou, Z.; Qiu, L. Highly Efficient Synthesis of a Class of Novel Chiral-Bridged Atropisomeric Monophosphine Ligands *via* Simple Desymmetrization and Their Applications in Asymmetric Suzuki–Miyaura Coupling Reaction. *Org. Lett.* **2012**, *14* (8), 1966–1969. https://doi.org/10.1021/ol300721p.

(178) Zhou, Y.; Wang, S.; Wu, W.; Li, Q.; He, Y.; Zhuang, Y.; Li, L.; Pang, J.; Zhou, Z.; Qiu, L. Enantioselective Synthesis of Axially Chiral Multifunctionalized Biaryls *via* Asymmetric Suzuki–Miyaura Coupling. *Org. Lett.* **2013**, *15* (21), 5508–5511. https://doi.org/10.1021/ol402666p.

(179) Zhou, Y.; Zhang, X.; Liang, H.; Cao, Z.; Zhao, X.; He, Y.; Wang, S.; Pang, J.; Zhou, Z.; Ke, Z.; Qiu, L. Enantioselective Synthesis of Axially Chiral Biaryl Monophosphine Oxides *via*

Direct Asymmetric Suzuki Coupling and DFT Investigations of the Enantioselectivity. *ACS Catal.* **2014**, *4* (5), 1390–1397. https://doi.org/10.1021/cs500208n.

(180) Ma, Y.-N.; Yang, S.-D. Asymmetric Synthesis of Chiral Atropisomeric Bis-Aryl Organophosphorus from Menthyl H-Phosphinate. *Chem. Rec.* **2016**, *16* (2), 977–986. https://doi.org/10.1002/tcr.201500242.

(181) Xie, P.; Wang, J.; Fan, J.; Liu, Y.; Wo, X.; Loh, T.-P. The C–OH/P–H Dehydrative Cross-Coupling for the Construction of the P–C Bond under Metal-Free Conditions. *Green Chem.* **2017**, *19* (9), 2135–2139. https://doi.org/10.1039/C7GC00882A.

(182) Zeng, H.; Dou, Q.; Li, C.-J. Photoinduced Transition-Metal-Free Cross-Coupling of Aryl Halides with H-Phosphonates. *Org. Lett.* **2019**, *21* (5), 1301–1305. https://doi.org/10.1021/acs.orglett.8b04081.

(183) Yuan, J.; To, W.-P.; Zhang, Z.-Y.; Yue, C.-D.; Meng, S.; Chen, J.; Liu, Y.; Yu, G.-A.; Che, C.-M. Visible-Light-Promoted Transition-Metal-Free Phosphinylation of Heteroaryl Halides in the Presence of Potassium Tert-Butoxide. *Org. Lett.* **2018**, *20* (24), 7816–7820. https://doi.org/10.1021/acs.orglett.8b03265.

(184) Dhokale, R. A.; Mhaske, S. B. P-Arylation: Arynes to Aryl-Phosphonates, -Phosphinates, and -Phosphine Oxides. *Org. Lett.* **2013**, *15* (9), 2218–2221. https://doi.org/10.1021/ol400780f.

(185) Doherty, S.; Knight, J. G.; Ward, N. A. B.; Perry, D. O.; Bittner, D. M.; Probert, M. R.; Westcott, S. A. Palladium-Catalyzed Suzuki–Miyaura Cross-Couplings with 2-Diethylphosphonato-Substituted Aryl- and Naphthylboronate Esters as the Nucleophilic Partner: A Complementary Approach to the Synthesis of Biaryl Monophosphonates. *Organometallics* **2014**, *33* (19), 5209–5219. https://doi.org/10.1021/om500520z.

(186) Xu, F.; Duke, O. M.; Rojas, D.; Eichelberger, H. M.; Kim, R. S.; Clark, T. B.; Watson, D. A. Arylphosphonate-Directed Ortho C–H Borylation: Rapid Entry into Highly-Substituted Phosphoarenes. *J. Am. Chem. Soc.* **2020**, *142* (28), 11988–11992. https://doi.org/10.1021/jacs.0c04159.

(187) Wen, J.; Wang, D.; Qian, J.; Wang, D.; Zhu, C.; Zhao, Y.; Shi, Z. Rhodium-Catalyzed PIII-Directed Ortho-C−H Borylation of Arylphosphines. *Angew. Chem. Int. Ed.* **2019**, *58* (7), 2078–2082. https://doi.org/10.1002/anie.201813452.

(188) Qiu, X.; Wang, M.; Zhao, Y.; Shi, Z. Rhodium(I)-Catalyzed Tertiary Phosphine Directed C−H Arylation: Rapid Construction of Ligand Libraries. *Angew. Chem. Int. Ed.* **2017**, *56* (25), 7233–7237. https://doi.org/10.1002/anie.201703354.

(189) Crawford, K. M.; Ramseyer, T. R.; Daley, C. J. A.; Clark, T. B. Phosphine-Directed C-H Borylation Reactions: Facile and Selective Access to Ambiphilic Phosphine Boronate Esters. *Angew. Chem.* **2014**, *126* (29), 7719–7723. https://doi.org/10.1002/ange.201402868.

(190) Wright, S. E.; Richardson-Solorzano, S.; Stewart, T. N.; Miller, C. D.; Morris, K. C.; Daley, C. J. A.; Clark, T. B. Accessing Ambiphilic Phosphine Boronates through C−H Borylation by an Unforeseen Cationic Iridium Complex. *Angew. Chem.* **2019**, *131* (9), 2860–2864. https://doi.org/10.1002/ange.201812857.

(191) Ishiyama, T.; Takagi, J.; Ishida, K.; Miyaura, N.; Anastasi, N. R.; Hartwig, J. F. Mild Iridium-Catalyzed Borylation of Arenes. High Turnover Numbers, Room Temperature Reactions, and Isolation of a Potential Intermediate. *J. Am. Chem. Soc.* **2002**, *124* (3), 390–391. https://doi.org/10.1021/ja0173019.

(192) Ishiyama, T.; Takagi, J.; Hartwig, J. F.; Miyaura, N. A Stoichiometric Aromatic C-H Borylation Catalyzed by Iridium(I)/2,2′-Bipyridine Complexes at Room Temperature. *Angew. Chem. Int. Ed.* **2002**, *41* (16), 3056–3058. https://doi.org/10.1002/1521-3773(20020816)41:16<3056::AID-ANIE3056>3.0.CO;2-#.

(193) Cho, J.-Y.; Tse, M. K.; Holmes, D.; Maleczka, R. E.; Smith, M. R. Remarkably Selective Iridium Catalysts for the Elaboration of Aromatic C-H Bonds. *Science* **2002**, *295* (5553), 305–308. https://doi.org/10.1126/science.1067074.

(194) Maleczka, Robert E.; Shi, F.; Holmes, D.; Smith, M. R. C−H Activation/Borylation/Oxidation: A One-Pot Unified Route To Meta-Substituted Phenols Bearing Ortho-/Para-Directing Groups. *J. Am. Chem. Soc.* **2003**, *125* (26), 7792–7793. https://doi.org/10.1021/ja0349857.

(195) Holmes, D.; Chotana, G. A.; Maleczka, Robert E.; Smith, M. R. One-Pot Borylation/Amination Reactions: Syntheses of Arylamine Boronate Esters from Halogenated Arenes. *Org. Lett.* **2006**, *8* (7), 1407–1410. https://doi.org/10.1021/ol060205y.

(196) Tzschucke, C. C.; Murphy, J. M.; Hartwig, J. F. Arenes to Anilines and Aryl Ethers by Sequential Iridium-Catalyzed Borylation and Copper-Catalyzed Coupling. *Org. Lett.* **2007**, *9* (5), 761–764. https://doi.org/10.1021/ol062902w.

(197) Murphy, J. M.; Tzschucke, C. C.; Hartwig, J. F. One-Pot Synthesis of Arylboronic Acids and Aryl Trifluoroborates by Ir-Catalyzed Borylation of Arenes. *Org. Lett.* **2007**, *9* (5), 757–760. https://doi.org/10.1021/ol062903o.

(198) Joliton, A.; Carreira, E. M. Ir-Catalyzed Preparation of SF5-Substituted Potassium Aryl Trifluoroborates *via* C–H Borylation and Their Application in the Suzuki–Miyaura Reaction. *Org. Lett.* **2013**, *15* (20), 5147–5149. https://doi.org/10.1021/ol4025666.

(199) Liskey, C. W.; Liao, X.; Hartwig, J. F. Cyanation of Arenes *via* Iridium-Catalyzed Borylation. *J. Am. Chem. Soc.* **2010**, *132* (33), 11389–11391. https://doi.org/10.1021/ja104442v.

(200) Li, X.; Deng, X.; Coyne, A. G.; Srinivasan, R. Meta-Nitration of Arenes Bearing Ortho/Para Directing Group(s) Using C−H Borylation. *Chem. Eur. J.* **2019**, *25* (34), 8018–8023. https://doi.org/10.1002/chem.201901633.

(201) Murphy, J. M.; Liao, X.; Hartwig, J. F. Meta Halogenation of 1,3-Disubstituted Arenes *via* Iridium-Catalyzed Arene Borylation. *J. Am. Chem. Soc.* **2007**, *129* (50), 15434–15435. https://doi.org/10.1021/ja076498n.

(202) Robbins, D. W.; Hartwig, J. F. Sterically Controlled Alkylation of Arenes through Iridium-Catalyzed C-H Borylation. *Angew. Chem.* **2013**, *125* (3), 967–971. https://doi.org/10.1002/ange.201208203.

(203) Feng, Z.; Min, Q.-Q.; Fu, X.-P.; An, L.; Zhang, X. Chlorodifluoromethane-Triggered Formation of Difluoromethylated Arenes Catalysed by Palladium. *Nat. Chem.* **2017**, *9*, 918–923. https://doi.org/10.1038/nchem.2746.

(204) Litvinas, N. D.; Fier, P. S.; Hartwig, J. F. A General Strategy for the Perfluoroalkylation of Arenes and Arylbromides by Using Arylboronate Esters and [(Phen)CuRF]. *Angew. Chem., Int. Ed.* **2012**, *51* (2), 536–539. https://doi.org/10.1002/anie.201106668.

(205) Liu, T.; Shao, X.; Wu, Y.; Shen, Q. Highly Selective Trifluoromethylation of 1,3-Disubstituted Arenes through Iridium-Catalyzed Arene Borylation. *Angew. Chem.* **2012**, *124* (2), 555–558. https://doi.org/10.1002/ange.201106673.

(206) Chotana, G. A.; Montero Bastidas, J. R.; Miller, S. L.; Smith, M. R.; Maleczka, R. E. One-Pot Iridium Catalyzed C–H Borylation/Sonogashira Cross-Coupling: Access to Borylated Aryl Alkynes. *Mol.* **2020**, *25* (7), 1754. https://doi.org/10.3390/molecules25071754.

(207) Wang, J.; Torigoe, T.; Kuninobu, Y. Hydrogen-Bond-Controlled Formal Meta-Selective C–H Transformations and Regioselective Synthesis of Multisubstituted Aromatic Compounds. *Org. Lett.* **2019**, *21* (5), 1342–1346. https://doi.org/10.1021/acs.orglett.9b00030.

(208) Kuninobu, Y.; Ida, H.; Nishi, M.; Kanai, M. A Meta-Selective C–H Borylation Directed by a Secondary Interaction between Ligand and Substrate. *Nature Chem.* **2015**, *7* (9), 712–717. https://doi.org/10.1038/nchem.2322.

(209) Davis, H. J.; Mihai, M. T.; Phipps, R. J. Ion Pair-Directed Regiocontrol in Transition-Metal Catalysis: A Meta-Selective C–H Borylation of Aromatic Quaternary Ammonium Salts. *J. Am. Chem. Soc.* **2016**, *138* (39), 12759–12762. https://doi.org/10.1021/jacs.6b08164.

(210) Yang, L.; Uemura, N.; Nakao, Y. Meta-Selective C–H Borylation of Benzamides and Pyridines by an Iridium–Lewis Acid Bifunctional Catalyst. *J. Am. Chem. Soc.* **2019**, *141* (19), 7972–7979. https://doi.org/10.1021/jacs.9b03138.

(211) Bisht, R.; Chattopadhyay, B. Formal Ir-Catalyzed Ligand-Enabled Ortho and Meta Borylation of Aromatic Aldehydes *via* in Situ-Generated Imines. *J. Am. Chem. Soc.* **2016**, *138* (1), 84–87. https://doi.org/10.1021/jacs.5b11683.

(212) Gao, P.; Szostak, M. Highly Selective and Divergent Acyl and Aryl Cross-Couplings of Amides *via* Ir-Catalyzed C–H Borylation/N–C(O) Activation. *Org. Lett.* **2020**, *22* (15), 6010–6015. https://doi.org/10.1021/acs.orglett.0c02105.

(213) Mkhalid, I. A. I.; Barnard, J. H.; Marder, T. B.; Murphy, J. M.; Hartwig, J. F. C−H Activation for the Construction of C−B Bonds. *Chem. Rev.* **2010**, *110* (2), 890–931. https://doi.org/10.1021/cr900206p.

(214) Hartwig, J. F. Borylation and Silylation of C–H Bonds: A Platform for Diverse C–H Bond Functionalizations. *Acc. Chem. Res.* **2012**, *45* (6), 864–873. https://doi.org/10.1021/ar200206a.

(215) Preshlock, S. M.; Ghaffari, B.; Maligres, P. E.; Krska, S. W.; Maleczka, R. E.; Smith, M. R. High-Throughput Optimization of Ir-Catalyzed C–H Borylation: A Tutorial for Practical Applications. *J. Am. Chem. Soc.* **2013**, *135* (20), 7572–7582. https://doi.org/10.1021/ja400295v.

(216) Liskey, C. W.; Hartwig, J. F. Iridium-Catalyzed Borylation of Secondary C–H Bonds in Cyclic Ethers. *J. Am. Chem. Soc.* **2012**, *134* (30), 12422–12425. https://doi.org/10.1021/ja305596v.

(217) Larsen, M. A.; Hartwig, J. F. Iridium-Catalyzed C–H Borylation of Heteroarenes: Scope, Regioselectivity, Application to Late-Stage Functionalization, and Mechanism. *J. Am. Chem. Soc.* **2014**, *136* (11), 4287–4299. https://doi.org/10.1021/ja412563e.

(218) Liskey, C. W.; Hartwig, J. F. Iridium-Catalyzed C–H Borylation of Cyclopropanes. *J. Am. Chem. Soc.* **2013**, *135* (9), 3375–3378. https://doi.org/10.1021/ja400103p.

(219) Li, Q.; Liskey, C. W.; Hartwig, J. F. Regioselective Borylation of the C–H Bonds in Alkylamines and Alkyl Ethers. Observation and Origin of High Reactivity of Primary C–H Bonds Beta to Nitrogen and Oxygen. *J. Am. Chem. Soc.* **2014**, *136* (24), 8755–8765. https://doi.org/10.1021/ja503676d.

(220) Boller, T. M.; Murphy, J. M.; Hapke, M.; Ishiyama, T.; Miyaura, N.; Hartwig, J. F. Mechanism of the Mild Functionalization of Arenes by Diboron Reagents Catalyzed by Iridium Complexes. Intermediacy and Chemistry of Bipyridine-Ligated Iridium Trisboryl Complexes. *J. Am. Chem. Soc.* **2005**, *127* (41), 14263–14278. https://doi.org/10.1021/ja053433g.

(221) Doherty, S.; Knight, J. G.; Tran, T. S. T.; Alharbi, H. Y.; Perry, D. O. The Synthesis of Biarylmonophosphonates *via* Palladium-Catalyzed Phosphonation, Iridium-Catalyzed C-H Borylation, Palladium-Catalyzed Suzuki–Miyaura Cross-Coupling. *Catal. Lett.* **2022**, *152* (2), 398–413. https://doi.org/10.1007/s10562-021-03643-3.

(222) Sabbioni, G.; Richter, E. Aromatic Amines, Nitroarenes, and Heterocyclic Aromatic Amines. In *Toxicology*; Elsevier, 1999; pp 729–741.

(223) Rothenberg, G. *Catalysis: Concepts and Green Applications*; John Wiley & Sons, 2017.

(224) Saha, A.; Ranu, B. Highly Chemoselective Reduction of Aromatic Nitro Compounds by Copper Nanoparticles/Ammonium Formate. *J. Org. Chem.* **2008**, *73* (17), 6867–6870. https://doi.org/10.1021/jo800863m.

(225) Wisniak, J.; Klein, M. Reduction of Nitrobenzene to Aniline. *Ind. Eng. Chem. Prod. Res. Dev.* **1984**, *23* (1), 44–50. https://doi.org/10.1021/i300013a009.

(226) Haber, F. Gradual Electrolytic Reduction of Nitrobenzene with Limited Cathode Potential. *Elektrochem. Angew. Phys. Chem.* **1898**, *22*, 506–514.

(227) Turáková, M.; Salmi, T.; Eränen, K.; Wärnå, J.; Murzin, D. Yu.; Králik, M. Liquid Phase Hydrogenation of Nitrobenzene. *Appl. Catal. A: Gen.* **2015**, *499*, 66–76. https://doi.org/10.1016/j.apcata.2015.04.002.

(228) Marozsán, N.; Horváth, H.; Erdei, A.; Joó, F. Dehalogenation of Organic Halides in Aqueous Media by Hydrogen Transfer from Formate Catalyzed by Water-Soluble Ru(II)-*N*-Heterocyclic Carbene Complexes. *J. Mol. Catal. A: Chem.* **2016**, *425*, 103–109. https://doi.org/10.1016/j.molcata.2016.09.036.

(229) Sarmah, P. P.; Dutta, D. K. Stabilized Rh0-Nanoparticles-Montmorillonite Clay Composite: Synthesis and Catalytic Transfer Hydrogenation Reaction. *Appl. Catal. A: Gen.* **2014**, *470*, 355–360. https://doi.org/10.1016/j.apcata.2013.10.049.

(230) Tuteja, J.; Nishimura, S.; Ebitani, K. RSC Adv., 2014, 4, 38241-38249;(k) L. Yu, Q. Zhang, S. *RSC Adv.* **2015**, *8*, 3029–3035.

(231) Perret, N.; Wang, X.; Onfroy, T.; Calers, C.; Keane, M. A. Selectivity in the Gas-Phase Hydrogenation of 4-Nitrobenzaldehyde over Supported Au Catalysts. *J. Catal.* **2014**, *309*, 333–342. https://doi.org/10.1016/j.jcat.2013.10.011.

(232) Nasir Baig, R. B.; Varma, R. S. Magnetic Silica-Supported Ruthenium Nanoparticles: An Efficient Catalyst for Transfer Hydrogenation of Carbonyl Compounds. *ACS Sustainable Chem. Eng.* **2013**, *1* (7), 805–809. https://doi.org/10.1021/sc400032k.

(233) Gao, Y.; Jaenicke, S.; Chuah, G.-K. Highly Efficient Transfer Hydrogenation of Aldehydes and Ketones Using Potassium Formate over AlO(OH)-Entrapped Ruthenium Catalysts. *Appl. Catal. A: Gen.* **2014**, *484*, 51–58. https://doi.org/10.1016/j.apcata.2014.07.010.

(234) Lu, Y.-M.; Zhu, H.-Z.; Li, W.-G.; Hu, B.; Yu, S.-H. Size-Controllable Palladium Nanoparticles Immobilized on Carbon Nanospheres for Nitroaromatic Hydrogenation. *J. Mater. Chem. A.* **2013**, *1* (11), 3783–3788. https://doi.org/10.1039/C3TA00159H.

(235) Su, Y.; Li, X.; Wang, Y.; Zhong, H.; Wang, R. Gold Nanoparticles Supported by Imidazolium-Based Porous Organic Polymers for Nitroarene Reduction. *Dalton Trans.* **2016**, *45* (42), 16896–16903. https://doi.org/10.1039/C6DT03050E.

(236) Tyler, J. H.; Nazari, S. H.; Patterson, R. H.; Udumula, V.; Smith, S. J.; Michaelis, D. J. Synthesis of *N*-Aryl and *N*-Heteroaryl Hydroxylamines *via* Partial Reduction of Nitroarenes with Soluble Nanoparticle Catalysts. *Tetrahedron Lett.* **2017**, *58* (1), 82–86. https://doi.org/10.1016/j.tetlet.2016.11.105.

(237) Zhong, H.; Gong, Y.; Liu, W.; Zhang, B.; Hu, S.; Wang, R. Robust Ultrafine Ruthenium Nanoparticles Enabled by Covalent Organic Gel Precursor for Selective Reduction of Nitrobenzene in Water. *Dalton Trans.* **2019**, *48* (7), 2345–2351. https://doi.org/10.1039/C8DT04717K.

(238) Mandi, U.; Salam, N.; K. Kundu, S.; Bhaumik, A.; Manirul Islam, S. Ruthenium Nanoparticles Supported over Mesoporous TiO_2 as an Efficient Bifunctional Nanocatalyst for Esterification of Biomass-Derived Levulinic Acid and Transfer-Hydrogenation Reactions. *RSC Adv.* **2016**, *6* (77), 73440–73449. https://doi.org/10.1039/C6RA10233F.

(239) Cai, X.; Nie, J.; Yang, G.; Wang, F.; Ma, C.; Lu, C.; Chen, Z. Phosphorus-Rich Network Polymer Supported Ruthenium Nanoparticles for Nitroarene Reduction. *Mater.* **2019**, *240*, 80–83. https://doi.org/10.1016/j.matlet.2018.12.140.

(240) Sharma, R.; Holland, G. P.; Solomon, V. C.; Zimmermann, H.; Schiffenhaus, S.; Amin, S. A.; Buttry, D. A.; Yarger, J. L. NMR Characterization of Ligand Binding and Exchange Dynamics in Triphenylphosphine-Capped Gold Nanoparticles. *J. Phys. Chem. C* **2009**, *113* (37), 16387–16393. https://doi.org/10.1021/jp905141h.

(241) Hardacre, C.; Parvulescu, V. *Catalysis in Ionic Liquids: From Catalyst Synthesis to Application*; RSC, 2014.

(242) Backhouse, T. Heteroatom-Modified Polymer Immobilised Ionic Liquid-Stabilised Metal Nanoparticles : Synthesis and Applications. Thesis, Newcastle University, 2019.

(243) Mayer, H. A.; Kaska, W. C. Stereochemical Control of Transition Metal Complexes by Polyphosphine Ligands. *Chem. Rev.* **1994**, *94* (5), 1239–1272. https://doi.org/10.1021/cr00029a004.

(244) Rabinowitz, R.; Marcus, R. Notes-Direct Synthesis of p-Styryldiphenylphosphine. *J. Org. Chem.* **1961**, *26* (10), 4157–4158. https://doi.org/10.1021/jo01068a637.

(245) Chen, W.; Zhang, Y.; Zhu, L.; Lan, J.; Xie, R.; You, J. A Concept of Supported Amino Acid Ionic Liquids and Their Application in Metal Scavenging and Heterogeneous Catalysis. *J. Am. Chem. Soc.* **2007**, *129* (45), 13879–13886. https://doi.org/10.1021/ja073633n.

(246) Gonnella, N. C.; Busacca, C.; Campbell, S.; Eriksson, M.; Grinberg, N.; Bartholomeyzik, T.; Ma, S.; Norwood, D. L. ^{31}P Solid State NMR Study of Structure and Chemical Stability of Dichlorotriphenylphosphorane. *Magn. Reson. Chem.* **2009**, *47* (6), 461–464. https://doi.org/10.1002/mrc.2412.

(247) Dubován, L.; Pöllnitz, A.; Silvestru, C. Tri(3-Pyridyl)- and Tri(4-Pyridyl)-phosphine Chalcogenides and Their Complexes with ZnTPP (TPP = Tetraphenylporphyrinate). *Eur. J. Inorg. Chem.* **2016**, *2016* (10), 1521–1527. https://doi.org/10.1002/ejic.201501333.

(248) Albright, T. A.; Freeman, W. J.; Schweizer, E. E. Nuclear Magnetic Resonance Studies. IV. Carbon and Phosphorus Nuclear Magnetic Resonance of Phosphine Oxides and Related Compounds. *J. Org. Chem.* **1975**, *40* (23), 3437–3441. https://doi.org/10.1021/jo00911a030.

(249) Attar, S.; Nelson, J. H.; Bearden, W. H.; Alcock, N. W.; Solujic', L.; Milosavljevic', E. B. Phosphole Complexes of Gold(III) Halides: Synthesis, Structure, Electrochemistry and Ligand Redistribution Reactions. *Polyhedron* **1991**, *10* (16), 1939–1949. https://doi.org/10.1016/S0277-5387(00)86058-1.

(250) Teets, T. S.; Nocera, D. G. Halogen Photoreductive Elimination from Gold(III) Centers. *J. Am. Chem. Soc.* **2009**, *131* (21), 7411–7420. https://doi.org/10.1021/ja9009937.

(251) Price, G. A.; Brisdon, A. K.; Flower, K. R.; Pritchard, R. G.; Quayle, P. Solvent Effects in Gold-Catalysed A3-Coupling Reactions. *Tetrahedron Lett.* **2014**, *55* (1), 151–154. https://doi.org/10.1016/j.tetlet.2013.10.141.

(252) Vasilikogiannaki, E.; Gryparis, C.; Kotzabasaki, V.; Lykakis, I. N.; Stratakis, M. Facile Reduction of Nitroarenes into Anilines and Nitroalkanes into Hydroxylamines *via* the Rapid Activation of Ammonia· Borane Complex by Supported Gold Nanoparticles. *Adv. Synth. Catal.* **2013**, 5.

(253) Andreou, D.; Iordanidou, D.; Tamiolakis, I.; Armatas, G. S.; Lykakis, I. N. Reduction of Nitroarenes into Aryl Amines and *N*-Aryl Hydroxylamines *via* Activation of NaBH$_4$ and Ammonia-Borane Complexes by Ag/TiO$_2$ Catalyst. *Nanomaterials* **2016**, *6* (3), 54.

(254) Tyler, J. H.; Nazari, S. H.; Patterson, R. H.; Udumula, V.; Smith, S. J.; Michaelis, D. J. Synthesis of *N*-Aryl and *N*-Heteroaryl Hydroxylamines *via* Partial Reduction of Nitroarenes with Soluble Nanoparticle Catalysts. *Tetrahedron Lett.* **2017**, *58* (1), 82–86. https://doi.org/10.1016/j.tetlet.2016.11.105.

(255) K. Shil, A.; Das, P. Solid Supported Platinum(0) Nanoparticles Catalyzed Chemo-Selective Reduction of Nitroarenes to *N*-Arylhydroxylamines. *Green Chem.* **2013**, *15* (12), 3421–3428. https://doi.org/10.1039/C3GC41179F.

(256) Liu, X.; Ye, S.; Li, H.-Q.; Liu, Y.-M.; Cao, Y.; Fan, K.-N. Mild, Selective and Switchable Transfer Reduction of Nitroarenes Catalyzed by Supported Gold Nanoparticles. *Catal. Sci. Technol.* **2013**, *3* (12), 3200–3206. https://doi.org/10.1039/C3CY00533J.

(257) Wei, Y.; Wu, J.; Xue, D.; Wang, C.; Liu, Z.; Zhang, Z.; Chen, G.; Xiao, J. Highly Efficient Rhodium-Catalyzed Transfer Hydrogenation of Nitroarenes into Amines and Formanilides. *Synlett* **2014**, *25* (9), 1295–1298. https://doi.org/10.1055/s-0033-1341250.

(258) Shi, Q.; Lu, R.; Jin, K.; Zhang, Z.; Zhao, D. Simple and Eco-Friendly Reduction of Nitroarenes to the Corresponding Aromatic Amines Using Polymer -Supported Hydrazine Hydrate over Iron Oxide Hydroxide Catalyst. *Green Chem.* **2006**, *8* (10), 868–870. https://doi.org/10.1039/B606705K.

(259) M. Patil, N.; A. Bhosale, M.; M. Bhanage, B. Transfer Hydrogenation of Nitroarenes into Anilines by Palladium Nanoparticles *via* Dehydrogenation of Dimethylamine Borane Complex. *RSC Adv.* **2015**, *5* (105), 86529–86535. https://doi.org/10.1039/C5RA14944D.

(260) Sridharan, V.; Suryavanshi, P. A.; Menéndez, J. C. Advances in the Chemistry of Tetrahydroquinolines. *Chem. Rev.* **2011**, *111* (11), 7157–7259. https://doi.org/10.1021/cr100307m.

(261) Omar-Amrani, R.; Thomas, A.; Brenner, E.; Schneider, R.; Fort, Y. Efficient Nickel-Mediated Intramolecular Amination of Aryl Chlorides. *Org. Lett.* **2003**, *5* (13), 2311–2314. https://doi.org/10.1021/ol034659w.

(262) Kubo, T.; Katoh, C.; Yamada, K.; Okano, K.; Tokuyama, H.; Fukuyama, T. A Mild Inter- and Intramolecular Amination of Aryl Halides with a Combination of CuI and CsOAc. *Tetrahedron* **2008**, *64* (49), 11230–11236. https://doi.org/10.1016/j.tet.2008.09.042.

(263) Maruoka, K.; Miyazaki, T.; Ando, M.; Matsumura, Y.; Sakane, S.; Hattori, K.; Yamamoto, H. Organoaluminum-Promoted Beckmann Rearrangement of Oxime Sulfonates. *J. Am. Chem. Soc.* **1983**, *105* (9), 2831–2843. https://doi.org/10.1021/ja00347a052.

(264) Fish, R. H.; Thormodsen, A. D.; Cremer, G. A. Homogeneous Catalytic Hydrogenation. 1. Regiospecific Reductions of Polynuclear Aromatic and Polynuclear Heteroaromatic Nitrogen Compounds Catalyzed by Transition Metal Carbonyl Hydrides. *J. Am. Chem. Soc.* **1982**, *104* (19), 5234–5237. https://doi.org/10.1021/ja00383a044.

(265) Wang, T.; Zhuo, L.-G.; Li, Z.; Chen, F.; Ding, Z.; He, Y.; Fan, Q.-H.; Xiang, J.; Yu, Z.-X.; Chan, A. S. C. Highly Enantioselective Hydrogenation of Quinolines Using Phosphine-Free Chiral Cationic Ruthenium Catalysts: Scope, Mechanism, and Origin of Enantioselectivity. *J. Am. Chem. Soc.* **2011**, *133* (25), 9878–9891. https://doi.org/10.1021/ja2023042.

(266) Kuwano, R.; Ikeda, R.; Hirasada, K. Catalytic Asymmetric Hydrogenation of Quinoline Carbocycles: Unusual Chemoselectivity in the Hydrogenation of Quinolines. *Chem. Commun.* **2015**, *51* (35), 7558–7561. https://doi.org/10.1039/C5CC01971K.

(267) Xu, C.; Zhang, L.; Dong, C.; Xu, J.; Pan, Y.; Li, Y.; Zhang, H.; Li, H.; Yu, Z.; Xu, L. Iridium-Catalyzed Transfer Hydrogenation of 1,10-Phenanthrolines Using Formic Acid as the

Hydrogen Source. *Adv. Synth. Catal.* **2016**, *358* (4), 567–572. https://doi.org/10.1002/adsc.201500909.

(268) Fleischer, S.; Zhou, S.; Werkmeister, S.; Junge, K.; Beller, M. Cooperative Iron-Brønsted Acid Catalysis: Enantioselective Hydrogenation of Quinoxalines and 2*H*-1,4-Benzoxazines. *Chem. Eur. J.* **2013**, *19* (16), 4997–5003. https://doi.org/10.1002/chem.201204236.

(269) Zhang, L.; Qiu, R.; Xue, X.; Pan, Y.; Xu, C.; Li, H.; Xu, L. Versatile (Pentamethylcyclopentadienyl)Rhodium-2,2′-Bipyridine (Cp*Rh-Bpy) Catalyst for Transfer Hydrogenation of *N*-Heterocycles in Water. *Adv. Synth. Catal.* **2015**, *357* (16–17), 3529–3537. https://doi.org/10.1002/adsc.201500491.

(270) Tu, X.-F.; Gong, L.-Z. Highly Enantioselective Transfer Hydrogenation of Quinolines Catalyzed by Gold Phosphates: Achiral Ligand Tuning and Chiral-Anion Control of Stereoselectivity. *Angew. Chem.* **2012**, *124* (45), 11508–11511. https://doi.org/10.1002/ange.201204179.

(271) Xu, R.; Chakraborty, S.; Yuan, H.; Jones, W. D. Acceptorless, Reversible Dehydrogenation and Hydrogenation of *N*-Heterocycles with a Cobalt Pincer Catalyst. *ACS Catal.* **2015**, *5* (11), 6350–6354. https://doi.org/10.1021/acscatal.5b02002.

(272) Wang, D.-S.; Chen, Q.-A.; Lu, S.-M.; Zhou, Y.-G. Asymmetric Hydrogenation of Heteroarenes and Arenes. *Chem. Rev.* **2012**, *112* (4), 2557–2590. https://doi.org/10.1021/cr200328h.

(273) Bravo-Suárez, J. J.; Chaudhari, R. V.; Subramaniam, B. Design of Heterogeneous Catalysts for Fuels and Chemicals Processing: An Overview. In *Novel Materials for Catalysis and Fuels Processing*; ACS Symposium Series; ACS, 2013; Vol. 1132, pp 3–68. https://doi.org/10.1021/bk-2013-1132.ch001.

(274) Gong, Y.; Li, M.; Li, H.; Wang, Y. Graphitic Carbon Nitride Polymers: Promising Catalysts or Catalyst Supports for Heterogeneous Oxidation and Hydrogenation. *Green Chem.* **2015**, *17* (2), 715–736. https://doi.org/10.1039/C4GC01847H.

(275) Zhang, Y.; Zhu, J.; Xia, Y.-T.; Sun, X.-T.; Wu, L. Efficient Hydrogenation of Nitrogen Heterocycles Catalyzed by Carbon-Metal Covalent Bonds-Stabilized Palladium Nanoparticles: Synergistic Effects of Particle Size and Water. *Adv. Synth. Catal.* **2016**, *358* (19), 3039–3045. https://doi.org/10.1002/adsc.201600505.

(276) Zhang, F.; Ma, C.; Chen, S.; Zhang, J.; Li, Z.; Zhang, X.-M. *N*-Doped Hierarchical Porous Carbon Anchored Tiny Pd NPs: A Mild and Efficient Quinolines Selective Hydrogenation Catalyst. *Mol. Catal.* **2018**, *452*, 145–153. https://doi.org/10.1016/j.mcat.2018.04.001.

(277) Zhang, S.; Xia, Z.; Ni, T.; Zhang, Z.; Ma, Y.; Qu, Y. Strong Electronic Metal-Support Interaction of Pt/CeO$_2$ Enables Efficient and Selective Hydrogenation of Quinolines at Room Temperature. *J. Catal.* **2018**, *359*, 101–111. https://doi.org/10.1016/j.jcat.2018.01.004.

(278) Shaikh, M. N.; Kalanthoden, A. N.; Ali, M.; Haque, Md. A.; Aziz, Md. A.; Abdelnaby, M. M.; Rani, S. K.; Bakare, A. I. Platinum Nanoparticle Based Dip-Catalyst for Facile Hydrogenation of Quinoline, Unfunctionalized Olefins, and Imines. *ChemistrySelect* **2020**, *5* (47), 14827–14838. https://doi.org/10.1002/slct.202003178.

(279) Zhang, L.; Wang, X.; Xue, Y.; Zeng, X.; Chen, H.; Li, R.; Wang, S. Cooperation between the Surface Hydroxyl Groups of Ru–SiO$_2$ @mSiO$_2$ and Water for Good Catalytic Performance for Hydrogenation of Quinoline. *Catal. Sci. Technol.* **2014**, *4* (7), 1939–1948. https://doi.org/10.1039/C3CY01071F.

(280) Ye, T.-N.; Li, J.; Kitano, M.; Hosono, H. Unique Nanocages of 12CaO$_7$Al$_2$O$_3$ Boost Heterolytic Hydrogen Activation and Selective Hydrogenation of Heteroarenes over Ruthenium Catalyst. *Green Chem.* **2017**, *19* (3), 749–756. https://doi.org/10.1039/C6GC02782B.

(281) Karakulina, A.; Gopakumar, A.; Akçok, İ.; Roulier, B. L.; LaGrange, T.; Katsyuba, S. A.; Das, S.; Dyson, P. J. A Rhodium Nanoparticle–Lewis Acidic Ionic Liquid Catalyst for the Chemoselective Reduction of Heteroarenes. *Angew. Chem.* **2016**, *128* (1), 300–304. https://doi.org/10.1002/ange.201507945.

(282) Guo, M.; Li, C.; Yang, Q. Accelerated Catalytic Activity of Pd NPs Supported on Amine-Rich Silica Hollow Nanospheres for Quinoline Hydrogenation. *Catal. Sci. Technol.* **2017**, *7* (11), 2221–2227. https://doi.org/10.1039/C7CY00394C.

(283) Ren, D.; He, L.; Yu, L.; Ding, R.-S.; Liu, Y.-M.; Cao, Y.; He, H.-Y.; Fan, K.-N. An Unusual Chemoselective Hydrogenation of Quinoline Compounds Using Supported Gold Catalysts. *J. Am. Chem. Soc.* **2012**, *134* (42), 17592–17598. https://doi.org/10.1021/ja3066978.

(284) Michel, C.; Zaffran, J.; Ruppert, A. M.; Matras-Michalska, J.; Jędrzejczyk, M.; Grams, J.; Sautet, P. Role of Water in Metal Catalyst Performance for Ketone Hydrogenation: A Joint Experimental and Theoretical Study on Levulinic Acid Conversion into Gamma-

Valerolactone. *Chem. Commun.* **2014**, *50* (83), 12450–12453. https://doi.org/10.1039/C4CC04401K.

(285) Mao, H.; Ma, J.; Liao, Y.; Zhao, S.; Liao, X. Using Plant Tannin as Natural Amphiphilic Stabilizer to Construct an Aqueous–Organic Biphasic System for Highly Active and Selective Hydrogenation of Quinoline. *Catal. Sci. Technol.* **2013**, *3* (6), 1612–1617. https://doi.org/10.1039/C3CY00108C.

(286) Mao, H.; Chen, C.; Liao, X.; Shi, B. Catalytic Hydrogenation of Quinoline over Recyclable Palladium Nanoparticles Supported on Tannin Grafted Collagen Fibers. *J. Mol. Catal. A Chem.* **2011**, *341* (1), 51–56. https://doi.org/10.1016/j.molcata.2011.03.023.

(287) Dell'Anna, M. M.; Capodiferro, V. F.; Mali, M.; Manno, D.; Cotugno, P.; Monopoli, A.; Mastrorilli, P. Highly Selective Hydrogenation of Quinolines Promoted by Recyclable Polymer Supported Palladium Nanoparticles under Mild Conditions in Aqueous Medium. *Appl. Catal. A: Gen.* **2014**, *481*, 89–95. https://doi.org/10.1016/j.apcata.2014.04.041.

(288) Iwai, T.; Harada, T.; Hara, K.; Sawamura, M. Threefold Cross-Linked Polystyrene–Triphenylphosphane Hybrids: Mono-P-Ligating Behavior and Catalytic Applications for Aryl Chloride Cross-Coupling and C(Sp^3)-H Borylation. *Angew. Chem., Int. Ed.* **2013**, *52* (47), 12322–12326. https://doi.org/10.1002/anie.201306769.

(289) Chambreau, S. D.; Schenk, A. C.; Sheppard, A. J.; Yandek, G. R.; Vaghjiani, G. L.; Maciejewski, J.; Koh, C. J.; Golan, A.; Leone, S. R. Thermal Decomposition Mechanisms of Alkylimidazolium Ionic Liquids with Cyano-Functionalized Anions. *J. Phys. Chem. A* **2014**, *118* (47), 11119–11132. https://doi.org/10.1021/jp5095855.

(290) Montolio, S.; Vicent, C.; Aseyev, V.; Alfonso, I.; Burguete, M. I.; Tenhu, H.; García-Verdugo, E.; Luis, S. V. AuNP–Polymeric Ionic Liquid Composite Multicatalytic Nanoreactors for One-Pot Cascade Reactions. *ACS Catal.* **2016**, *6* (10), 7230–7237. https://doi.org/10.1021/acscatal.6b01759.

(291) Yamada, Y. M. A.; Uozumi, Y. Development of a Convoluted Polymeric Nanopalladium Catalyst: α-Alkylation of Ketones and Ring-Opening Alkylation of Cyclic 1,3-Diketones with Primary Alcohols. *Tetrahedron* **2007**, *63* (35), 8492–8498. https://doi.org/10.1016/j.tet.2007.05.071.

(292) Costa, N. J. S.; Kiyohara, P. K.; Monteiro, A. L.; Coppel, Y.; Philippot, K.; Rossi, L. M. A Single-Step Procedure for the Preparation of Palladium Nanoparticles and a Phosphine-

Functionalized Support as Catalyst for Suzuki Cross-Coupling Reactions. *J. Catal.* **2010**, *276* (2), 382–389. https://doi.org/10.1016/j.jcat.2010.09.028.

(293) Luska, K. L.; Moores, A. Improved Stability and Catalytic Activity of Palladium Nanoparticle Catalysts Using Phosphine-Functionalized Imidazolium Ionic Liquids. *Adv. Synth. Catal.* **2011**, *353* (17), 3167–3177. https://doi.org/10.1002/adsc.201100551.

(294) Son, S. U.; Jang, Y.; Yoon, K. Y.; Kang, E.; Hyeon, T. Facile Synthesis of Various Phosphine-Stabilized Monodisperse Palladium Nanoparticles through the Understanding of Coordination Chemistry of the Nanoparticles. *Nano Lett.* **2004**, *4* (6), 1147–1151. https://doi.org/10.1021/nl049519+.

(295) Xia, Y.-T.; Ma, J.; Wang, X.-D.; Yang, L.; Wu, L. Enantioselective Hydrogenation of *N*-Heteroaromatics Catalyzed by Chiral Diphosphine Modified Binaphthyl Palladium Nanoparticles. *Catal. Sci. Technol.* **2017**, *7* (23), 5515–5520. https://doi.org/10.1039/C7CY01672G.

(296) Joule, J. A.; Mills, K.; Smith, G. F. *Heterocyclic Chemistry*, 3rd ed.; CRC Press: London, 2020. https://doi.org/10.1201/9781003072850.

(297) Guella, G.; Zanchetta, C.; Patton, B.; Miotello, A. New Insights on the Mechanism of Palladium-Catalyzed Hydrolysis of Sodium Borohydride from ^{11}B NMR Measurements. *J. Phys. Chem. B* **2006**, *110* (34), 17024–17033. https://doi.org/10.1021/jp063362n.

(298) Li, G.; Yang, H.; Zhang, H.; Qi, Z.; Chen, M.; Hu, W.; Tian, L.; Nie, R.; Huang, W. Encapsulation of Nonprecious Metal into Ordered Mesoporous *N*-Doped Carbon for Efficient Quinoline Transfer Hydrogenation with Formic Acid. *ACS Catal.* **2018**, *8* (9), 8396–8405. https://doi.org/10.1021/acscatal.8b01404.

(299) Wan, H.; Vitter, A.; Chaudhari, R. V.; Subramaniam, B. Kinetic Investigations of Unusual Solvent Effects during Ru/C Catalyzed Hydrogenation of Model Oxygenates. *J. Catal.* **2014**, *309*, 174–184. https://doi.org/10.1016/j.jcat.2013.09.020.

(300) Sun, B.; Carnevale, D.; Süss-Fink, G. Selective *N*-Cycle Hydrogenation of Quinolines with Sodium Borohydride in Aqueous Media Catalyzed by Hectorite-Supported Ruthenium Nanoparticles. *J. Organomet. Chem.* **2016**, *821*, 197–205. https://doi.org/10.1016/j.jorganchem.2016.07.010.

(301) Zhang, L.; Wang, X.; Xue, Y.; Zeng, X.; Chen, H.; Li, R.; Wang, S. Cooperation between the Surface Hydroxyl Groups of Ru-SiO$_2$@mSiO$_2$ and Water for Good Catalytic

Performance for Hydrogenation of Quinoline. *Catal. Sci. Technol.* **2014**, *4* (7), 1939–1948. https://doi.org/10.1039/c3cy01071f.

(302) Sun, B.; Khan, F.-A.; Vallat, A.; Süss-Fink, G. NanoRu@hectorite: A Heterogeneous Catalyst with Switchable Selectivity for the Hydrogenation of Quinoline. *Appl. Catal. A: Gen.* **2013**, *467*, 310–314. https://doi.org/10.1016/j.apcata.2013.07.037.

(303) Dell'Anna, M. M.; Romanazzi, G.; Intini, S.; Rizzuti, A.; Leonelli, C.; Piccinni, A. F.; Mastrorilli, P. A Polymer Supported Palladium(II) *β*-Ketoesterate Complex as Active and Recyclable Pre-Catalyst for Selective Reduction of Quinolines in Water with Sodium Borohydride. *J. Mol. Catal. A Chem.* **2015**, *402*, 83–91. https://doi.org/10.1016/j.molcata.2015.03.013.

(304) Appendix A: Why Is Saturation Not Observed in Catalysts That Display Conventional Kinetics? In *Mechanical Catalysis*; John Wiley & Sons, Ltd, 2008; pp 337–339. https://doi.org/10.1002/9780470384190.app1.

(305) Mohr, S. H.; Wang, J.; Ellem, G.; Ward, J.; Giurco, D. Projection of World Fossil Fuels by Country. *Fuel* **2015**, *141*, 120–135. https://doi.org/10.1016/j.fuel.2014.10.030.

(306) Li, Z.; Xu, Q. Metal-Nanoparticle-Catalyzed Hydrogen Generation from Formic Acid. *Acc. Chem. Res.* **2017**, *50* (6), 1449–1458. https://doi.org/10.1021/acs.accounts.7b00132.

(307) Chen, W.; Shen, J.; Huang, Y.; Liu, X.; Astruc, D. Catalyzed Hydrolysis of Tetrahydroxydiboron by Graphene Quantum Dot-Stabilized Transition-Metal Nanoparticles for Hydrogen Evolution. *ACS Sustainable Chem. Eng.* **2020**, *8* (19), 7513–7522. https://doi.org/10.1021/acssuschemeng.0c02496.

(308) Perera, F. Pollution from Fossil-Fuel Combustion Is the Leading Environmental Threat to Global Pediatric Health and Equity: Solutions Exist. *Int. J. Environ. Res.* **2018**, *15* (1), 16. https://doi.org/10.3390/ijerph15010016.

(309) Olivier, J.; Schure, K.; Peters, J. Trends in Global CO_2 and Total Greenhouse Gas Emissions. 2017. *URL https://tinyurl. com/ycnx7at6* **2019**.

(310) Sanz-Pérez, E. S.; Murdock, C. R.; Didas, S. A.; Jones, C. W. Direct Capture of CO_2 from Ambient Air. *Chem. Rev.* **2016**, *116* (19), 11840–11876. https://doi.org/10.1021/acs.chemrev.6b00173.

(311) Jain, I. P.; Lal, C.; Jain, A. Hydrogen Storage in Mg: A Most Promising Material. *Int. J. Hydrog. Energy* **2010**, *35* (10), 5133–5144. https://doi.org/10.1016/j.ijhydene.2009.08.088.

(312) Schlapbach, L.; Züttel, A. Hydrogen-Storage Materials for Mobile Applications. In *Materials for Sustainable Energy*; Co-Published with Macmillan Publishers Ltd, UK, 2010; pp 265–270. https://doi.org/10.1142/9789814317665_0038.

(313) Brack, P.; Dann, S. E.; Wijayantha, K. G. U. Heterogeneous and Homogenous Catalysts for Hydrogen Generation by Hydrolysis of Aqueous Sodium Borohydride ($NaBH_4$) Solutions. *Energy Sci. Eng.* **2015**, *3* (3), 174–188. https://doi.org/10.1002/ese3.67.

(314) R. Shaner, M.; A. Atwater, H.; S. Lewis, N.; W. McFarland, E. A Comparative Technoeconomic Analysis of Renewable Hydrogen Production Using Solar Energy. *Energy Environ. Sci.* **2016**, *9* (7), 2354–2371. https://doi.org/10.1039/C5EE02573G.

(315) Koumi Ngoh, S.; Njomo, D. An Overview of Hydrogen Gas Production from Solar Energy. *Renew. Sust. Energ. Rev.* **2012**, *16* (9), 6782–6792. https://doi.org/10.1016/j.rser.2012.07.027.

(316) Hosseini, S. E.; Wahid, M. A. Hydrogen from Solar Energy, a Clean Energy Carrier from a Sustainable Source of Energy. *Int. J. Energy Res.* **2020**, *44* (6), 4110–4131. https://doi.org/10.1002/er.4930.

(317) Turner, J.; Sverdrup, G.; Mann, M. K.; Maness, P.-C.; Kroposki, B.; Ghirardi, M.; Evans, R. J.; Blake, D. Renewable Hydrogen Production. *Int. J. Energy Res.* **2008**, *32* (5), 379–407. https://doi.org/10.1002/er.1372.

(318) Yu, X.; Tang, Z.; Sun, D.; Ouyang, L.; Zhu, M. Recent Advances and Remaining Challenges of Nanostructured Materials for Hydrogen Storage Applications. *Prog. Mater. Sci.* **2017**, *88*, 1–48. https://doi.org/10.1016/j.pmatsci.2017.03.001.

(319) de Bruijn, F. A. Hydrogen as a Future Energy Carrier. Edited by Andreas Züttel, Andreas Borgschulte, and Louis Schlapbach. *ChemSusChem* **2008**, *1* (8–9), 782–783. https://doi.org/10.1002/cssc.200800119.

(320) K. Mandal, T.; H. Gregory, D. Hydrogen Storage Materials: Present Scenarios and Future Directions. *Annu. Rep. Prog. Chem., Sect. A: Inorg. Chem.* **2009**, *105* (0), 21–54. https://doi.org/10.1039/B818951J.

(321) Cipriani, G.; Di Dio, V.; Genduso, F.; La Cascia, D.; Liga, R.; Miceli, R.; Ricco Galluzzo, G. Perspective on Hydrogen Energy Carrier and Its Automotive Applications. *Int. J. Hydrog. Energy* **2014**, *39* (16), 8482–8494. https://doi.org/10.1016/j.ijhydene.2014.03.174.

(322) Duman, S.; Kaya, B.; Caf, F.; Enez, B.; Fincan, S. A. Innovative Hydrogen Release from Sodium Borohydride Hydrolysis Using Biocatalyst-like Fe_2O_3 Nanoparticles Impregnated

on Bacillus Simplex Bacteria. *Int. J. Hydrog. Energy* **2021**, *46* (29), 15410–15430. https://doi.org/10.1016/j.ijhydene.2021.02.028.

(323) Lang, C.; Jia, Y.; Yao, X. Recent Advances in Liquid-Phase Chemical Hydrogen Storage. *Energy Storage Mater.* **2020**, *26*, 290–312. https://doi.org/10.1016/j.ensm.2020.01.010.

(324) Felderhoff, M.; Weidenthaler, C.; Helmolt, R. von; Eberle, U. Hydrogen Storage: The Remaining Scientific and Technological Challenges. *Phys. Chem. Chem. Phys.* **2007**, *9* (21), 2643–2653. https://doi.org/10.1039/B701563C.

(325) Sun, Q.; Wang, N.; Xu, Q.; Yu, J. Nanopore-Supported Metal Nanocatalysts for Efficient Hydrogen Generation from Liquid-Phase Chemical Hydrogen Storage Materials. *Adv. Mater.* **2020**, *32* (44), 2001818. https://doi.org/10.1002/adma.202001818.

(326) He, T.; Pachfule, P.; Wu, H.; Xu, Q.; Chen, P. Hydrogen Carriers. Vol. 1. *Nat. Rev. Mater.* **2016**, 16059.

(327) Demirci, U. B.; Akdim, O.; Andrieux, J.; Hannauer, J.; Chamoun, R.; Miele, P. Sodium Borohydride Hydrolysis as Hydrogen Generator: Issues, State of the Art and Applicability Upstream from a Fuel Cell. *Fuel Cells.* **2010**, *10* (3), 335–350. https://doi.org/10.1002/fuce.200800171.

(328) Santos, D. M. F.; Sequeira, C. A. C. Sodium Borohydride as a Fuel for the Future. *Renew. Sust. Energ. Rev.* **2011**, *15* (8), 3980–4001. https://doi.org/10.1016/j.rser.2011.07.018.

(329) Patel, N.; Fernandes, R.; Gupta, S.; Edla, R.; Kothari, D. C.; Miotello, A. Co-B Catalyst Supported over Mesoporous Silica for Hydrogen Production by Catalytic Hydrolysis of Ammonia Borane: A Study on Influence of Pore Structure. *Appl. Catal. B: Environ.* **2013**, *140–141*, 125–132. https://doi.org/10.1016/j.apcatb.2013.03.046.

(330) Sordakis, K.; Tang, C.; Vogt, L. K.; Junge, H.; Dyson, P. J.; Beller, M.; Laurenczy, G. Homogeneous Catalysis for Sustainable Hydrogen Storage in Formic Acid and Alcohols. *Chem. Rev.* **2018**, *118* (2), 372–433. https://doi.org/10.1021/acs.chemrev.7b00182.

(331) Onishi, N.; Laurenczy, G.; Beller, M.; Himeda, Y. Recent Progress for Reversible Homogeneous Catalytic Hydrogen Storage in Formic Acid and in Methanol. *Coord. Chem. Rev.* **2018**, *373*, 317–332. https://doi.org/10.1016/j.ccr.2017.11.021.

(332) W. Hamilton, C.; Tom Baker, R.; Staubitz, A.; Manners, I. B–N Compounds for Chemical Hydrogen Storage. *Chem. Soc. Rev.* **2009**, *38* (1), 279–293. https://doi.org/10.1039/B800312M.

(333) Onishi, N.; Iguchi, M.; Yang, X.; Kanega, R.; Kawanami, H.; Xu, Q.; Himeda, Y. Development of Effective Catalysts for Hydrogen Storage Technology Using Formic Acid. *Adv. Energy Mater.* **2019**, *9* (23), 1801275. https://doi.org/10.1002/aenm.201801275.

(334) Zhan, W.-W.; Zhu, Q.-L.; Xu, Q. Dehydrogenation of Ammonia Borane by Metal Nanoparticle Catalysts. *ACS Catal.* **2016**, *6* (10), 6892–6905. https://doi.org/10.1021/acscatal.6b02209.

(335) Zeng, M.; Li, Y. Recent Advances in Heterogeneous Electrocatalysts for the Hydrogen Evolution Reaction. *J. Mater. Chem. A* **2015**, *3* (29), 14942–14962. https://doi.org/10.1039/C5TA02974K.

(336) Liu, K.-H.; Zhong, H.-X.; Li, S.-J.; Duan, Y.-X.; Shi, M.-M.; Zhang, X.-B.; Yan, J.-M.; Jiang, Q. Advanced Catalysts for Sustainable Hydrogen Generation and Storage *via* Hydrogen Evolution and Carbon Dioxide/Nitrogen Reduction Reactions. *Prog. Mater. Sci.* **2018**, *92*, 64–111. https://doi.org/10.1016/j.pmatsci.2017.09.001.

(337) Deng, X.; Huang, Z.; Wang, W.; Davé, R. N. Investigation of Nanoparticle Agglomerates Properties Using Monte Carlo Simulations. *Adv. Powder Technol.* **2016**, *27* (5), 1971–1979. https://doi.org/10.1016/j.apt.2016.06.029.

(338) Min, Y.; Akbulut, M.; Kristiansen, K.; Golan, Y.; Israelachvili, J. The Role of Interparticle and External Forces in Nanoparticle Assembly. In *Nanoscience and Technology*; Co-Published with Macmillan Publishers Ltd, UK, 2009; pp 38–49. https://doi.org/10.1142/9789814287005_0005.

(339) Yang, X.-F.; Wang, A.; Qiao, B.; Li, J.; Liu, J.; Zhang, T. Single-Atom Catalysts: A New Frontier in Heterogeneous Catalysis. *Acc. Chem. Res.* **2013**, *46* (8), 1740–1748. https://doi.org/10.1021/ar300361m.

(340) Cao, A.; Lu, R.; Veser, G. Stabilizing Metal Nanoparticles for Heterogeneous Catalysis. *Phys. Chem. Chem. Phys.* **2010**, *12* (41), 13499–13510. https://doi.org/10.1039/C0CP00729C.

(341) Schmid, G. *Nanoparticles: From Theory to Application*; John Wiley & Sons, 2011.

(342) Qu, X.; Jiang, R.; Li, Q.; Zeng, F.; Zheng, X.; Xu, Z.; Chen, C.; Peng, J. The Hydrolysis of Ammonia Borane Catalyzed by NiCoP/OPC-300 Nanocatalysts: High Selectivity and Efficiency, and Mechanism. *Green Chem.* **2019**, *21* (4), 850–860. https://doi.org/10.1039/C8GC03536A.

(343) Cai, Y.-Y.; Li, X.-H.; Zhang, Y.-N.; Wei, X.; Wang, K.-X.; Chen, J.-S. Highly Efficient Dehydrogenation of Formic Acid over a Palladium-Nanoparticle-Based Mott–Schottky Photocatalyst. *Angew. Chem., Int. Ed.* **2013**, *125* (45), 12038–12041. https://doi.org/10.1002/ange.201304652.

(344) Song, F.-Z.; Zhu, Q.-L.; Yang, X.; Zhan, W.-W.; Pachfule, P.; Tsumori, N.; Xu, Q. Metal–Organic Framework Templated Porous Carbon-Metal Oxide/Reduced Graphene Oxide as Superior Support of Bimetallic Nanoparticles for Efficient Hydrogen Generation from Formic Acid. *Adv. Energy Mater.* **2018**, *8* (1), 1701416. https://doi.org/10.1002/aenm.201701416.

(345) Li, Y.-T.; Zhang, X.-L.; Peng, Z.-K.; Liu, P.; Zheng, X.-C. Hierarchical Porous G-C3N4 Coupled Ultrafine RuNi Alloys as Extremely Active Catalysts for the Hydrolytic Dehydrogenation of Ammonia Borane. *ACS Sustainable Chem. Eng.* **2020**, *8* (22), 8458–8468. https://doi.org/10.1021/acssuschemeng.0c03009.

(346) Yin, L.; Zhang, T.; Dai, K.; Zhang, B.; Xiang, X.; Shang, H. Ultrafine PtCo Alloy Nanoclusters Confined in *N*-Doped Mesoporous Carbon Spheres for Efficient Ammonia Borane Hydrolysis. *ACS Sustainable Chem. Eng.* **2021**, *9* (2), 822–832. https://doi.org/10.1021/acssuschemeng.0c07385.

(347) Ding, R.; Chen, Q.; Luo, Q.; Zhou, L.; Wang, Y.; Zhang, Y.; Fan, G. Salt Template-Assisted in Situ Construction of Ru Nanoclusters and Porous Carbon: Excellent Catalysts toward Hydrogen Evolution, Ammonia-Borane Hydrolysis, and 4-Nitrophenol Reduction. *Green Chem.* **2020**, *22* (3), 835–842. https://doi.org/10.1039/C9GC03986D.

(348) Sun, Q.; Wang, N.; Bing, Q.; Si, R.; Liu, J.; Bai, R.; Zhang, P.; Jia, M.; Yu, J. Subnanometric Hybrid Pd-M(OH)₂, M = Ni, Co, Clusters in Zeolites as Highly Efficient Nanocatalysts for Hydrogen Generation. *Chem.* **2017**, *3* (3), 477–493. https://doi.org/10.1016/j.chempr.2017.07.001.

(349) Wang, N.; Sun, Q.; Bai, R.; Li, X.; Guo, G.; Yu, J. In Situ Confinement of Ultrasmall Pd Clusters within Nanosized Silicalite-1 Zeolite for Highly Efficient Catalysis of Hydrogen Generation. *J. Am. Chem. Soc.* **2016**, *138* (24), 7484–7487. https://doi.org/10.1021/jacs.6b03518.

(350) Sun, Q.; Wang, N.; Zhang, T.; Bai, R.; Mayoral, A.; Zhang, P.; Zhang, Q.; Terasaki, O.; Yu, J. Zeolite-Encaged Single-Atom Rhodium Catalysts: Highly-Efficient Hydrogen Generation

and Shape-Selective Tandem Hydrogenation of Nitroarenes. *Angew. Chem. Int. Ed.* **2019**, *58* (51), 18570–18576. https://doi.org/10.1002/anie.201912367.

(351) Sun, Q.; Wang, N.; Zhang, T.; Bai, R.; Mayoral, A.; Zhang, P.; Zhang, Q.; Terasaki, O.; Yu, J. Zeolite-Encaged Single-Atom Rhodium Catalysts: Highly-Efficient Hydrogen Generation and Shape-Selective Tandem Hydrogenation of Nitroarenes. *Angew. Chem. Int. Ed.* **2019**, *58* (51), 18570–18576. https://doi.org/10.1002/anie.201912367.

(352) Verma, P.; Yuan, K.; Kuwahara, Y.; Mori, K.; Yamashita, H. Enhancement of Plasmonic Activity by Pt/Ag Bimetallic Nanocatalyst Supported on Mesoporous Silica in the Hydrogen Production from Hydrogen Storage Material. *Appl. Catal. B: Environ.* **2018**, *223*, 10–15. https://doi.org/10.1016/j.apcatb.2017.05.017.

(353) Mori, K.; Futamura, Y.; Masuda, S.; Kobayashi, H.; Yamashita, H. Controlled Release of Hydrogen Isotope Compounds and Tunneling Effect in the Heterogeneously-Catalyzed Formic Acid Dehydrogenation. *Nat. Commun.* **2019**, *10* (1), 4094. https://doi.org/10.1038/s41467-019-12018-7.

(354) Zhong, H.; Su, Y.; Cui, C.; Zhou, F.; Li, X.; Wang, R. Palladium Nanoparticles Supported by Carboxylate-Functionalized Porous Organic Polymers for Additive-Free Hydrogen Generation from Formic Acid. *ACS Sustainable Chem. Eng.* **2017**, *5* (9), 8061–8069. https://doi.org/10.1021/acssuschemeng.7b01675.

(355) Cui, C.; Tang, Y.; Ziaee, M. A.; Tian, D.; Wang, R. Highly Dispersed Ultrafine Palladium Nanoparticles Enabled by Functionalized Porous Organic Polymer for Additive-Free Dehydrogenation of Formic Acid. *ChemCatChem* **2018**, *10* (6), 1431–1437. https://doi.org/10.1002/cctc.201701805.

(356) Wang, C.; Tuninetti, J.; Wang, Z.; Zhang, C.; Ciganda, R.; Salmon, L.; Moya, S.; Ruiz, J.; Astruc, D. Hydrolysis of Ammonia-Borane over Ni/ZIF-8 Nanocatalyst: High Efficiency, Mechanism, and Controlled Hydrogen Release. *J. Am. Chem. Soc.* **2017**, *139* (33), 11610–11615. https://doi.org/10.1021/jacs.7b06859.

(357) Fu, F.; Wang, C.; Wang, Q.; Martinez-Villacorta, A. M.; Escobar, A.; Chong, H.; Wang, X.; Moya, S.; Salmon, L.; Fouquet, E.; Ruiz, J.; Astruc, D. Highly Selective and Sharp Volcano-Type Synergistic $Ni_2Pt@ZIF-8$-Catalyzed Hydrogen Evolution from Ammonia Borane Hydrolysis. *J. Am. Chem. Soc.* **2018**, *140* (31), 10034–10042. https://doi.org/10.1021/jacs.8b06511.

(358) Gu, X.; Lu, Z.-H.; Jiang, H.-L.; Akita, T.; Xu, Q. Synergistic Catalysis of Metal–Organic Framework-Immobilized Au–Pd Nanoparticles in Dehydrogenation of Formic Acid for Chemical Hydrogen Storage. *J. Am. Chem. Soc.* **2011**, *133* (31), 11822–11825. https://doi.org/10.1021/ja200122f.

(359) Kang, N.; Djeda, R.; Wang, Q.; Fu, F.; Ruiz, J.; Pozzo, J.-L.; Astruc, D. Efficient "Click"-Dendrimer-Supported Synergistic Bimetallic Nanocatalysis for Hydrogen Evolution by Sodium Borohydride Hydrolysis. *ChemCatChem* **2019**, *11* (9), 2341–2349. https://doi.org/10.1002/cctc.201900246.

(360) Wang, Q.; Fu, F.; Escobar, A.; Moya, S.; Ruiz, J.; Astruc, D. "Click" Dendrimer-Stabilized Nanocatalysts for Efficient Hydrogen Release upon Ammonia-Borane Hydrolysis. *ChemCatChem* **2018**, *10* (12), 2673–2680. https://doi.org/10.1002/cctc.201800407.

(361) Wang, Q.; Fu, F.; Yang, S.; Martinez Moro, M.; Ramirez, M. de los A.; Moya, S.; Salmon, L.; Ruiz, J.; Astruc, D. Dramatic Synergy in CoPt Nanocatalysts Stabilized by "Click" Dendrimers for Evolution of Hydrogen from Hydrolysis of Ammonia Borane. *ACS Catal.* **2019**, *9* (2), 1110–1119. https://doi.org/10.1021/acscatal.8b04498.

(362) Yang, Q.; Jayakumar, S.; Modak, A.; Guo, M.; Li, H.; Hu, X. Ultrasmall Pt Stabilized on Triphenylphosphine Modified Silica for Chemoselective Hydrogenation. *Chem. Eur. J.* **2017**, *23*. https://doi.org/10.1002/chem.201700980.

(363) Han, K. N.; Li, C. A.; Bui, M.-P. N.; Pham, X.-H.; Kim, B. S.; Choa, Y. H.; Seong, G. H. Development of Pt/TiO$_2$ Nanohybrids-Modified SWCNT Electrode for Sensitive Hydrogen Peroxide Detection. *Sens. Actuators B Chem.* **2012**, *174*, 406–413. https://doi.org/10.1016/j.snb.2012.08.066.

(364) Simagina, V. I.; Storozhenko, P. A.; Netskina, O. V.; Komova, O. V.; Odegova, G. V.; Samoilenko, T. Yu.; Gentsler, A. G. Effect of the Nature of the Active Component and Support on the Activity of Catalysts for the Hydrolysis of Sodium Borohydride. *Kinet. Catal.* **2007**, *48* (1), 168–175. https://doi.org/10.1134/S0023158407010223.

(365) Guella, G.; Patton, B.; Miotello, A. Kinetic Features of the Platinum Catalyzed Hydrolysis of Sodium Borohydride from ^{11}B NMR Measurements. *J. Phys. Chem. C* **2007**, *111* (50), 18744–18750. https://doi.org/10.1021/jp0759527.

(366) Salameh, C.; Bruma, A.; Malo, S.; B. Demirci, U.; Miele, P.; Bernard, S. Monodisperse Platinum Nanoparticles Supported on Highly Ordered Mesoporous Silicon Nitride

Nanoblocks: Superior Catalytic Activity for Hydrogen Generation from Sodium Borohydride. *RSC Adv.* **2015**, *5* (72), 58943–58951. https://doi.org/10.1039/C5RA05901A.

(367) Lale, A.; Wasan, A.; Kumar, R.; Miele, P.; Demirci, U. B.; Bernard, S. Organosilicon Polymer-Derived Mesoporous 3D Silicon Carbide, Carbonitride and Nitride Structures as Platinum Supports for Hydrogen Generation by Hydrolysis of Sodium Borohydride. *Int. J. Hydrog. Energy* **2016**, *41* (34), 15477–15488. https://doi.org/10.1016/j.ijhydene.2016.06.186.

(368) Uzundurukan, A.; Devrim, Y. Hydrogen Generation from Sodium Borohydride Hydrolysis by Multi-Walled Carbon Nanotube Supported Platinum Catalyst: A Kinetic Study. *Int. J. Hydrog. Energy* **2019**, *44* (33), 17586–17594. https://doi.org/10.1016/j.ijhydene.2019.04.188.

(369) Saha, S.; Basak, V.; Dasgupta, A.; Ganguly, S.; Banerjee, D.; Kargupta, K. Graphene Supported Bimetallic G–Co–Pt Nanohybrid Catalyst for Enhanced and Cost Effective Hydrogen Generation. *Int. J. Hydrog. Energy* **2014**, *39* (22), 11566–11577. https://doi.org/10.1016/j.ijhydene.2014.05.131.

(370) Wu, C.; Zhang, J.; Guo, J.; Sun, L.; Ming, J.; Dong, H.; Zhao, Y.; Tian, J.; Yang, X. Ceria-Induced Strategy To Tailor Pt Atomic Clusters on Cobalt–Nickel Oxide and the Synergetic Effect for Superior Hydrogen Generation. *ACS Sustain. Chem. Eng.* **2018**, *6* (6), 7451–7457. https://doi.org/10.1021/acssuschemeng.8b00061.

(371) Dai, P.; Zhao, X.; Xu, D.; Wang, C.; Tao, X.; Liu, X.; Gao, J. Preparation, Characterization, and Properties of Pt/Al$_2$O$_3$/Cordierite Monolith Catalyst for Hydrogen Generation from Hydrolysis of Sodium Borohydride in a Flow Reactor. *Int. J. Hydrog. Energy* **2019**, *44* (53), 28463–28470. https://doi.org/10.1016/j.ijhydene.2019.02.013.

(372) Majoulet, O.; Salameh, C.; Schuster, M. E.; Demirci, U. B.; Sugahara, Y.; Bernard, S.; Miele, P. Synthesis of Periodic Mesoporous Silicon-Aluminum-Carbon-Nitrogen Frameworks Surface-Decorated with Pt Nanoparticles. *chem. Mater.* **2013**, *25*, 3957–3970.

(373) Wang, X.; Zhao, Y.; Peng, X.; Wang, J.; Jing, C.; Tian, J. Synthesis and Characterizations of CoPt Nanoparticles Supported on Poly(3,4-Ethylenedioxythiophene)/Poly(Styrenesulfonate) Functionalized Multi-Walled Carbon Nanotubes with Superior Activity for NaBH$_4$ Hydrolysis. *Mater. Sci. Eng. B: Solid-State Mater. Adv. Technol.* **2015**, *200*, 99–106. https://doi.org/10.1016/j.mseb.2015.07.002.

(374) Lale, A.; Mallmann, M. D.; Tada, S.; Bruma, A.; Özkar, S.; Kumar, R.; Haneda, M.; Francisco Machado, R. A.; Iwamoto, Y.; Demirci, U. B.; Bernard, S. Highly Active, Robust and Reusable Micro-/Mesoporous TiN/Si$_3$N$_4$ Nanocomposite-Based Catalysts for Clean Energy: Understanding the Key Role of TiN Nanoclusters and Amorphous Si3N4 Matrix in the Performance of the Catalyst System. *Appl. Catal. B: Environ.* **2020**, *272*, 118975. https://doi.org/10.1016/j.apcatb.2020.118975.

(375) Zabielaitė, A.; Balčiūnaitė, A.; Stalnionienė, I.; Lichušina, S.; Šimkūnaitė, D.; Vaičiūnienė, J.; Šimkūnaitė-Stanynienė, B.; Selskis, A.; Tamašauskaitė-Tamašiūnaitė, L.; Norkus, E. Fiber-Shaped Co Modified with Au and Pt Crystallites for Enhanced Hydrogen Generation from Sodium Borohydride. *Int. J. Hydrog. Energy* **2018**, *43* (52), 23310–23318. https://doi.org/10.1016/j.ijhydene.2018.10.179.

(376) Sachau, S.; Zaheer, M.; Lale, A.; Friedrich, M.; Denner, C.; Demirci, P.; Bernard, S.; Motz, G.; Kempe, Prof. D. Micro-/Mesoporous Platinum–SiCN Nanocomposite Catalysts (Pt@SiCN): From Design to Catalytic Applications. *Chem. Eur. J.* **2016**, *22*. https://doi.org/10.1002/chem.201603266.

(377) Semiz, L.; Abdullayeva, N.; Sankir, M. Nanoporous Pt and Ru Catalysts by Chemical Dealloying of Pt-Al and Ru-Al Alloys for Ultrafast Hydrogen Generation. *J. Alloys Compd.* **2018**, *744*, 110–115. https://doi.org/10.1016/j.jallcom.2018.02.082.

(378) Luo, C.; Fu, F.; Yang, X.; Wei, J.; Wang, C.; Zhu, J.; Huang, D.; Astruc, D.; Zhao, P. Highly Efficient and Selective Co@ZIF-8 Nanocatalyst for Hydrogen Release from Sodium Borohydride Hydrolysis. *ChemCatChem* **2019**, *11* (6), 1643–1649. https://doi.org/10.1002/cctc.201900051.

(379) Yao, Q.; Yang, K.; Hong, X.; Chen, X.; Lu, Z.-H. Base-Promoted Hydrolytic Dehydrogenation of Ammonia Borane Catalyzed by Noble-Metal-Free Nanoparticles. *Catal. Sci. Technol.* **2018**, *8* (3), 870–877. https://doi.org/10.1039/C7CY02365K.

(380) Wang, Q.; Fu, F.; Escobar, A.; Moya, S.; Ruiz, J.; Astruc, D. "Click" Dendrimer-Stabilized Nanocatalysts for Efficient Hydrogen Release upon Ammonia-Borane Hydrolysis. *ChemCatChem* **2018**, *10* (12), 2673–2680. https://doi.org/10.1002/cctc.201800407.

(381) Huff, C.; Biehler, E.; Quach, Q.; Long, J. M.; Abdel-Fattah, T. M. Synthesis of Highly Dispersive Platinum Nanoparticles and Their Application in a Hydrogen Generation Reaction. *Colloids Surf. A Physicochem. Eng.* **2021**, *610*, 125734. https://doi.org/10.1016/j.colsurfa.2020.125734.

(382) Wei, Y.; Wang, Y.; Wei, L.; Zhao, X.; Zhou, X.; Liu, H. Highly Efficient and Reactivated Electrocatalyst of Ruthenium Electrodeposited on Nickel Foam for Hydrogen Evolution from NaBH$_4$ Alkaline Solution. *Int. J. Hydrog. Energy* **2018**, *43* (2), 592–600. https://doi.org/10.1016/j.ijhydene.2017.11.010.

(383) Karataş, Y.; Aygun, A.; Gülcan, M.; Şen, F. A New Highly Active Polymer Supported Ruthenium Nanocatalyst for the Hydrolytic Dehydrogenation of Dimethylamine-Borane. *J. Taiwan Inst. Chem. Eng.* **2019**, *99*, 60–65. https://doi.org/10.1016/j.jtice.2019.02.032.

(384) Zhang, N.; Liu, G.; Sun, Y.; Wang, Y.; Yan, J.; Liu, X. H$_2$ Evolution Upon Hydrolysis of Ammonia-Borane Catalyzed by Porphyrin Stabilized Nanocatalysts. *Catal. Lett.* **2021**, *151* (8), 2272–2278. https://doi.org/10.1007/s10562-020-03501-8.

(385) Lang, C.; Jia, Y.; Yao, X. Recent Advances in Liquid-Phase Chemical Hydrogen Storage. *Energy Storage Mater.* **2020**, *26*, 290–312. https://doi.org/10.1016/j.ensm.2020.01.010.

(386) B. Demirci, U.; Miele, P. Sodium Borohydride versus Ammonia Borane, in Hydrogen Storage and Direct Fuel Cell Applications. *Energy Environ. Sci.* **2009**, *2* (6), 627–637. https://doi.org/10.1039/B900595A.

(387) Zhan, W.-W.; Zhu, Q.-L.; Xu, Q. Dehydrogenation of Ammonia Borane by Metal Nanoparticle Catalysts. *ACS Catal.* **2016**, *6* (10), 6892–6905. https://doi.org/10.1021/acscatal.6b02209.

(388) Liu, B. H.; Li, Z. P. A Review: Hydrogen Generation from Borohydride Hydrolysis Reaction. *J. Power Sources* **2009**, *187* (2), 527–534. https://doi.org/10.1016/j.jpowsour.2008.11.032.

(389) Retnamma, R.; Novais, A. Q.; Rangel, C. M. Kinetics of Hydrolysis of Sodium Borohydride for Hydrogen Production in Fuel Cell Applications: A Review. *Int. J. Hydrog. Energy* **2011**, *36* (16), 9772–9790. https://doi.org/10.1016/j.ijhydene.2011.04.223.

(390) Schneemann, A.; White, J. L.; Kang, S.; Jeong, S.; Wan, L. F.; Cho, E. S.; Heo, T. W.; Prendergast, D.; Urban, J. J.; Wood, B. C.; Allendorf, M. D.; Stavila, V. Nanostructured Metal Hydrides for Hydrogen Storage. *Chem. Rev.* **2018**, *118* (22), 10775–10839. https://doi.org/10.1021/acs.chemrev.8b00313.

(391) Zhang, S.; Zhou, L.; Chen, M. Amine-Functionalized MIL-53(Al) with Embedded Ruthenium Nanoparticles as a Highly Efficient Catalyst for the Hydrolytic Dehydrogenation of Ammonia Borane. *RSC Adv.* **2018**, *8* (22), 12282–12291. https://doi.org/10.1039/C8RA01507D.

(392) Ramsay, W. J.; Bell, N. A. W.; Qing, Y.; Bayley, H. Single-Molecule Observation of the Intermediates in a Catalytic Cycle. *J. Am. Chem. Soc.* **2018**, *140* (50), 17538–17546. https://doi.org/10.1021/jacs.8b09282.